OCS Study
MMS-2001-098

FINAL REPORT – November 2001

NUMERICAL MODELING EVALUATION OF THE CUMULATIVE PHYSICAL EFFECTS OF OFFSHORE SAND DREDGING FOR BEACH NOURISHMENT

Prepared by:

Sean W. Kelley
John S. Ramsey
Mark R. Byrnes

Applied Coastal Research and Engineering, Inc.
766 Falmouth Road, Suite A-1
Mashpee, MA 02649

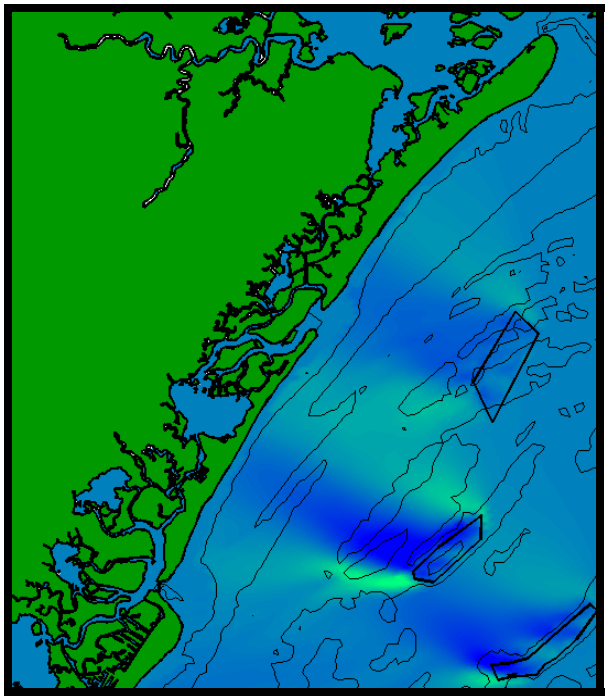

Prepared for:

U.S. Department of the Interior
Minerals Management Service
International Activities and Marine
Minerals Division (INTERMAR)

Funded Under Contract Number 1435-01-99-CT-30993

DISCLAIMER

SUGGESTED CITATION

Kelley, S.W., J.S. Ramsey, M.R. Byrnes, 2001. Numerical Modeling Evaluation of the Cumulative Physical Effects of Offshore Sand Dredging for Beach Nourishment. U.S. Department of the Interior, Minerals Management Service, International Activities and Marine Minerals Division (INTERMAR), Herndon, VA. OCS Report MMS 2001-098, 95 pp. + 106 pp. appendices.

OCS Study
MMS-2001-098

FINAL REPORT

Numerical Modeling Evaluation Of The Cumulative Physical Effects Of Offshore Sand Dredging For Beach Nourishment

November 2001

Sean W. Kelley
John S. Ramsey
Mark R. Byrnes

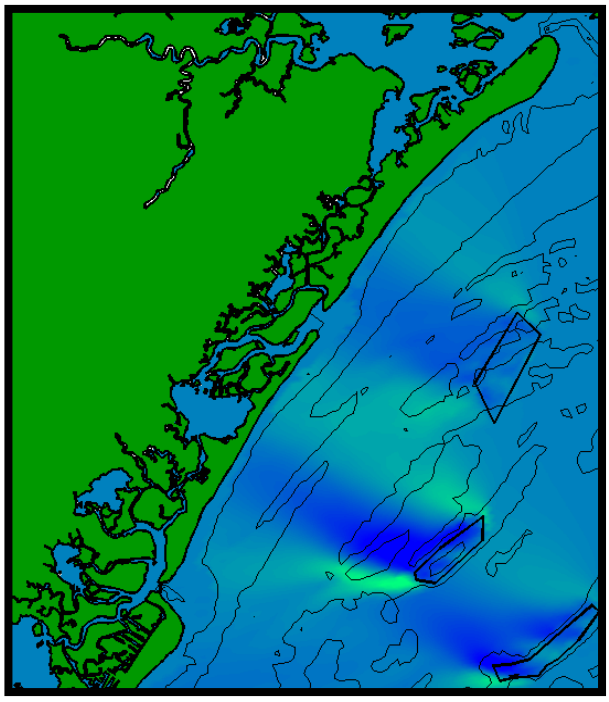

Prepared by:

Applied Coastal Research and Engineering, Inc.
766 Falmouth Road, Suite A-1
Mashpee, MA 02649

Prepared for:

U.S. Department of the Interior
Minerals Management Service
International Activities and Marine
Minerals Division (INTERMAR)

Funded Under Contract Number 1435-01-99-CT-30993

ACKNOWLEDGMENTS

This project was funded by the U.S. Department of the Interior (DOI), Minerals Management Service (MMS), International Activities and Marine Minerals Division (INTERMAR) under Contract #1435-01-99-CT-30993. Mr. Barry S. Drucker was the MMS Contracting Officer's Technical Representative (COTR) and provided valuable assistance throughout the project. Ms. Jane Carlson served as the MMS Contracting Officer. Mr. Barry Drucker and Mr. Roger Amato of the MMS reviewed the draft document.

Mr. Sean W. Kelley authored Sections 3.0 (Modeling Approach and Applications), 4.0 (Cumulative Impacts), and Appendices B through E. Mr. John S. Ramsey authored Sections 2.0 (Physical Processes) and 5.0 (Conclusions). Dr. Mark R. Byrnes served as Project Manager and Editor of the report, and authored Section 1.0 (Introduction). Ms. Elizabeth Hunt was responsible for report compilation and editorial assistance during production of the report.

TABLE OF CONTENTS

LIST OF FIGURES

APPENDIX B: NEW JERSEY WAVE MODEL OUTPUT

APPENDIX C: VIRGINIA WAVE MODEL OUTPUT

APPENDIX D: NORTH CAROLINA WAVE MODEL OUTPUT

APPENDIX E: FLORIDA WAVE MODEL OUTPUT

LIST OF TABLES

1.0 INTRODUCTION

The Minerals Management Service (MMS), a bureau within the U.S. Department of the Interior, has responsibility for managing all mineral resources on the Federal Outer Continental Shelf (OCS), a zone that extends three (3) miles seaward from State coastline boundaries to 200 miles offshore. Although most interest in this zone relates to oil and gas resources, the potential for exploitation of sand resources as a source for beach and barrier island restoration has grown rapidly in the last several years as similar resources in State waters are being depleted or polluted. Extraction of sand resources in Federal waters may be preferred relative to State waters due to concerns over changes in physical oceanographic conditions resulting from large quantities of material dredged from resource sites impacted by waves and currents. This has generated a need for technical information to ensure that offshore minerals are developed with due concern for potential environmental considerations.

In 1983, the MMS established the Office of Strategic and International Minerals for evaluating the prospects for and conditions under which sand and gravel mining would develop in the U.S. In 1991, the Office of International Activities and Marine Minerals (INTERMAR; now referred to as the International Activities and Marine Minerals Division) was created to develop strategies for addressing specific concerns regarding offshore sand and gravel mining operations (Hammer et al., 1993). The MMS has significant responsibilities with respect to potential environmental impacts of sand and gravel mining. Existing regulations governing sand and gravel mining provide a framework for comprehensive environmental protection during operations. Specific requirements exist for evaluations and lease stipulations that include appropriate mitigation measures (Hammer et al., 1993). Guidelines for protecting the environment stem from a wide variety of laws, including the OCS Lands Act (OCSLA), National Environmental Policy Act (NEPA), and others. Regulations require activities to be conducted in a manner which prevents or minimizes the likelihood of any occurrences that may cause damage to the environment. The MMS takes a case-by-case approach in conducting environmental analyses, as required by NEPA and the Council on Environmental Quality (CEQ) regulations.

In recent years, there has been increasing interest in sand and gravel mining on the OCS. Currently, eight State-Federal task forces, several cooperative agreements, at least five negotiated agreements, and seven environmental surveys exist to ensure substantive government and public involvement and attention to regional, State, and local concerns regarding leasing, engineering, economic, and environmental aspects of sand and gravel mining (to obtain specific information regarding these activities, visit http://www.mms.gov/intermar/marineac.htm). Under the OCSLA, the MMS is required to conduct environmental studies to obtain information useful for decisions related to negotiated agreements and lease activities. As such, the MMS pursues its responsibilities for management of offshore sand and gravel mining vigorously by:

- protecting ocean and coastal environments by ensuring that all OCS sand and gravel mining activities are environmentally acceptable;
- ensuring the OCS sand and gravel activities are compatible with other uses of the ocean;
- involving coastal States in all aspects of sand and gravel mining activities; and
- evaluating the potential of the OCS as a domestic source for sand and gravel.

1.1 STUDY PURPOSE

The overall study purpose addresses the need for physical environmental information to support potential lease decisions offshore the east coast of the U.S. from southern New Jersey to Cape Canaveral, Florida. Specifically, the study examines the potential for negative impacts to coastal and nearshore environments, particularly from alterations to the local wave and sediment transport regime, due to long-term dredging and significant removal of sand from shoals offshore southern New Jersey, southeastern Virginia (Sandbridge Shoal), North Carolina (north of Oregon Inlet), and Cape Canaveral, Florida. Shoals in these areas are expected to serve as long-term and continual sources of borrow material, due to existing beach renourishment cycles, and to repair damage from severe coastal storms. In certain instances, such as Sandbridge Shoal offshore southeastern Virginia, several jurisdictions or entities want to use the same borrow area(s) on different cycles. This raises the issue of cumulative effects of multiple sand dredging events and/or dredging at multiple sites, particularly related to alterations to the local wave and sediment transport regime. In natural continental shelf settings, wave energy typically concentrates at shoals and diverges at holes due to wave refraction and diffraction. The interaction between waves and bathymetric surface geometry dictates the resultant pattern of wave energy propagation. As such, patterns of wave energy transformation across the continental shelf depend on changes in bathymetry and the level of incident energy.

The most effective means of quantifying incremental and cumulative physical environmental effects of sand dredging from shoals on the continental shelf is through the use of wave transformation numerical modeling tools that recognize the random nature of incident waves as they propagate onshore. Spectral wave models, such as STWAVE, REF/DIF-S, SWAN, and others, typically provide more realistic results than monochromatic wave models relative to field measurements (see Appendix A). As such, spectral wave transformation modeling was applied in this study to evaluate the potential negative impacts to coastal and nearshore sites from long-term dredging and significant removal of sand from offshore sand borrow sites. Although the interpretation of wave modeling results is relatively straightforward, evaluating the significance of predicted changes for accepting or rejecting a borrow site is more complicated. A substantial part of this study was aimed at assessing the significance of simulated changes between existing and post-dredging conditions versus natural variability in wave climate and potential sediment transport rates to determine the relative importance of predicted changes. It is expected that information generated will enable the MMS to assess potential impacts of long-term offshore dredging and to identify potential dredging alternatives aimed at minimizing or precluding adverse physical environmental impacts.

1.2 STUDY AREAS AND BORROW SITE CHARACTERISTICS

The inshore portion of the continental shelf, seaward of the State-Federal OCS boundary and within the Exclusive Economic Zone (EEZ), encompasses the project study areas offshore southern New Jersey (Figure 1-1), southeastern Virginia (Figure 1-2), North Carolina (north of Oregon Inlet; Figure 1-3), and Cape Canaveral, Florida (Figure 1-4). The seaward limit of all borrow sites is generally within about 30 km of the shoreline and located between the 10- and 20-m depth contours.

The continental shelf surface offshore southern New Jersey contains many first-, second-, and third-order morphologic features formed during the Holocene transgression (McKinney et al., 1974; Figure 1-1). Sand ridges 2- to 5-m high and 0.5- to 1.5-km apart

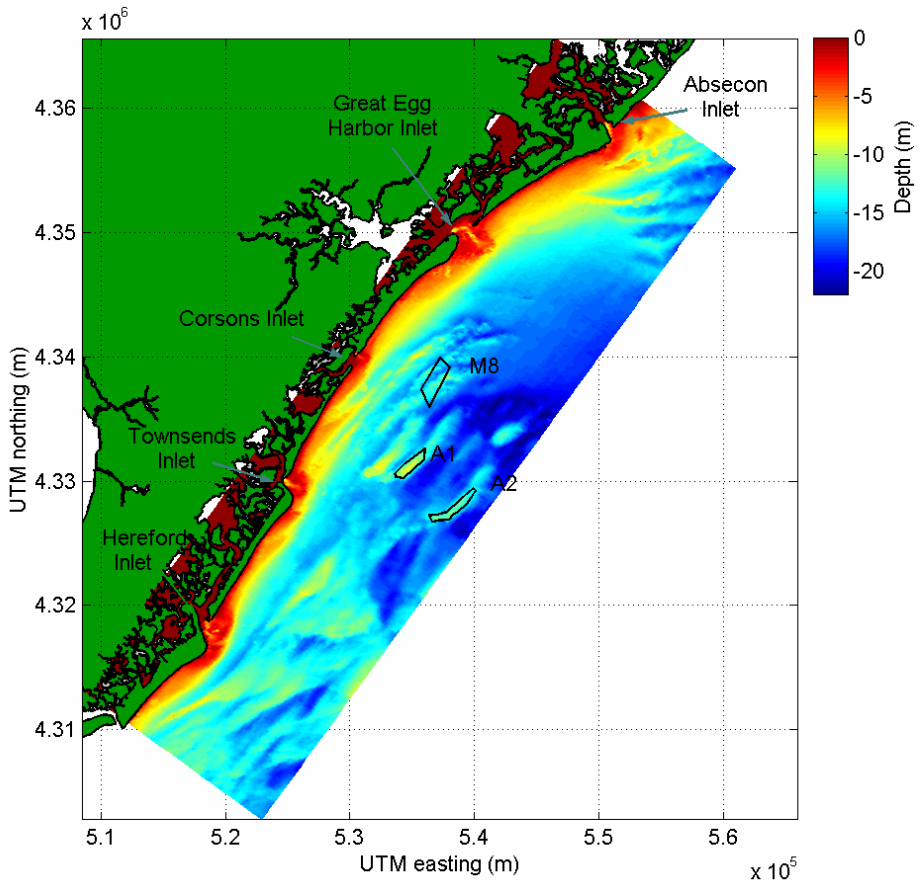

Figure 1-1. Location diagram illustrating sand borrow sites M8 (USACE designation), A1 and A2 (NJ State designation), and State-Federal boundary relative to 1934/77 bathymetry.

represent second-order features that are the primary sand resource targets of this study. Average shoal relief is about 3 m. Three potential borrow sites were modeled for southern New Jersey to evaluate the cumulative effects of multiple simultaneous dredging operations and repetitive dredging with time at one site. Table 1-1 lists proposed maximum dredging volumes and depths for sites A-1, A-2, and M8.

Continental shelf topography offshore southeastern Virginia is dominated by ridge and swale features formed during the Holocene (Williams et al., 1987; Kimball et al., 1991). Many potential sand resource sites are associated with ridges approximately 20 km offshore Virginia Beach (known as the Virginia Beach Ridges) and seaward of False Cape (False Cape Ridges). Kimball and Dame (1989) identified Sandbridge Shoal as a viable sand resource site for beach nourishment along the southeastern Virginia coast. The horseshoe-shaped shoal was characterized as a northward and eastward thinning wedge of sand approximately 48 km^2 in area and up to 6 m thick. Maximum relief over the ambient shelf surface was about 4 m (Kimball et al., 1991). Two sand borrow sites were identified on this shoal (Sites A and B; Figure 1-2), and approximately 1.5 MCY has been extracted from Site A for beach nourishment along Dam Neck Beach and Sandbridge Beach to date. Table 1-1 lists proposed maximum dredging volumes and depths for sites A and B.

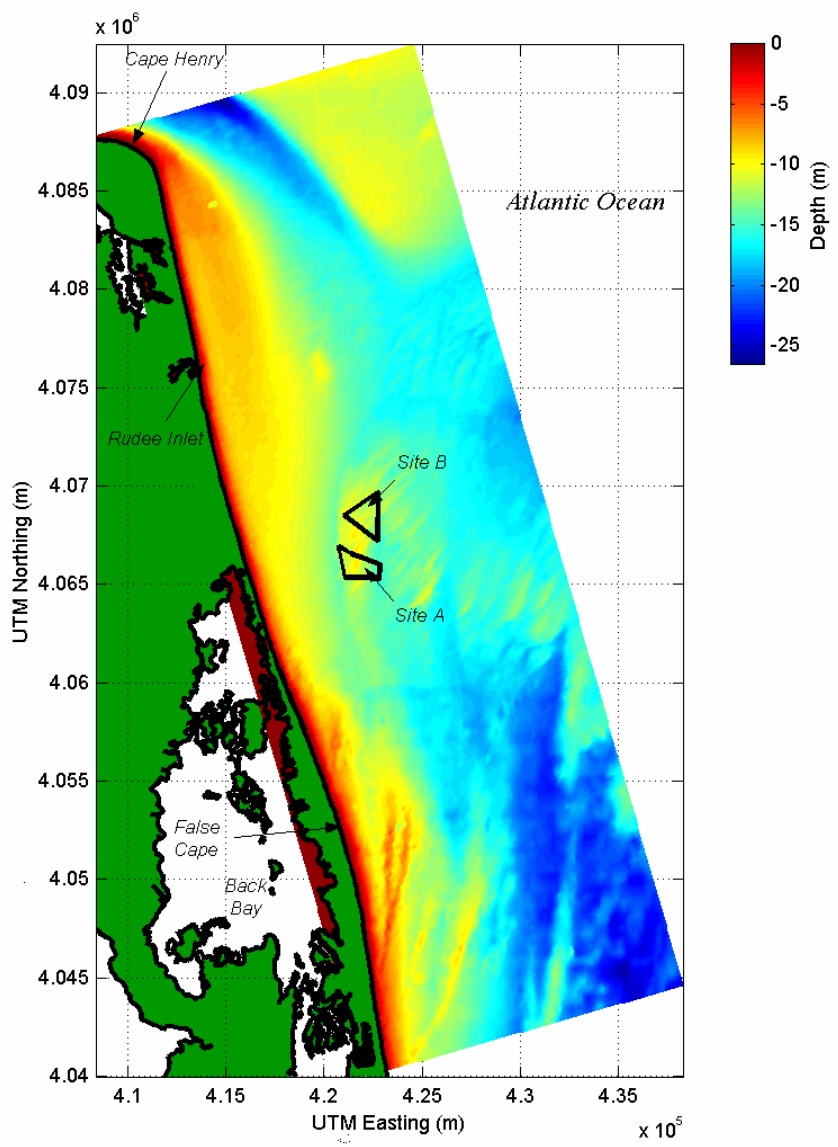

Figure 1-2. Location diagram illustrating sand borrow sites A and B and State-Federal boundary relative to 1934/77 bathymetry.

Table 1-1. Borrow site characteristics for the four sand resource areas.

Region	Site Designation	Volume (10^6 m^3)	Area (10^6 m^2)	Average Excavation Depth (m)
Southern New Jersey	A1	8.8	2.2	4.0
	A2	7.8	2.6	3.0
	M8	8.0	4.0	2.0
Southeastern Virginia	A	5.3	1.8	3.0
	B	6.9	2.3	3.0
North Carolina	3 East	1.4	0.7	2.0
	3 West	2.5	0.8	3.0
Offshore Cape Canaveral, Florida	2	26.0	5.0	5.2

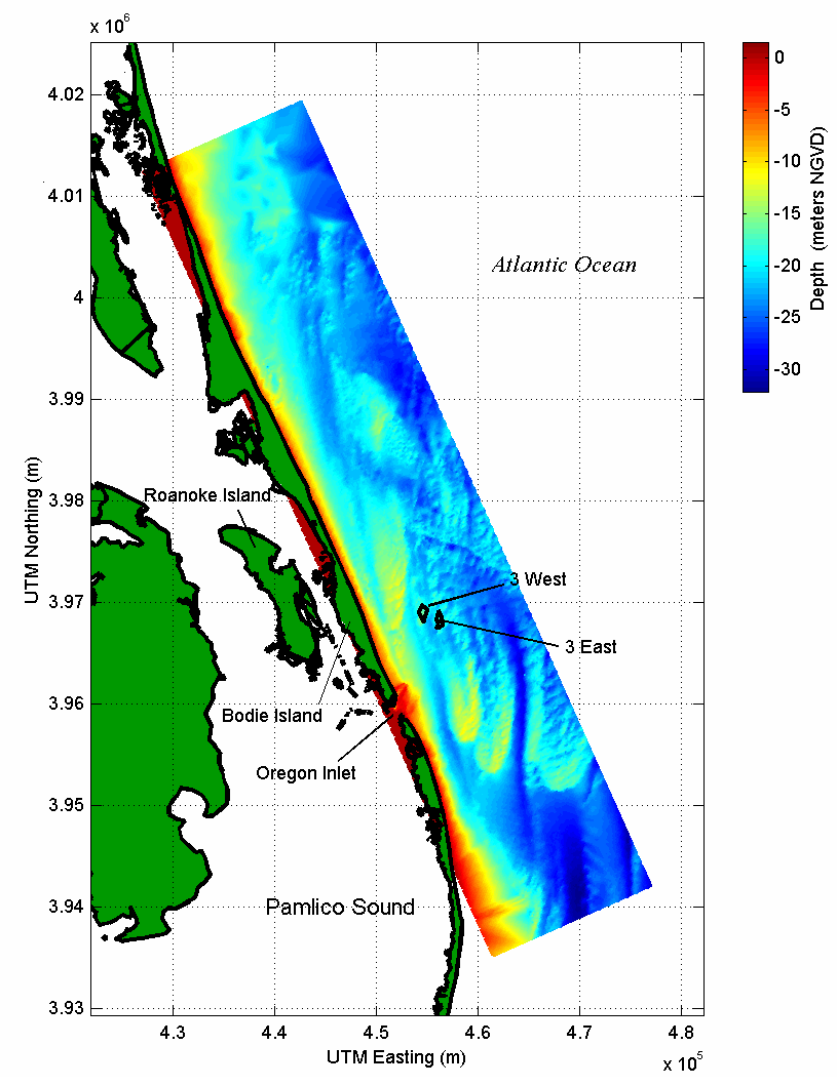

Figure 1-3. Location diagram illustrating sand borrow sites 3 West and 3 East and State-Federal boundary relative to 1934/77 bathymetry.

In the vicinity of Oregon Inlet, North Carolina shelf topography is characterized by sub-parallel ridges and swales that trend approximately north-south making an angle of about 20° to 30° with the shoreline trend (Inman and Dolan, 1989). The ridges are about 1.5 to 6 km apart, extend 12 to 60 km, and have an average relief of 2 to 6 m (Swift et al., 1972). The North Carolina Geological Survey identified four sand resource areas in OCS waters northeast of Oregon Inlet (Hoffman, 1998). Two sand borrow sites were selected in Resource Area 3 (3 East and 3 West; Figure 1-3) for evaluating the potential impact of simultaneous dredging at multiple sites on coastal wave and sediment transport processes. Table 1-1 lists proposed maximum dredging volumes and depths for sites 3 West and 3 East.

Cape Canaveral Shoals was the fourth sand resource area evaluated in this study. A potential offshore borrow site was identified by the U.S. Army Corps of Engineers, Jacksonville District, (USACE, 1999). Borrow Area 2 is located along the seaward margin of Canaveral Shoals about 15 to 20 km offshore in an area referred to

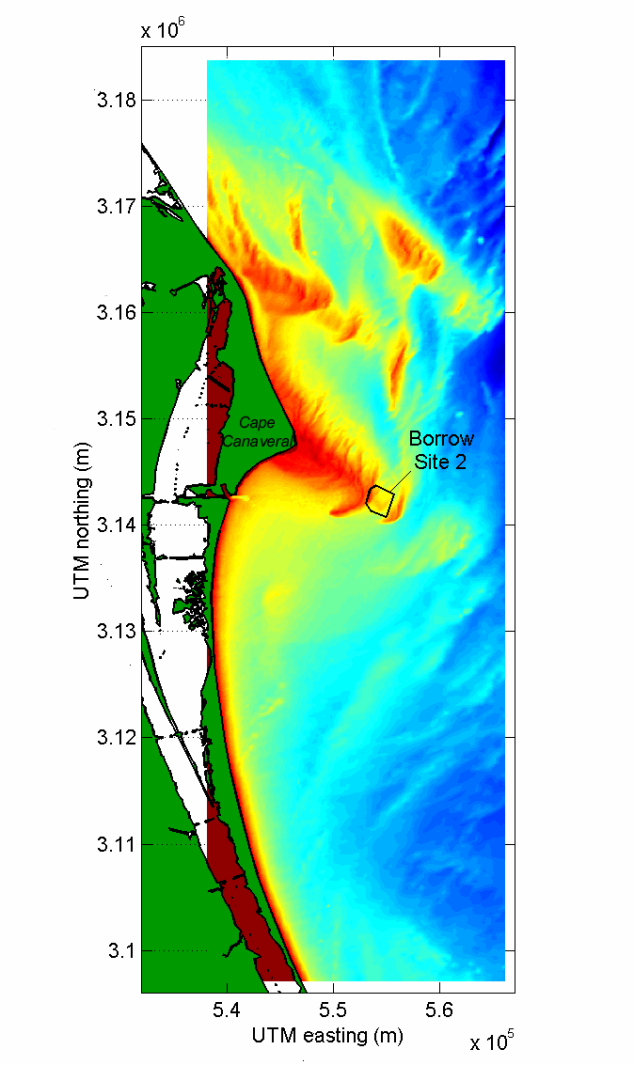

Figure 1-4. Location diagram illustrating sand Borrow Site II and State-Federal boundary relative to 1934/77 bathymetry.

as “Southeast Shoals”, in water depths ranging from 7 to 14 m (Figure 1-4). Core data from the borrow site suggest that beach quality sand is present at thicknesses of 3 to 5 m. Average median grain size is about 0.35 mm. Table 1-1 lists the proposed maximum dredging volume and depth for sand Borrow Site 2.

1.3 STUDY APPROACH

To address the overall study purpose, a four-phase approach was implemented. First, a detailed evaluation of three readily-available, project-tested spectral wave models was conducted to determine the most effective simulation routine for predicting potential wave impacts due to dredging at offshore borrow sites. Appendix A contains the final report for the spectral wave model evaluation task. Our analysis recommended that the U.S. Army Corps of Engineer STeady-state spectral WAVE model (STWAVE) be used on future MMS wave transformation modeling studies. Second, a standard method was developed to qualify the significance of changes associated with borrow site

excavation to determine the influence of borrow site geometry on local wave refraction and sediment transport patterns. Because large natural spatial and temporal variability exists within the wave climate at a particular site, determination of physical impacts associated with sand mining must consider the influence of process variability. The method developed for this study is based on historical wave climate variability, as well as local wave climate changes directly attributable to borrow site excavation.

The third phase of the project focused on wave spectra development, wave transformation modeling, and coastal sediment transport calculations. This phase of the project represents the bulk of analyses performed to document potential impacts associated with dredging at selected offshore sand borrow sites. Wave transformation modeling and sediment transport potential calculations were performed for existing and post-dredging bathymetric conditions. Comparison of computations for existing and post-dredging conditions are used to illustrate the relative maximum impact of borrow site excavation on wave-induced coastal processes.

The fourth and most significant phase of the project addressed potential cumulative effects and significance of sand dredging from offshore sand borrow sites. A site-specific determination of acceptable limits of borrow site impacts relative to sediment transport potential was determined for each case. In addition to the site-specific investigations, two model studies of incremental cumulative impacts from different borrow site configurations were investigated. The first study group of incremental impacts involved the interaction of multiple sites in close proximity to one another, such that overlapping areas of shoreline impact exist. The second study grouping of incremental impacts involves multiple dredging events at a single site, and how effects vary as excavation depth is increased (e.g., due to multiple dredging events over time). These analyses were designed to determine how potential wave impacts at individual sites may interact to produce additive physical environmental effects along the coast.

1.4 DOCUMENT ORGANIZATION

Information presented in this document represents the culmination of a year and a half of work among experts in the fields of oceanography, coastal processes, and numerical wave and sediment transport modeling, under the direction of Mr. Barry Drucker (MMS INTERMAR). This document was organized into six major sections as follows:

- Introduction
- Physical Processes
- Modeling Approach and Applications
- Cumulative Effects
- Conclusions
- Literature Cited

In addition to the main document, appendices were prepared in support of many of the analyses presented in each section of the report. Furthermore, an Executive Summary, a Technical Summary, and a Non-Technical Summary will be prepared as separate documents to provide a brief description of study methods and findings for audiences ranging from researchers to non-technical people.

2.0 PHYSICAL PROCESSES

During the past few decades, there has been increased focus on the nearshore zone due to rapid development of this region and the need to protect infrastructure from devastating storm impacts and long-term coastal erosion. A significant portion of this effort has been concentrated on developing analytical tools to evaluate the transformation of waves in shallow water and to quantify sediment transport induced by breaking waves along the shoreline. Although our understanding has improved, evaluation of coastal processes still requires a blend of analytical capability, interpretation of many complex and often apparently conflicting data sets, and experience gained from analyzing a variety of shorelines. The primary reason for this relevance on qualitative and quantitative approaches is that the equations governing sediment movement by waves are not yet fully known.

The primary quantitative technique used to evaluate nearshore processes is wave transformation modeling. Wave models have been developed to numerically solve the equations governing changes in wave height and direction (through processes such as refraction, shoaling, and breaking). As better offshore wave data sets become available (e.g., wave gauge and hindcast information), wave transformation models have become standard tools for evaluating changes in nearshore wave climate. Due to the complexities of surf zone hydrodynamics, sediment transport analysis techniques typically depend on information from wave models at the line of wave breaking. Unfortunately, calculations involving sediment transport are dependent on empirical or semi-empirical relationships; therefore, these techniques are not as theoretically rigorous as wave modeling. In addition, shoreline modifications (e.g., coastal engineering structures, natural hardbottom, and beach nourishment projects) are not included and sediment transport equations assume that an infinite supply of material is available, hence the term “sediment transport potential”. Although these simplifications can limit the applicability of the approach, proper interpretation of wave modeling and associated longshore sediment transport analysis results can provide a powerful tool for coastal engineering design and assessment of shoreline dynamics.

The analysis techniques presented in this report involve spectral wave modeling, based primarily on wave hindcast information, combined with standard longshore sediment transport equations to evaluate impacts associated with offshore sand mining. A general description of nearshore wave transformation and longshore sediment transport is provided. In addition, nearshore wave transformations and alterations to longshore sediment transport potential are shown for an idealized borrow site.

2.1 NEARSHORE WAVE TRANSFORMATION

Open ocean waves primarily are generated by wind that induces drag across the water surface. Over time, persistent strong winds can generate long waves with large heights, replacing less energetic waves initially created. Because wind patterns are complex, blowing in various directions with different speeds for varying amounts of time, the resulting sea is complicated as well. Due to the restoring force provided by gravity, ocean waves can travel long distances across the surface of the ocean with relatively little change in shape. As waves travel, energy is exchanged between the different component waves of the spectrum, and a small amount of wave energy is dissipated through surface tension and whitecapping. However, waves in the open ocean remain fairly uniform as they travel through deep water. As waves propagate into intermediate

and shallow water depths, the effects of the seafloor tend to dominate wave transformations. Although a small amount of energy is lost through bottom stresses (frictional drag), most nearshore wave transformation results from six processes: 1) refraction, 2) shoaling, 3) breaking, 4) diffraction, 5) reflection, and 6) wave-current interactions. These processes determine the size and incident angle of breaking waves, the dominant driving force for nearshore sediment transport. Although minor wave diffraction and reflection may occur at an offshore borrow site, wave refraction, shoaling, and breaking dominate transformation processes associated with offshore sand mining. Therefore, consideration of wave refraction, shoaling, and breaking are critical components of any spectral analysis used to evaluate alterations to a wave field associated with offshore sand mining.

As a wave propagates into shallow water, the wavelength shortens and the wave period remains constant (assuming the wave field is constant in time). The wave period is defined as the time required for successive wave crests to pass a particular location. Consequently, waves travel at slower speeds in shallow water. This process causes wave crests to bend, or refract, toward regions of shallow water and away from regions of deep water. As shown in Figure 2-1, wave crests approaching the beach at an angle become more parallel to the shoreline as they approach the beach and the water depth decreases. Refraction also serves to focus wave energy on headlands, reefs, and shoals, while diverting energy from deep holes and channels. This, in turn, directly impacts the erosional pressures on the shoreline. Because longshore sediment transport rates are dependent upon the wave angle at breaking, determined by the effects of refraction, underwater features such as troughs and ridges can serve to exacerbate erosion in certain regions. These erosional *hot spots* will exist where the bathymetry tends to focus wave energy. Along a wave crest, variations in wave height may occur due to a focusing of wave energy from refraction processes, a change in wave height from shoaling processes, or a shielding of wave energy from an obstruction.

Neglecting small energy losses due to frictional effects, the total energy in a propagating waveform is conserved. As a wave enters shallow water its propagation speed tends to slow. Because wave energy is dependent upon wave height and wave speed, and wave speed slows with decreasing depth, wave height increases as the wave propagates into shallow water. Depending on offshore bottom slope, the change in wave height due to shoaling can be significant. Computation of the longshore transport rate is dependent on the incident wave angle at breaking and wave height. Therefore, shoaling characteristics are important for evaluating beach erosion. In general, areas with relatively gentle offshore slopes allow wave energy to concentrate over a wide surf zone, and sediment transport volumes are high relative to incident wave height. However, beaches with gentle slopes usually have a significant sediment volume in storage, and because the wide surf zone causes transport to be distributed over a large area, the effects of sediment movement may not be evident. Conversely, beaches with very steep offshore slopes do not allow waves to completely shoal before breaking takes place. Thus, wave heights at breaking are reduced; however, breaking wave energy is dissipated within a narrow surf zone. Although transport volumes may not be as high as beaches with gentle slopes, the concentration of transport within a narrow region may cause the effects of beach erosion to be more pronounced.

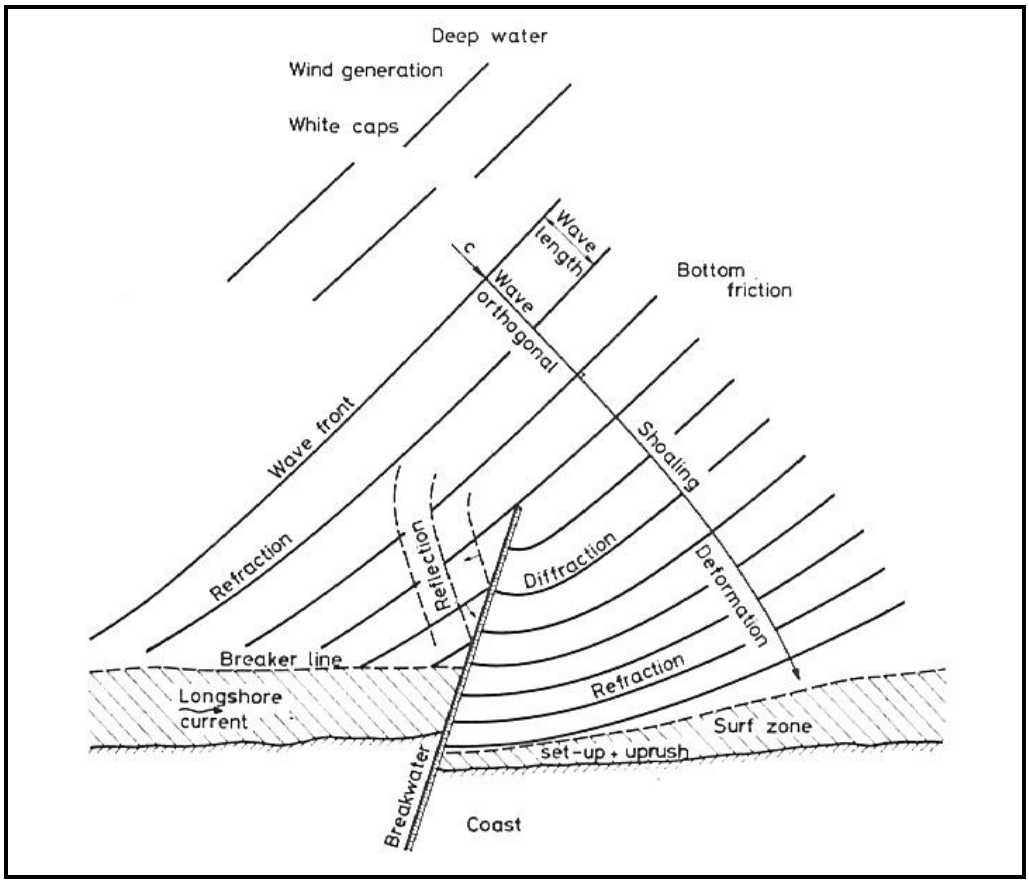

Figure 2-1. Diagram illustrating the effects of refraction and diffraction as waves approach the coastline (from Svendsen and Jonsson, 1976).

The most significant nearshore wave transformation occurs when waves break. In very shallow water (proportional to the wave height), the combined effects of refraction, shoaling, diffraction, and reflection produce a wave form that is unstable. When a wave becomes too steep, and the speed of the crest exceeds that of the entire wave form, the wave topples over and breaks. Breaking drastically reduces the wave height. Much of the wave energy is dissipated through the breaking process in a very narrow surf zone, where large amounts of sediment are lifted from the bottom and transported by nearshore waves and currents.

2.2 NEARSHORE SEDIMENT TRANSPORT PATTERNS

Nearshore wave and current motions are complex, and the surf zone system is further complicated by the capability of these motions to lift and transport beach sediment. An integrated study of wave processes, shoreline geometry, and sediment characteristics is required for predicting erosional trends and naturally occurring beach profile and planform shapes. Qualitatively, an understanding of the nearshore littoral system is obtained by focusing on cross-shore and longshore sediment transport trends, and on the influence of severe storm events versus typical wave conditions.

Generally, beach profile shape is governed by relatively short-term catastrophic events such as severe storms. For example, on the East Coast of the United States, beach profile shapes are dramatically changed by northeast storms and hurricanes.

Large volumes of sand are eroded from the beach face and deposited offshore in sand bars during these storm events. However, much of this material is recovered over longer time scales as milder waves move sediment landward, causing the beach face to accrete. Seasonal trends in wave climate influence cross-shore sediment transport as well. Typically, larger winter waves erode the beach face and milder summer waves build the beach. Therefore, the beach profile is dynamic, and the best estimate of a typical profile is the stable beach shape that forms when exposed to average annual waves. A stable beach is defined as an equilibrium condition and may be predicted using coastal engineering analyses. Cross-shore transport (or profile) modeling is usually based on the concept of equilibrium conditions forming a "stable" profile. This condition is used as a baseline for determining the potential changes in shoreline position due to a severe storm.

While large volumes of beach sediment are moved during isolated storm events, it is seasonal or average annual waves that dictate beach planform shape. Planform shape can be evaluated using longshore sediment transport models based on average annual wave conditions. Although large storm events may transport large volumes of sand along the coast, the short-term effects of storms tend to be minimal when long-term transport is evaluated. Waves incident from the north transport sediment to the south and vice-versa. Seasonal trends exist on the East Coast because winter waves generally are incident from the north, and summer waves generally are incident from the south. Of course, transport trends are highly dependent upon shoreline orientation. Varying volumes of sediment transported north and south may be estimated over time and superimposed to determine the net annual longshore sediment transport direction and volume. Another approach is to estimate the net annual transport from average annual wave conditions.

2.3 IDEALIZED OFFSHORE BORROW SITE

To assess alterations to wave patterns and associated longshore sediment transport processes, evaluation of an idealized offshore borrow site was performed using the spectral wave model STWAVE (described in Section 3) and standard sediment transport potential equations. A comparison of wave/sediment transport modeling results between transformations resulting from typical nearshore bathymetric conditions and those created by the existence of an offshore borrow site reveals the potential influence of sand mining on the littoral system.

First, a bathymetric grid was developed to represent generalized variations in water depth. Based on a typical cross-shore profile for New Jersey (Dean, 1977), the grid was developed assuming straight and parallel bathymetric contours using the equation: $h = Ay^m$, where h is the water depth, y is the distance offshore, A is a profile scale factor (indirectly related to beach grain size), and m is profile shape factor. For the southern New Jersey shoreline example, A was set at 0.0793 and m was set at 0.822. The idealized borrow site was centered on the 10 m bathymetric contour (see Figure 2-2) and consisted of an excavation of approximately 3 m. The borrow site was assumed to be square in the x-y direction with dimensions of 225 by 225 m. Total volume of the borrow site was approximately 153,000 cu m (200,000 cu yds).

The grid used for spectral wave refraction modeling extended 2,000 m alongshore and 850 m in the cross-shore direction, with a grid spacing of 5 m. A series of wave model runs were developed to provide conditions consistent with the southern New

Jersey shoreline: an incident spectral significant wave height of 1.2 m, a peak wave period of 8 sec, relatively narrow directional spreading, and a frequency distribution based on the work of Bretschneider (1968) and Mitsuyasu (1975). Wave model runs were performed for conditions with no borrow site (referred to as existing conditions) and for conditions with the borrow site described above (referred to as post-dredging conditions). To assess the range of wave transformations possible, wave spectra centered at -30°, -15°, 0°, 15°, and 30° relative to shore normal were modeled.

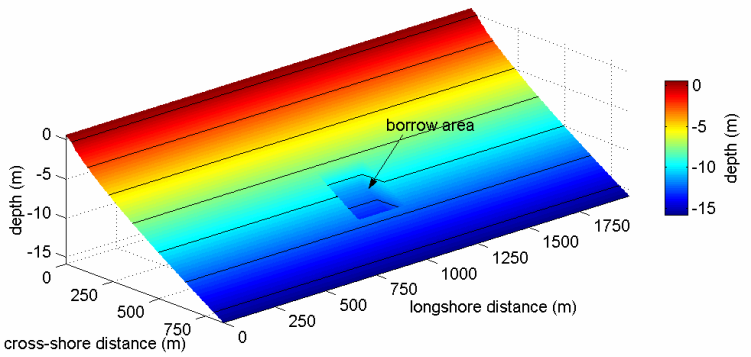

Figure 2-2. Surface plot with 2.5 m contours of bathymetry grid used for idealized borrow site model runs.

As an example of the wave modeling results, Figure 2-3 illustrates the influence of the idealized borrow site on the nearshore wave field for the -30º condition. Waves propagating across the borrow site tend to refract toward shallower water along the edges; therefore, areas of wave energy focusing (increase in wave heights) occur along each side of the borrow site. In addition, the wave refraction effect for the various spectral components generally creates a shadow zone landward of the borrow site. Due to the proximity of this borrow site to the beach (approximately 350 m offshore), the influence of the idealized borrow site on nearshore wave processes is much more pronounced than for a sand borrow site further offshore. However, the nearshore location of the borrow site creates a rather limited longshore region of influence. For the wave model case shown in Figure 2-3, the influence of the borrow site on the wave climate can be seen most clearly by comparing existing and post-dredging conditions as shown in Figure 2-4 (H_{post} - H_{pre}). For this wave modeling case, the longshore influence of the borrow site extends for an approximate distance of 900 m measured at the breaker line. In addition, the maximum increase and decrease in wave height created by the borrow site excavation are of similar magnitude (approximately ±0.3 m).

Although the influence of a borrow site excavation on the wave field is important, an evaluation of the wave field alterations alone does not directly provide information needed to assess potential borrow site impacts. Calculation of longshore sediment transport potential for a series of wave cases provides a method for determining the extent and magnitude of alterations to nearshore processes. For the idealized borrow site, annualized sediment transport potential curves were generated for each of the five spectral wave conditions (Figure 2-5). As expected, the influence of the borrow site for the 0° case is distributed evenly, where positive sediment transport is from left-to-right. Cases with a negative approach angle relative to shore normal (-15° and -30°) illustrate

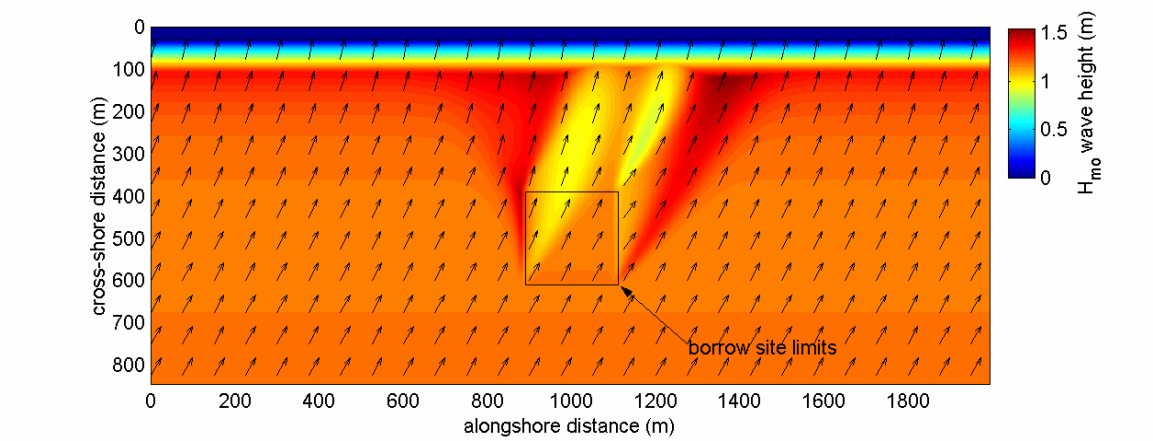

Figure 2-3. Example color contour plot of modeled wave heights, with vectors indicating mean wave direction for idealized borrow site (incident wave height of 1.2 m and period of 8 sec approaching shoreline at -30º from shore-normal).

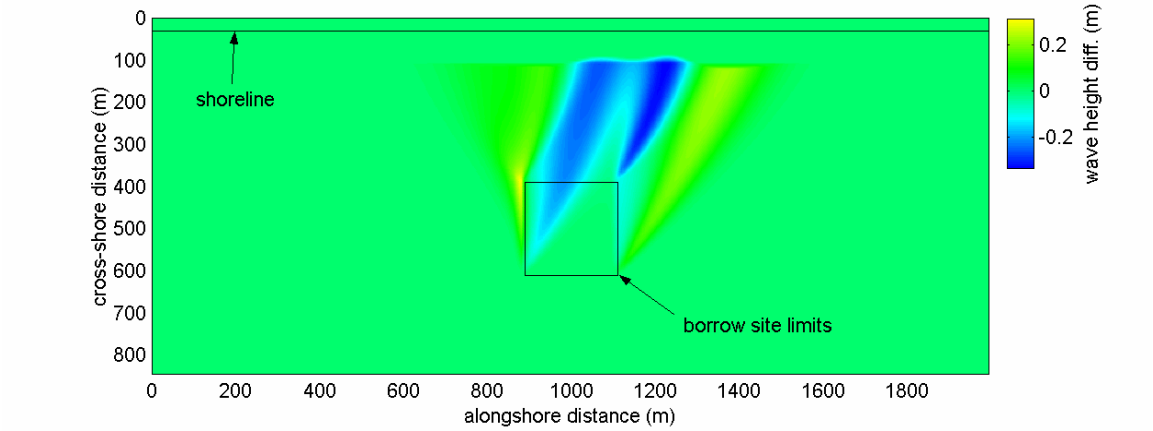

Figure 2-4. Color surface plot of wave height difference (H_{post} - H_{pre}) resulting from borrow site excavation, for wave case shown in Figure 2-3.

the influence of the borrow site shifted to the right and a left-to-right transport potential. Cases with a positive approach angle relative to shore normal (15° and 30°) show the opposite trend.

As part of the idealized borrow site evaluation, it first was assumed that each of the five modeled wave conditions occurred for 20% of the time. By superimposing each of the sediment transport potential curves shown in Figure 2-5 and weighting them by the appropriate percent occurrence (20%), a composite sediment transport potential curve can be developed (Figure 2-6). Because the modeled borrow site is so close to the shoreline, the influence of the borrow site on wave refraction and associated nearshore sediment transport patterns is substantial. Without the borrow site influence,

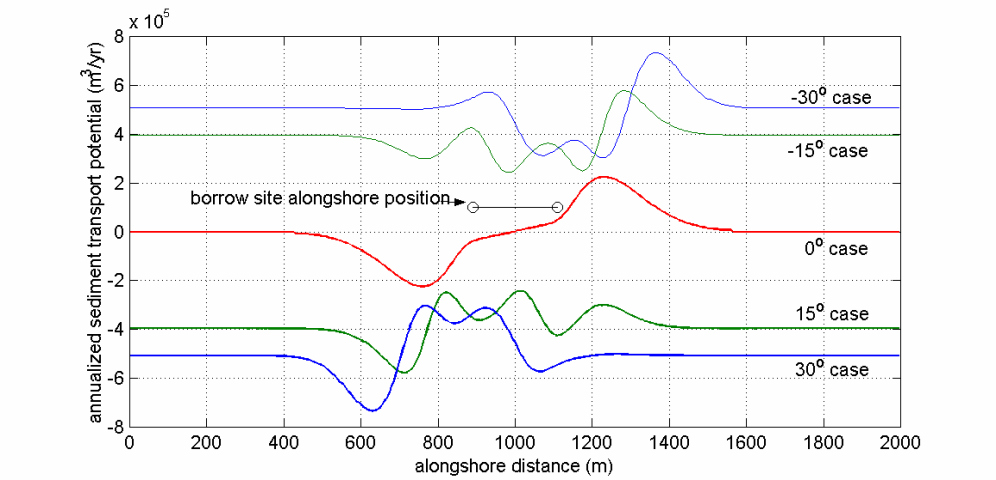

Figure 2-5. Computed annualized longshore sediment transport potential for idealized borrow site for five wave cases.

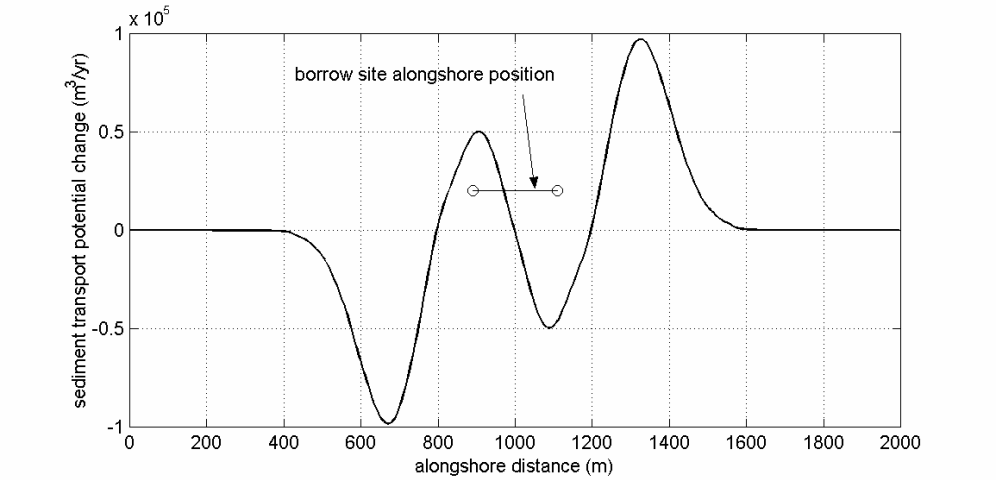

Figure 2-6. Change in computed longshore sediment transport potential for idealized borrow site.

the even distribution of wave conditions would cause a net sediment transport potential of zero for this shoreline; however, Figure 2-6 indicates that peak transport rates would increase to nearly 100,000 cu m annually at an alongshore distance of approximately 350 m from the center of the borrow site. These large increases in sediment transport potential directed away from the borrow site are a result of wave focusing. In contrast, the small peaks in sediment transport potential in between the two large peaks result from the "shadowing" effect of the borrow site created by the wave condition combinations. For example, waves propagating over the borrow site from the right (15° and 30° wave conditions) create a shadow region along the shoreline that is centered slightly to the left of the borrow site (the +50,000 cu m/yr transport peak in Figure 2-6). This shadow region is characterized by a decrease in left-directed sediment transport for these cases. Therefore, the overall effect is to create an increase in net right-directed (left-to-right) transport.

By computing the change in sediment transport potential over the shoreline distance (dQ/dy), a normalized curve of anticipated shoreline change resulting from excavation of an offshore borrows site can be developed. Figure 2-7 illustrates shoreline

change resulting from wave conditions presented above. Due to wave focusing caused by the borrow site configuration, increased erosion occurs along the shoreline on either side of the borrow site. Material eroded from these two areas feeds the central "shadow zone", as well as shoreline regions further from the borrow site center.

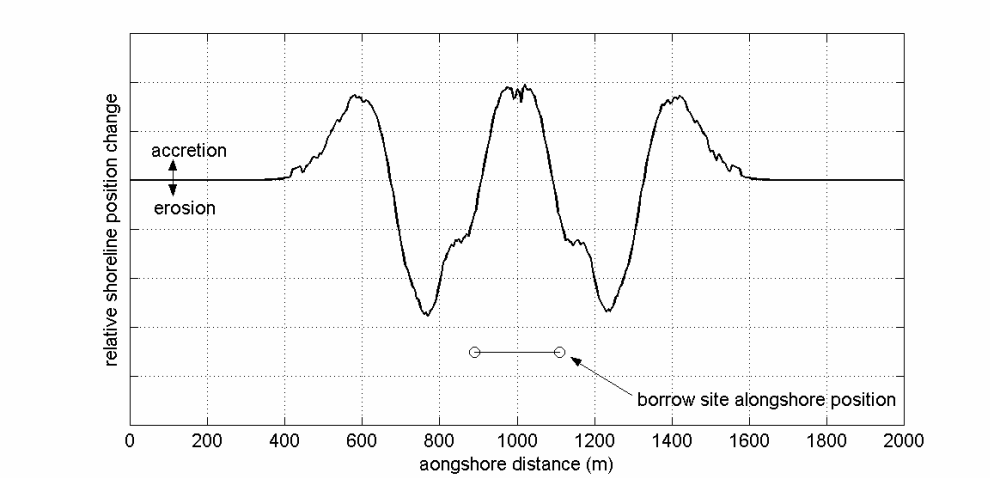

Figure 2-7. Computed cross-shore change in shoreline position based on modifications to longshore sediment transport potential by idealized borrow site.

To illustrate the influence of variable wave conditions on nearshore sediment transport dynamics, a second evaluation for the idealized borrow site was performed with a different distribution of input wave conditions. The percent occurrence for wave conditions presented above were altered to represent conditions dominated by a single direction as shown in Table 2-1. Figures 2-8 and 2-9 represent results from this redistribution of wave energy. As expected, the higher percent occurrence of the right-directed wave cases (-30° and -15°) increases the influence of these conditions on sediment transport potential (Figure 2-8). Although the longshore location of sediment transport and erosion/accretion peaks remains the same, the magnitude is different. For this case, the higher percent occurrence of right-directed transport creates a greater increase in shoreline erosion potential to the right of the borrow site.

Table 2-1. Redistributed wave energy for idealized borrow site case illustrating the effects of a case dominated by one wave direction.

	Wave Direction (center of wave spectra)				
	-30°	-15°	0°	15°	30°
% Occurrence	20	35	20	15	10

Because actual wave conditions at a borrow site are dominated by a single direction, the asymmetric distribution of sediment transport potential and associated shoreline change are characteristic of conditions expected at borrow sites along the U.S. East Coast. This asymmetric distribution naturally causes impacts associated with sand mining to be focused along a shoreline area that generally is not directly landward of the borrow site. By performing a wave refraction and longshore sediment transport analysis based on site conditions, the anticipated influence of a specific borrow site on local littoral processes can be determined. In this manner, the numerical modeling process can be used to optimize borrow site excavation strategies, or alternatively, to determine acceptable volume limits of a sand mining operation.

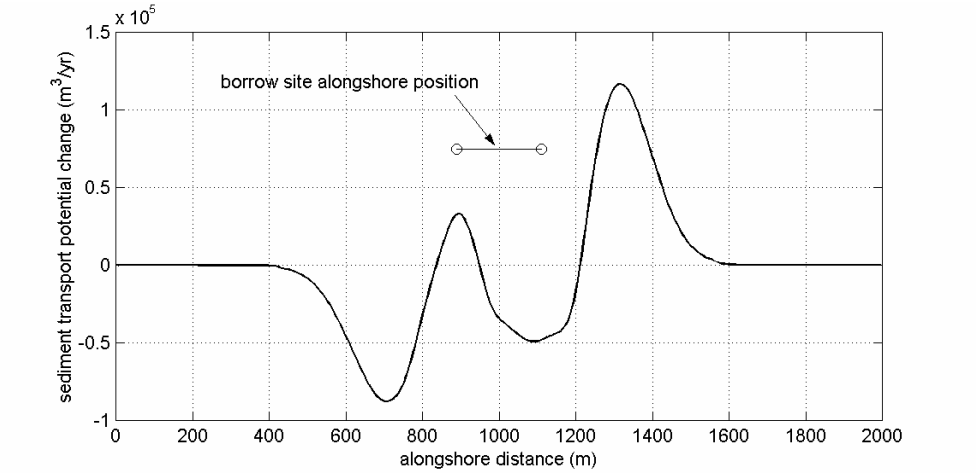

Figure 2-8. Change in computed longshore sediment transport potential based on alternate distribution of wave percent occurrences.

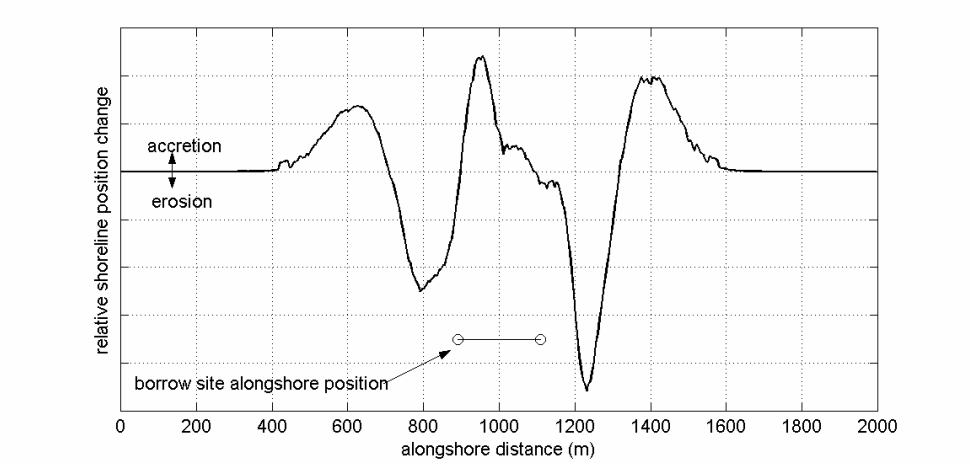

Figure 2-9. Computed cross-shore change in shoreline position based on modifications to longshore sediment transport potential using alternate distribution of wave percent occurrences.

2.4 SIGNIFICANCE OF BORROW SITE IMPACTS

As part of any offshore sand mining effort, the MMS requires an evaluation of potential environmental impacts associated with alterations to nearshore wave patterns. To determine potential impacts associated with borrow site excavation, the influence of borrow site geometry on local wave refraction patterns is evaluated; however, standard methodologies have not been developed to determine the significance of changes associated with these impacts. Because large natural spatial and temporal variability exists within the wave climate at a particular site, determination of physical impacts associated with sand mining must consider the influence of process variability. A method based on historical wave climate variability, as well as local wave climate changes directly attributable to borrow site excavation, has been applied to determine appropriate criteria for assessing impact significance.

Over the past two decades, advances in numerical wave modeling techniques have resulted in more accurate analysis of nearshore wave field transformation. In addition, the availability of long-term wave data and hindcast information has improved the boundary conditions necessary to drive these models. Although future work likely will improve some of the simplifying assumptions inherent in nearshore wave models, as well as the limitations associated with wave model input data (wave and bathymetric information), available spectral wave models can be used to develop reliable estimates of impacts associated with offshore sand mining. As shown in Appendix A, spectral wave models are reliable tools for simulating observed wave conditions affected by rapidly changing nearshore bathymetry (e.g., shoals and/or channels).

2.4.1 Available Methods for Assessing Borrow Site Impacts

One standard method for evaluating borrow site impacts is to perform wave and sediment transport modeling. Information developed from these modeling efforts is used to quantify potential physical environmental impacts associated with dredging activities. Although changes in sediment transport potential and wave energy flux associated with re-direction of wave energy generally are used as impact evaluation criteria, determining acceptable limits for these impacts is not a straightforward process. First, the wave climate in the vicinity of a borrow site exhibits temporal and spatial variations. Therefore, appropriate evaluation criteria must include the temporal and spatial variability of the wave field. Additionally, although past methodologies have described alterations to the wave field at various locations (e.g., immediately landward of the borrow site, at a fixed reference line, at the breaker line), the shoreline or breaker line appears to be most appropriate. In this manner, calculated longshore transport rates (based on wave modeling results) can be validated through evaluation of observed shoreline change.

Over the past few years, the MMS has employed two techniques for determining the significance of borrow site impacts associated with re-direction of nearshore wave energy. In 1999, a statistical approach was developed to evaluate changes in wave climate at a pre-defined offshore reference line, as well as a method for determining the statistical significance of impacts (Basco, 1999). For borrow site studies in Alabama (Byrnes et al., 1999) and New Jersey (Byrnes et al., 2000), the significance of borrow site impacts were evaluated relative to potential error estimates associated with wave height and direction (Rosati and Kraus, 1991). It was concluded that if percent changes in longshore sediment transport caused by offshore sand mining were less than the percent error determined for wave height/direction estimates, the impact was insignificant.

Although the above methodologies provide reasonable quantitative estimates of impact significance associated with offshore sand mining, the present study introduces a new methodology for evaluating borrow site impacts that incorporates temporal and spatial changes in the wave field. All three approaches use site-specific wave analyses as the basis for quantifying potential alterations to nearshore processes; however, the method presented in this study incorporates natural, site-specific variability in wave climate as a basis for determining impact significance. The following sections describe each method in more detail and provide the benefits and shortcomings, associated with each evaluation technique.

2.4.2 Reference Line Statistical Approach

To quantify changes in wave climate associated with sand mining, Basco (1999) applied a linear wave transformation model that incorporated a unit offshore wave height at the model domain boundary. Fifty (50) direction/period band combinations represented the wave climate for the chosen site (Sandbridge Shoal, Virginia), each with appropriate wave height multiplier coefficients. A reference line was defined landward of the borrow area, but seaward of the breaker line for 99% of the incident waves. In this manner, the use of a unit offshore wave height could be justified. The frequency-weighted wave energy variation along the reference line was then calculated to determine the percent change in total wave energy between existing and post-dredging conditions.

Following the development of wave energy changes, basic statistical theory was used to test for the significance of impacts. The method tests the difference in median wave energy between existing and post-dredging conditions at a 95% confidence level for various locations along the reference line. The length of the reference line is chosen to ensure that no wave energy change exists at either end. The evaluation criterion imposed indicates that if more than 50% of the total reference line is negatively impacted under the 95% confidence level, the borrow site should be rejected (Basco, 1999). Figure 2-10 illustrates the application of this significance criterion for Sandbridge Shoal, where borrow site dredging creates significant wave energy change for 12.6 km of the 20-km-long reference line (63% of the reference line length). Therefore, the report concluded "that since over 50 percent of the reference line experiences a wave climate modification, long-term dredging of sand from Sandbridge Shoal will significantly alter the wave climate." Based on this assumption, it was suggested that the site should be rejected.

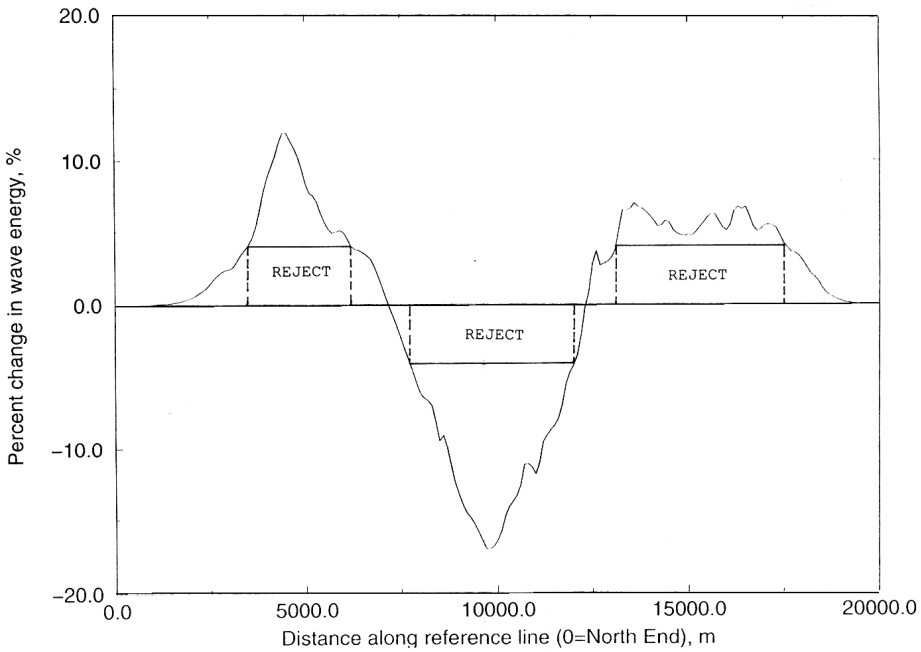

Figure 2-10. Percent change in wave energy showing regions of acceptance and rejection of the null-hypothesis using ≥ 4.0 percent as the cut-off value (from Basco, 1999).

Although the above methodology incorporates a significant numerical wave modeling effort and is statistically rigorous, it requires use of arbitrary limits. For example, rejection of the borrow site was based on greater than 50% of the reference line experiencing significant wave climate modifications. The 50% modification criteria and the length of the reference line are based on the user's judgment rather than scientific principles. Although some type of acceptable limit is required to make the process useful, it should be based on similar statistical arguments as the remainder of the methodology. In addition, waves approach the coast from all directions facing the shoreline. Generally, wave modelers make the decision to limit the angle of wave approach because waves propagating nearly parallel to the shoreline generally occur infrequently and contain little wave energy. However, the selection of reference line length is heavily dependent on the modeler's choice of wave direction limits. For a relatively narrow range of wave directions, the reference line becomes shorter, and the more likely wave impacts will be determined significant for a dredging project (and *vice versa*).

2.4.3 Potential Uncertainties in Wave Information Approach

Rather than focusing on the differences between wave and/or sediment transport processes directly associated with sand mining, borrow site studies offshore Alabama (Byrnes et al., 1999) and New Jersey (Byrnes et al., 2000) determined the significance of borrow site impacts from the error associated with wave height and direction estimates (Rosati and Kraus, 1991). Using conservative estimates for error associated with wave height and wave direction of 10%, sediment transport rates can be predicted to within ±35%. These errors can be attributed to the inherent uncertainties in the WIS data set (wave height and directional accuracy) used to develop offshore wave conditions. The ±35% value is significantly higher than the impacts associated with any of the borrow sites evaluated for either Alabama or New Jersey.

Analysis of uncertainties related to longshore sediment transport estimates indicates that variations in transport associated with potential dredging scenarios are an order of magnitude lower than the uncertainty associated with sediment transport calculations. Therefore, the potential effects of offshore sand mining on longshore sand transport rates was determined to be insignificant for the scenarios tested in Alabama and New Jersey. Alternative scenarios were not expected to pose any greater effects unless the quantity of sand dredged from a site was substantially larger than potential dredged volumes selected for these studies.

One advantage of using the above methodology for estimating dredging impact significance is the direct incorporation of sediment transport calculations, rather than the indirect impact associated with changes in wave energy. Impacts to sediment transport patterns can be readily observed, since modifications to longshore transport patterns will alter the shoreline position along a sandy coast. Basco (1999) indicated that calculation of sediment transport quantities and volumes would improve the utility of the reference line statistical approach as a management tool. However, incorporation of shoreline change and sediment transport calculations was left to future work.

Although use of wave information uncertainties offers a simple tool to address borrow site impacts, it also contains inherent shortcomings. The method indicates the potential errors in wave information; however, it does not evaluate any potential errors directly associated with the wave models. If the same offshore wave field is defined for

existing and post-dredging conditions, the error associated with wave measurements (direction and wave height) may not be the best indicator of borrow site impacts.

2.4.4 Spatial and Temporal Variations in Wave Climate Approach

To directly assess the impacts to coastal processes associated with sand mining, a new approach has been developed that considers spatial (longshore) and temporal aspects of the local wave climate. This method uses a similar wave modeling effort as those needed for the previous two methods; however, modeling of waves is performed for the entire 20-year WIS record and five 4-year blocks of the WIS record. In this manner, temporal variations in the wave climate are considered relative to average annual conditions. From these wave model runs, sediment transport potential curves are derived for average annual conditions (based on the full 20-year WIS record) and each 4-year period (based on the five 4-year wave records parsed from the full record). Applying this information, the average and standard deviation in calculated longshore sediment transport potential is determined every 200 m along the shoreline.

Assuming the temporal component of sediment transport potential is normally distributed, the suggested criterion for accepting or rejecting a potential borrow site is based on a range of one standard deviation about the mean. If any portion of the sediment transport potential curve associated with a sand mining project exceeds one standard deviation of the natural temporal variability (which incorporates 2/3 of the variability) in sediment transport potential, the site would be rejected. Although using the standard deviation of each 4-year period is more conservative than using a 1-year period, the methodology provides a useful indication of sediment transport variability relative to the natural system.

An example of this method is shown in Figure 2-11, where the alterations in wave climate caused by dredging of Sandbridge Shoal, Virginia were determined to be insignificant relative to natural variability. The maximum variation in sediment transport potential caused by dredging Sandbridge Shoal was determined to be approximately 25,000 m^3 per year, where the standard deviation of the natural sediment transport variability was approximately 100,000 m^3/yr. Due to the orientation of the shoreline and the relatively high natural variability in wave climate, an observer on the shoreline is unlikely to notice alterations in shoreline position caused by borrow site dredging. For this reason, sites with large natural variation in wave climate and associated sediment transport potential would be allowed to have larger impacts associated with an offshore sand mining project.

As a management tool for the MMS, this methodology provides several advantages over methods previously employed to assess the significance of borrow site impacts. The primary advantages include:

1. Observed long-term shoreline change is compared with computed longshore change in sediment transport potential. Close comparison between these two curves indicates that longshore sediment transport potential calculations are appropriate for assessing long-term natural change. Therefore, this methodology has a model-independent component (observed shoreline change) used to ground truth the model results.

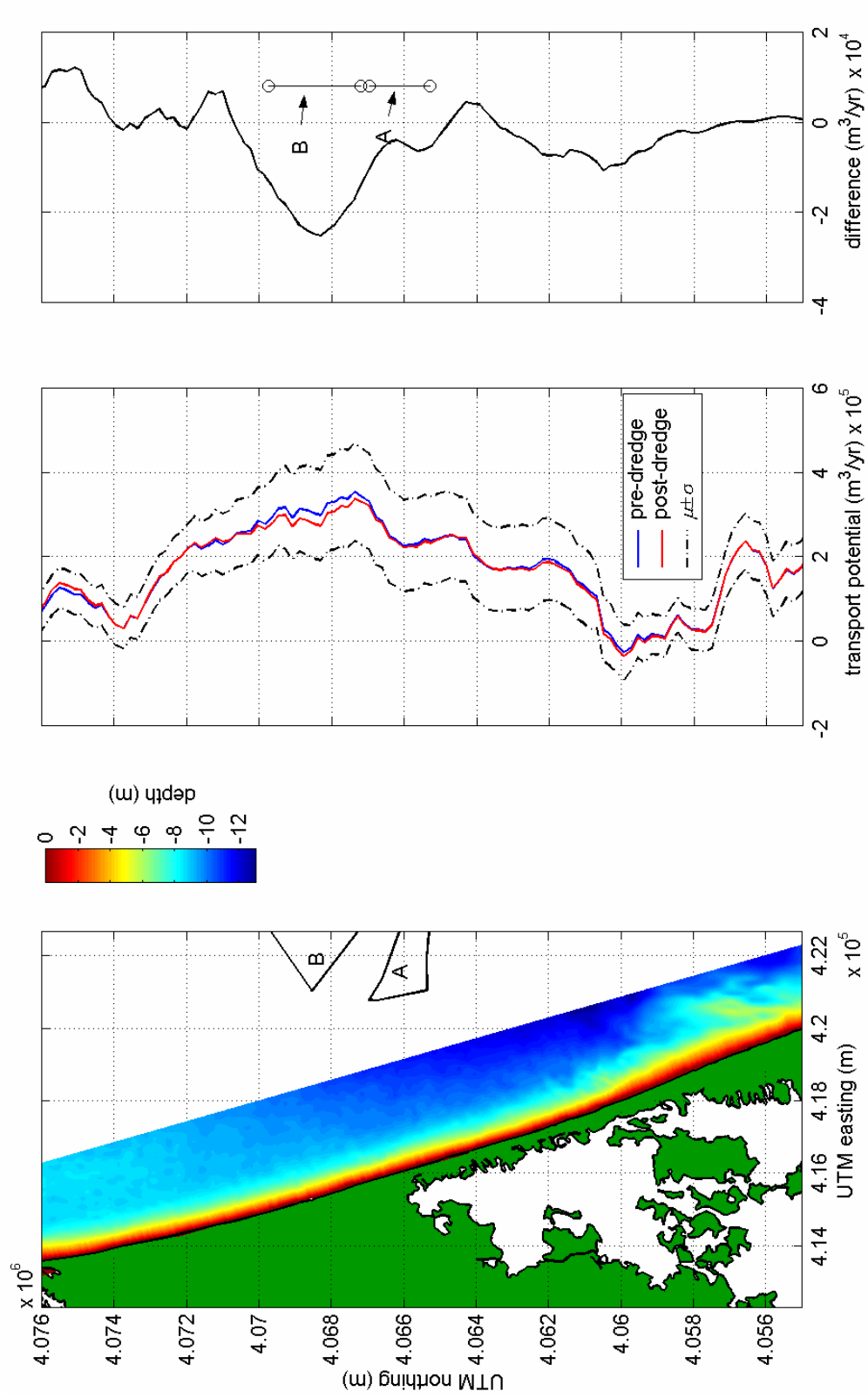

Figure 2-11. Example of results for spatial/temporal variability method for determining significance of borrow site dredging impacts. Plots of modeled net transport potential and post-dredging change in transport for borrow sites located offshore Sandbridge, Virginia. Middle plot shows dredging significance criterion envelope ($\pm\sigma$) determined for this shoreline. The left plot of the shoreline is given for reference.

2. The method is directly related to sediment transport potential and associated shoreline change. Therefore, impacts associated with borrow site excavation can be directly related to their potential influence on observed coastal processes (annualized variability in shoreline position).
3. Site-specific temporal variability in wave climate and sediment transport potential is calculated as part of the methodology. For sites that show little natural variability in inter-annual wave climate, allowable coastal processes impacts associated with borrow site dredging similarly would be limited, and *vice versa*. In this manner, the inter-annual temporal component of the natural wave climate is a major component in the determination of impact significance.
4. Similar to methodologies incorporated in previous MMS studies, the longshore spatial distribution of borrow site impacts is considered. However, the allowable limit of longshore sediment transport variability is computed from the temporal component of the analysis. Therefore, the final results of this analysis provide a spatially-varying envelope of allowable impacts in addition to the modeled impacts directly associated with borrow site excavation. The methodology accounts for spatial and temporal variability in wave climate, as well as providing a defensible means of assessing significance of impacts relative to site-specific conditions.

3.0 MODELING APPROACH AND APPLICATIONS

Excavation of a nearshore borrow site can affect wave heights and the direction of wave propagation. The existence of an offshore trough or trench can cause waves to refract toward the shallower edges of the borrow site. This alteration to the wave field by a borrow area may change local sediment transport rates along the shoreline, where some areas may experience a reduction in longshore transport and other areas may show an increase. In this study, four offshore areas were investigated to determine the potential cumulative physical impacts associated with dredging selected borrow sites to their maximum design limits, including 1) southern New Jersey, in the vicinity of Townsends and Corsons Inlets; 2) southeastern Virginia, in the vicinity of Sandbridge Shoal off Virginia Beach; 3) the North Carolina Outer Banks, between Duck, NC and Oregon Inlet; and 4) Canaveral Shoals, southeast of Cape Canaveral, Florida. Wave transformation modeling and sediment transport potential calculations were performed for existing and post-dredging bathymetric conditions. Comparison of computations for existing and post-dredging conditions are used to illustrate the relative maximum impact of borrow site excavation on wave-induced coastal processes.

3.1 ANALYSIS APPROACH

Sediment transport rates along a coastline are dependent on the wave climate in that area. For this study, nearshore wave heights and directions along the shoreline landward of proposed borrow sites were estimated using the spectral wave model STWAVE to simulate the propagation of offshore waves to the shoreline. Offshore wave conditions used as input for wave modeling were derived from two sources: 1) measured spectral wave data from offshore data buoys, and 2) hindcast simulation time series data, available from the U.S. Army Corps of Engineer's (USACE) Wave Information Study (WIS).

3.1.1 Wave Modeling

Developed by the U.S. Army Engineer Waterways Experiment Station (WES), STWAVE v2.0 is a steady state, spectral wave transformation model (Smith, et al., 1999). Two-dimensional (frequency and direction vs. energy) spectra are used as input to the model. STWAVE is able to simulate wave refraction and shoaling induced by changes in bathymetry and by wave interactions with currents. The model includes a wave breaking model based on water depth and wave steepness. Model output includes significant wave height (H_s), peak period (T_p), and mean wave direction ($\overline{\theta}$).

STWAVE is an efficient program that requires moderate computing resources to run well. The model is implemented using a finite-difference scheme on a regular Cartesian grid (grid increments in the *x* and *y* directions are equal). During a model run, the solution is computed starting from the offshore open boundary and is marched in the onshore direction in a single pass of the model domain. This is why STWAVE can propagate waves only in directions within the $\pm 87.5°$ half plane. A benefit of using this single pass approach is that it uses minimal computer memory, because the only memory-resident spectral data are for two grid columns. As such, the changing wave spectra across each grid column are in turn computed using the information solely from the previous grid column.

STWAVE is based on a form of the wave action balance equation. For this model the wave action density spectrum, which includes the effects of currents, is conserved along wave rays. In the absence of currents, wave rays, correspond to wave orthogonals, and the action density spectrum is equivalent to the wave energy density spectrum. A diagram showing the relationship between wave orthogonal, wave ray and current directions is shown in Figure 3-1. The governing equation of wave transformation, using the action balance spectrum, in tensor notation is written as (Smith et al., 1999)

$$\left(C_{ga}\right)_i \frac{\partial}{\partial x_i} \frac{C_a C_{ga} \cos(\mu - \alpha) E}{\omega_r} = \sum \frac{S}{\omega_r} \tag{3.1}$$

where

$E = E(f, \theta)$ wave energy density spectrum,
S = energy source and sink terms (e.g., whitecapping, breaking, wind input),
α = wave orthogonal direction,
μ = wave ray direction (direction of energy propagation),
ω_r = relative angular frequency ($2\pi f_r$),
C_a, C_{ga} = absolute wave celerity and group celerity, respectively.

The breaking model in STWAVE is based on a form of the Miche criterion as discussed by Battjes and Janssen (1978). It sets a maximum limit on the zero-moment wave height (H_{mo}), the wave height based on the distribution of energy in the wave spectrum. The formulation of this model is

$$H_{mo(max)} = 0.1L \tanh(kd) \tag{3.2}$$

where L is the wavelength, k is the wave number ($k = 2\pi/L$), and d is the depth at the point where the breaking limit is being evaluated. This equation is used with a simpler

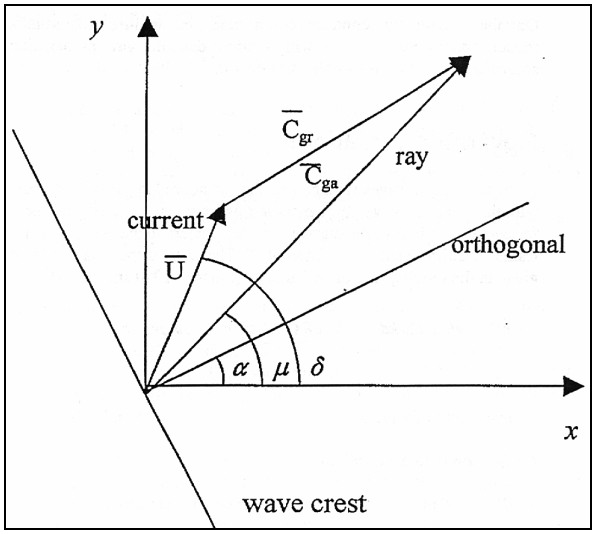

Figure 3-1. Diagram of wave and current vectors used in STWAVE (from Smith et al., 1999). Subscript *a* denotes values in the *absolute* frame of reference, and subscript *r* denotes values in the *relative* frame of reference (with currents).

breaking model, as applied in earlier versions of STWAVE, where the maximum H_{mo} wave height is always expressed as a constant ratio of water depth

$$H_{mo(max)} = 0.64\, d\ . \tag{3.3}$$

An advantage to using Equation 3.2 versus Equation 3.3 is that it accounts for increased wave breaking resulting from wave steepening caused by wave-current interactions. Once model wave heights exceed $H_{mo(max)}$, STWAVE uses a simple method to reduce the energy spectrum, essentially to set the value of $H_{mo} = H_{mo(max)}$. Energy at each frequency and direction is reduced by the same percentage. As a result, non-linear transfers of energy to high frequencies during breaking are not included in STWAVE.

3.1.2 Input Spectra Development

Spectral wave input for STWAVE model runs performed for each of the study areas was developed using WIS hindcast data for borrow sites offshore southern New Jersey, Dam Neck/Sandbridge Beach (Virginia), Dare County North Carolina, and Cape Canaveral (Florida). Alternatively, for the Sandbridge Shoal area offshore southeastern Virginia, a five-year spectral wave data record from an offshore buoy maintained by the National Data Buoy Center (NDBC) was used to develop model input spectra. The NDBC data were used over available WIS data for southeastern Virginia because the buoy record was adequately long and represented actual long-term wave conditions in the area. In general, buoy data are the preferred source of wave information for modeling, because they represent actual offshore measurements rather than hindcast information derived from large-scale models. However, very few sites along the U. S. East Coast have wave measurement records of sufficient length to justify their use as a source of long-term information.

3.1.2.1 Southern New Jersey WIS Data

Wave data for model runs offshore southern New Jersey and Townsends Inlet were developed using WIS station AU2067 (Figure 3-2), located approximately 22 km southeast of Townsends Inlet, NJ. This WIS record covers a 20-year period from January 1976 to December 1995 and includes 58,440 wave events (eight records per day). Two wave roses showing percent occurrence of different wave conditions are shown in Figure 3-3. The first rose shows how wave height distribution varies with direction. The majority of waves (68%) in the WIS record fall within the compass sector between 90° and 180°. The dominant wave direction is east-northeast, from which 28% of waves in the record propagate. The mean height for all waves in the record is 1.2 m, with a standard deviation of 0.7 m. The mean height for waves along the dominant wave direction is 1.1 m, with a standard deviation of 0.8 m. The second rose in Figure 3-3 shows the distribution of peak periods in the record. The mean peak periods for the entire record is 7.7 sec, and 26% of the simulated waves in the record have peak period greater than 9 sec.

3.1.2.2 Southeastern Virginia WIS Data

Wave input conditions for model simulations offshore southern Virginia were developed using WIS hindcast data from station AU2058 (Figure 3-2), The data from this station were used to develop the dredging significance envelope discussed in the following sections. Station AU2058 is located approximately 17 km offshore Sandbridge, VA. The hindcast data for this site cover the same 20-year period as the New Jersey

record from WIS station AU2067. The two wave roses showing wave height and wave period distributions for station AU2058 are presented in Figure 3-4. Most waves in this record (68%) are from the 60 degree compass sector around due east. The prevailing wave direction is east-northeast, where 38% of the wave of the WIS record propagate. The mean wave height for all waves in the record is 1.2 m, with a standard deviation of 0.7 m. From the prevailing east-northeast compass sector, the mean wave height is 1.3 m, with a standard deviation of 0.9 m. The second plot of Figure 3-4 shows the distribution of wave periods in the WIS record. The mean period for the entire hindcast record is 8.7 sec.

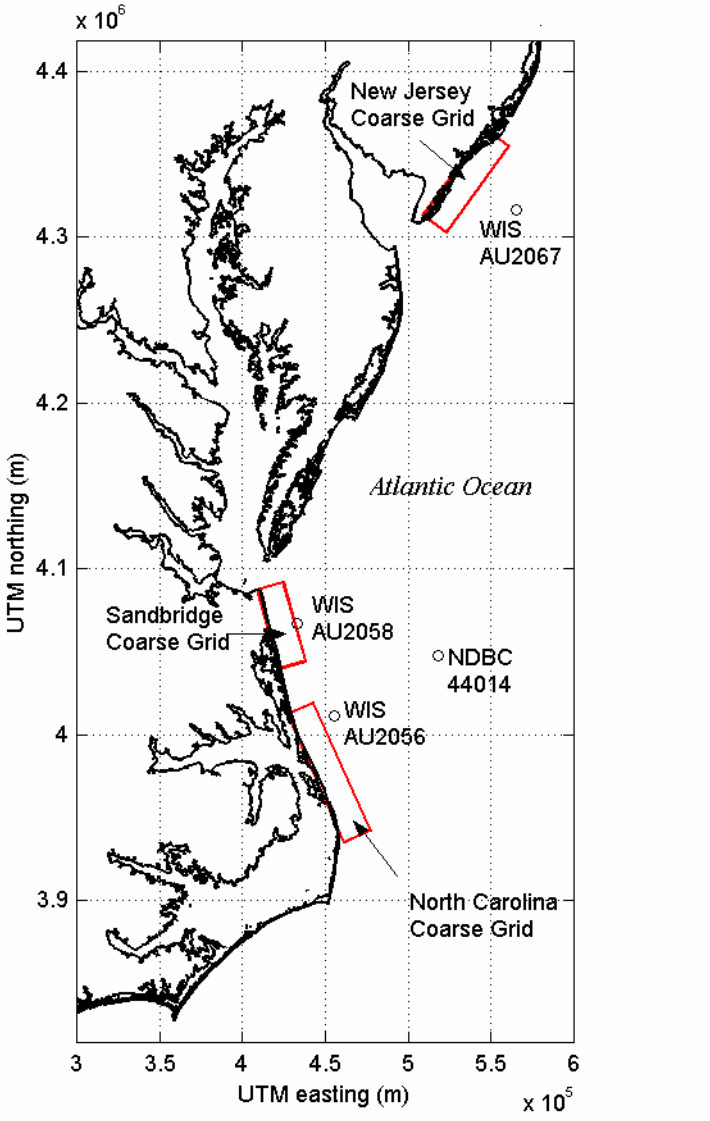

Figure 3-2. Shoreline from New Jersey to North Carolina with coarse grid limits and wave input data stations used to determine dredging impacts from offshore sand mining.

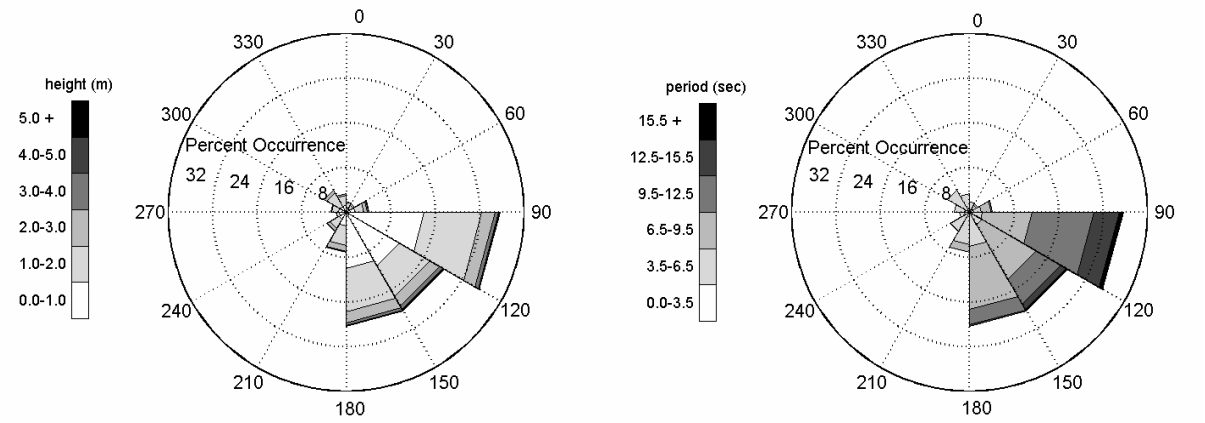

Figure 3-3. Wave height and period for hindcast data from WIS station AU2067 (offshore New Jersey) for the 20-year period between January 1976 and December 1995. Direction indicates from where waves were traveling, relative to true north. Radial length of gray tone segments indicates percent occurrence for each range of wave heights and periods. Combined length of segments in each sector indicate percent occurrence of all waves from that direction.

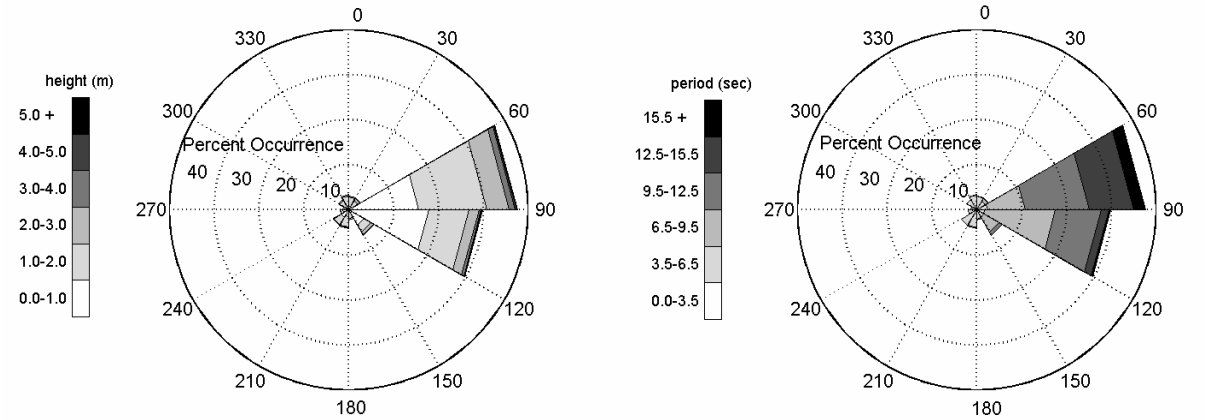

Figure 3-4. Wave height and period for hindcast data from WIS station AU2058 (offshore southern Virginia) for the 20-year period between January 1976 and December 1995. Direction indicates from where waves were traveling, relative to true north. Radial length of gray tone segments indicates percent occurrence for each range of wave heights and periods. Combined length of segments in each sector indicate percent occurrence of all waves from that direction.

3.1.2.3 North Carolina WIS Data

Wave input conditions for simulations offshore North Carolina were developed using hindcast data from WIS station AU2056 (Figure 3-2), which is located approximately 33 km northeast of Bodie Island, NC. This WIS record covers a 20-year period from January 1976 to December 1995. Two wave roses showing percent occurrence of different wave conditions are shown in Figure 3-5. The first rose shows how wave height distribution varies with direction. The majority of waves (52%) in the WIS record fall within the compass sector between 60° and 120°. The dominant wave direction is east-northeast, from which 32% of waves in the record propagate. The mean height for all waves in the record is 1.5 m, with a standard deviation of 0.9 m. The mean height for waves along the dominant wave direction is 1.2 m, with a standard

deviation of 0.8 m. The second rose in Figure 3-5 shows the distribution of peak periods in the record. A significant number of wave events (32%) have peak periods greater than 9 sec, and the mean peak period for the entire record is 8.3 sec.

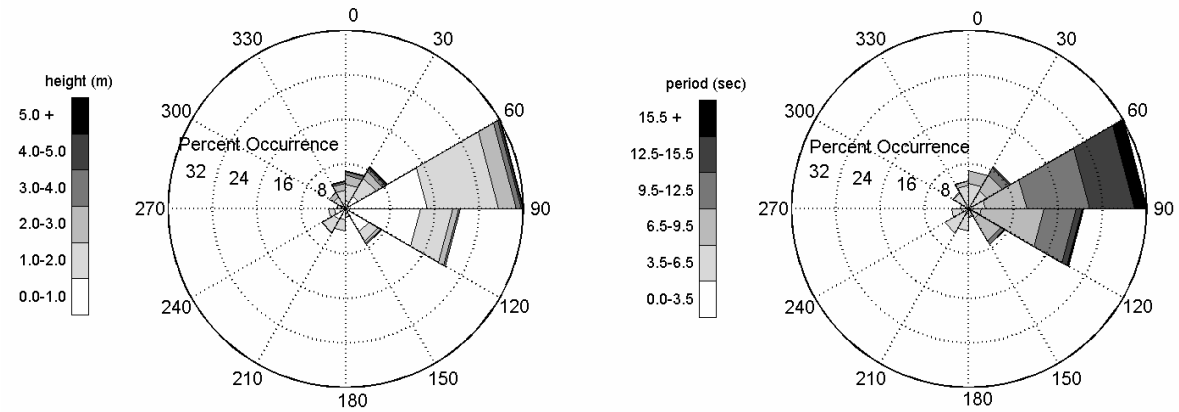

Figure 3-5. Wave height and period for hindcast data from WIS station AU2056 (offshore North Carolina) for the 20-year period between January 1976 and December 1995. Direction indicates from where waves were traveling, relative to true north. Radial length of gray tone segments indicates percent occurrence for each range of wave heights and periods. Combined length of segments in each sector indicate percent occurrence of all waves from that direction.

3.1.2.4 Cape Canaveral WIS Data

Wave data for model runs offshore Cape Canaveral were developed using WIS station AU2019 (Figure 3-6), which is located approximately 29 km east-northeast of Cape Canaveral, FL. Two wave roses showing percent occurrence of different wave conditions are shown in Figure 3-7. The first rose shows how wave height distribution varies with direction. Most waves (90%) in the record fall within the compass sector between 30° and 120°, and the greatest percentage of waves (43%) are from the east-northeast sector. The mean height for all waves in the record is 1.3 m, with a standard deviation of 0.7 m. The mean height for waves along the dominant wave direction is 1.4 m, with a standard deviation of 0.7 m. The second rose in Figure 3-7 shows the distribution of peak periods in the record. The mean peak period for the entire record is 9.3 sec, and 38% of simulated waves in the record have peak periods greater than 9 sec.

3.1.2.5 Development of Model Spectra from WIS Data

In order to reduce the offshore extent of the computational grid used by STWAVE, the program WAVETRAN was used to propagate WIS waves closer to shore. For the New Jersey WIS data, waves were propagated from a depth of 18 m at the station to a depth of 17 m, the mean depth along the offshore open boundary of the coarse model grid. For the North Carolina data, waves were propagated from a 37-m water depth to a 24-m water depth approximately 17 km offshore (the seaward limit of the STWAVE grid). For the Cape Canaveral model grid, WIS data were propagated from a depth of 27 m to 24-m water depth at the offshore boundary of the coarse model grid. WAVETRAN is part of the Shoreline Modeling System (SMS) developed by WES (Jensen, 1983).

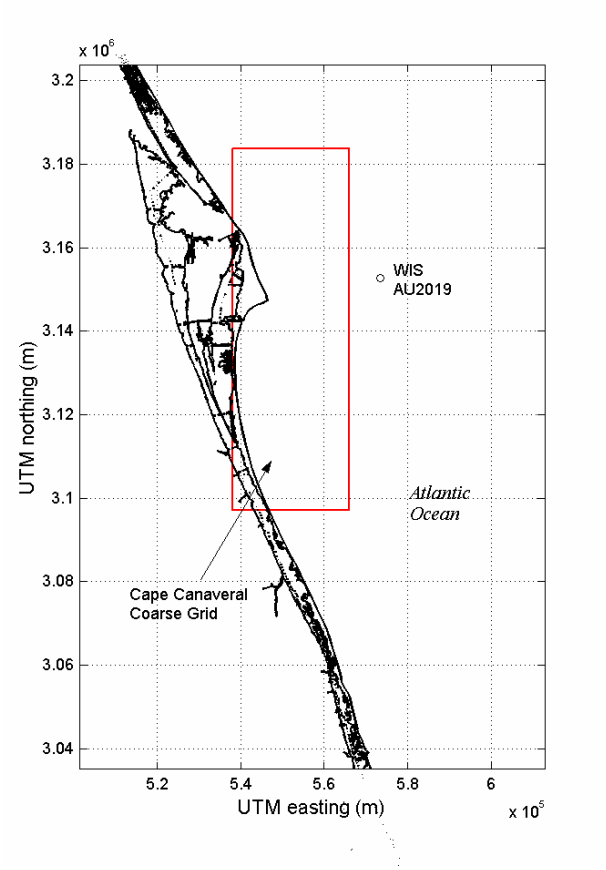

Figure 3-6. East Florida shoreline at Cape Canaveral with coarse grid limits and wave input data station used to determine dredging impacts from offshore sand mining.

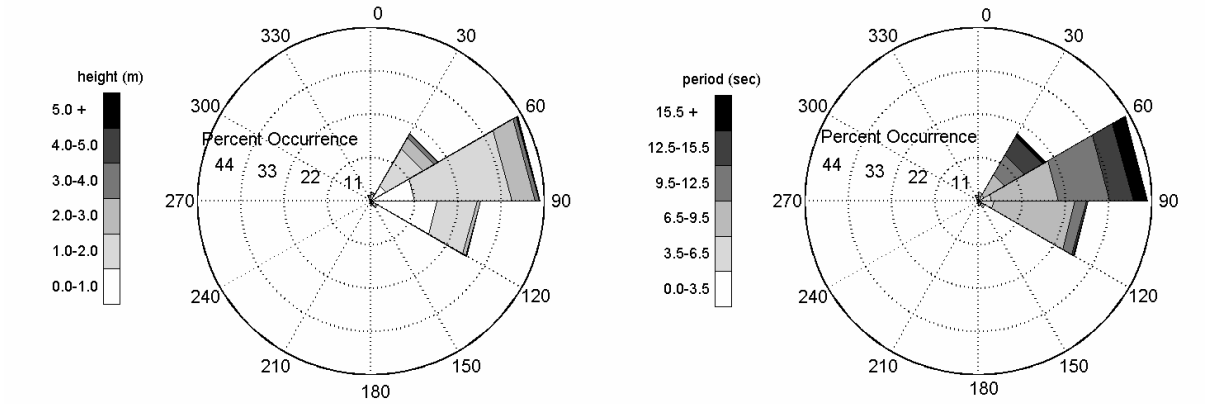

Figure 3-7. Wave height and period for hindcast data from WIS station AU2019 (Cape Canaveral) for the 20-year period between January 1976 and December 1995. Direction indicates from where waves were traveling, relative to true north. Radial length of gray tone segments indicates percent occurrence for each range of wave heights and periods. Combined length of segments in each sector indicate percent occurrence of all waves from that direction.

STWAVE input spectra were developed using a second numerical routine which re-creates a two dimensional spectrum for each individual wave condition in the transformed WIS record. This program computes the frequency and directional spread of a wave energy spectrum based on significant wave parameters (i.e., wave height, peak period, and peak direction), as well as wind speed. This method is described by Goda (1985). The frequency spectrum $S(f)$ is computed using the relationship

$$S(f) = 0.257 H_{1/3}^2 T_{1/3} (T_{1/3} f)^{-5} \exp\left[-1.03 (T_{1/3} f)^{-4}\right] \tag{3.4}$$

known as the Bretschneider-Mitsuyasu spectrum, where $H_{1/3}$ is the significant wave height, f is the discrete frequency where $S(f)$ is evaluated, and $T_{1/3}$ is the significant period, estimated from the peak wave frequency (f_p) by

$$T_{1/3} = 1/(1.05 f_p). \tag{3.5}$$

To compute the two-dimensional energy spectrum, a directional spreading function $G(f,\theta)$ must be applied to the frequency spectrum such that

$$S(f,\theta) = S(f) G(f,\theta). \tag{3.6}$$

In this method, the directional spreading function is computed using the relationship

$$G(f,\theta) = G_o \cos^{2s}\left(\frac{\theta}{2}\right) \tag{3.7}$$

where s is a spreading parameter related to wind speed and frequency, θ is the azimuth angle relative to the principle direction of wave travel, and G_o is a constant dependent upon θ and s. The spreading parameter s is evaluated using the expression

$$s = \begin{cases} s_{\max} \cdot (f / f_p)^5 : f \le f_p \\ s_{\max} \cdot (f / f_p)^{-2.5} : f \ge f_p \end{cases} \tag{3.8}$$

where $s_{\max} = 11.5(2\pi f_p U / g)^{-2.5}$. Wind speed U is therefore used to control the directional spread of the spectrum by increasing the directional spread with increasing wind speed. Finally, the constant G_o is computed by evaluating the integral

$$G_o = \left[\int_{\theta_{\min}}^{\theta_{\max}} \cos^{2s}\left(\frac{\theta}{2}\right) d\theta \right]^{-1}. \tag{3.9}$$

The result is a wave energy spectrum that is based on parameters from the WIS record, where spectral energy is distributed based on wave peak frequency and wind speed. An example of a two-dimensional spectrum generated by this method is presented in Figure 3-8.

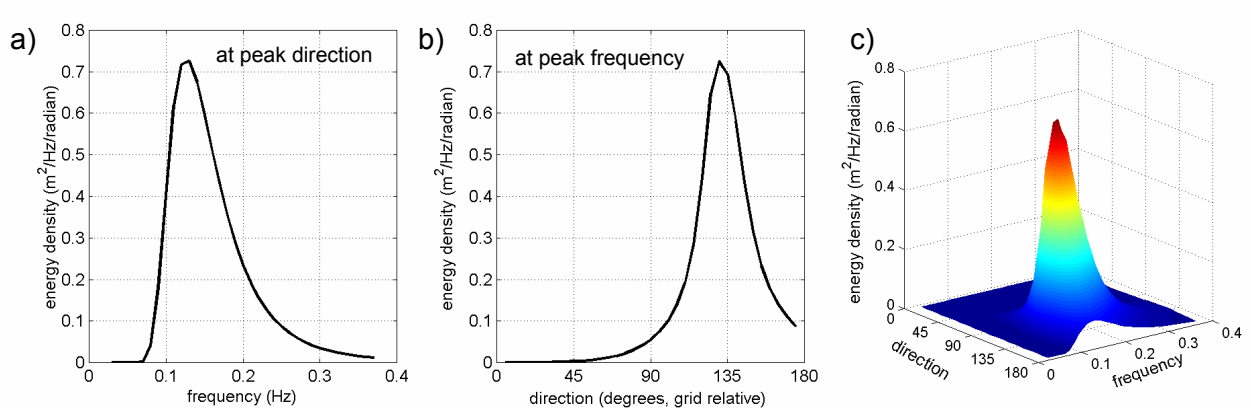

Figure 3-8. Example of STWAVE input spectrum developed using WIS 20-year hindcast data and Goda method of computing frequency and direction spectrum. Plots show a) frequency distribution of energy at peak direction, b) directional distribution of energy at peak frequency, and c) surface plot of two-dimensional energy spectrum. Example is model case 5 (H_{mo} = 0.9 m, θ_{mean} = 130° grid relative).

After re-creating a two-dimensional spectrum from the parameters given in the WIS record, each individual spectrum is sorted (or binned) by peak direction and peak period. Wave spectra computed from wave parameters that fall within the limits of individual direction and period bins are added together, and a mean spectrum for all waves in each bin is computed based on the total number of wave events in the bin. In total, six direction bins and two period bins were used to characterize wave data. From the 12 total bins, conditions used in the model runs of STWAVE were selected based on the percent occurrence and percent energy for conditions in each bin. Selected conditions have a percent occurrence greater than two percent and contain more than 2.5 percent of the energy of the entire wave record. For the four modeled regions conditions selected for model runs are shown in Tables 3-1 through 3-4, with significant parameters for each input spectrum.

Table 3-1. Significant parameters of input wave spectra used for existing and post-dredging STWAVE model runs for New Jersey model grid.

	STWAVE model input condition	% occurrence	H_{mo} wave height	Mean wave period, T_p	Peak wave direction, θ_p	Peak wave direction, θ_p	Direction bin
			m	sec	deg. true north	grid relative	grid relative
Period Band 1	1	6.4	1.4	7.7	61	25	0-30
	2	14.1	1.1	8.3	86	50	30-60
	3	14.1	1.2	7.7	111	75	60-90
	4	17.7	1.2	7.1	131	95	90-120
	5	6.6	0.8	5.0	161	125	120-150
Period Band 2	6	5.1	1.3	11.1	61	25	0-30
	7	14.5	1.6	11.1	81	45	30-60
	8	5.8	2.0	10.0	96	60	60-90

Table 3-2. Significant parameters of input wave spectra used for existing and post-dredging STWAVE model runs for Virginia model grid.

	STWAVE model input condition	% occurrence	H_{mo} wave height	Mean wave period, T_p	Peak wave direction, θ_p	Peak wave direction, θ_p	Direction bin
			m	sec	deg. true north	grid relative	grid relative
Period Band 1	1	5.4	0.5	4.4	14	30	0-30
	2	9.1	1.3	5.3	34	50	30-60
	3	8.2	1.4	6.7	64	80	60-90
	4	10.4	1.1	7.3	89	105	90-120
	5	14.2	0.9	7.6	114	130	120-150
	6	3.4	1.0	4.8	139	155	150-180
Period Band 2	7	9.7	1.5	11.8	74	90	60-90
	8	18.8	1.5	12.9	79	95	90-120
	9	6.1	1.3	11.2	109	125	120-150

Table 3-3. Significant parameters of input wave spectra used for existing and post-dredging STWAVE model runs for North Carolina model grid.

	STWAVE model input condition	% occurrence	H_{mo} wave height	Mean wave period, T_p	Peak wave direction, θ_p	Peak wave direction, θ_p	Direction bin
			m	sec	deg. true north	grid relative	grid relative
Period Band 1	1	9.4	1.1	5.1	1	25	0-30
	2	8.1	1.9	6.0	21	45	30-60
	3	8.7	1.5	6.7	56	80	60-90
	4	10.1	1.2	7.4	86	110	90-120
	5	16.3	0.9	7.6	106	130	120-150
	6	8.1	0.6	4.6	131	155	150-180
Period Band 2	7	6.0	1.9	11.5	66	90	60-90
	8	19.2	1.5	12.8	71	95	90-120
	9	6.3	1.3	11.3	101	125	120-150

Table 3-4. Significant parameters of input wave spectra used for existing and post-dredging STWAVE model runs for Florida model grid.

	STWAVE model input condition	% occurrence	H_{mo} wave height	Mean wave period, T_p	Peak wave direction, θ_p	Peak wave direction, θ_p	Direction bin
			m	sec	deg. true north	grid relative	grid relative
Period Band 1	1	8.2	1.7	7.7	55	55	30-60
	2	20.8	1.4	7.7	80	80	60-90
	3	24.6	1.0	7.7	100	100	90-120
	4	2.3	1.5	6.3	130	130	120-150
Period Band 2	5	6.5	1.7	12.5	60	60	30-60
	6	28.5	1.6	14.3	65	65	60-90
	7	3.4	1.5	11.1	100	100	90-120

3.1.2.6 Spectral Development from Wave Buoy Data

An alternate method was used to develop wave spectra for the southeastern Virginia region model. In addition to the WIS record, which was used in model runs to determine the dredging significance envelope, spectral input for the Sandbridge Shoal STWAVE model was developed using NDBC spectral wave buoy data (NDBC buoy 44014), which is located approximately 95 km east of False Cape, VA. The buoy record was used for model runs executed to determine post-dredging impacts caused by the two sites offshore Sandbridge, VA. This buoy record covers a 5-year period from January 1996 to December 2000. Wave roses showing the percent occurrence of different wave conditions is illustrated in Figure 3-9.

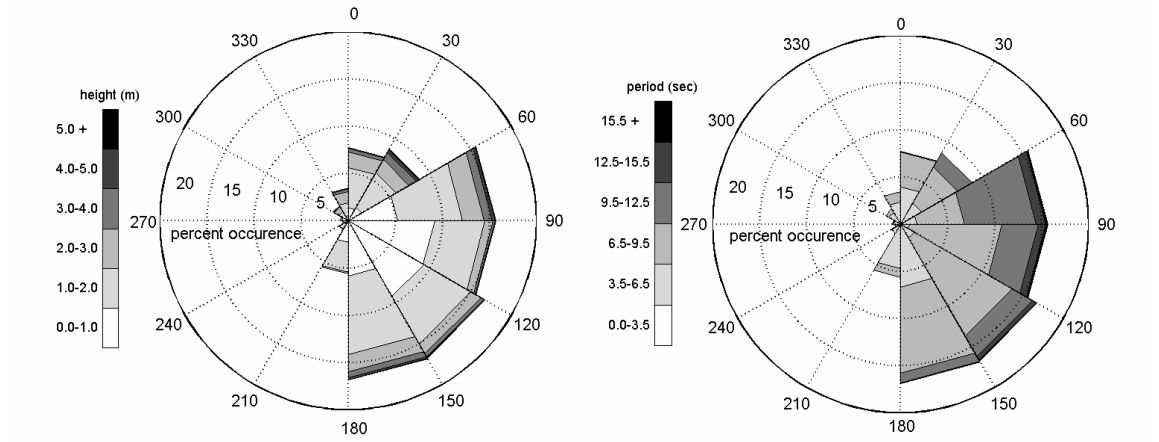

Figure 3-9. Wave height and wave period roses for data recorded by NDBC buoy 44014 (offshore Virginia Beach) for the 5-year period between January 1996 and December 2000. Direction indicates the direction waves were propagating from relative to true north. Radial length of gray tone segments indicates percent occurrence of each range of wave condition (height or period). Combined length of segments in each sector indicates percent occurrence of all waves from that direction.

The first rose shows how wave height distribution varies with direction. The majority of waves (69%) in the buoy record fall within the broad compass sector between

60° and 180°. The dominant wave direction is south-southeast, where 18% of waves in the record propagate. The mean significant wave height for all conditions in the record is 1.4 m, with a standard deviation of 0.9 m. The second rose in Figure 3-8 shows the distribution of peak periods in the record. A significant number of wave events (22%) have peak period greater than 10 sec, and the mean dominant periods for the entire record is 7.9 sec.

In order to reduce the offshore extent of the computational grid used by STWAVE, a computer program was developed to propagate buoy spectra, from 47.5-m water depth at the buoy to 16.6-m water depth approximately 15 km offshore (the seaward limit of the coarse STWAVE grid). The method employed to refract buoy spectra also was used in WIS Phase III (Jensen, 1983). This method is based on the conservation of energy along wave rays and Snell's law. For monochromatic waves, assuming straight and parallel bottom contours, shallow water wave height after shoaling and refraction is expressed as the product of the offshore wave height H_0 with the shoaling and refraction coefficients (K_s and K_r respectively):

$$H = H_0 K_s K_r \tag{3.10}$$

where the shoaling coefficient is determined using the group velocity of offshore (C_{g0}) and shallow water (C_g) wave conditions, expressed as $K_s=(C_{g0}/C_g)^{0.5}$, and the refraction coefficient is determined using the approach angle of the incident offshore wave θ_0 and the angle of the refracted shallow water wave θ, expressed as $K_r=(\cos\theta_0/\cos\theta)^{0.5}$. In terms of energy for a wave spectrum, the total energy of the refracted spectrum can be expressed in terms of the initial two-dimensional (f frequency, and θ direction) energy spectrum $E(f, \theta)$ (Jensen, 1983),

$$E_t = \int_0^{\infty}\int_0^{2\pi} E(f,\theta)\frac{(cc_g)_0}{(cc_g)}\left|\frac{\partial\theta}{\partial\theta_0}\right| d\theta df \tag{3.11}$$

where the term

$$\frac{(cc_g)_0}{(cc_g)}\left|\frac{\partial\theta}{\partial\theta_0}\right| \tag{3.12}$$

is essentially the combined refraction and shoaling coefficients. Therefore, Equation 3.11 is applied to individual spectral components, using Snell's law to determine $\partial\theta/\partial\theta_0$ for each direction bin in the spectrum. Finally, the shallow water wave angle of the refracted component is determined using Snell's law directly, $\theta(f, d, \theta_0)=\sin^{-1}(c/c_0\sin\theta_0)$.

Before transforming buoy spectra to the offshore limit of the computational grid, an additional numerical routine was used to sort the spectral data for each individual wave record in the transformed buoy data. Each wave record was sorted by peak direction and peak period. Wave spectral components computed from wave parameters that fall within the limits of individual direction and period bins are summed, and a two-dimensional (frequency and direction) mean spectrum for all waves in each bin is computed based on the total number of wave events in the bin. In total, a matrix of six direction bins *versus* two period bins were used to characterize the wave data. From the 12 total bins, conditions used in the STWAVE model runs were selected based on

percent occurrence and energy content of conditions in each bin. The 11 conditions selected for model runs are shown in Table 3-5, with significant parameters for each input spectrum.

Table 3-5. Significant parameters for input wave spectra used for existing and post-dredging STWAVE model runs for offshore southeastern Virginia sites.

	STWAVE model input condition	% occurrence	H_{mo} wave height	Peak wave period, T_p	Peak wave direction, θ_p	Peak wave direction, θ_p	Direction bin
			m	sec	deg. true north	grid relative	grid relative
Period Band 1	1	7.2	1.6	7.7	359	15	0-30
	2	7.7	1.6	8.3	34	50	30-60
	3	8.1	1.4	9.1	54	70	60-90
	4	10.1	1.1	8.3	104	120	90-120
	5	13.2	1.1	8.3	119	135	120-150
	6	15.2	1.2	8.3	149	165	150-180
Period Band 2	7	2.0	2.8	11.1	39	55	30-60
	8	7.5	2.0	11.1	64	80	60-90
	9	5.2	1.6	11.1	79	95	90-120
	10	3.4	1.8	10.0	134	150	120-150
	11	1.2	2.4	10.0	144	160	150-180

3.1.3 Grid Development

Along with input spectra, bathymetry grids were developed for existing and post-dredging scenarios. Plots of coarse and fine-nested grids for modeled regions are shown in Figures 3-10 through 3-17. For each of the four modeled areas, two coarse grids were developed that have the same geographical coverage and differ only by modifications to bathymetry in the borrow area. The maximum cumulative dredged volumes and mean depths for the modeled borrow sites for each region are shown in Table 3-6. The National Ocean Service (NOS) was the primary source of bathymetric data used to create the grids (NOS, 1998). However, these data were supplemented by other sources of data when needed (i.e., digitized NOAA chart bathymetry for areas along the North Carolina shoreline), or when more recent survey data were available (i.e., recent USACE surveys of the nearshore region along Cape Canaveral, FL). Depths at the offshore open boundary of the coarse grids vary between 9.2 and 21.4 m for the southern New Jersey coarse grid, 10.5 and 24.6 m for the southeastern Virginia coarse grid, 19.0 and 31.0 m for the North Carolina grid, and 19.3 and 29.7 m for the Cape Canaveral grid.

The spatial extent of each model coarse grid is given in Table 3-7. The geographical limits of the grids were chosen based on wave conditions available for model runs. Wave conditions with relatively small angles to the shoreline require a large grid in the longshore direction so the site of interest (i.e., the borrow site and affected shoreline) does not fall within the “shadow” of lateral grid boundaries. The grids all have a node spacing of 200 m. Grid axes are rotated to match the orientation of the shoreline in the modeled area.

Fine grids also were developed for each region in order to obtain greater resolution of waves in the nearshore behind the borrow site (Figure 3-11, 3-13, 3-15, and 3-17),

particularly in the surf zone. For each region, the same fine grid was used for existing and post-dredging conditions. Alongshore and cross-shore node spacing for fine grids is 20 m for all four regions. Boundary conditions (wave spectra) at the offshore and lateral boundaries of the fine grids were extracted from coarse-grid model runs. Therefore, boundary conditions vary along the length of the open boundary of the fine grid (nested into the coarse grid model solution).

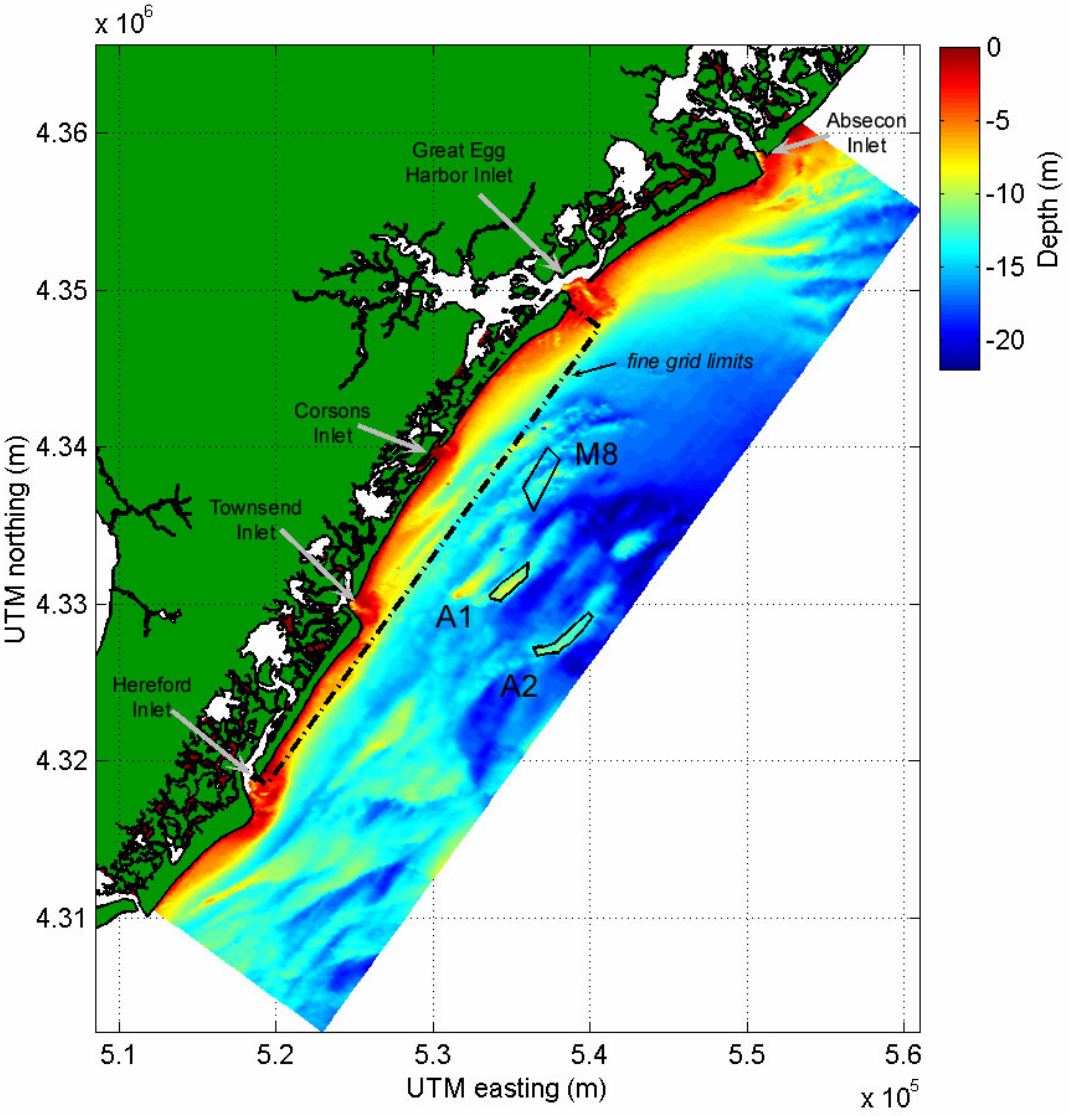

Figure 3-10. Color contour plot of coarse model grid (200 m x 200 m grid spacing) of offshore New Jersey. Depths are relative to NVGD. Borrow site locations are indicated by solid black lines, and fine grid limits are indicated by a dashed line.

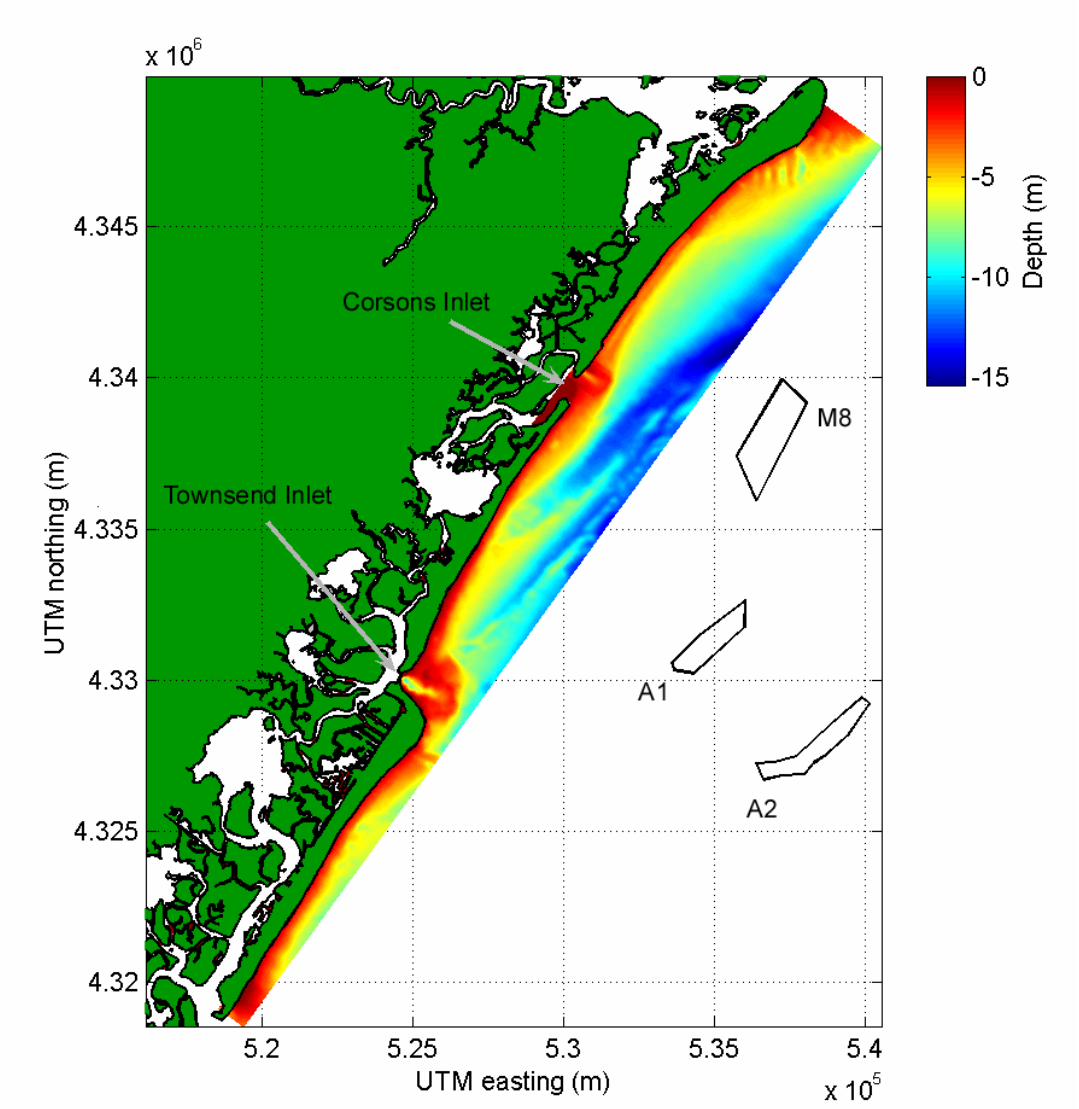

Figure 3-11. Color contour plot of the nested fine model grid (20 m x 20 m grid spacing) used with STWAVE for offshore New Jersey. Depths are relative to NVGD. Borrow site location is indicated by solid black line, and fine grid limits are indicated by dashed line.

Table 3-6. Maximum estimated cumulative borrow site excavation dimensions for the four sand resource areas.

Region	Site Designation	Volume (10^6 m^3)	Area (10^6 m^2)	Excavation Mean Depth (m)
New Jersey	A1	8.8	2.2	4.0
	A2	7.8	2.6	3.0
	M8	8.0	4.0	2.0
Virginia	A	5.3	1.8	3.0
	B	6.9	2.3	3.0
North Carolina	3 east	1.4	0.7	2.0
	3 west	2.5	0.8	3.0
Florida	2	26.0	5.0	5.2

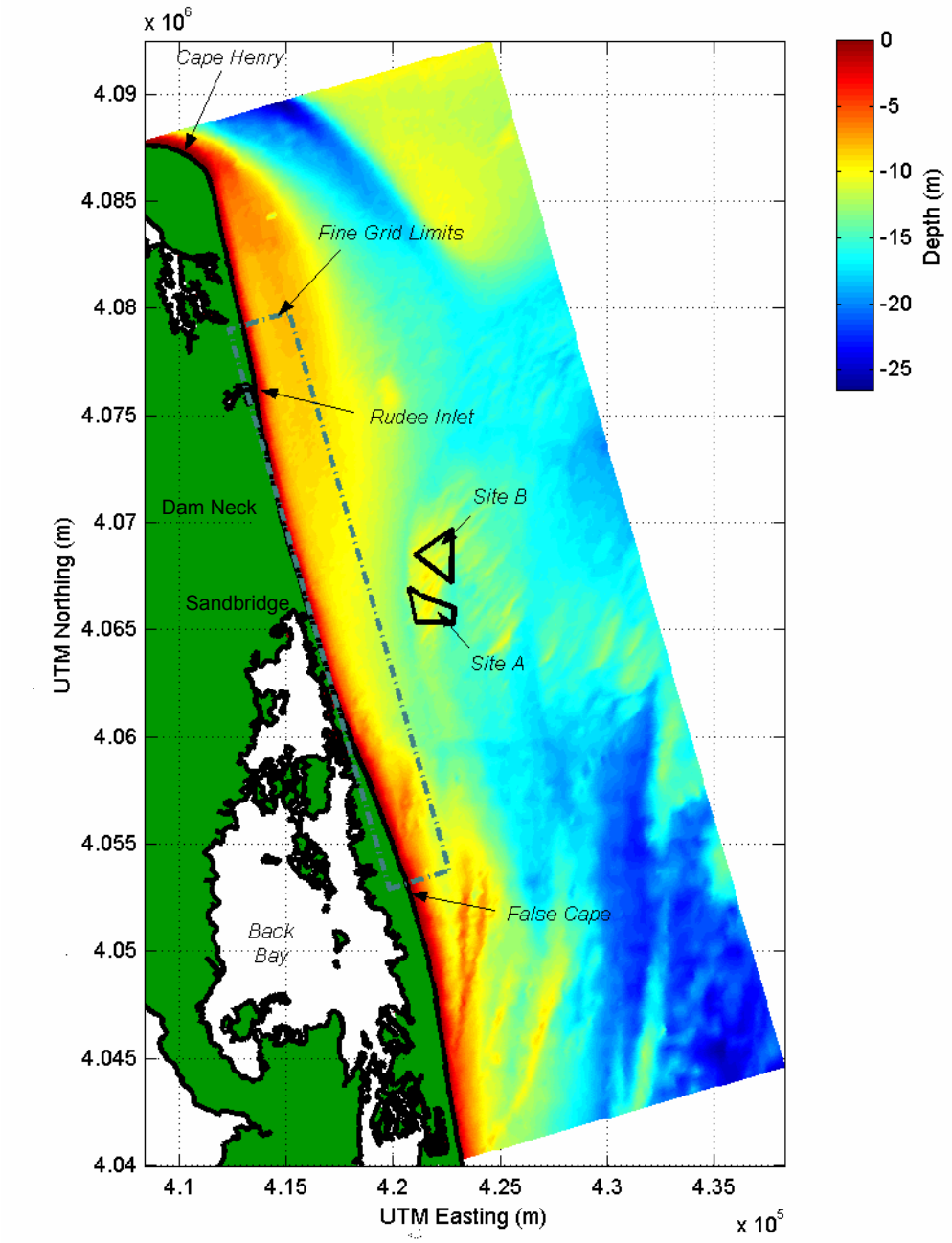

Figure 3-12. Color contour plot of coarse model grid (200 m x 200 m grid spacing) of offshore southeastern Virginia. Depths are relative to NVGD. Borrow site locations are indicated by solid black lines, and fine grid limits are indicated by a dashed line.

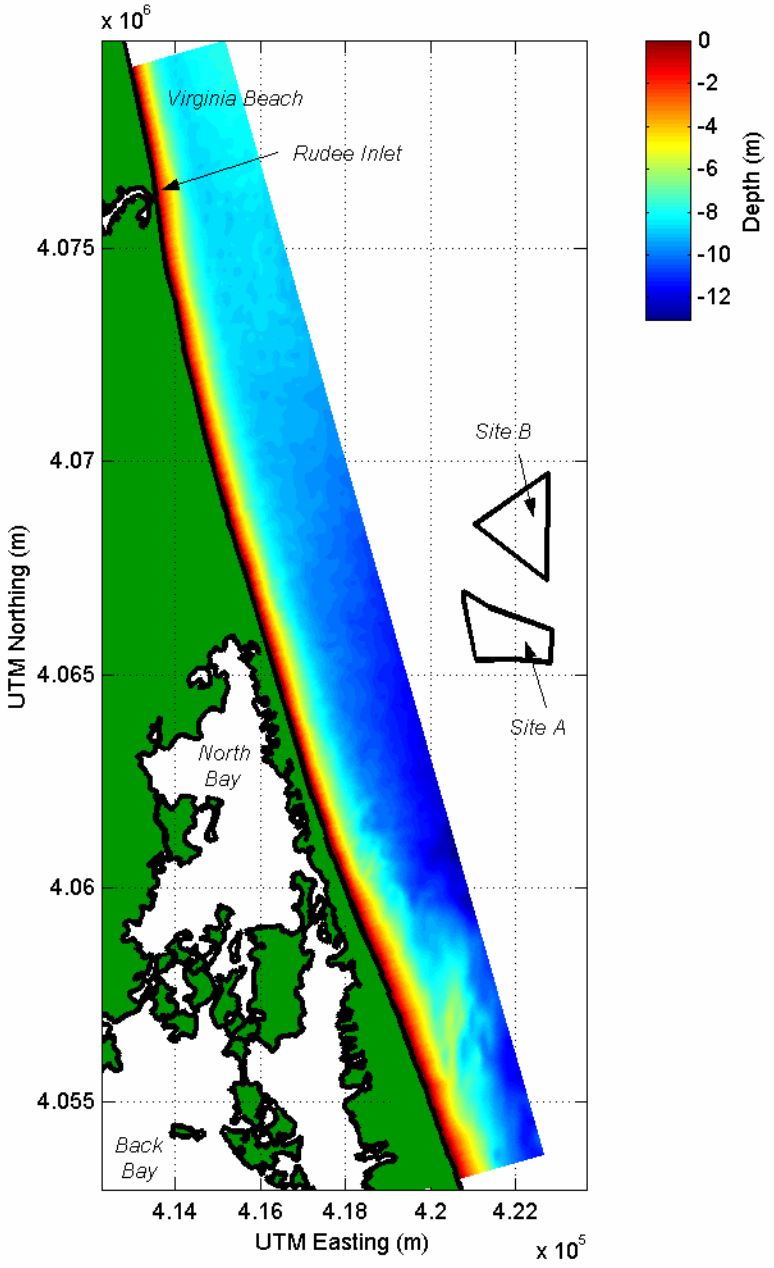

Figure 3-13. Color contour plot of the nested fine model grid (20 m x 20 m grid spacing) of offshore southern Virginia used with STWAVE. Depths are relative to NVGD. Borrow site location is indicated by solid black line, and fine grid limits are indicated by dashed line.

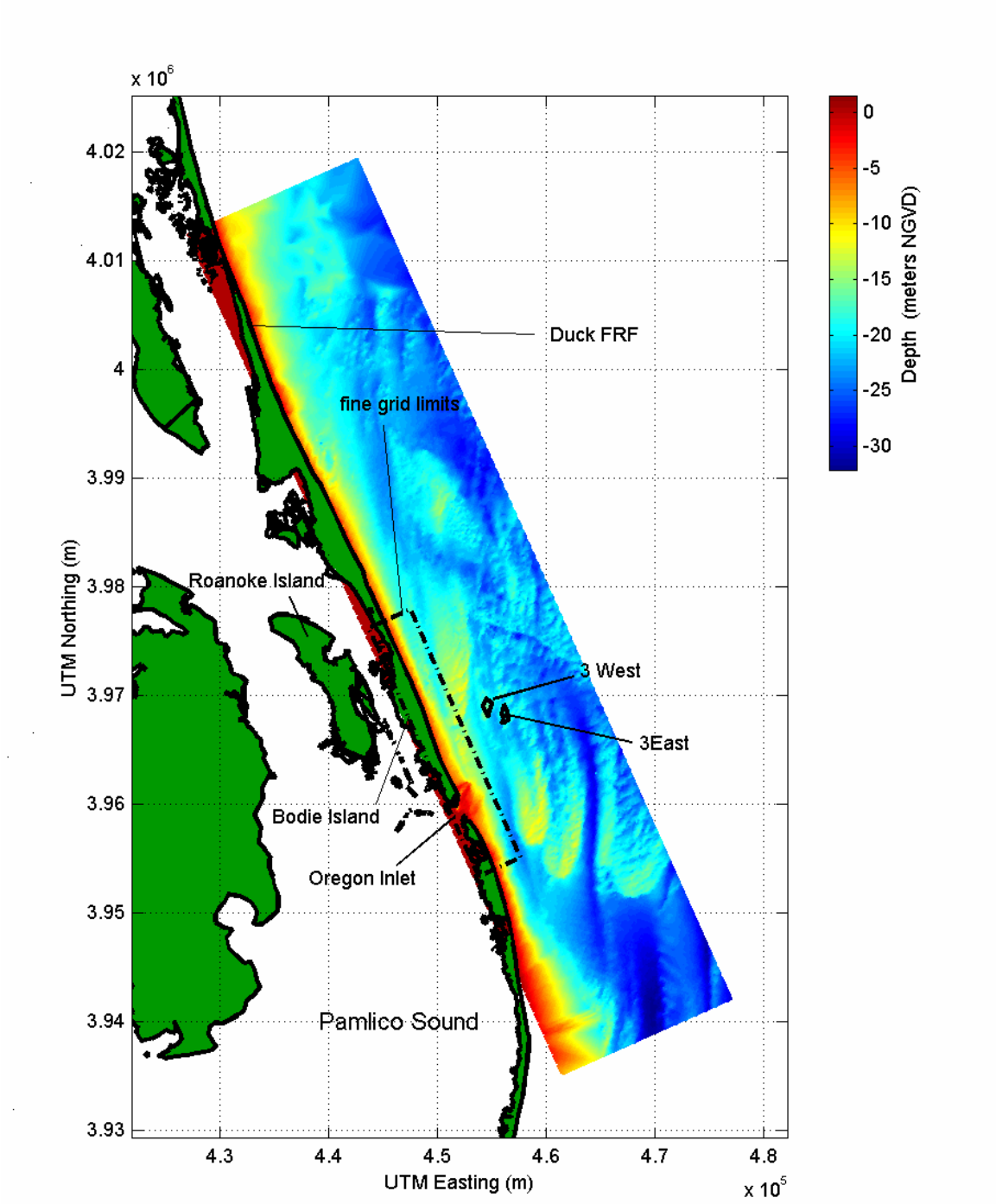

Figure 3-14. Color contour plot of coarse model grid (200 m x 200 m grid spacing) for offshore North Carolina. Depths are relative to NVGD. Borrow site locations are indicated by solid black lines, and fine grid limits are indicated by a dashed line.

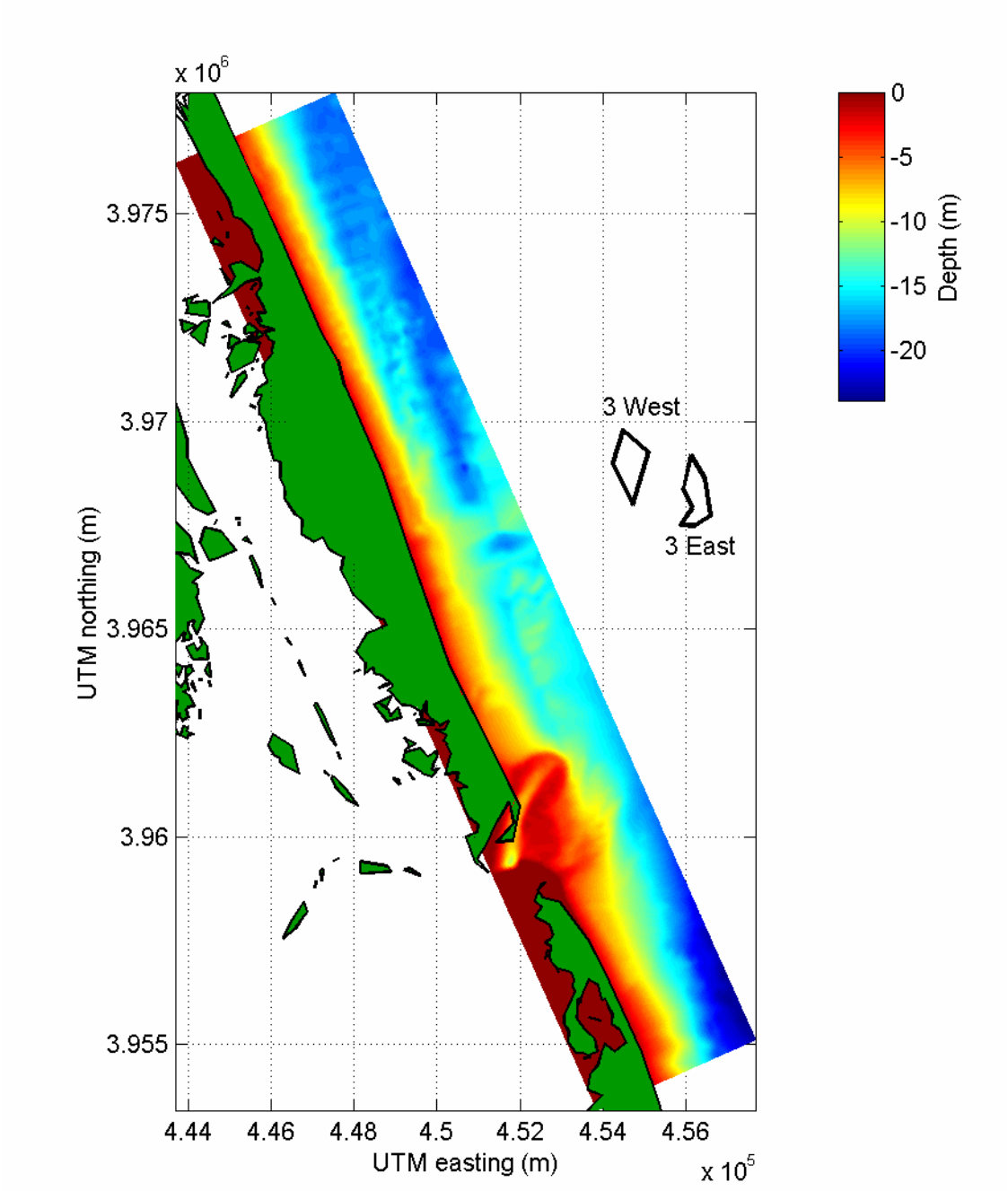

Figure 3-15. Color contour plot of the nested fine model grid (20 m x 20 m grid spacing) for offshore North Carolina. Depths are relative to NVGD. Borrow site location is indicated by solid black line, and fine grid limits are indicated by dashed line.

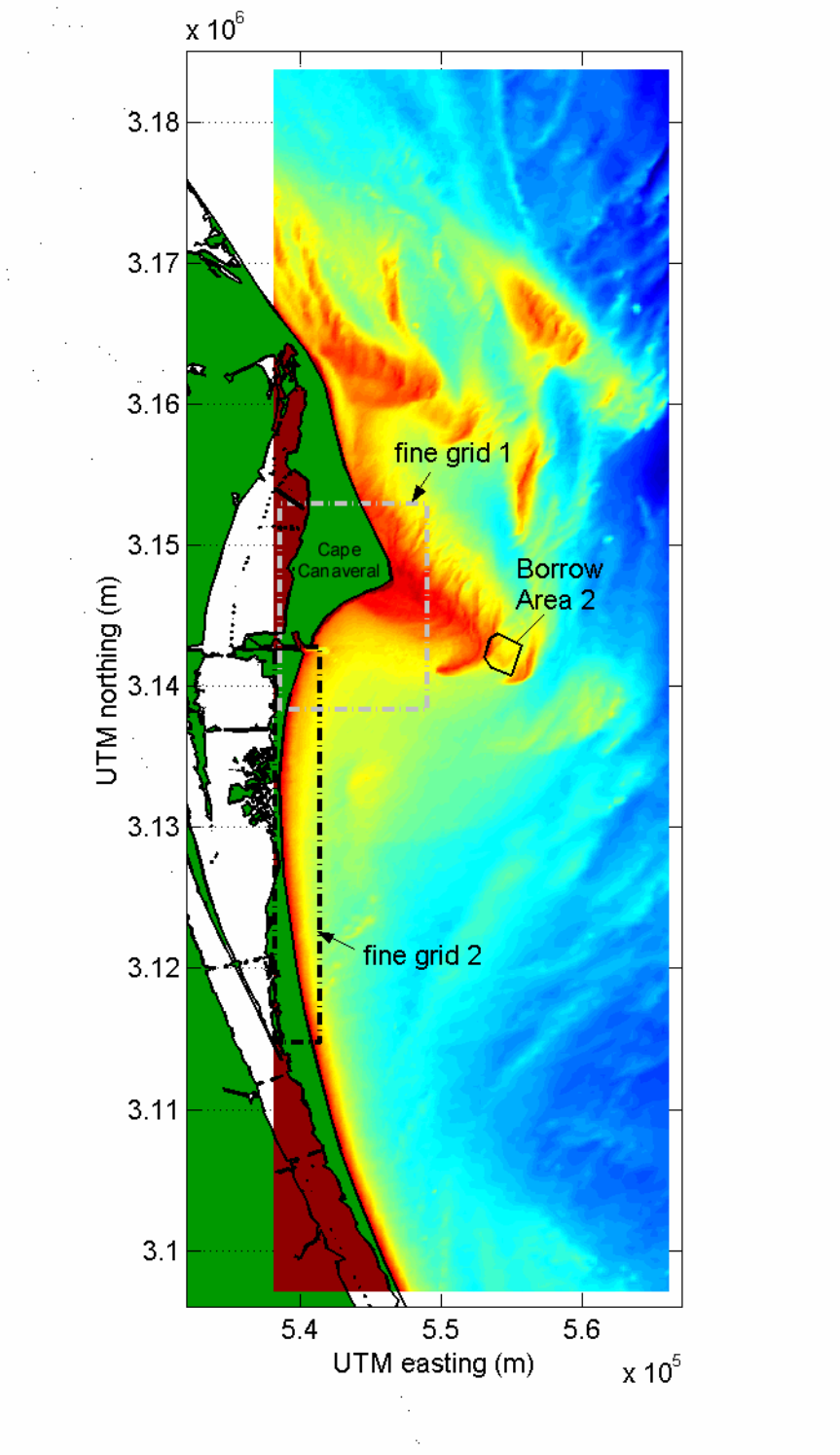

Figure 3-16. Color contour plot of coarse model grid (200 m x 200 m grid spacing) for offshore Cape Canaveral, FL. Depths are relative to NVGD. Borrow site locations are indicated by solid black lines, and fine grid limits are indicated by a dashed line.

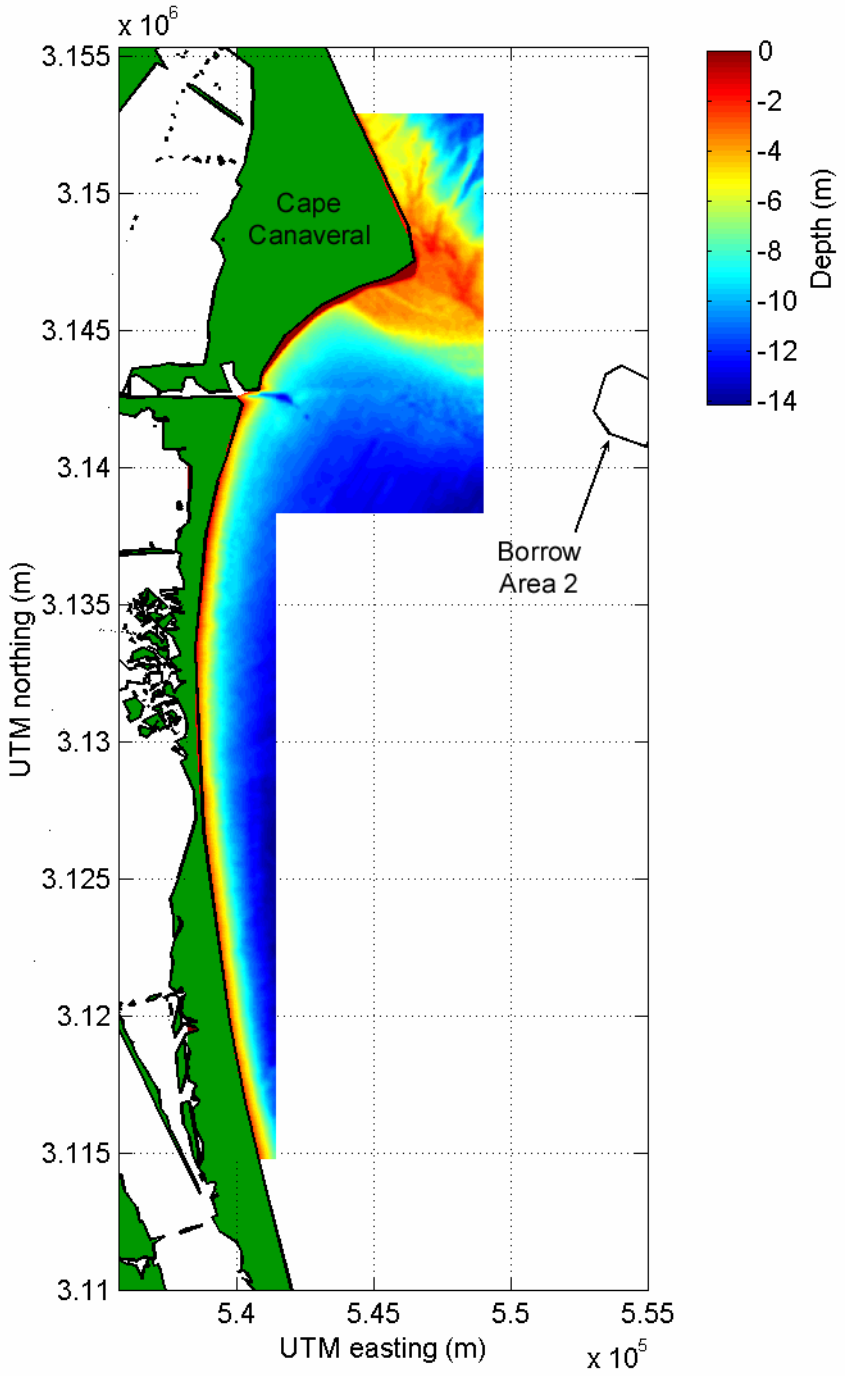

Figure 3-17. Color contour plot of the nested fine model grid (20 m x 20 m grid spacing) for offshore Cape Canaveral, FL. Depths are relative to NVGD. Borrow site location is indicated by solid black line, and fine grid limits are indicated by dashed line.

Table 3-7. Numerical grid dimensions for offshore (coarse) and nearshore (fine) grids. Dimensions are given as (cross-shore x alongshore).

Region	Coarse Grid (200 m spacing)		Fine Grid (20 m spacing)		grid angle (deg CW from north)
	nodes	distance (km)	nodes	distance (km)	
New Jersey	90 x 325	18 x 65	200 x 1800	4 x 36	36
Virginia	85 x 250	17 x 50	150 x 1360	3 x 27	-16
North Carolina	87 x 425	17 x 85	210 x 1250	4 x 25	-24
Florida	141 x 434	28 x 87	520 x 730	10 x 15	0
			160 x 1400	3 x 28	

3.1.4 Sediment Transport Potential

Initially, calculations of sediment transport potential were performed to indicate the maximum quantity of transport possible based on a sediment-rich environment. Results from spectral wave modeling formed the basis for evaluating changes in sediment transport rates along the beach. Longshore transport depends on long-term fluctuations in incident wave energy and the resulting longshore current. Therefore, annual transport rates were calculated from long-term wave statistics.

The longshore sediment transport equation employed in this study is based on the formulation presented by the U.S. Army Corps of Engineers (USACE, 1984). In general, the longshore sediment transport rate is assumed to be proportional to the longshore wave energy flux at the breaker line, which is dependent on wave height and direction. Because the transport equation was developed using data from sediment-rich environments (no hardened structures), it typically over-predicts sediment transport rates along many coasts. However, the formula provides a useful technique for comparing erosion/accretion trends along a shoreline of interest.

The volumetric longshore transport, *Q*, past a point on a shoreline is computed using the relationship:

$$Q = \frac{I}{(s-1)\rho g a'} \tag{3.13}$$

where *I* is the immersed weight longshore sediment transport rate, *s* is the specific gravity of sediment, *a*' is the void ratio of the sediment, and ρ is the density of seawater.

The immersed weight longshore sediment transport, *I*, can be computed using the CERC formula (USACE, 1984),

$$I = KP_{ls} \tag{3.14}$$

where *K* is a dimensionless coefficient and P_{ls} is the longshore energy flux factor computed using the following relationship:

$$P_{ls} = \frac{\rho g^{3/2}}{16\sqrt{\gamma}} H_{sb}^{5/2} \sin 2\alpha_b \tag{3.15}$$

where H_{sb} is the significant wave height at breaking, γ is the coefficient for the inception of wave breaking ($\gamma=H_b/h_b$), and α_b is the breaking wave angle. Generally, a value of K=0.4 is used with significant wave heights (as computed by STWAVE), or the more familiar value K=0.77 is used with RMS wave height.

For this study, an alternate method was used to compute immersed weight longshore sediment transport, as described by Kamphuis (1990). This method is a modification to the original CERC formula that adds a dependency on the median grain diameter of beach sediment and incorporates the surf similarity parameter, ξ_b, expressed as

$$\xi_b = \frac{m}{\left(H_b / L_0\right)^{0.5}} \tag{3.16}$$

where m is the bottom slope and L_o is the deep water wavelength. The complete expression of Kamphuis is given by

$$I = K^* \rho g \left(\frac{g}{2\pi}\right)^{0.75} \xi_b T^{0.5} \left(m d_{50}\right)^{-0.25} H_s^{2.5} \sin^{0.6}\left(2\theta_b\right) \tag{3.17}$$

where the coefficient K^* = 0.0013.

Sediment transport computations were based on wave information at breaking for each grid cell along the modeled coastline. The shoreline segment incorporates the influence of all changes to nearshore wave climate associated with proposed dredging activities. Computations of sediment transport rates for each wave condition were performed and then weighted by the annual percent occurrence. Sediment transport potential was computed for existing and post-dredging conditions.

3.2 MODEL RESULTS

Due to the redistribution of wave energy and alteration of wave directions resulting from offshore sand excavation, changes to longshore sediment transport patterns will occur. Depending on the net direction of local sediment transport, the influence of borrow site conditions can either increase or decrease net littoral drift. Example model cases for each of the four sites are discussed in the following subsections. Complete wave model output for the four modeled regions, showing wave heights and wave height difference plots between existing and post-dredging conditions for all modeled wave cases, are given in Appendices B through E.

3.2.1 Wave Modeling

Overall, post-dredging wave model output for the four study sites illustrates reduced wave heights landward of borrow sites and increased wave heights at the longshore limits of the borrow site. This effect is more pronounced for cases with larger wave heights and longer periods. As waves propagate across a borrow site (deeper water than the surrounding area), wave refraction bends waves away from the center of the borrow site and toward the shallower edges. The net effect is to create a shadow zone of reduced wave energy immediately landward of the borrow site and a zone of increased wave energy updrift and downdrift of the borrow site.

This shadowing effect is apparent in model results presented in Figure 3-18 for offshore southern New Jersey. In this figure, color contours represent coarse grid wave height differences between model results computed for existing and post-dredging conditions. In the immediate vicinity of the borrow site, wave heights increased by a maximum of 0.20 m at the northern and southern edges of the borrow site and decreased by a maximum of 0.19 m behind the borrow site. In Figure 3-19, fine grid model results for the same wave condition (case 7) show how waves propagate toward shore landward of proposed borrow sites. The wave shadow generated by Site M8 is most prominent. For this wave case, the maximum wave height difference between existing and post-dredging conditions is 0.27 m at the borrow site, but closer to shore within the fine grid, the maximum wave height difference is reduced to 0.06 m.

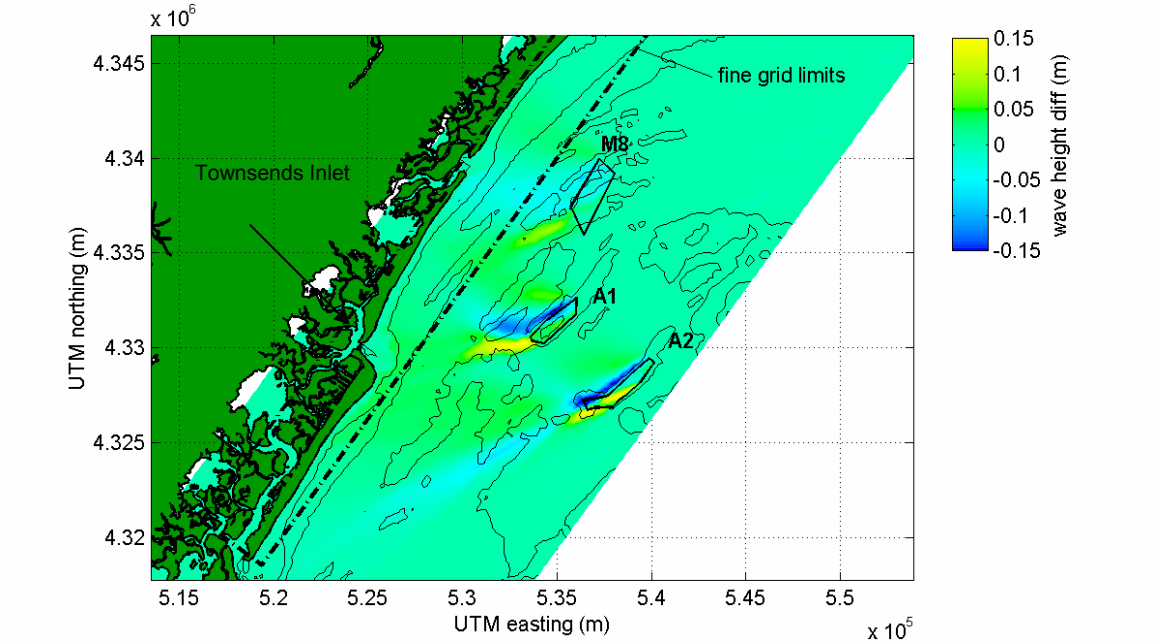

Figure 3-18. Example of coarse grid wave height difference plot between existing and post-dredging bathymetry conditions offshore Townsends Inlet, NJ. This result is for NJ wave case 7; 1.6 m wave height and 11.1 sec period.

Because these are spectral wave model results, and because different frequencies in the spectrum are refracted by varying degrees at the borrow area, the areas of increased and reduced wave height gradually diffuse as the wave field approaches shore. As a result, the extent of this energy diffusion can be considerably longer than the borrow area. For this particular example, the length of shoreline affected by Site M8 is approximately three times greater than the alongshore dimension of the borrow site.

Although borrow sites that are further offshore impact a longer length of shoreline, the actual magnitude of impact is lower because the affected wave field has had a greater distance over which to diffuse energy. This is illustrated in a comparison of wave transformation impacts for borrow sites M8 and A1 in Figure 3-18. Borrow Site A1 causes a greater local difference in wave heights primarily because it has a greater excavated depth. However, because the borrow site is further offshore, wave height change from existing to post-dredging conditions at the shoreline is less than the changes that are caused by borrow Site M8, as seen in Figure 3-19.

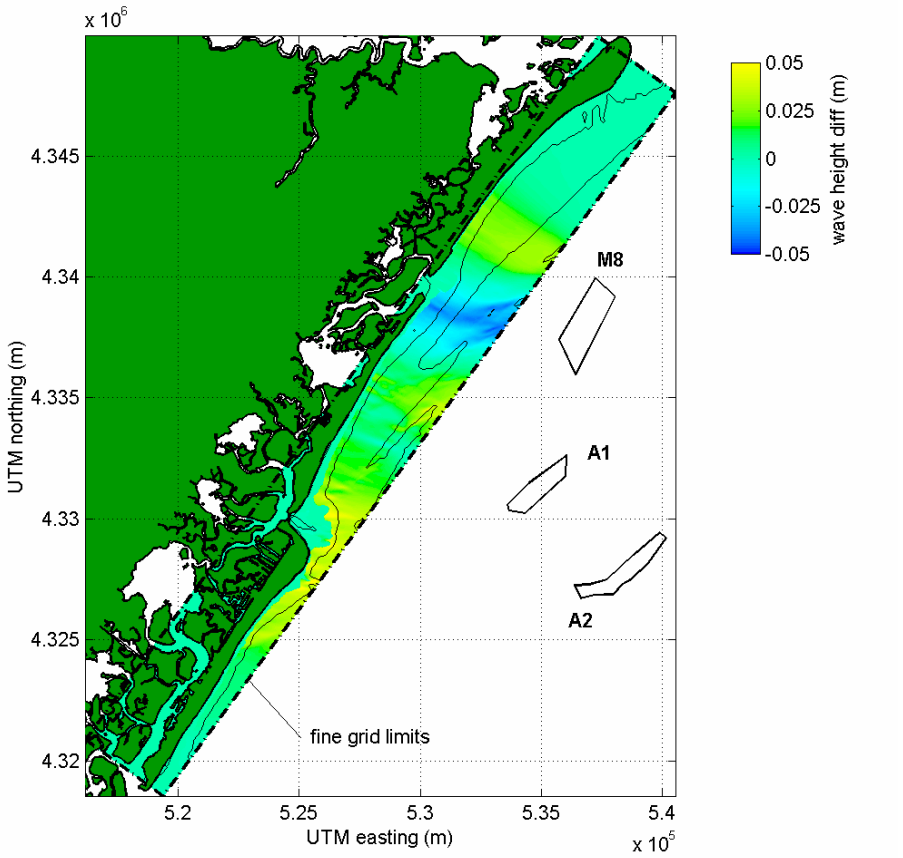

Figure 3-19. Example of fine grid wave height difference plot between existing and post-dredging bathymetry conditions offshore Townsends Inlet, NJ. This result is for NJ wave case 7; 1.6 m wave height and 11.1 sec period.

In addition to wave impacts resulting from borrow site excavation, wave heights and directions are modified by natural offshore bottom features as well. From the existing conditions model results for offshore North Carolina, it is seen how bottom features offshore the Outer Banks modify the wave field as it propagates shoreward. Model output presented in Figure 3-20 shows how waves respond to offshore shoals, even in relatively deep water (>15 m). For example, an area of reduced wave heights starting in the vicinity of 450,000 E, 3,985,000 N is caused by shallower areas immediately north and south. The shoal areas refract the wave field, causing a slight focusing of wave energy behind each feature. Because energy is conserved, the focusing of wave energy behind the shoal causes a reduction in energy at the northern and southern edges of the shoal, which is apparent by reduced wave heights in these areas. Another example of energy focusing caused by offshore features is show in Figure 3-21, for Sandbridge Shoal offshore Virginia Beach. The focusing effect of shoals is clear in this southeast wave condition. As wave energy is focused on the shoreline in the vicinity of Rudee Inlet in this example, there is a concurrent decrease in wave energy to the southwest of the shoals.

In addition to the effects of bottom features far offshore, waves are refracted by the straight and parallel bottom contours in the nearshore. In Figure 3-22, fine grid results show how wave directions change as the wave field propagates shoreward. For this SE wave condition (as in Figure 3-21) waves refract and the mean direction of wave

propagation becomes more shore-normal (perpendicular to the shoreline). In addition to the change in wave direction, wave heights are also modified by nearshore bathymetry. Waves begin to shoal (increase in height) about 440 m offshore, and increase in height by 0.1 m before breaking begins. Wave heights are reduced as energy is dissipated in the surf zone, which is about 120 m wide in this example.

The following discussion summarizes wave modeling results for the most common wave approach conditions at each potential sand resource area. Existing and post-dredging model results are described with reference to natural offshore bottom features and bathymetry changes resulting from proposed sand dredging.

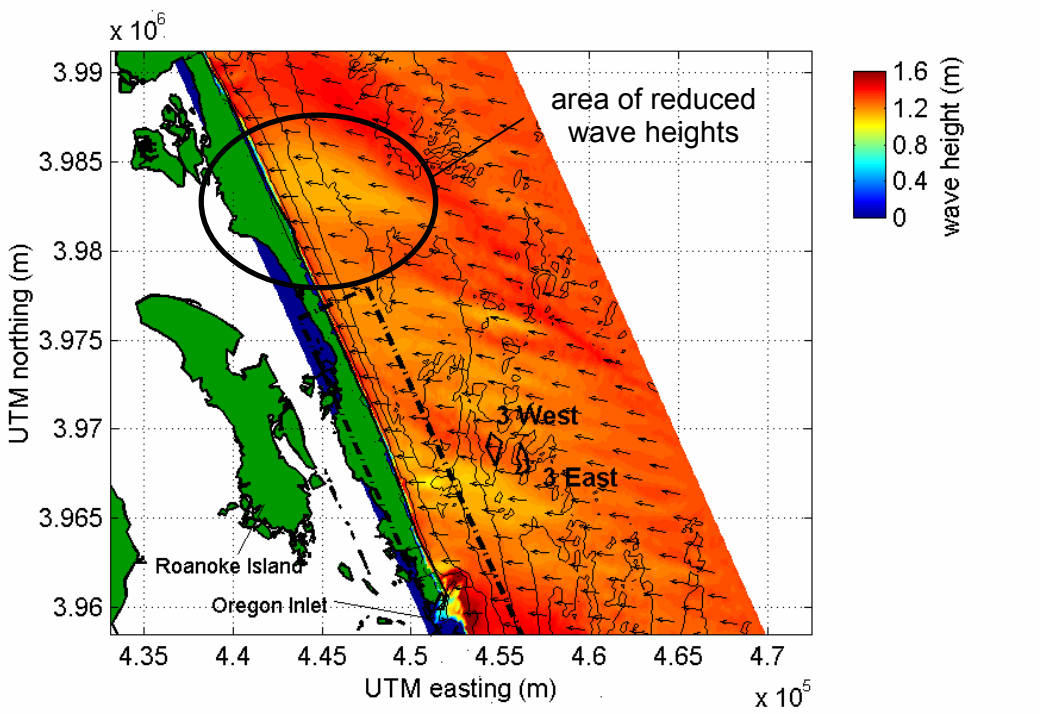

Figure 3-20. Coarse grid model results for offshore North Carolina (wave case 9; 1.3 m wave height, 11.3 sec period) illustrating area of reduced wave heights resulting from refraction of wave energy due to bottom bathymetry.

3.2.1.1 Offshore New Jersey

Examples of wave model output for existing conditions offshore southern New Jersey are shown in Figures 3-23 and 3-24 (wave cases 4 and 7 of Table 3-1). Case 4 has 1.2 m waves with a 7.1 sec peak period propagating from the southeast. The coarse grid results presented in Figure 3-23 illustrate that the direction of wave propagation is directly onshore; therefore, the effects of wave refraction are not discernable until waves are well within a kilometer of the shoreline. Waves increase in height and break on the shoals present in the vicinity of each of the modeled inlets. The highest refracted wave height for this case is about 1.5 m, which occurs in the shoals near Great Egg Harbor Inlet. Immediately offshore the coastline between Townsends and Great Egg Harbor Inlet, wave height reductions are observed that result from wave energy spreading by refraction along the gently crescent-shaped bottom contours of this area.

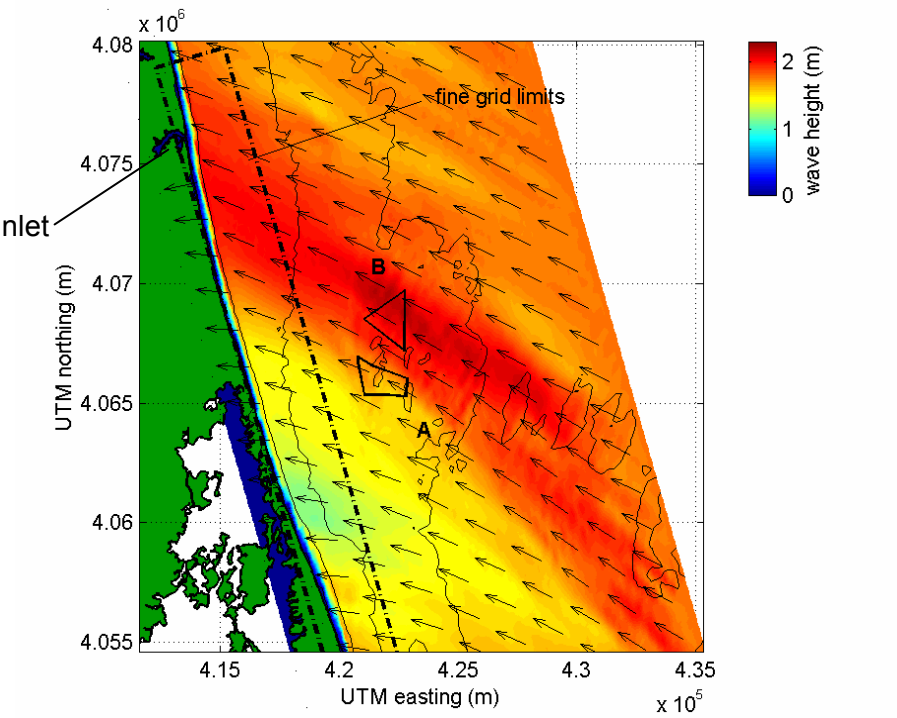

Figure 3-21. Coarse grid model results for Sandbridge Shoal, Virginia for wave case 10 (1.8 m wave height, 10.0 sec wave period) showing wave focusing effect of natural shoal deposits and area of reduced wave heights to the southwest of the shoals.

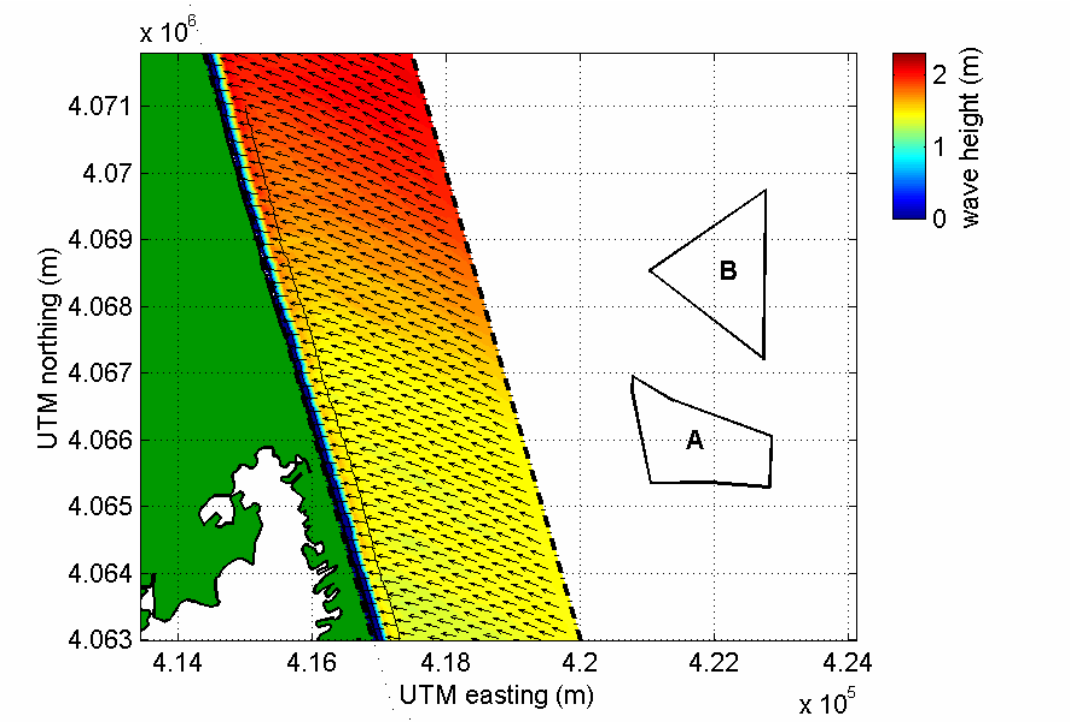

Figure 3-22. Fine grid model results for Sandbridge Shoal, Virginia for the same wave case presented in Figure 3-21. Detailed analysis illustrates nearshore refraction of waves and wave height reductions through the width of the surf zone.

In Figure 3-24, the results of wave Case 7 illustrate how 1.6 m, 11.1 sec waves propagating from the east are transformed as they approach the coast. The effects of wave refraction are more pronounced in this example as wave rays are seen to gradually arc toward shore-normal about 4 km offshore. Offshore wave height differences are more dramatic than the previous example due to the combination of the higher wave height, longer wavelength, and a more oblique offshore approach angle. In several offshore regions, wave heights have been reduced by approximately 0.25 m due to spreading of wave energy by refraction. In contrast to Case 4, where highest wave heights in the model grid occur are associated with inlet ebb shoals, the highest wave heights for Case 7 occur on the offshore shoal in the vicinity of borrow site A2. At this shoal, wave heights reach 2.1 m, a half-meter increase over the offshore boundary condition.

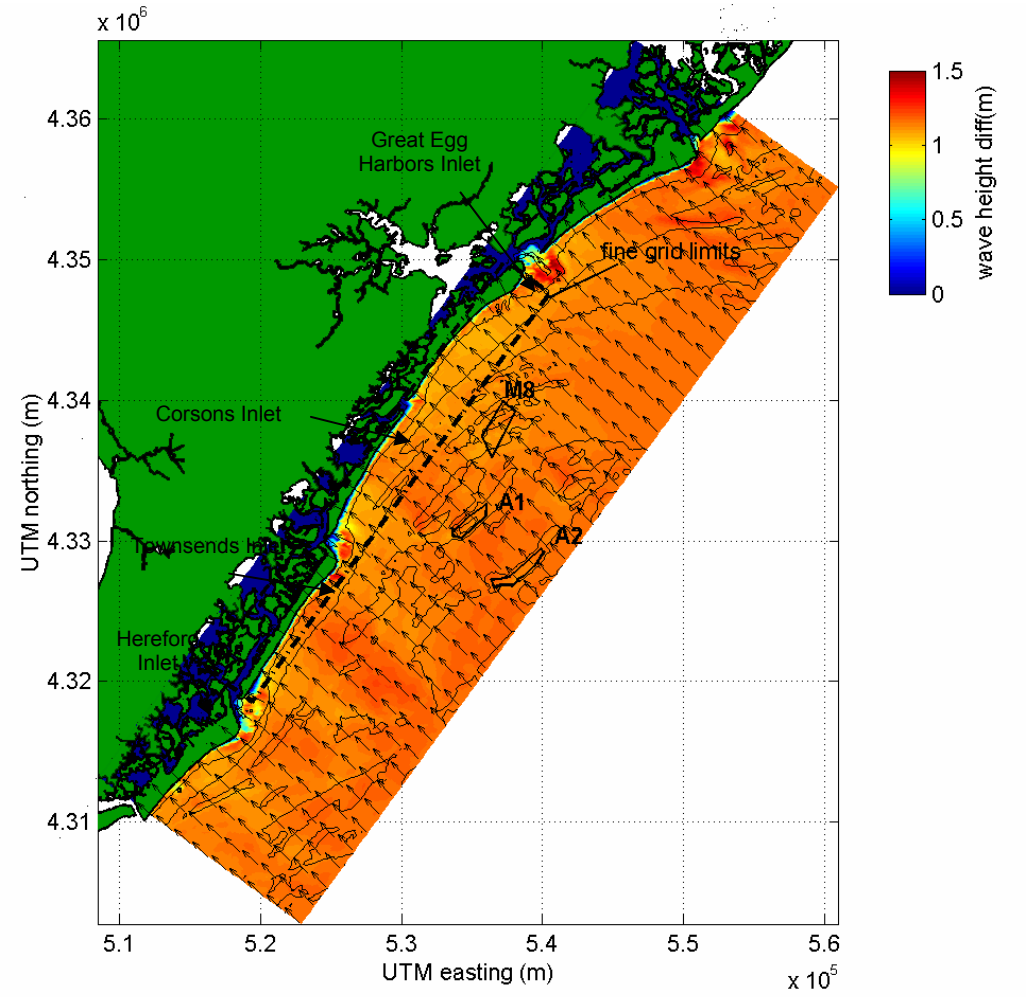

Figure 3-23. Plot of STWAVE model output for southern New Jersey wave Case 4 (H_s=1.2 m, T_{peak}=7.1 sec, θ_{peak}=131 deg). Color contours indicate wave height, and vectors show mean direction of wave propagation.

Plots of wave height difference between existing and post-dredging conditions for Cases 4 and 7 are presented in Figures 3-25 and 3-26. For Case 4, the maximum change in wave heights is ±0.05 m. Borrow Site A1 has a greater influence on wave

heights than other sites, where wave heights increase at the northeast and southwest edges due to wave refraction, and a corresponding decrease in wave heights is present between these margins. For wave Case 4, the length of shoreline impacted by the combination of the three borrow sites is approximately 20 km between Townsends and Great Egg Harbor Inlets.

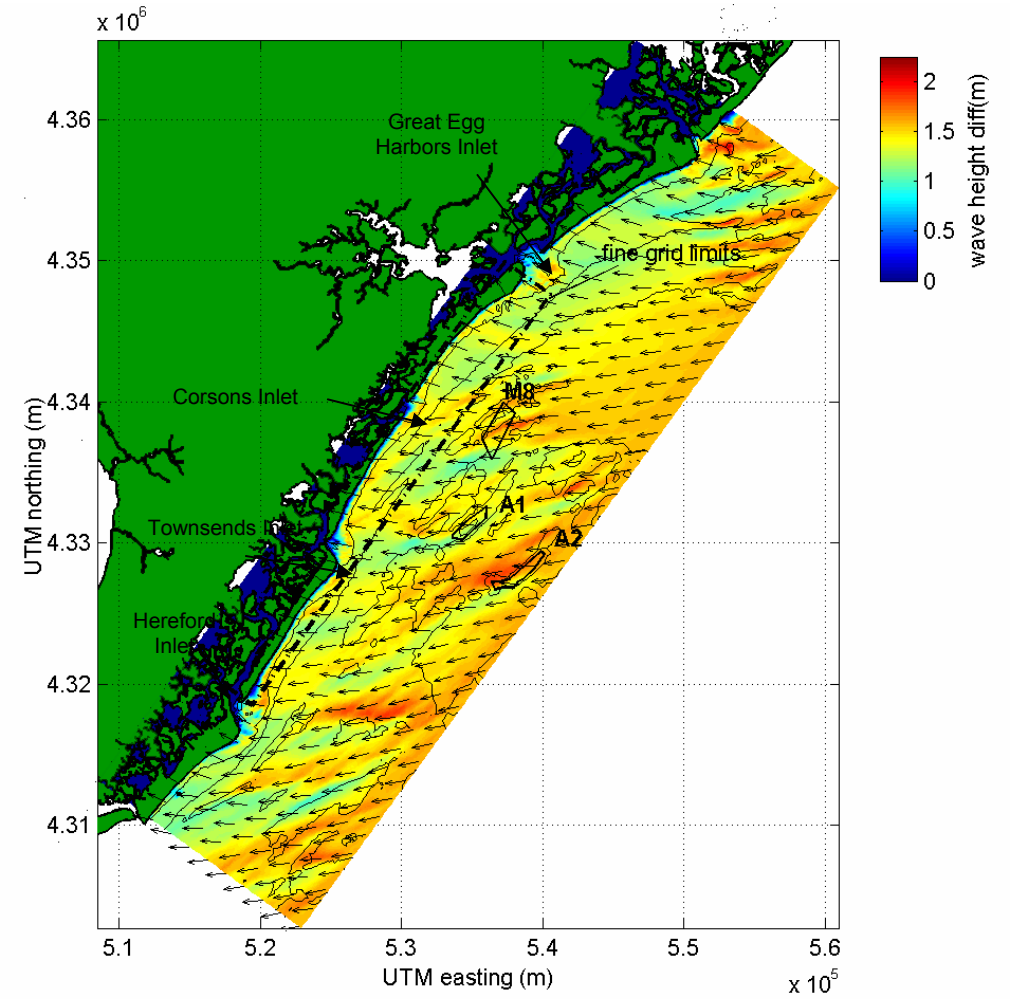

Figure 3-24. Plot of STWAVE model output for southern New Jersey wave Case 7 (H_s=1.6 m, T_{peak}=11.1 sec, θ_{peak}=81 deg). Color contours indicate wave height, and vectors show mean direction of wave propagation.

The wave difference plot for Case 7 in Figure 3-26 again shows that site A1 has the greatest influence on wave heights. Maximum wave height changes are ±0.25 m, near Site A1. The greatest increase in wave heights occurs long the southwestern margin of Site A1. For Site A2, the resulting wave shadow from the borrow site is much more focused than what is indicated for Case 4. This results from the geometry of the site, which is long and narrow, because waves are propagating along the major axis of the site in this case. Because offshore waves propagate from a more oblique angle relative to the shoreline than in Case 4, the area of shoreline influence for the three sites is considerably longer. For this case, approximately 30 km of shoreline between Hereford and Great Egg Harbor Inlets is in the zone of influence of the three sites.

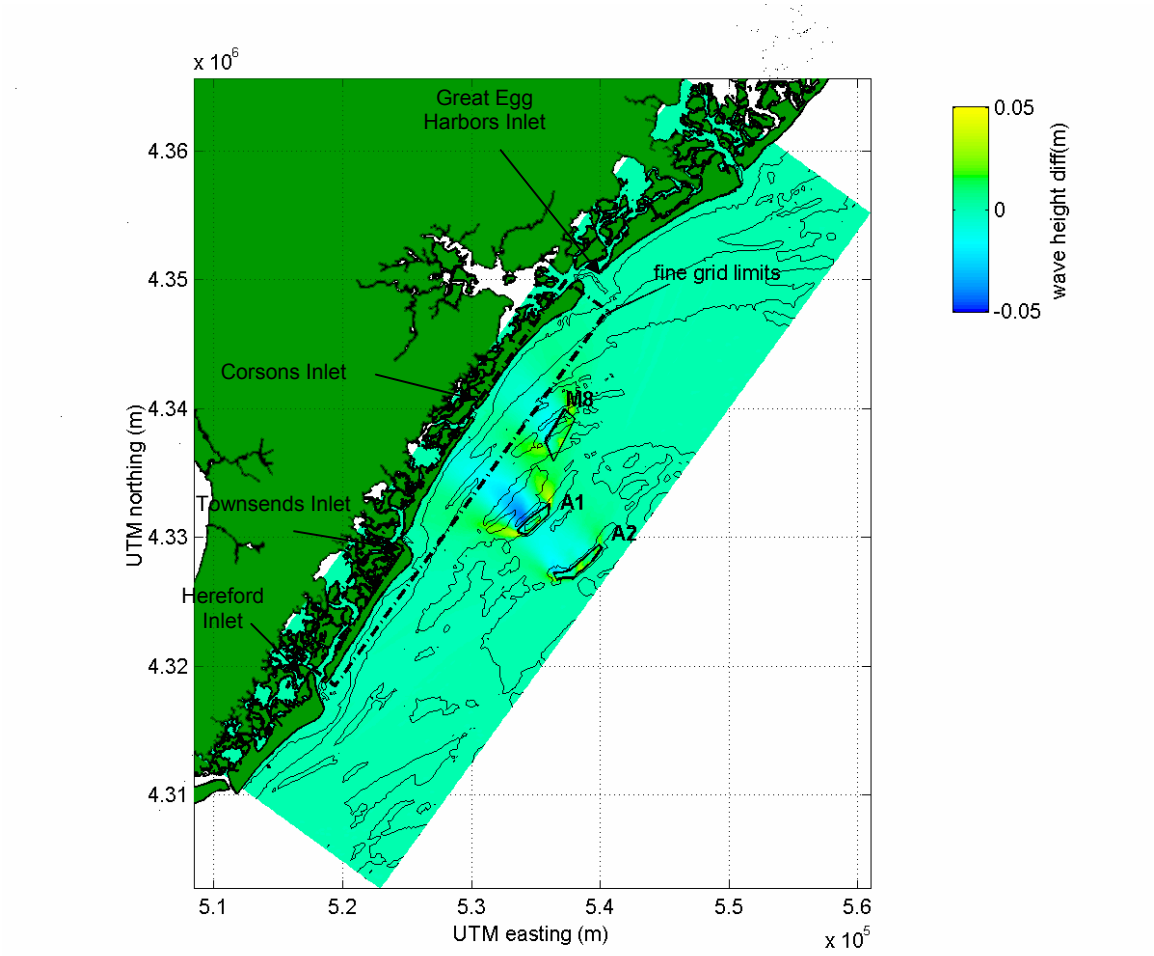

Figure 3-25. Plot of wave height change between existing and post-dredging ($\Delta=H_{post}-H_{pre}$) conditions at indicated borrow sites for STWAVE model output of southern New Jersey wave Case 4 (H_s=1.2 m, T_{peak}=7.1 sec, θ_{peak}=131 deg).

3.2.1.2 Offshore Southeastern Virginia

Wave model output for wave Cases 7 and 10 (see Table 3-5) for southern Virginia are presented in Figures 3-27 and 3-28. The results of Case 7 are for a 2.8 m wave with a peak period of 11.1 sec, propagating from the northeast. Because these waves basically are moving directly onshore and nearshore bathymetric contours are generally parallel to the shoreline, wave directions do not change significantly until they are very close to shore. The maximum refracted wave height in the model grid is 3.3 m, which is 0.5 m greater than the boundary condition. These maximum wave heights occur just outside the seaward extent of the surf zone, prior to the inception of wave breaking. Aside from wave height reductions seen near the top lateral boundary of the model grid (at the entrance to Chesapeake Bay), significant differences in offshore wave heights are not present due to the limited effect of refraction in this onshore wave condition.

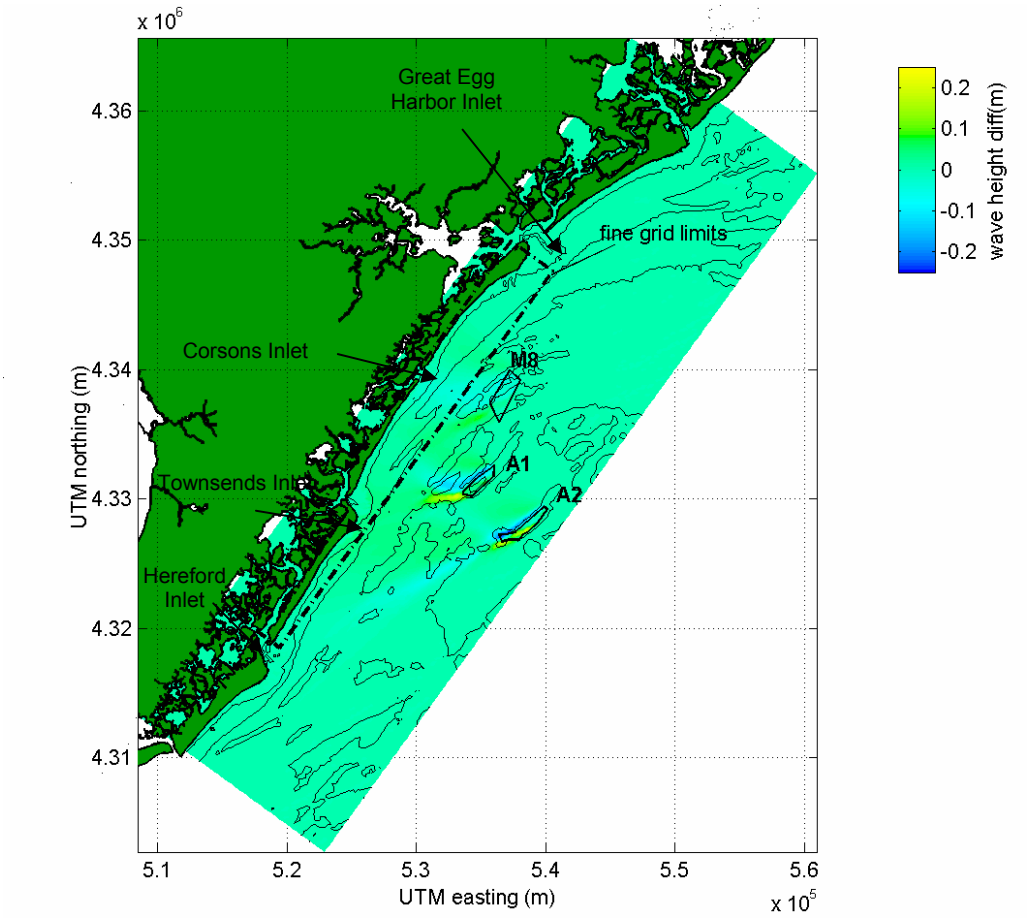

Figure 3-26. Plot of wave height change between existing and post-dredging ($\Delta=H_{post}-H_{pre}$) conditions at indicated borrow sites for STWAVE model output of southern New Jersey wave Case 7 (H_s=1.6 m, T_{peak}=11.1 sec, θ_{peak}=81 deg).

A second example of model output for southeastern Virginia is shown in Figure 3-28, for Case 10 (see Table 3-5). The offshore wave condition used for this model run was a 1.8 m high, 10 sec peak period wave that propagates from the southeast. The plot of this wave condition shows significant modifications to the offshore wave field that result from complex bathymetric features present at Sandbridge Shoal. Wave energy in this case is focused by the shoals, which results in an area of increased wave heights in the vicinity of Rudee Inlet. Maximum increased wave heights in this zone are 0.5 m above the offshore condition, or 2.3 m. This zone of increased wave heights extends approximately 10 km on either side of Rudee Inlet. As a result of the wave focusing by the shoals, there is a corresponding decrease in wave heights south of the shoals, shoreward to Sandbridge. An area of maximum decrease in wave height is indicated just seaward of Sandbridge, where wave heights are approximately 0.8 m less than at the offshore boundary. The full extent of the area of reduced wave heights is approximately 15 km.

Additional plots showing wave height changes that result from dredging the full design volumes at sites A and B for Cases 7 and 10 are shown in Figures 3-29 and 3-30. For waves modeled in Case 7, a case where waves are propagating almost directly onshore, maximum wave height changes are ±0.35 m. The largest decreases in wave heights after dredging are illustrated near Site B, at the western vertex of the triangle

that defines this site. The region of maximum wave height increase is found in the area between the two sites, resulting from the combined influence of Sites A and B. Wave energy is refracted by Site B to the south, where it combines with wave energy that has been refracted to the northwest by Site A, resulting in the observed increased wave heights. The shoreline potentially impacted by the presence of the two sites for wave model case 7 extends approximately 10 km alongshore in the vicinity of Sandbridge.

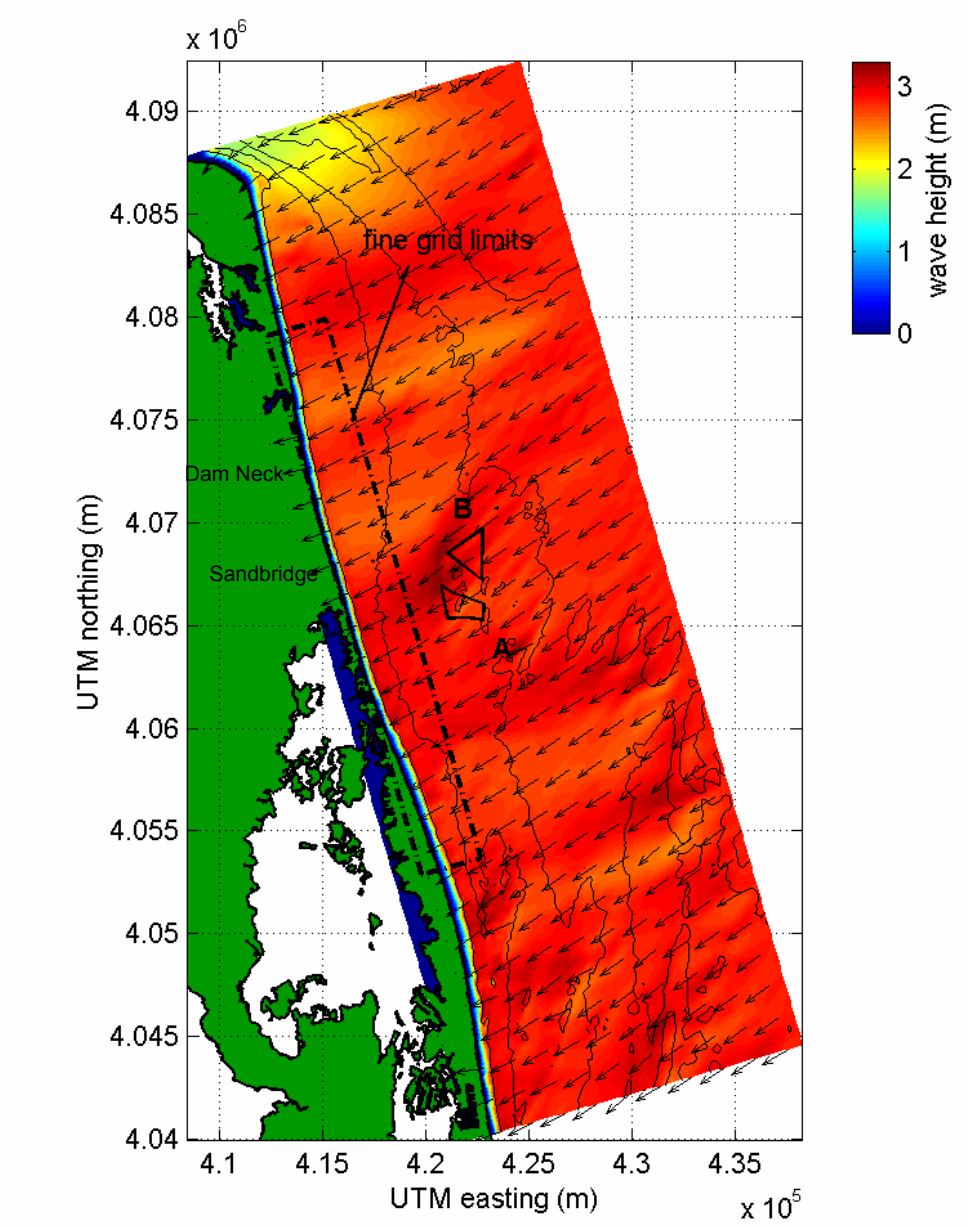

Figure 3-27. Plot of STWAVE model output for southeastern Virginia wave Case 7 (H_s=2.8 m, T_{peak}=11.1 sec, θ_{peak}=39 deg). Color contours indicate wave height, and vectors show mean direction of wave propagation.

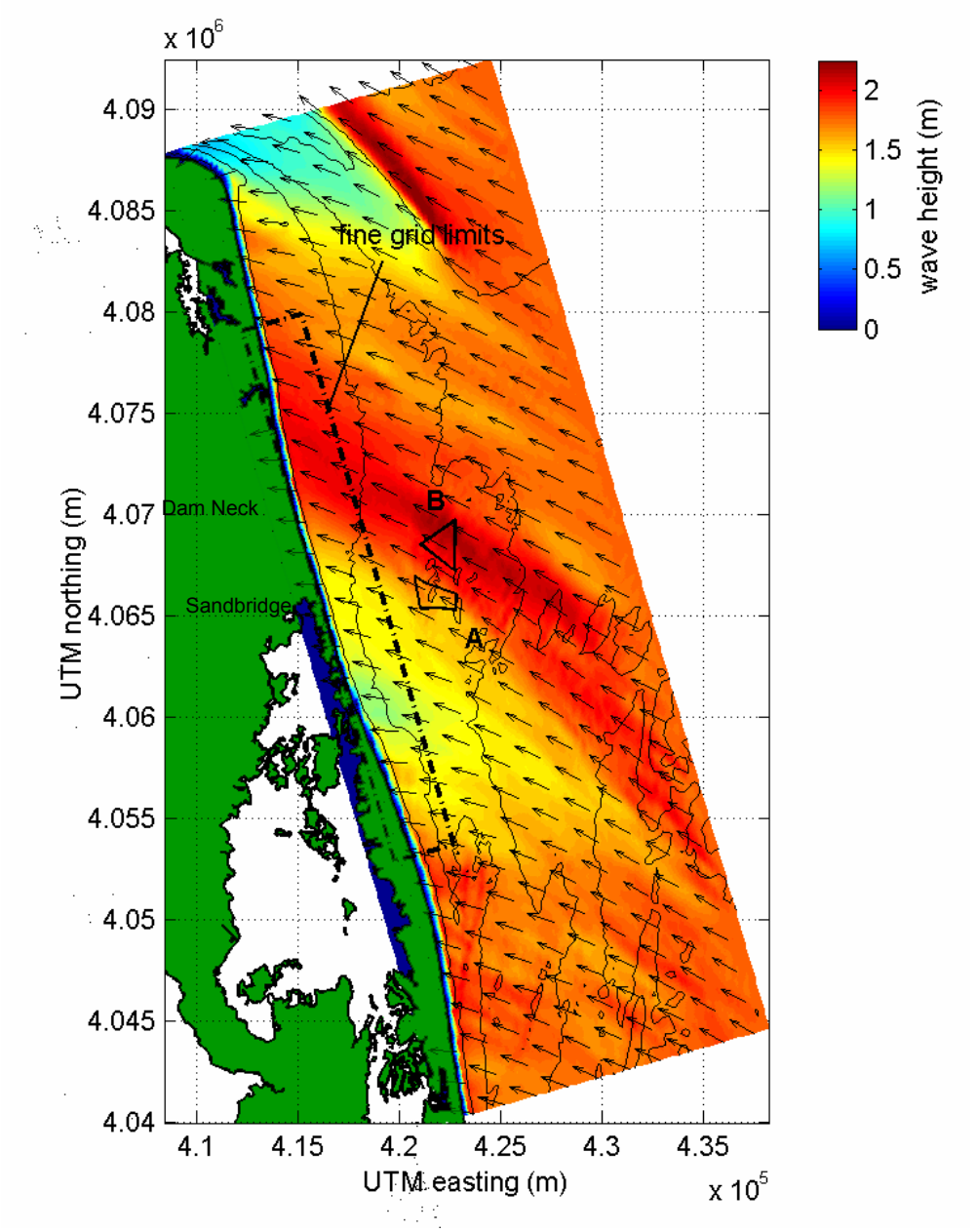

Figure 3-28. Plot of STWAVE model output for southeastern Virginia wave Case 10 (H_s=1.8 m, T_{peak}=10.0 sec, θ_{peak}=134 deg). Color contours indicate wave height, and vectors show mean direction of wave propagation.

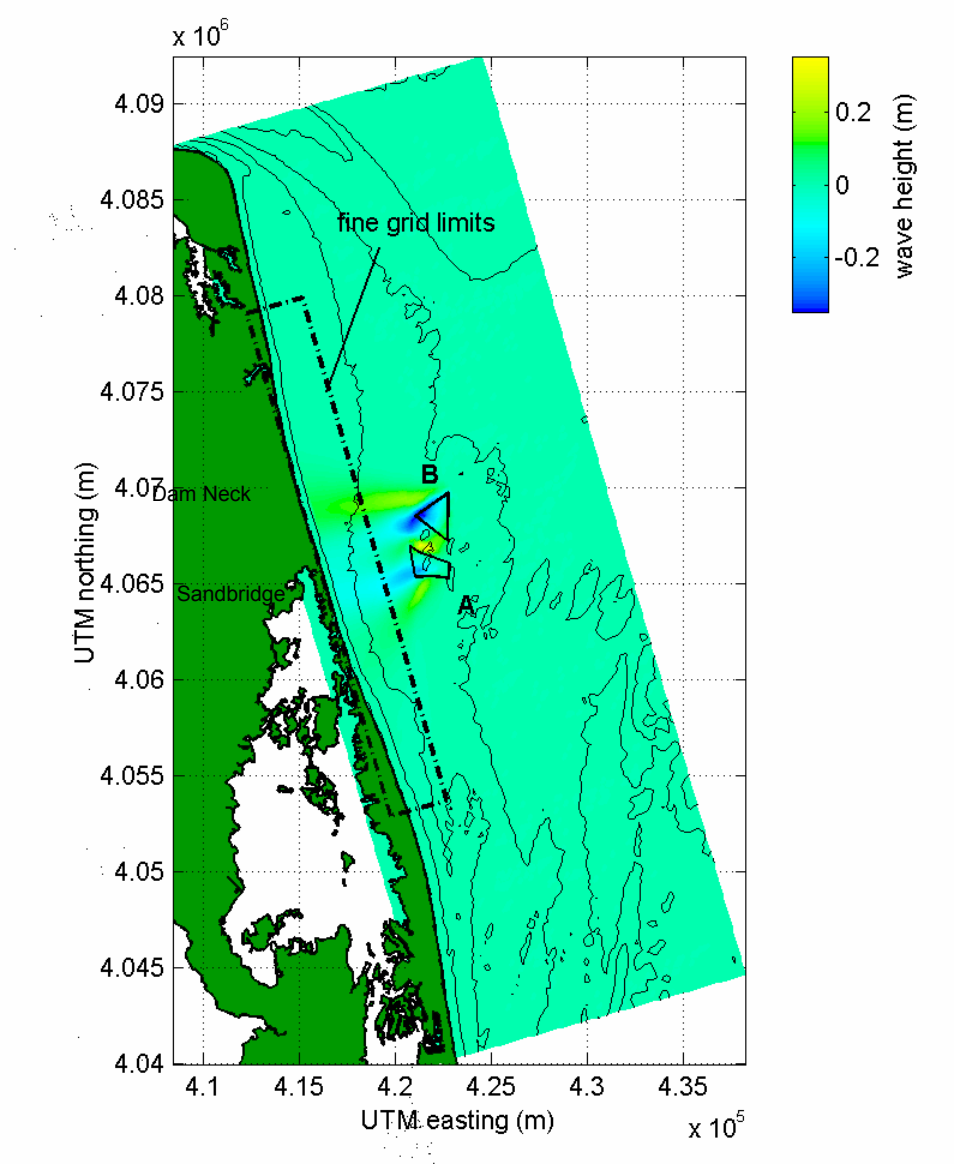

Figure 3-29. Plot of wave height change between existing and post-dredging (Δ=H_{post}-H_{pre}) conditions at borrow sites A and B for STWAVE model output for southeastern Virginia wave Case 7 (H_s=2.8 m, T_{peak}=11.1 sec, θ_{peak}=39 deg).

A plot of wave height changes for Case 10 between existing and post-dredging model conditions is shown in Figure 3-30. Modeled wave height changes range between 0.2 and -0.35 m. The zone of influence along the shoreline for the two sites extends approximately 12 km, from just north of Rudee inlet to Sandbridge. Maximum wave height reductions occur near Site A for this case, and the greatest increased wave heights occur in the area between the two sites. The shadow zones (areas of reduced wave height) from each borrow site merge to form a single shadow zone at about 3 km offshore.

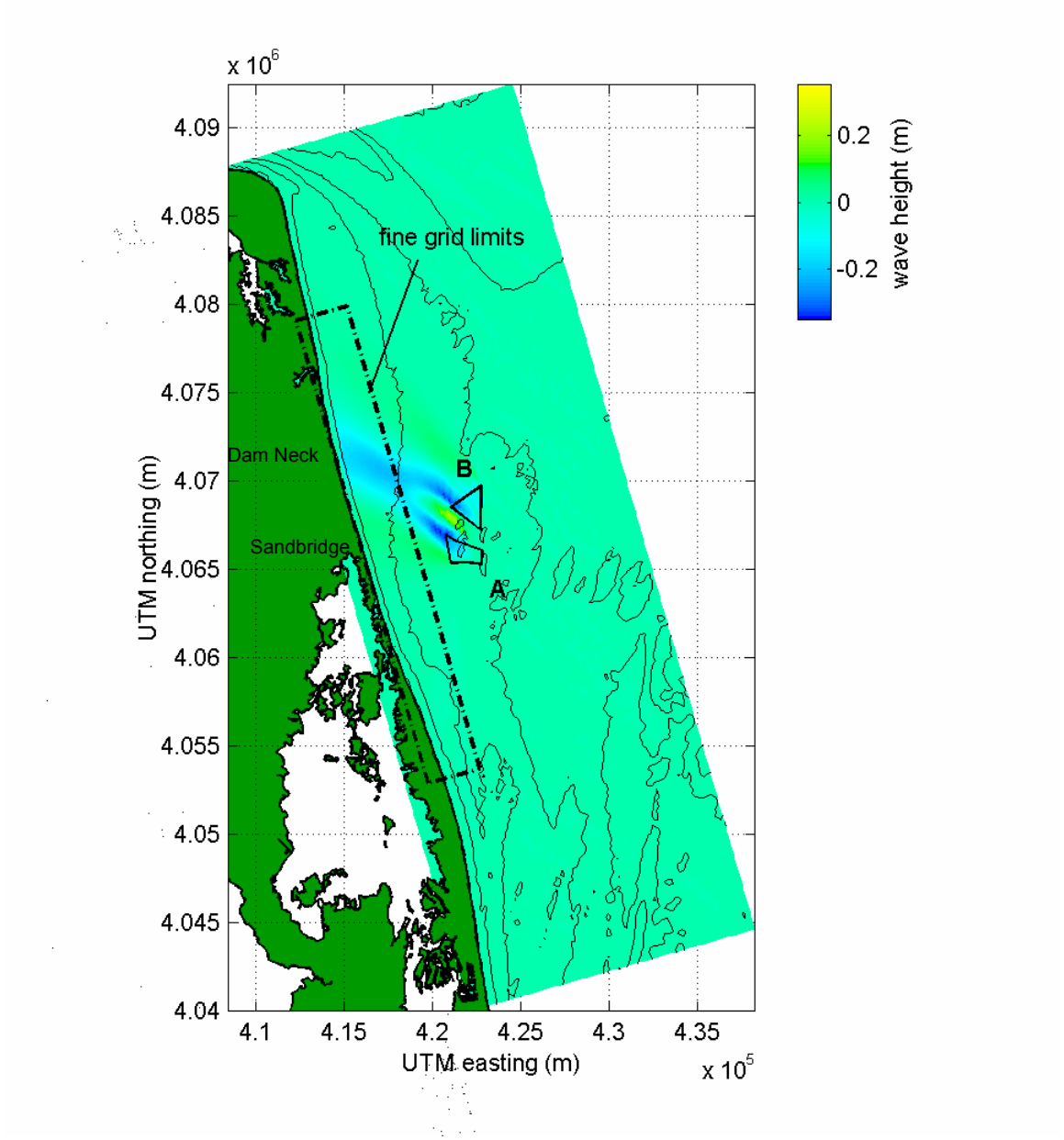

Figure 3-30. Plot of wave height change between existing and post-dredging ($\Delta=H_{post}-H_{pre}$) conditions at borrow sites A and B for STWAVE model output for southeastern Virginia wave Case 10 (H_s=1.8 m, T_{peak}=10.0 sec, θ_{peak}=134 deg).

3.2.1.3 Offshore North Carolina

Examples of wave model output for offshore North Carolina are illustrated in Figures 3-31 (Case 2) and 3-32 (Case 8). For Case 2, shoals offshore Oregon Inlet produce a small increase in wave heights landward of the shoals, with a corresponding small decrease in wave heights seaward of the shoals. Otherwise, no significant shoaling or refraction is observed in this relatively short period wave case.

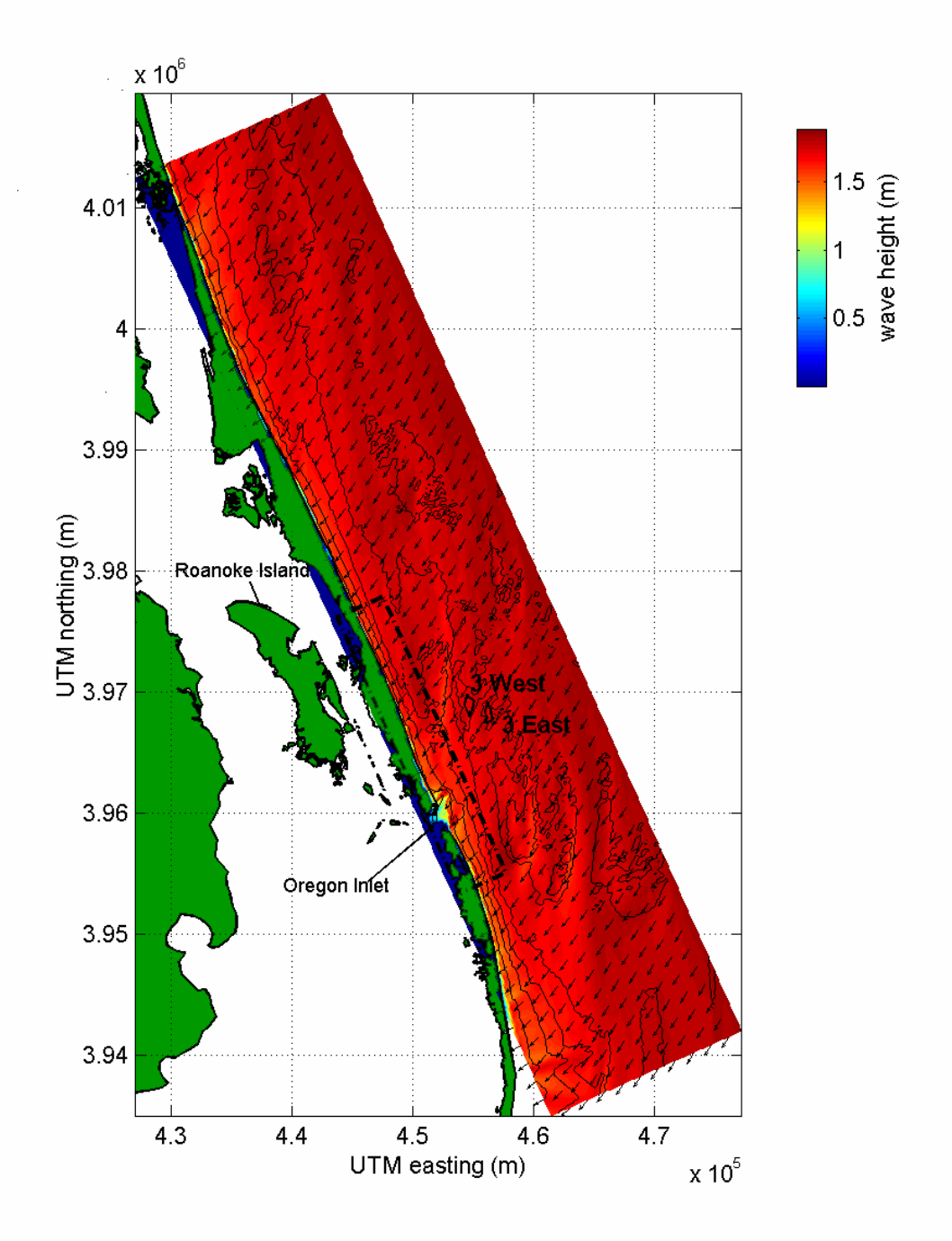

Figure 3-31. Plot of STWAVE model output for offshore North Carolina wave Case 2 (H_s=1.9 m, T_{peak}=6.0 sec, θ_{peak}=21 deg). Color contours indicate wave height, and vectors show mean direction of wave propagation.

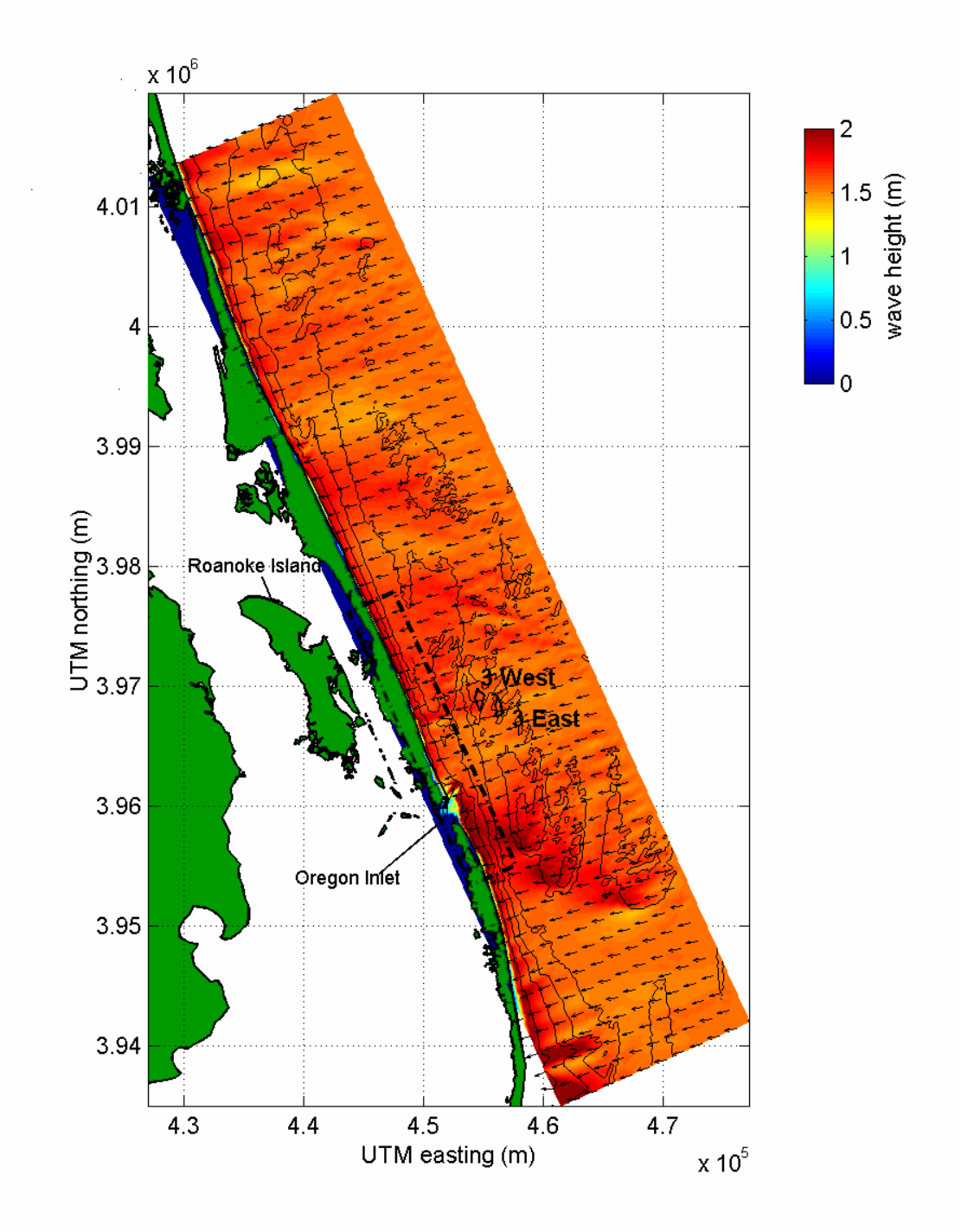

Figure 3-32. Plot of STWAVE model output for offshore North Carolina wave Case 8 (H_s=1.5 m, T_{peak}=12.8 sec, θ_{peak}=71 deg). Color contours indicate wave height, and vectors show mean direction of wave propagation.

Model output for wave Case 8 (see Table 3-5) is shown in Figure 3-32. This wave condition has a significantly longer period than the previous example, and as a result, waves are much more affected by offshore bathymetry gradients. Although the direction of wave propagation is not modified as much as was indicated in previous examples,

wave heights have changed significantly (e.g., a maximum height of 2.4 m at the southern side of Oregon Inlet) relative to offshore conditions. At the offshore shoals directly east of the inlet, wave heights increase approximately 0.7 m over the offshore boundary condition. Several shoal areas along the modeled coastline show similar impacts on wave heights, including the area encompassing the two modeled borrow sites.

Plots of wave height change from existing and post-dredging conditions at the two borrow sites are shown in Figures 3-33 and 3-34 for wave Cases 2 and 8. For Case 2 results (Figure 3-33), the area of influence for sites 3 East and 3 West extends approximately 20 km around Oregon Inlet. The extent of influence is the result of the approach angle for offshore waves. The greatest increase in wave heights resulting from the potential dredging was south of the western borrow site, where wave heights increased 0.04 m over existing conditions. The area of greatest wave height reduction also is located near the western borrow site, where wave heights decreased 0.07 m from existing conditions.

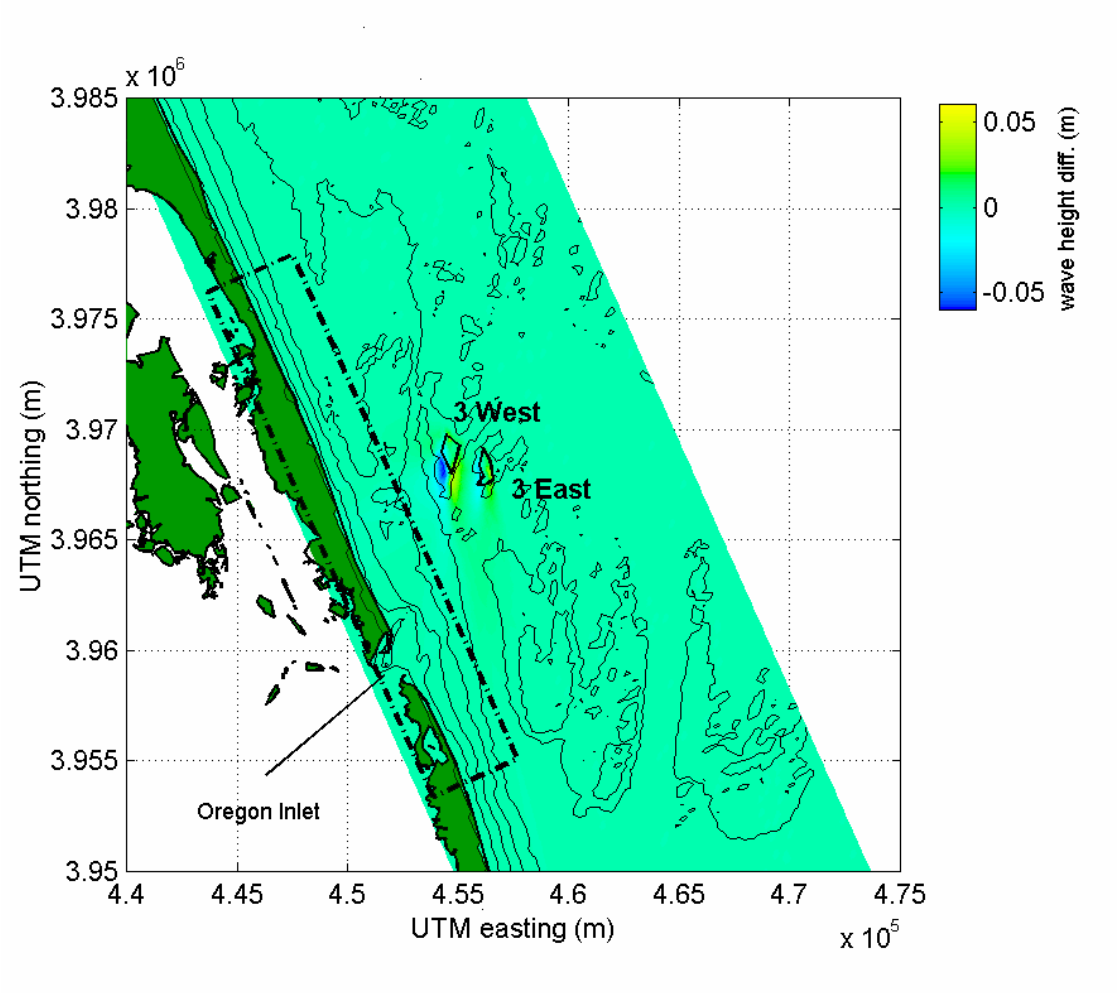

Figure 3-33. Plot of wave height change between existing and post-dredging ($\Delta=H_{post}-H_{pre}$) conditions at borrow sites 3 East and 3 West for STWAVE model output for offshore North Carolina wave Case 2 (H_s=1.9 m, T_{peak}=6.0 sec, θ_{peak}=21 deg).

Figure 3-34 presents the wave height difference plot for Case 8 (see Table 3-5). The two borrow sites have an overlapping region of influence, as site 3 West is located directly landward of the site 3 East along the direction of wave propagation. The area of maximum increased wave heights for post-dredging conditions is located at the northern corner site 3 West, where wave heights increase 0.06 m over existing conditions. Similar to the southeastern Virginia examples, wave height increase is the result of the combined influence of the two sites. The area of maximum wave height decrease is located landward of site 3 West, where wave heights are reduced by 0.07 m from existing conditions. Again, this maximum wave height reduction results from the combined impacts of the two sites. In a later section of this report (Section 4), it is determined that the cumulative impact of changes at each site are simply additive.

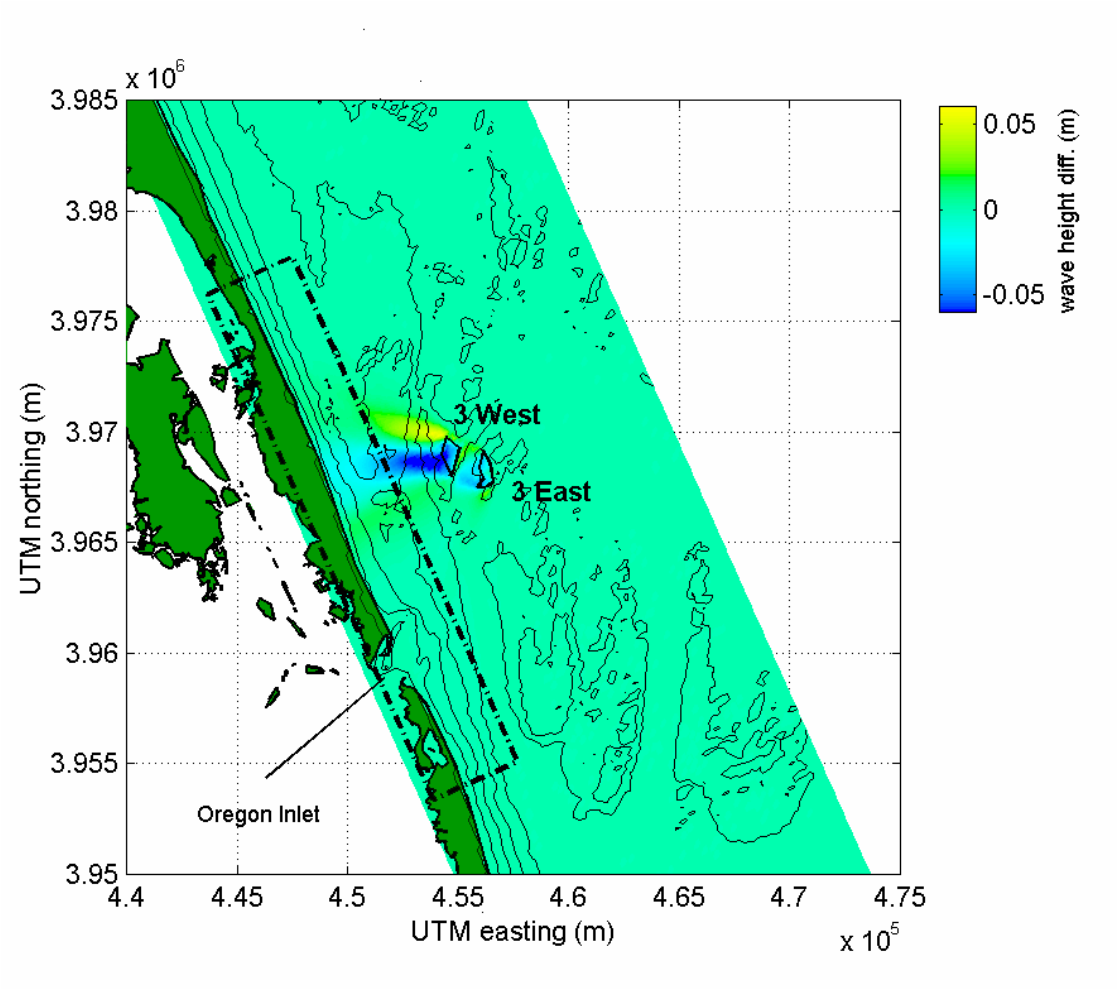

Figure 3-34. Plot of wave height change between existing and post-dredging ($\Delta=H_{post}-H_{pre}$) conditions at borrow sites 3 East and 3 West for STWAVE model output for offshore North Carolina wave Case 8 (H_s=1.5 m, T_{peak}=12.8 sec, θ_{peak}=71 deg).

3.2.1.4 Offshore Cape Canaveral

The results of two example wave cases are presented for offshore Florida in Figures 3-35 and 3-36. Output for existing conditions offshore Cape Canaveral for wave Case 3 (Table 3-4) is presented in Figure 3-35. Canaveral Shoals, the complex of

ridges and troughs that extend southeast from Cape Canaveral, cause significant increases in wave heights as waves propagate over this area. As waves refract over the shoals, wave heights increase by 0.5 m over the offshore boundary condition. In the

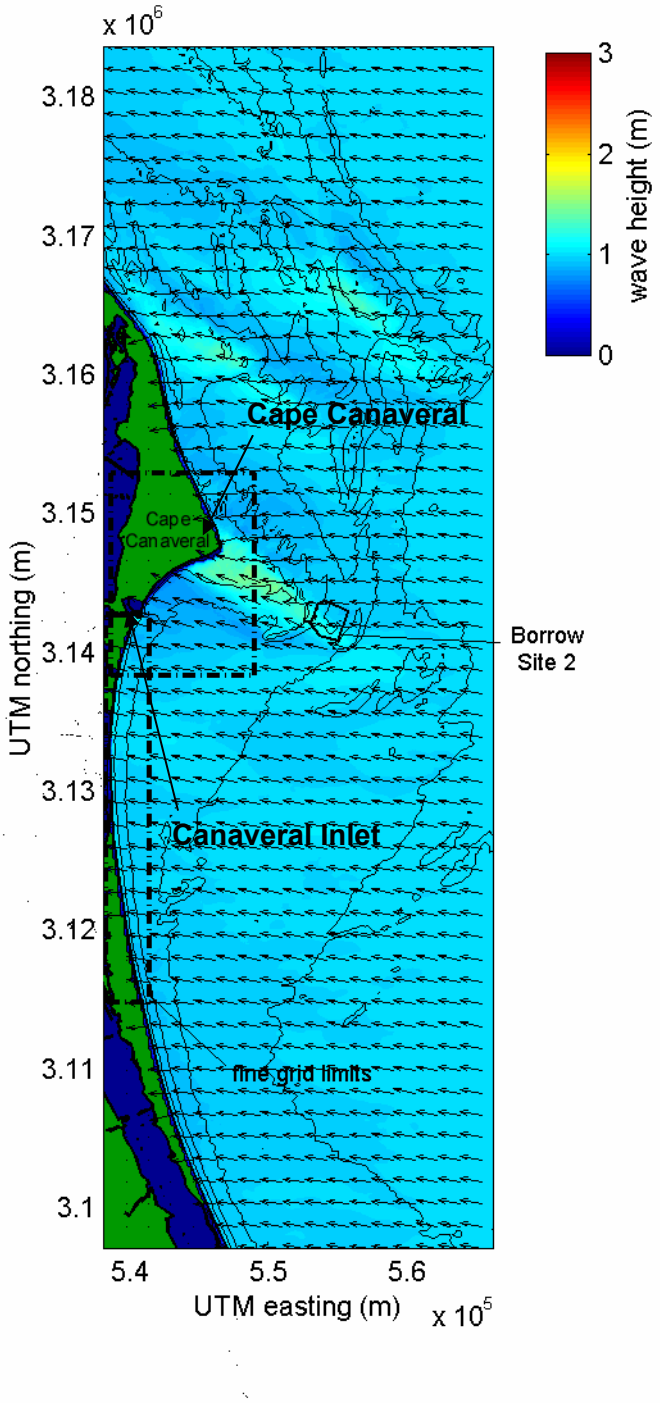

Figure 3-35. Plot of STWAVE model output for Cape Canaveral, Florida wave Case 3 (H_s=1.0 m, T_{peak}=7.7 sec, θ_{peak}=100 deg). Color contours indicate wave height, and vectors show mean direction of wave propagation.

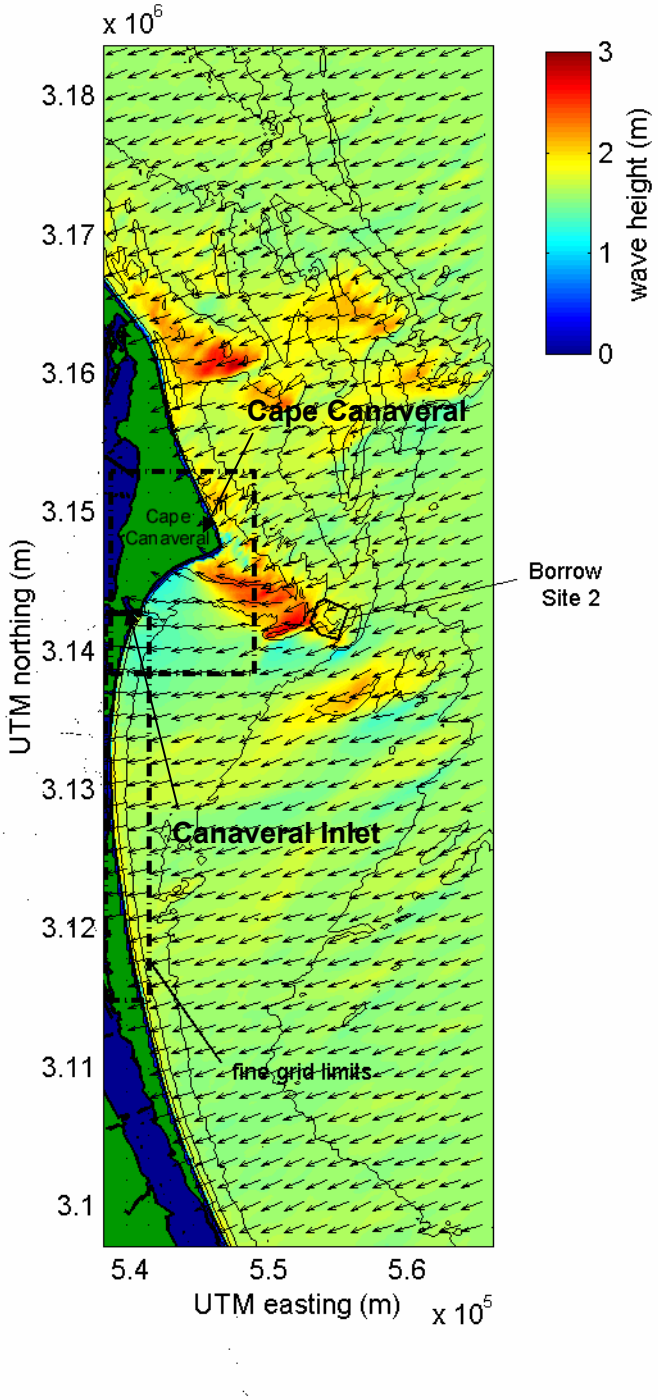

Figure 3-36. Plot of STWAVE model output for Cape Canaveral, Florida wave Case 6 (H_s=1.6 m, T_{peak}=14.3 sec, θ_{peak}=65 deg). Color contours indicate wave height, and vectors show mean direction of wave propagation.

shoal areas located northeast of the Cape, wave heights increase by about 0.3 m above offshore wave heights. Wave direction changes also are observed at the shoals.

A greater degree of direction change is seen in the model output for Case 6 (Figure 3-36). The offshore wave boundary condition is a 1.6 m, 14.3 sec wave propagating from the east-northeast. Vectors indicating wave direction illustrate that for some nearshore regions adjacent to the Cape, the direction of wave propagation changes more than 45 degrees, following the gradient in bathymetric contours. The largest waves in the model domain occur at the shoals north of Cape Canaveral, and are 1.3 m higher than offshore waves. At shoals in the vicinity of the borrow site, wave heights increase to a maximum of 2.8 m, 1.2 m above offshore conditions. Shoals tend to refract wave energy and focus it near the cusp of the Cape. Wave energy is focused away from the coast south of Cape Canaveral, and an area of reduced wave heights is created.

Wave height change plots are shown in Figures 3-37 and 3-38 for Cases 3 and 6, respectively. For Case 3, maximum wave height increase resulting from dredging the borrow site is 0.2 m, and the maximum decrease in the shadow zone of the site is 0.3 m. The overall area of influence of this borrow site extends approximately 14 km north of the Cape to about 4 km south of Port Canaveral.

Similar wave difference results are illustrated for Case 6 (Figure 3-38). Maximum changes in post-dredging wave heights were ±0.7 m, which are substantially greater than changes observed at previous sites. The area of greatest wave height increase occurs at the northwest corner of the site. Wave heights do not increase by the same amount at the southwest corner, likely due to the geometry and bathymetry of the site. Deeper excavation depths at the northwest corner cause a greater degree of wave refraction. The alongshore extent of influence is similar to that of Case 3, but it is shifted slightly southward due to the different direction of wave propagation.

3.2.2 Sediment Transport Potential

Comparisons of average annual sediment transport potential were performed for existing and post-dredging conditions to indicate the relative impact of dredging to longshore sediment transport processes. Sediment transport potential is a useful indicator of shoreline impacts caused by offshore borrow sites because the computations include the borrow site influence on wave height and direction. For each study area, the net sediment transport potential associated with average annual conditions was computed. Post-dredging model conditions in each study area are listed in Table 3-7. These values represent the recommended maximum excavation depths for each individual site, whether dredged during the course of one project or over the coarse of several projects.

3.2.2.1 Model Comparison with Historical Shoreline Change

To ensure that the spectral wave modeling and the associated longshore sediment transport potential could be utilized effectively to evaluate long-term alterations to the littoral system, a comparison of model predictions with observed shoreline change was performed. This analysis provides a semi-quantitative method for determining whether a) longshore wave-induced transport is responsible for observed shoreline change, and b) the long-term shoreline change trends are consistent with the shorter time-period (20-year) sediment transport potential analyses. For the four potential sand resource areas,

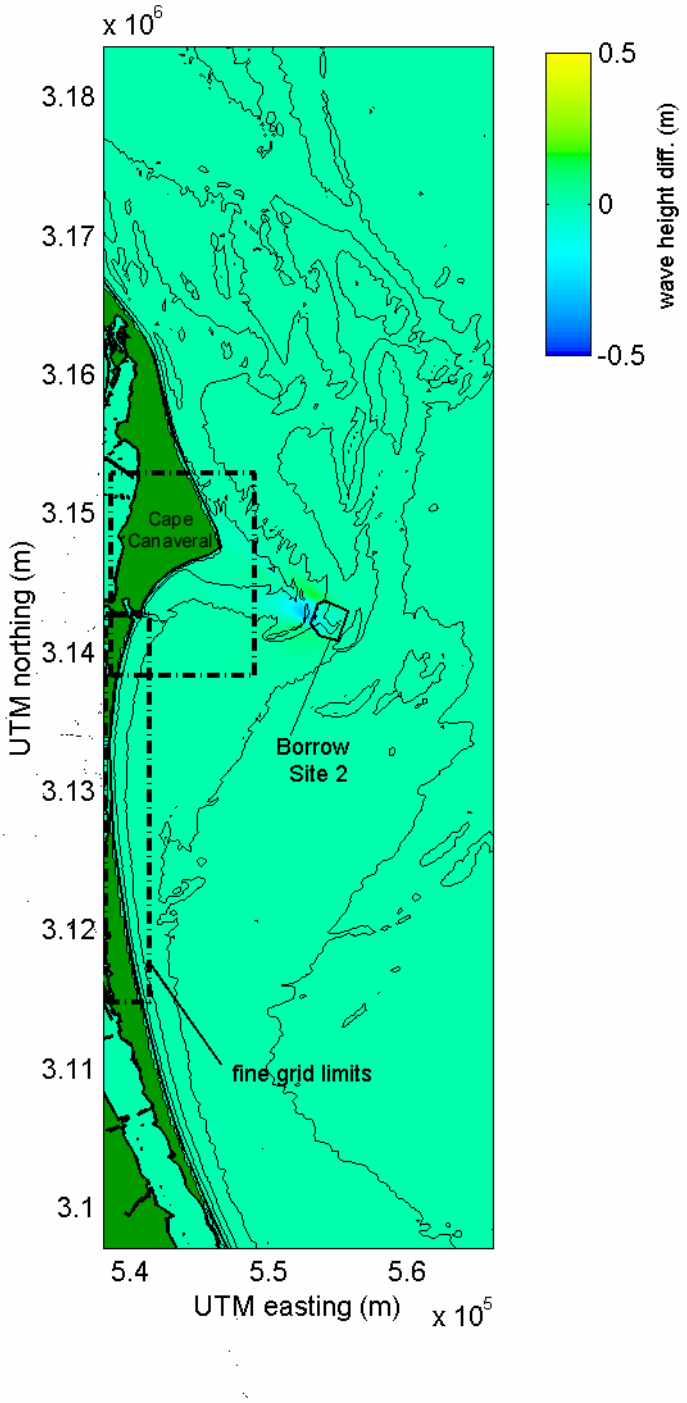

Figure 3-37. Plot of wave height change between existing and post-dredging ($\Delta=H_{post}-H_{pre}$) conditions at Borrow Site 2 for STWAVE model output for Cape Canaveral, Florida wave Case 3 (H_s=1.0 m, T_{peak}=7.7 sec, θ_{peak}=100 deg).

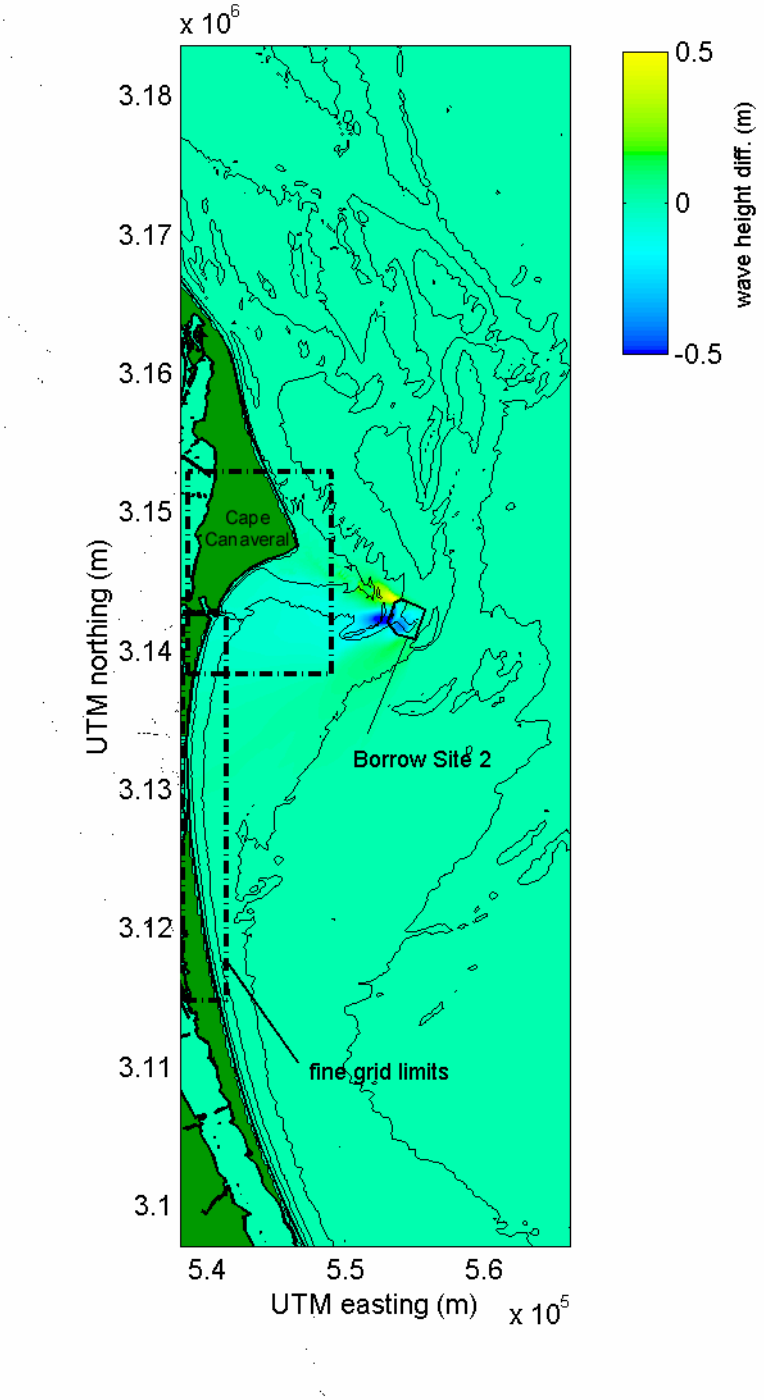

Figure 3-38. Plot of wave height change between existing and post-dredging ($\Delta=H_{post}-H_{pre}$) conditions at Borrow Site 2 for STWAVE model output for Cape Canaveral, Florida wave Case 6 (H_s=1.6 m, T_{peak}=14.3 sec, θ_{peak}=65 deg).

an evaluation of model output was performed using a comparison of computed gradients in sediment transport to historical shoreline change data. The basis for this comparison is the relationship between shoreline movement and the longshore gradient of sediment transport. Simply expressed, this relationship is

$$\frac{\partial Q}{\partial y} \propto \frac{\partial x}{\partial t} \tag{3.17}$$

where Q is sediment transport, y is alongshore distance, x is the cross-shore position of the shoreline, and t is time. A comparison of results should illustrate similar trends in long-term shoreline change and transport potential computed using wave conditions that represent long-term average conditions. Good general agreement between these two quantities would suggest that the transport potential model reasonably represents long-term costal processes for a given area, and thus, the model's ability to predict the likely impacts that would result from offshore dredging.

The time variation in shoreline position was determined from an analysis of historical shoreline data for each of the study areas. Regional change analysis provides a without-project assessment of shoreline response for comparison with predicted changes in wave-energy focusing at the shoreline resulting from potential offshore sand dredging activities. Because continuous measurements of historical shoreline change are available at 50-m alongshore intervals, model results (wave and sediment transport) at discreet intervals along the coast can be compared with historical data to develop process/response relationships for evaluating potential impacts. In this study, shoreline data covering the periods 1842 to 1977 for southern New Jersey (Byrnes et al., 2000); 1859 to 1980 for Sandbridge, southeastern Virginia (completed as part of this study); 1849 to 1980 for Dare County, North Carolina (Byrnes et al., 2001); and 1877 to 1996 for the shoreline south of Cape Canaveral, Florida (Byrnes and Kraus, 1999; Kraus et al., 1999) was used to quantify trends. Methods used for compiling and analyzing historical data sets are described in Byrnes and Hiland (1994). Alongshore variations in sediment transport were determined using the computed values of transport potential for each shoreline for modeled existing conditions. Comparisons of shoreline change to the modeled transport gradient are shown in Figures 3-39 to 3-42.

Southern New Jersey. For the modeled New Jersey shoreline shown in Figure 3-39, there is general agreement between shoreline change and transport gradient. Shoreline change data from Great Egg Harbor Inlet to Corsons Inlet show a trend from stable to erosional at the northeast side of Corsons Inlet. This trend is indicated in the transport gradient as well. From Corsons to Townsends Inlets, the shoreline change trend is from slightly erosional to slightly accretional, which is also the general trend documented in the gradient of transport potential. At the southwestern side of Townsends Inlet, a highly erosional area followed by an area of accretion is illustrated in shoreline change data and the modeled transport gradient. However, south of this area, agreement between modeled shoreline change trends and measured shoreline change do not appear to match well. Although the modeling predicts an area of significant accretion centered at approximately UTM Northing 4,325,000 meters, measurements indicate a stable shoreline in this region. Other than this one portion of the grid, which is not influenced by proposed borrow sites, agreement between the modeled gradient in transport potential and measured shoreline change is good. Even erosion and accretion trends

are predicted well in the vicinity of tidal inlets, where tidal current processes often dominate nearshore sediment transport patterns.

Southeastern Virginia. For the modeled shoreline of southeastern Virginia, the comparison of modeled transport gradient and measured shoreline change is shown in Figure 3-40. Shoreline change data and model results indicate a fairly stable shoreline between Rudee Inlet (north end of the plot) and Sandbridge (immediately landward of Borrow Sites A and B). South of Sandbridge, both analyses show a change to an erosional shoreline. Farther south from the maximum negative gradient in transport potential, the gradient changes to an accretional trend where shoreline change data indicate a change to a stable shoreline. Overall, the agreement between trends in longshore sediment transport potential gradient and observed shoreline change was good for the Virginia coast. This suggests that the 5-year offshore wave record used for calculating sediment transport potential represented long-term wave conditions responsible for regional shoreline change.

North Carolina. Trends in shoreline change generally agree with modeled transport gradients for the North Carolina coast north of Oregon Inlet (Figure 3-41). Results of both analyses illustrate a stable to erosional shoreline, with an area of maximum erosion between 5 and 7 km north of Oregon Inlet. For the modeled transport gradient, there is an area of accretion approximately 3 km north of the point of maximum erosion that is not indicated in the shoreline change analysis. This may be due to al lack of detailed nearshore bathymetry data for a 2 km section of coastline at this location. Bathymetry data used for developing the model grid was digitized from a NOAA navigational chart and does no have a high level of detail as is available in the data used for adjacent sections of coast. In addition, severe erosion observed immediately north of Oregon Inlet may have created an erosion hot-spot that has propagated to the north as shoreline orientation changed over the past century. The gradient in sediment transport potential was not expected to simulate this process that likely occurs over a time period spanning several decades. Significant migration of Oregon Inlet also may be responsible for some of the differences between observed and modeled shoreline change trends, where the peak in erosion likely has migrated south with the inlet. Therefore, the peak erosion area determined from the gradient of modeled transport potential, based on 20 years of recent wave information, may be more representative of present conditions than the long-term shoreline change (based on more than 100 years of shoreline data). Overall, good agreement exists between observed shoreline change and longshore gradient in modeled transport potential. Minor differences between the two methods, especially in the region of maximum erosion, likely are due to long-term alterations (spanning several decades) in shoreline position and the historical migration of Oregon Inlet.

Cape Canaveral. Model results and shoreline change data for the Cape Canaveral area are shown in Figure 3-42. Both analyses show that the shoreline is stable about 6 km south of Canaveral Inlet. In the shoreline change results, the trend from the Cape headland south to Port Canaveral is highly accretional to accretional. This trend is not duplicated in the modeled transport gradient, which shows an area of high accretion at the cusp of the Cape, followed by an area of significant erosion between the Cape and the Inlet. The model likely has difficulty in this area due to complex offshore bathymetric features associated with Canaveral Shoals and limitations related to wave modeling (wave diffraction presently not included in STWAVE). In addition, STWAVE propagates wave energy within a $\pm$90 degree sector from the cross-shore axis of the grid, which is important in areas where the shoreline angle is steeply inclined from the axis of the grid

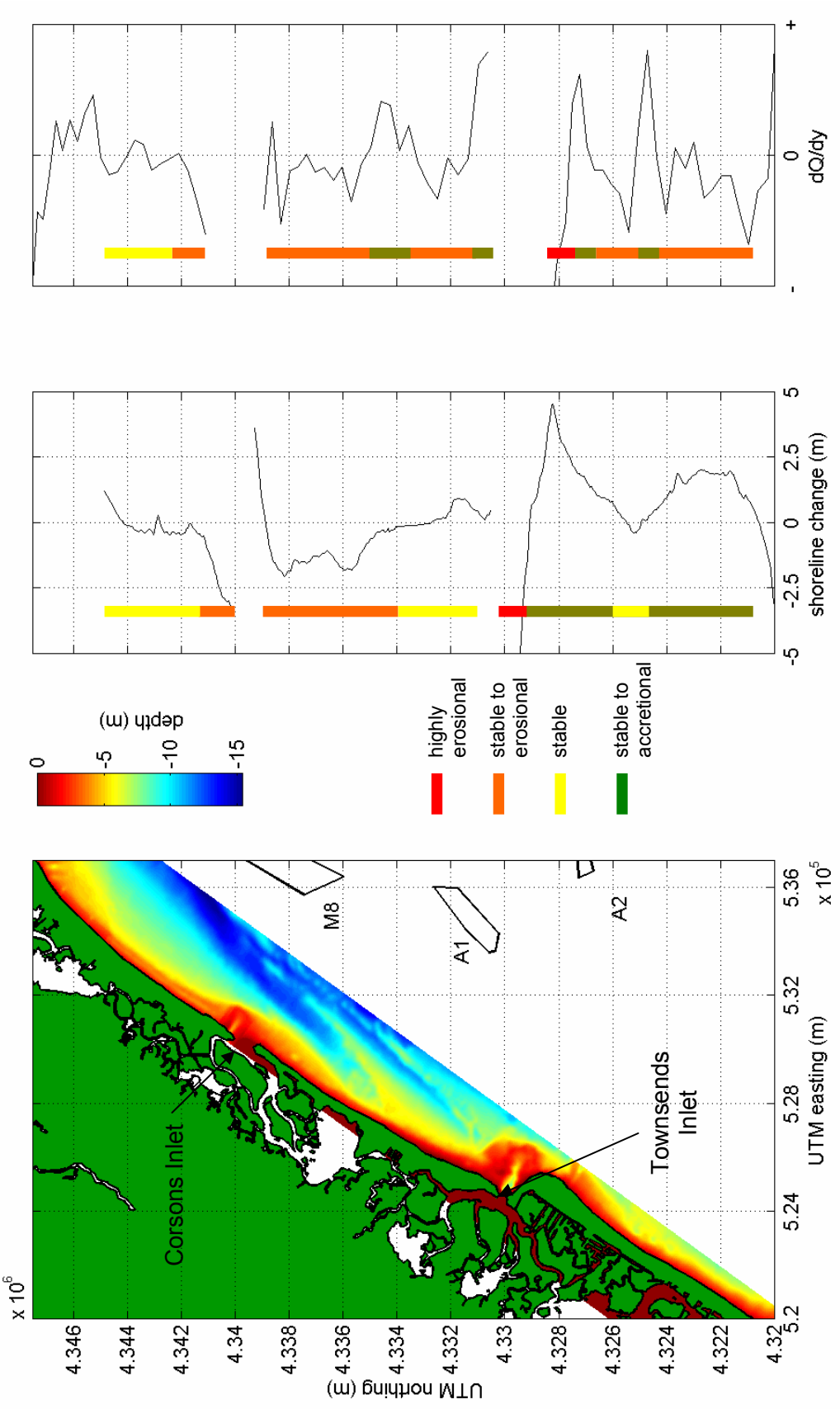

Figure 3-39. Comparison of historical shoreline change and gradient of modeled transport potential (dQ/dy) for the southern New Jersey shoreline. Color bars indicate whether the shoreline is accretional, stable, or erosional.

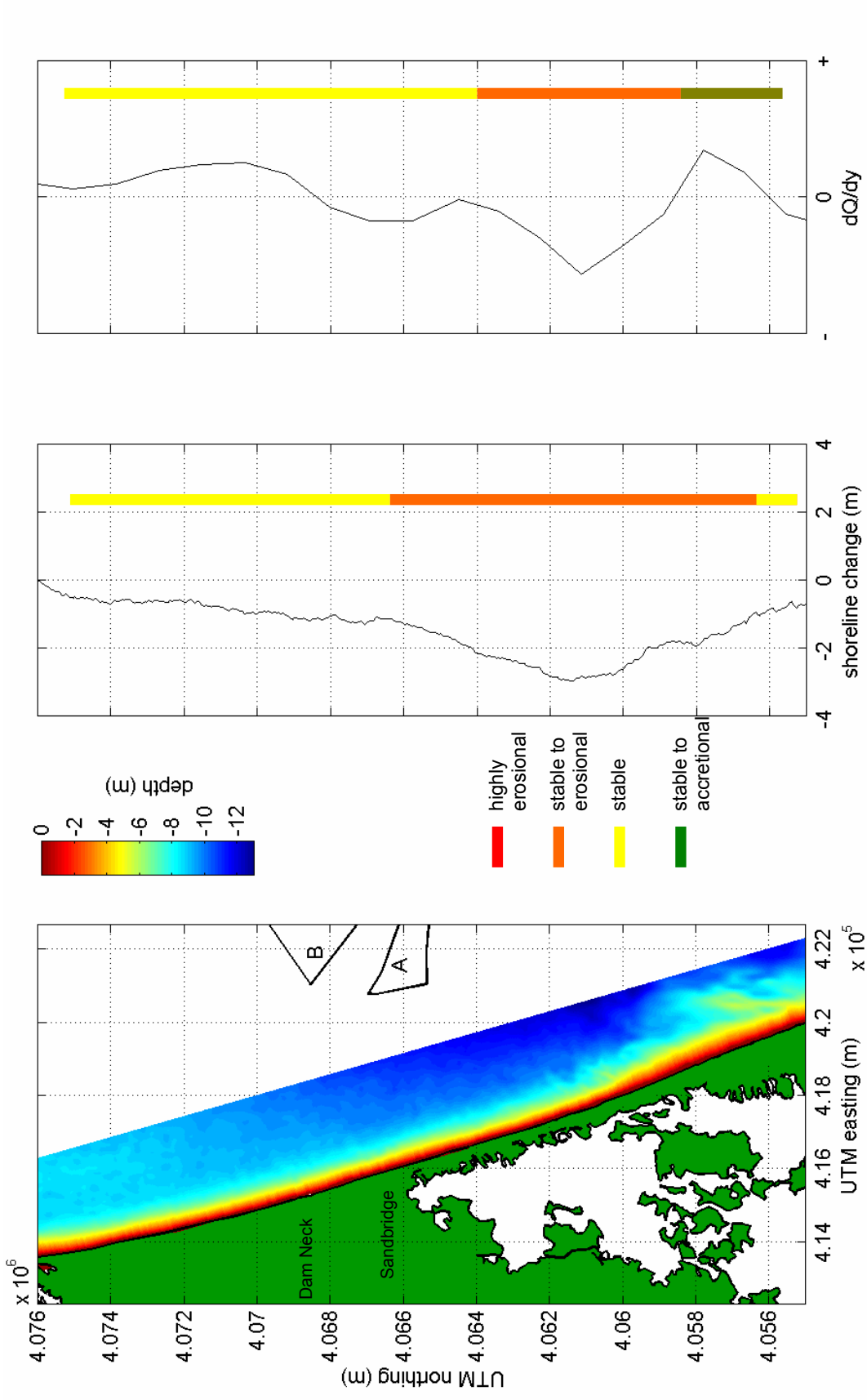

Figure 3-40. Comparison of historical shoreline change and gradient of modeled transport potential (dQ/dy) for the southeastern Virginia shoreline. Color bars indicate whether the shoreline is accretional, stable, or erosional.

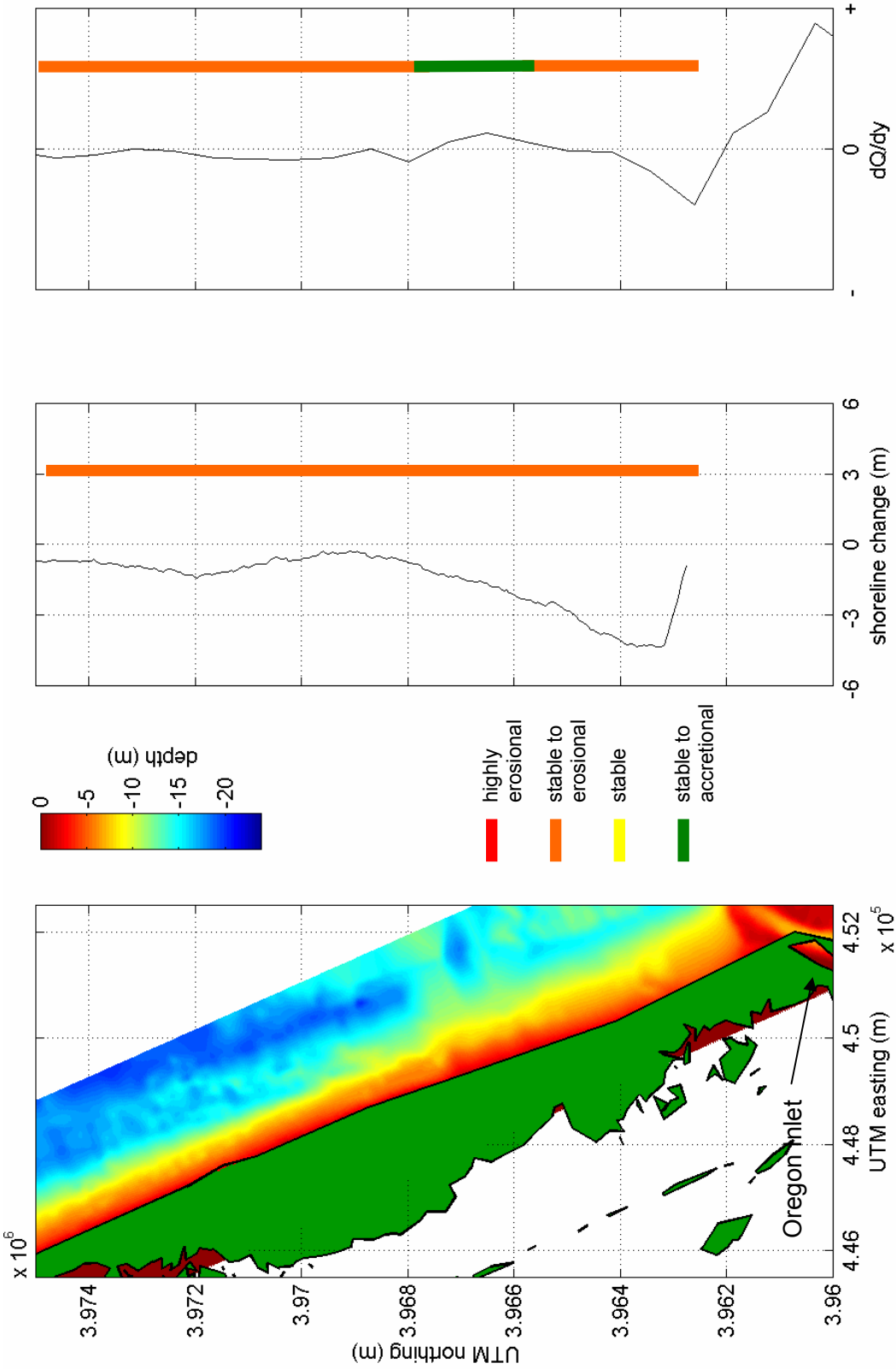

Figure 3-41. Comparison of historical shoreline change and gradient of modeled transport potential (dQ/dy) for the North Carolina shoreline. Color bars indicate whether the shoreline is accretional, stable, or erosional.

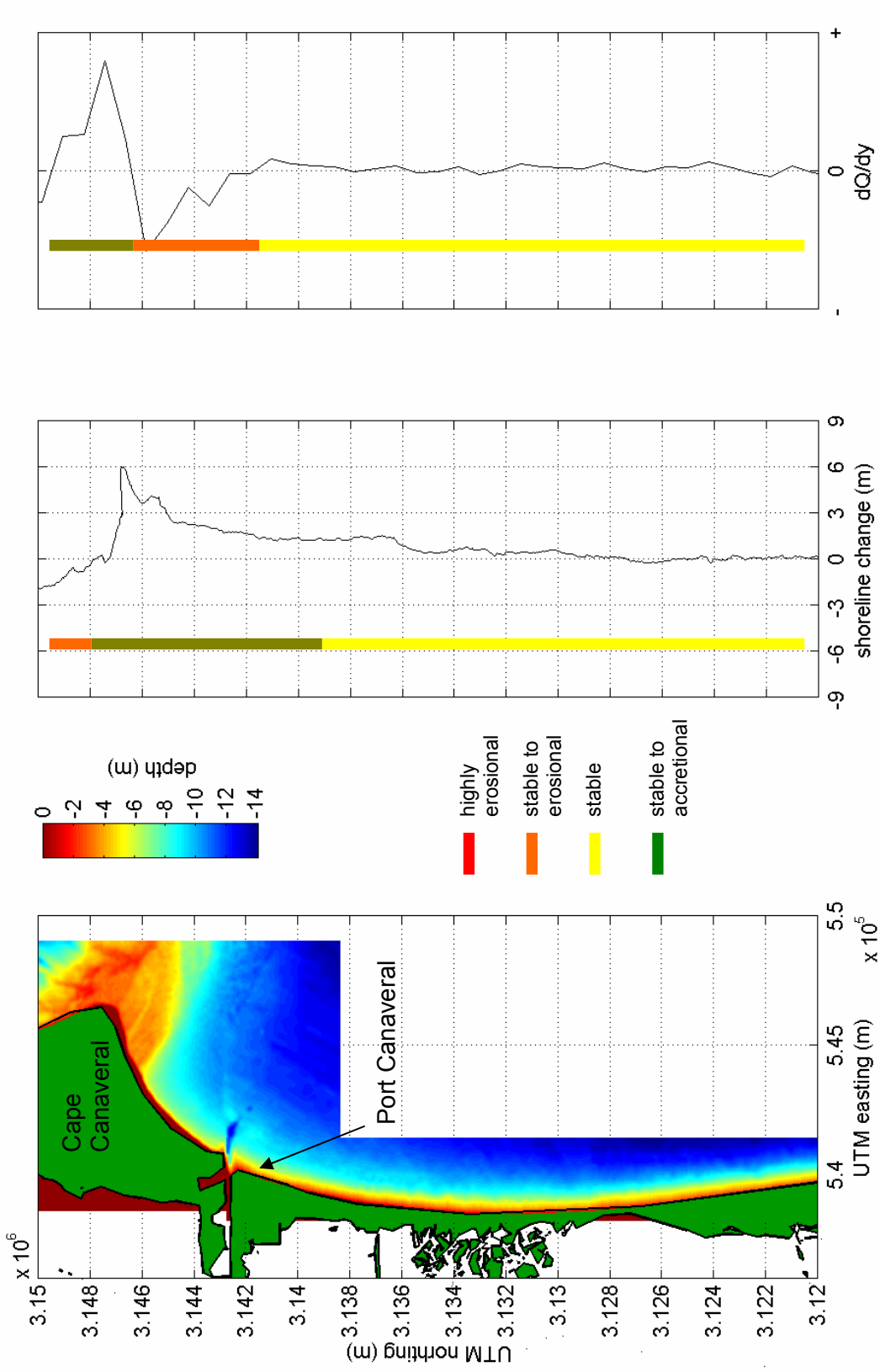

Figure 3-42. Comparison of historical shoreline change and gradient of modeled transport potential (dQ/dy) for the Cape Canaveral shoreline. Color bars indicate whether the shoreline is accretional, stable, or erosional.

(e.g., just south of the cusp of the Cape). Based on the curvature of the shoreline north of Port Canaveral, significant erosion is anticipated immediately south of the cusp of Cape Canaveral (as indicated by the modeled gradient of transport potential). However, shoreline change data indicate substantial accretion in this area. The primary reason for this accretion likely is due to the shoal serving as a sediment source for beaches to the south. This cross-shore transport mechanism is not considered in longshore sediment transport analyses. For shorelines where nearshore shoals exhibit significant diffraction and potentially serve as a sediment source to the beach system, modeled sediment transport potential cannot match observed trends in shoreline change. South of Port Canaveral, away from the influence of the Cape's topographic and bathymetric features, the trends predicted by the sediment transport potential model match well with historical shoreline change.

3.2.2.2 Modeled Transport and Dredging Impacts

To quantitatively assess impacts to coastal processes associated with sand mining, a new approach was developed that considers the spatial (longshore) and temporal variability of local wave climate. This methodology uses similar wave modeling results as those required for two previous analyses (Basco, 1999 and Byrnes, et al., 1999); however, wave modeling is performed for the entire 20-year WIS record as well as five 4-year blocks of the WIS record. In this manner, temporal variations in wave climate are considered relative to average annual conditions. From these wave model runs, sediment transport potential curves are derived for average annual conditions (using the full 20-year WIS record) and each 4-year period (using five 4-year wave records parsed from the full record). Based on this information, the average and standard deviation in calculated longshore sediment transport potential is determined every 200 m along the shoreline. Results of each of the four investigated areas are shown in Figures 3-43 through 3-46.

The purpose of segmenting the wave time series into five 4-year segments was to reduce the number of wave model runs without sacrificing information and to compute a more conservative estimate of wave variability (smaller range) for determining the significance of predicted impacts. Because the evaluation of sediment transport potential was performed to indicate long-term trends and not seasonal variations, the minimum length of wave record needed is one complete year. By grouping the 20-year wave record into 4-year blocks rather than into individual years, a more conservative standard deviation (smaller range) about the mean transport rate was derived. By definition, the standard deviation of a normally distributed variable would be reduced if the number of variables were reduced by grouping the original data.

Assuming the temporal component of sediment transport potential is normally distributed, the suggested criterion for accepting or rejecting a potential borrow site is based on one standard deviation about the mean. If any portion of the sediment transport potential curve associated with a sand mining project exceeds one standard deviation of the natural temporal variability (which incorporates 2/3 of the variability) in sediment transport potential, the site would be rejected. Because the standard deviation of each 4-year period is more realistic for documenting long-term variability than using a 1-year period, the methodology provides a useful indication of sediment transport variability relative to the natural system.

The methodology used to determine impact significance depended on a region's site-specific wave characteristics by considering temporal (inter-annual) and spatial variability in wave conditions. For this reason, the statistical envelope defining the limits of acceptable borrow site impacts varies along a given shoreline. A shoreline that experiences a wide variety of wave conditions (in direction, peak period, and significant wave height) from year to year naturally experiences large variability in sediment transport rates; therefore, the level of acceptable borrow site impacts would be relatively high. Conversely, a shoreline that experiences a limited range of wave conditions cannot accept a high level of borrow site impacts. An offshore site that is dominated by swell conditions from a single narrow direction band would be a good example of this latter case. Because the natural variability in inter-annual shoreline migration changes along the coast, certain portions of the shoreline will be more tolerant of alterations to the wave climate and associated sediment transport patterns. The methodology used to evaluate borrow site impacts provides a reliable quantitative technique for developing acceptable site-specific limits associated with changes in sediment transport potential.

Offshore Southern New Jersey. An illustration of sediment transport potential for existing and post-dredging conditions for the southern New Jersey coastline is plotted with the acceptable limits for post-dredging based on the dredging significance criterion (Figure 3-43). Typically, net transport potential values are around 300,000 m^3/yr to the south, with minimum values occurring in the vicinity of Townsends and Corsons Inlets. Post-dredging changes fall within the limits of the dredging significance criterion envelope, and therefore, the proposed excavation depths would be acceptable in terms of impact on transport patterns in the modeled area. For this section of modeled coastline, the significance criterion envelope is $\pm$10 to 15% of the modeled annualized net transport potential, with values of about $\pm$30% close to Great Egg Harbor Inlet, north of Corsons Inlet. Overall, the significance criterion envelope (representing plus or minus one standard deviation about the mean) for southern New Jersey was relatively narrow compared with the other three modeled areas. This results from the limited variability in inter-annual wave climate along this portion of the New Jersey coast.

Figure 3-43 includes the difference between existing and post-dredging conditions for all borrow sites (cumulative impacts). Generally, the greatest impact is indicated between Townsends and Corsons Inlets, with maximum changes in net transport potential of about -22,000 m^3/yr. In this case, negative transport changes mean that there has been an *increase* in southerly-directed transport. Based on the model results, nearly all of the borrow sites cause an increase in southerly-directed transport with the exception of regions immediately south of Townsends and Corsons Inlets. Because the magnitude of impacts north and south of Corsons Inlet appears to be significantly larger than the impacts south of Townsends Inlet, borrow sites A1 and M8 appear to have greatest influence on transport rates. The impact of offshore site A2 likely is distributed over a longer stretch of shoreline; however, the magnitude is reduced.

Offshore Southeastern Virginia. The results from wave model runs encompassing Sandbridge Shoal are presented in Figure 3-44. Sediment transport potential is directed to the north, with a maximum value of around 300,000 m^3/yr. A nodal point exists in the model output near False Cape. The significance criterion envelope is typically $\pm$20 to 35% of the modeled annualized net transport potential, which is larger than that for the modeled New Jersey shoreline. This means that borrow sites in this area would be able to impact sediment transport by a greater percentage than in the New Jersey simulations, because the sediment transport potential is more variable than it is in New

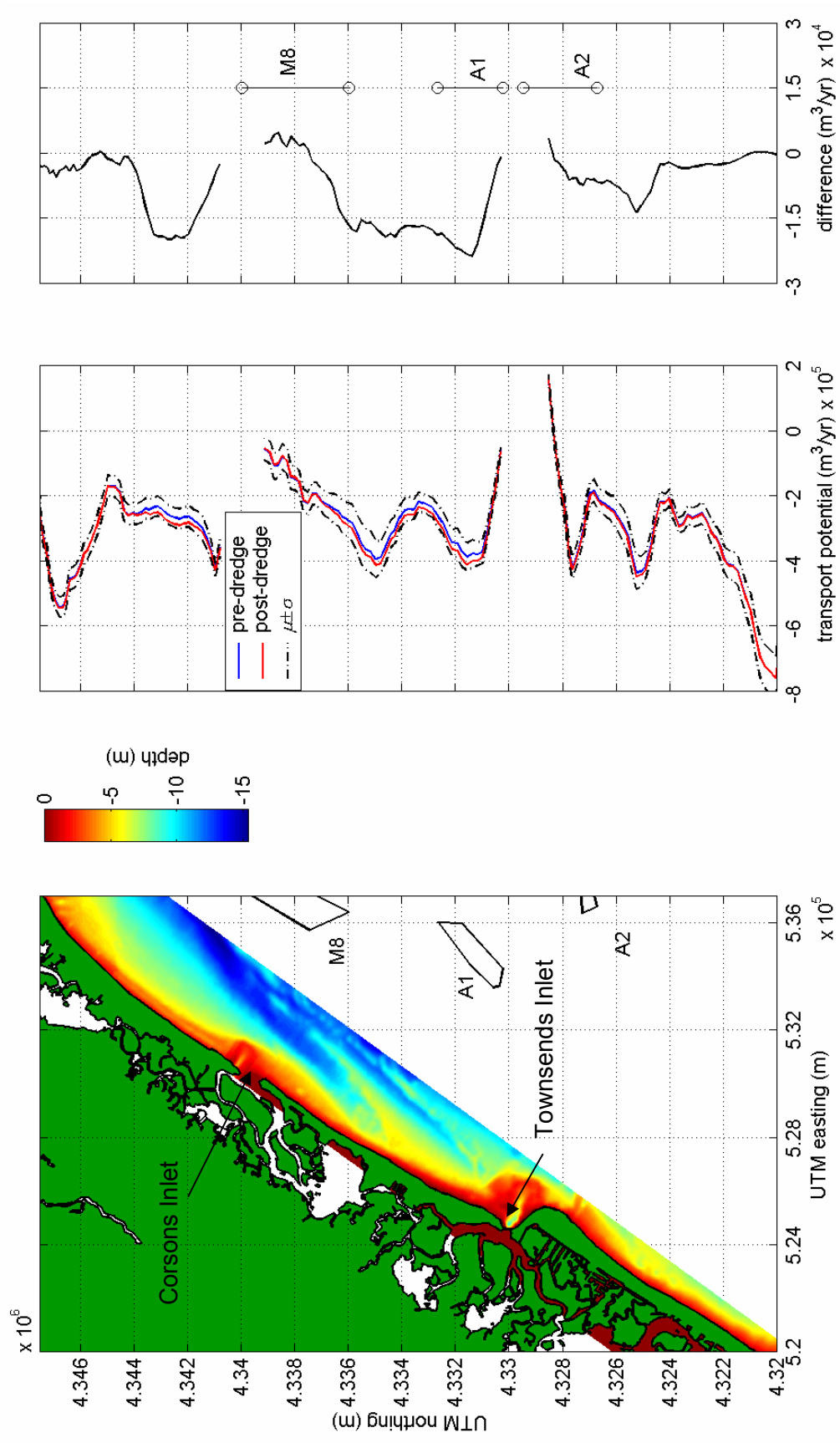

Figure 3-43. Plots of modeled net transport potential and post-dredging change in transport for borrow sites located offshore southern New Jersey. The middle plot shows the dredging significance criterion envelope ($\pm\sigma$), and the plot of the shoreline and bathymetry is given for reference.

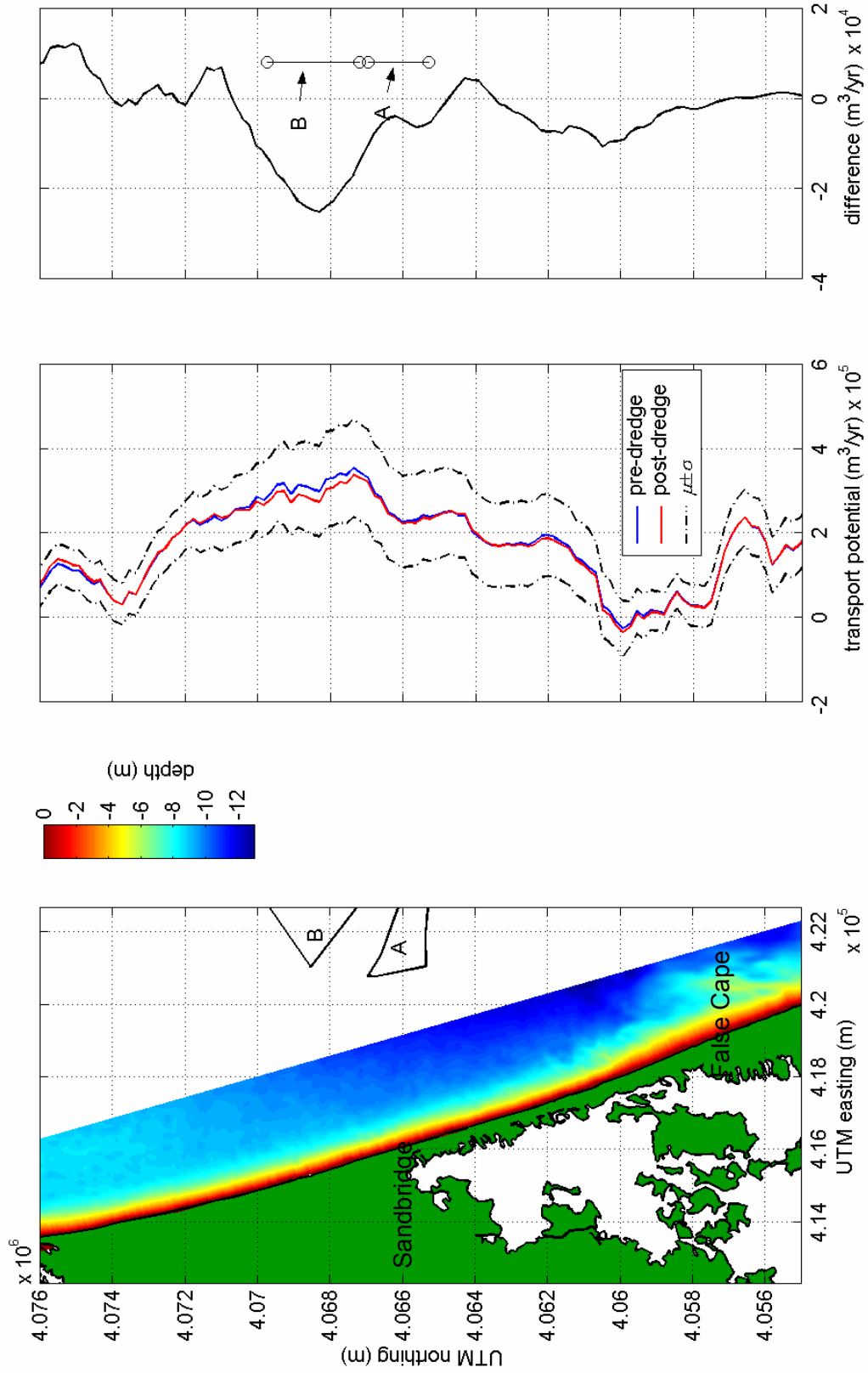

Figure 3-44. Plots of modeled net transport potential and post-dredging change in transport for borrow sites located offshore southeastern Virginia, the middle plot shows the dredging significance criterion envelope ($\pm\sigma$), and the plot of the shoreline and bathymetry is given for reference.

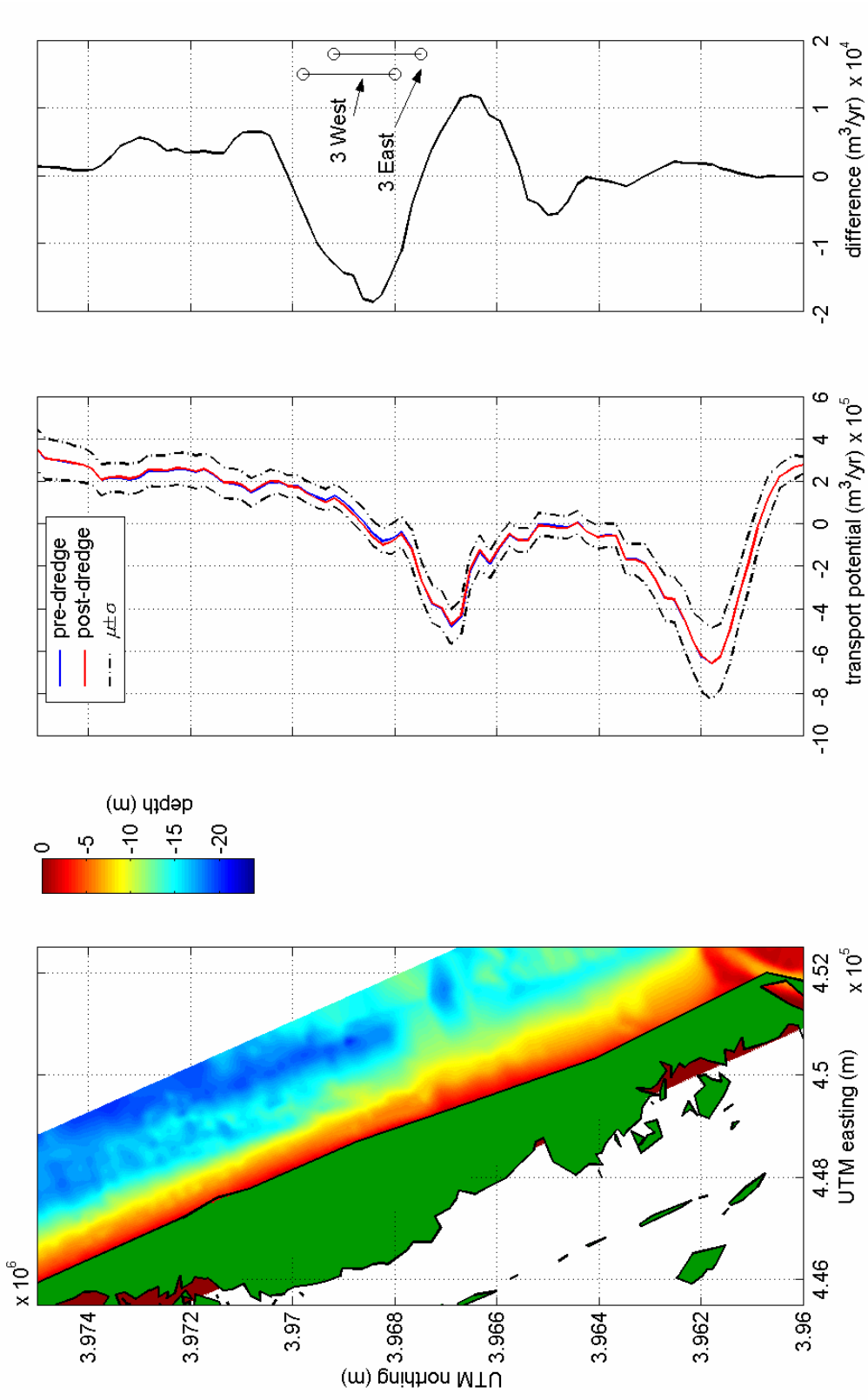

Figure 3-45. Plots of modeled net transport potential and post-dredging change in transport for borrow sites located offshore North Carolina, north of Oregon Inlet. The middle plot shows the dredging significance criterion envelope ($\pm\sigma$), and the plot of the shoreline and bathymetry is given for reference.

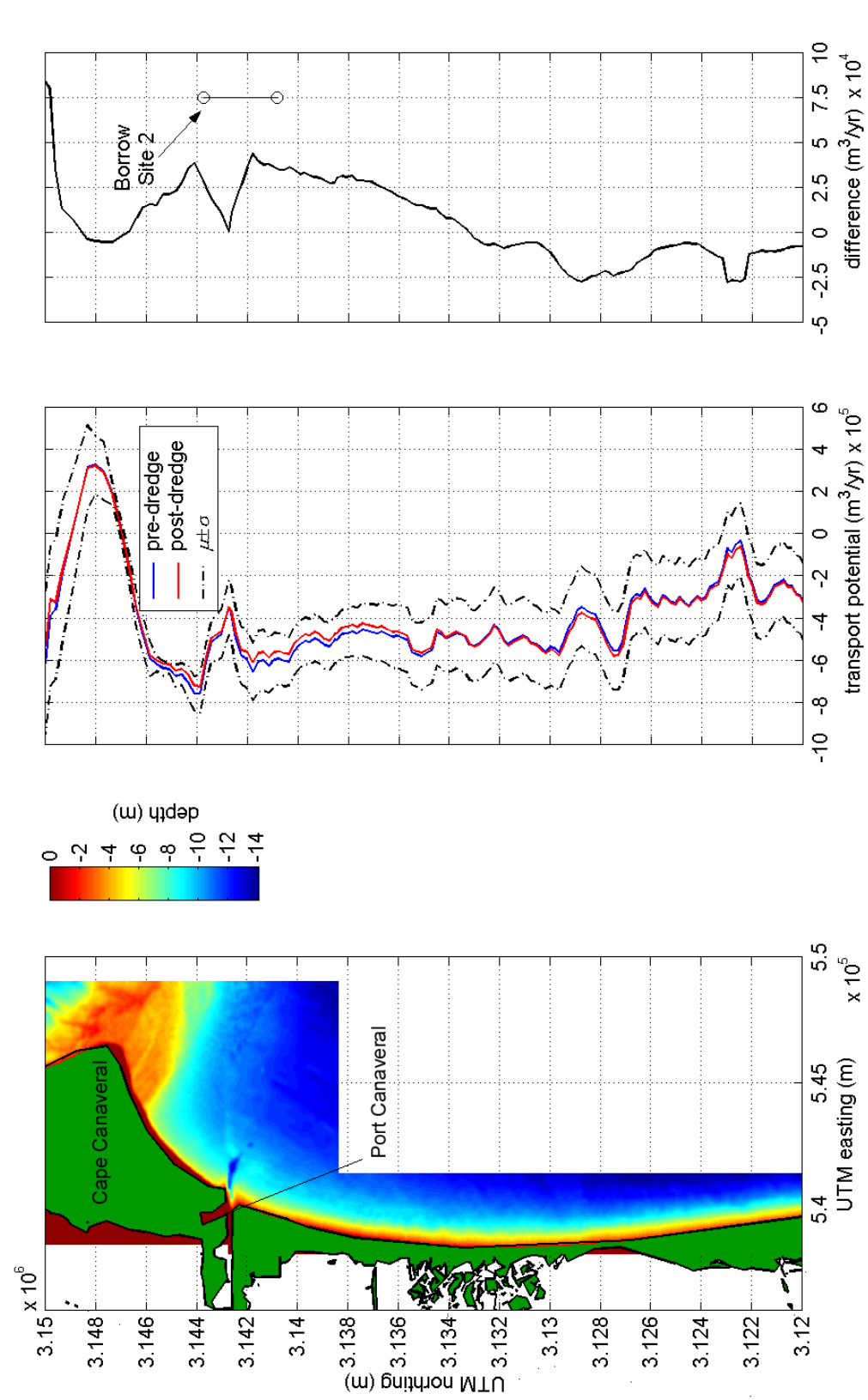

Figure 3-46. Plots of modeled net transport potential and post-dredging change in transport for borrow sites located offshore Florida, near Cape Canaveral. The middle plot shows the dredging significance criterion envelope ($\pm\sigma$), and the plot of the shoreline and bathymetry is given for reference.

Jersey. For the modeled borrow sites (see Table 3-7, with depths not to exceed 50 ft NGVD), change in sediment transport potential for post-dredging conditions falls within the limits of the dredging significance criterion. So again, these proposed excavation depths (and sediment volumes) would be acceptable.

The existing and post-dredging difference plot shows that the greatest impact from the two borrow sites is located in the vicinity of Sandbridge and Dam Neck (approximately 25,000 m^3/yr *decrease* in northerly directed transport), while approximately a 20 km segment of shoreline is affected in total. The shoreline region of borrow site impacts exists within the area of maximum inter-annual variability in sediment transport potential. In this area, the standard deviation of the sediment transport potential variability exceeds ±100,000 cubic meters per year. Based on the difference plot, it is not possible to discern the impacts associated with Sites A and B separately; however, the greatest influence of sand mining at both sites is to decrease northerly-directed littoral drift. Therefore, the region to the north of Dam Neck will have a reduced supply of sand and the region immediately landward of the borrow sites will experience in increase in shoreline stability as a result of the dredging. The magnitude of these anticipated alterations to the local sediment transport regime is within one standard deviation of the natural inter-annual variability.

Offshore North Carolina. Figure 3-45 illustrates model output to estimate the impact of sites 3 East and 3 West offshore North Carolina. North of the inlet, simulated net potential transport is to the north at approximately 250,000 m^3/yr. Gross annualized north and south transport values are about 450,000 m^3/yr and 200,000 m^3/yr, respectively. Closer to the inlet, net transport values are primarily to the south, with largest potential transport values around 600,000 m^3/yr and very little north-directed transport (approaching zero). The dredging significance criterion generally falls within ±30 to 40% of the computed net transport values, suggesting that the transport climate is similar to, but slightly more variable than, the southeastern Virginia example. For the modeled sand excavation conditions (Table 3-7), post-dredging model results fall within the significance criterion envelope, so again the modeled dredging plan would be acceptable.

The plot that presents transport differences between existing to post-dredging conditions at the two modeled sites indicates that the maximum impact from sand dredging at both borrow sites is an approximate 20,000 m^3/yr *increase* in south directed transport. These borrow sites represent the smallest sand mining sites evaluated, with 3 East containing approximately 1,400,000 m^3 and 3 West containing approximately 2,500,000 m^3. Although the borrow sites are relatively small, impacts associated with sand mining in this region are comparable in magnitude to the Dam Neck/Sandbridge Shoal sites described above. This impact magnitude likely is a result of the combined influence of the two borrow sites along a relatively short section of shoreline, where the longshore region of influence is approximately 10 km. A more complete discussion of combined impacts associated with borrow sites in close proximity to each other is presented in Section 4 (Cumulative Effects).

Because the region of impacts associated with the North Carolina borrow sites straddles a sediment transport nodal point, the influence of an *increase* in south-directed transport (between UTM northing 3,967,500 and 3,970,000 m) will reduce the supply of sediment north of this region and increase the amount of sediment leaving this region to the south. Therefore, simulated sand dredging at 3 East and 3 West may generate an

erosion hot spot. However, the magnitude of impacts to sediment transport patterns is anticipated to be small relative to natural inter-annual variability of the local littoral processes.

Offshore Cape Canaveral. Due to the influence of Cape Canaveral and the series of migrating ridges and troughs on Canaveral Shoals, a direct relationship between the observed shoreline change and the longshore gradient in sediment transport potential could not be established. Therefore, the utility of comparing the changes in sediment transport potential associated with sand mining to the natural variability of sediment transport patterns may have limited applicability in the region north of Port Canaveral. This is most clearly illustrated by the change in transport rates at the northern limit of the model grid, where a *decrease* in south-directed transport of 80,000 m^3/yr is predicted. Because the STWAVE model used for analysis does not include the influence of wave diffraction, modeled transport rates in regions influenced by diffraction effects are suspect. For Brevard County, this region influenced by wave diffraction would be north of Canaveral Inlet.

Model output for the region south of Port Canaveral (Brevard County) illustrates that in the area of greatest impact from the borrow site, the significance envelope is approximately ±20% of the mean computed net transport potential (Figure 3-46). The maximum modeled change for post-dredging conditions at the borrow site is about a 40,000 m^3/yr *decrease* in south directed transport, just south of Port Canaveral. The modeled sand excavation volume of 26 MCM is considerably greater than the estimated 3.4 MCM for present beach nourishment requirements in Brevard County (USACE, 1999). Though the modeled difference is within the transport significance envelope, the magnitude of impact resulting from cumulative dredging of the full volume at this site suggests further analysis should be required to ensure that no detrimental impacts would occur.

3.2.2.3 Dredging Impacts at East Coast Sites

To establish useful criteria for estimating impacts of sand mining on the nearshore littoral system, a comparison of sediment transport potential analysis and long-term shoreline change was performed at each of the four sand borrow sites. The analysis provided a quantitative method for determining whether longshore wave-induced transport was responsible for observed shoreline change and whether the long-term shoreline change trends were consistent with the shorter time-period (20-year) sediment transport potential analysis. In general, the comparison indicated that the longshore gradient in computed wave-induced sediment transport followed similar trends as observed long-term shoreline change for nearly all cases. Exceptions occurred at locations where STWAVE modeling was not applicable (areas where wave diffraction was important) or where wave-induced processes may not govern sediment transport (in the vicinity of tidal inlets).

For the southern New Jersey shoreline, erosion and accretion trends are predicted well at all locations, including in the vicinity of tidal inlets. Along the southeastern Virginia coast, model results predict similar trends as observed long-term shoreline change, where much of the coastline is stable or slightly erosional. The location of highest erosion rates is predicted accurately by the modeling analysis. Overall agreement between modeled trends and measured shoreline change also was achieved for the North Carolina coast north of Oregon Inlet. Discrepancies between predicted and

measured results likely are a result of the significant historical migration of Oregon Inlet. Therefore, the peak erosion area determined from the gradient of modeled transport potential, based on 20 years of recent wave information, may be more representative of present conditions than long-term shoreline change (based on more than 100 years of shoreline data). Along the Cape Canaveral coast, STWAVE modeling was not capable of evaluating changes in wave climate resulting from wave diffraction processes across Canaveral Shoals. In addition, these shoals likely serve as a sediment source to the beach in this region. For shorelines where nearshore shoals exhibit significant diffraction and potentially serve as a sediment source to the beach system, modeled sediment transport potential cannot match observed trends in shoreline change. South of Port Canaveral, away from the influence of the Cape's topographic and bathymetric features, the trends predicted by the sediment transport potential model match well with historical shoreline change.

Because modeled longshore gradients in sediment transport potential generally matched the trends in observed shoreline change, wave and sediment transport modeling provided an appropriate basis for evaluating long-term impacts associated with offshore sand mining. The methodology utilized to determine impact significance depended on a region's site-specific wave characteristics, where the method considered temporal (inter-annual) and spatial variability in wave conditions. Because the natural variability in inter-annual shoreline migration changes along the coast, certain portions of a given shoreline naturally will be more tolerant of alterations to the wave climate and associated sediment transport. The methodology used to evaluate borrow site impacts provided a reliable quantitative technique for developing acceptable site-specific limits associated with changes in sediment transport potential.

Based on site-specific analyses for each of the four sites, the impacts associated with dredging at all borrow sites were deemed acceptable. For the southern New Jersey coastline, the significance criterion envelope was typically $\pm$10 to 15% of the modeled annualized net transport potential, with values of about $\pm$30% close to Great Egg Harbor Inlet. Overall, the significance criterion envelope (representing plus or minus one standard deviation about the mean) for New Jersey was relatively narrow compared with the other three modeled areas. This results from limited variability in inter-annual wave climate along the southern New Jersey coast.

For southeastern Virginia and North Carolina coastal regions, the dredging significance criterion envelope generally falls within $\pm$20 to 40% of the computed net transport values. For the modeled sand excavation conditions (Table 3-7), post-dredging model results fall within the significance criterion envelope for both cases, so again the modeled dredging plan would be acceptable. Model output for the region south of Port Canaveral, Florida (Brevard County) illustrates that in the area of greatest impact from the borrow site, the significance envelope is approximately $\pm$20% of the mean computed net transport potential. Again, the modeled impacts in this region associated with potential offshore dredging are well within the significance envelope. However, due to limitations with the wave modeling effort, further analyses would be required to accurately assess impacts caused by dredging for the shoreline north of Port Canaveral.

4.0 CUMULATIVE IMPACTS

The borrow site analyses described in Section 3 document potential impacts associated with large-scale dredging of various offshore borrow areas. As shown in Table 3-6, all borrow sites contain a substantial volume of sand, most in excess of 5,000,000 m^3. Because typical beach nourishment projects require significantly less sand than exists within these borrow sites, it is likely that several dredging events will occur before the entire borrow site is excavated. The analysis in Section 3 assumes that the entire borrow site is excavated at one time; therefore, this analysis provides the cumulative impacts associated with potentially numerous dredging events at a single site.

To evaluate cumulative impacts associated with incremental dredging of a single site and/or the combined effects of dredging borrow sites in the same region, a cumulative assessment strategy was developed. For evaluating cumulative impacts of sand dredging at an offshore borrow site, two types of borrow site configurations were investigated. The first group of cumulative impacts involves the interaction of multiple sites in close proximity, such that they have overlapping areas of shoreline impact. The second grouping of cumulative impacts involves multiple dredging events at a single site.

4.1 SITES IN CLOSE PROXIMITY

An investigation of cumulative impacts resulting from borrow sites in close proximity was performed to determine how potential wave impacts at individual sites may interact to produce additive effects along the coast. The assumption is that net changes in sediment transport patterns along a section of coast, where multiple borrow sites have an overlapping influence, can be evaluated by superimposing individual changes resulting from excavation at each borrow site, as if the other sites in the grouping did not exist.

To determine the validity of the stated assumption, two areas were studied, 1) Sandbridge Shoal, offshore southeastern Virginia, and 2) offshore North Carolina, in the vicinity of Oregon Inlet. At Sandbridge Shoal, the two borrow sites are oriented side-by-side and parallel to the shoreline. An example of wave model output for these sites is given in Figure 4-1, which shows wave height changes between existing and post-dredging conditions. It appears that the two sites have an overlapping influence on offshore wave heights. For offshore North Carolina, sites 3 East and 3 West are oriented front-to-back in a line perpendicular to the shoreline. Wave model output for this simulation illustrates how site 3 East has an area of influence which includes the perimeter of site 3 West (Figure 4-2).

Wave model runs were executed for the wave conditions presented in Section 3.2. However, each borrow site was modeled independently, so that each site's own area of influence could be determined. Sediment transport potential computations also were performed. Figure 4-3 shows the results of model runs for Sandbridge Shoal. Transport potential difference for three modeled cases is shown for Sites A and B modeled individually and for these two sites modeled together. In addition, the sum of the differences computed for Sites A and B alone is included. In this case, the influence on sediment transport potential along the shoreline by these two sites individually is roughly of the same magnitude, which would be expected in a case where the borrow sites are positioned similar distances offshore and are similar in size. Differences resulting from

the two sites modeled together is similar to differences derived by adding the results of the two sites modeled independently (i.e., both methods correlate well). These results suggest that any possible interaction of sites positioned side-by-side is weak.

For sites 3 East and 3 West in North Carolina, Figure 4-4 shows transport potential difference computed for cases similar to the Sandbridge Shoal model runs. In this case, the eastern borrow site has much less influence on transport potential change than the western site, which is located closer to the shoreline. Similar to the southeastern Virginia example, the sum of transport potential difference, computed for model runs at each site modeled separately, correlates well with differences computed using model output from the two sites modeled together. Therefore, for sites positioned front-to-back and perpendicular to the shoreline, interaction between these sites also is limited.

The results from these two cases (Virginia and North Carolina) suggest that borrow sites located in close proximity illustrate additive impacts. Therefore, the influence of multiple sites on sediment transport along a coastline is a simple additive effect, rather than a more complicated non-linear effect or amplification.

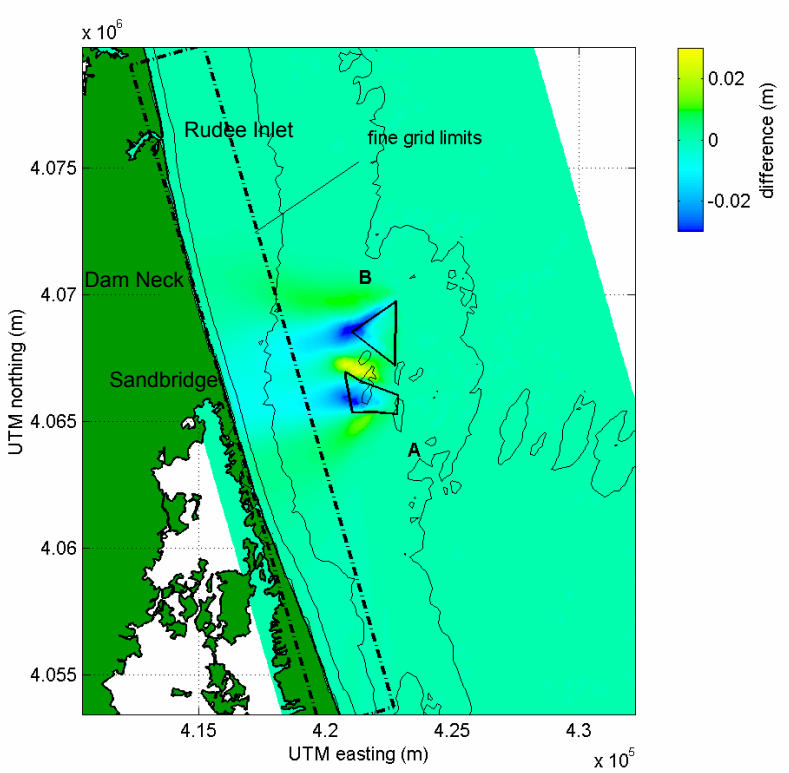

Figure 4-1. Difference plot of wave heights for existing and post-dredging conditions at sites A and B for Sandbridge model wave case 3.

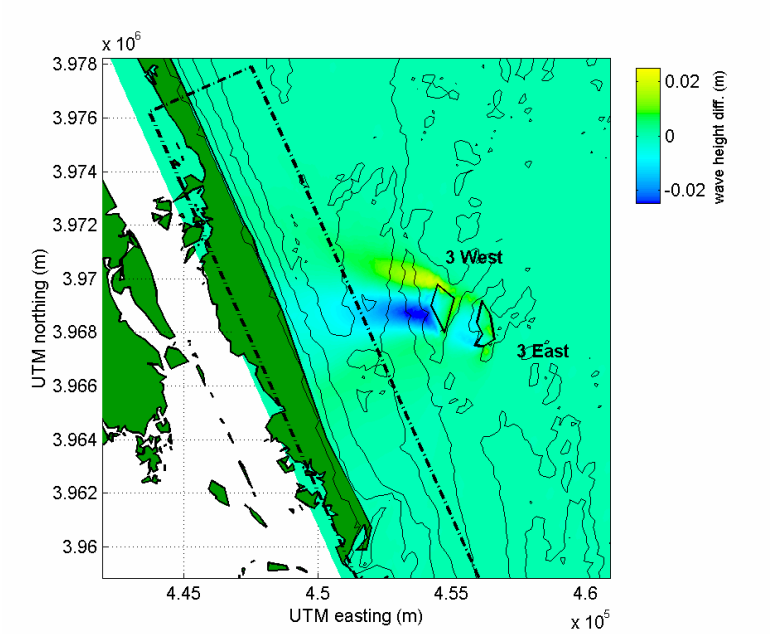

Figure 4-2. Difference plot of wave heights for existing and post-dredging conditions at sites 3 East and 3 West for North Carolina model wave case 4.

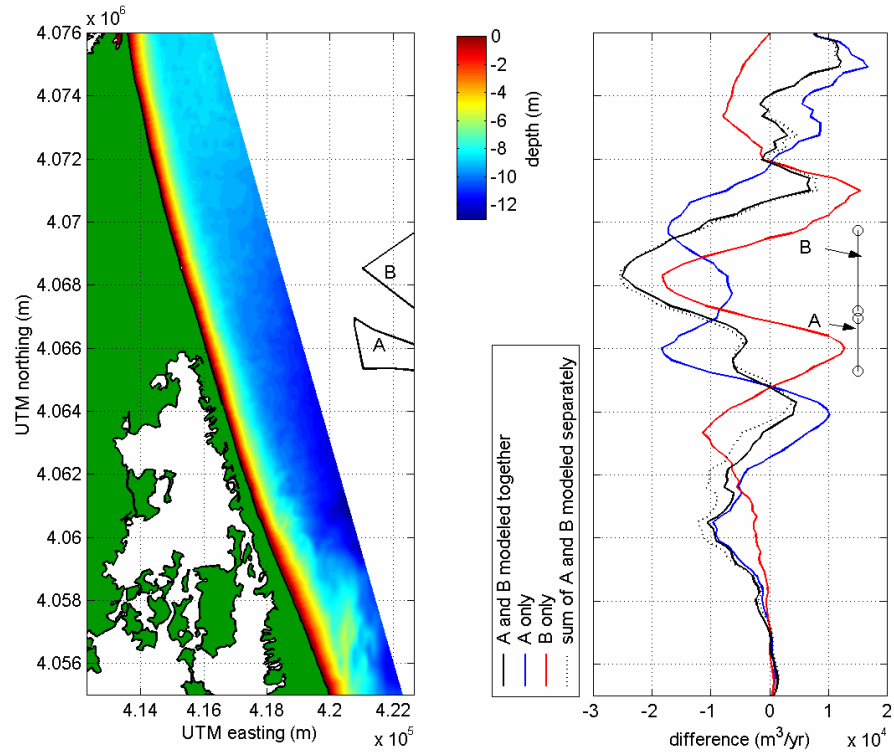

Figure 4-3. Plot of sediment transport potential difference between existing and post-dredging model runs including Sites A and B (southeastern Virginia) modeled together (solid black line) and separately (solid blue and red lines). The sum of transport difference computed for the separate runs of A and B (dotted black line) is presented for comparison with the curve of A and B modeled together (coefficient of determination, r^2=0.970).

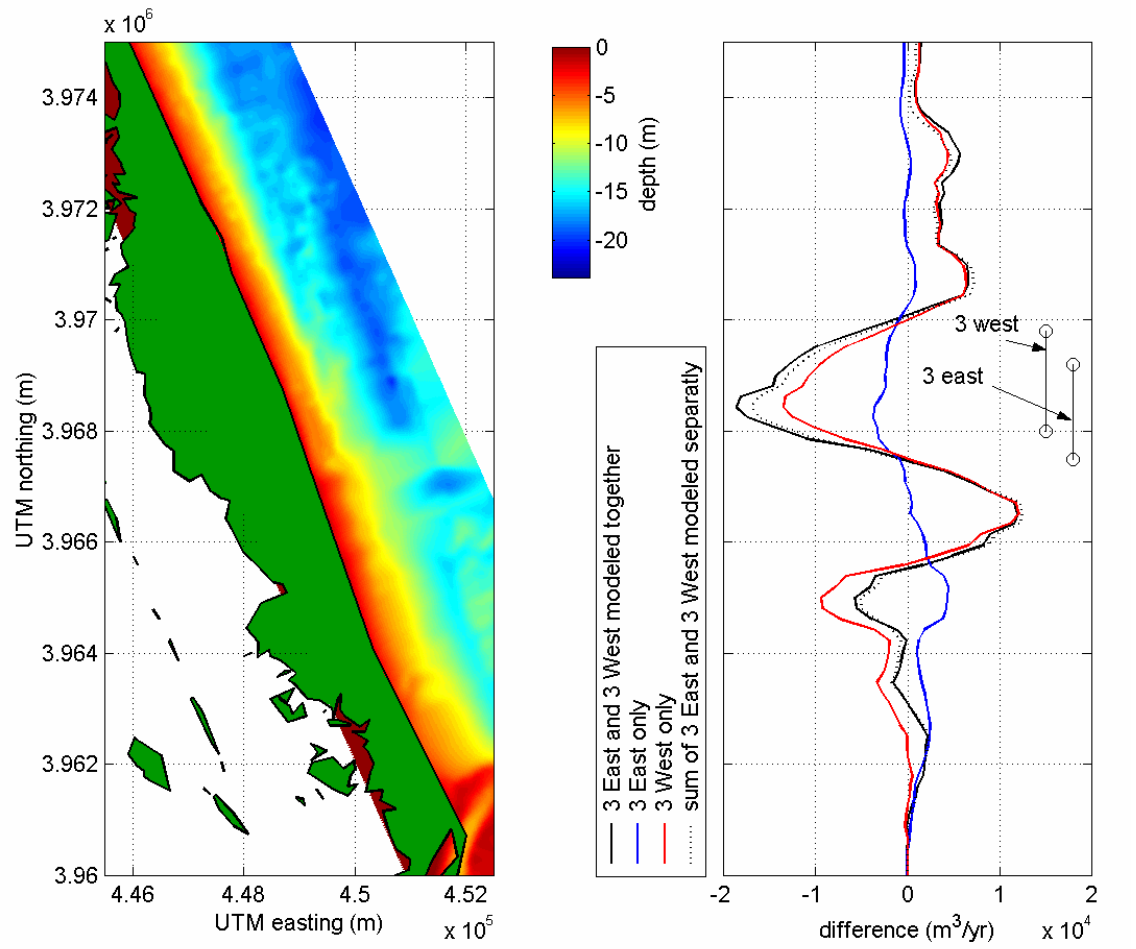

Figure 4-4. Plot of sediment transport potential difference between existing and post-dredging model runs including sites 3 East and 3 West (North Carolina) modeled together (solid black line) and separately (solid blue and red lines). The sum of transport difference computed for the separate runs of 3 East and 3 West (dotted black line) is presented for comparison to the curve of 3 East and 3 West modeled together (coefficient of determination, r^2=0.990).

4.2 MULTIPLE DREDGING EVENTS AT A SINGLE SITE

The second type of cumulative impact analysis evaluated the effect of multiple dredging events at a single site. As a borrow site is excavated to greater depths, the impact that it has on sediment transport along the shoreline will increase. Taken to extreme depths, the magnitude of impacts would be expected to reach some asymptotic value, but how these impacts vary through a range of reasonable depths was the emphasis of this study. In addition, the performance significance criterion established in Chapter 3 was tested to see what depths of excavation the criterion would be violated. Site M8, offshore southern New Jersey, was used in this analysis because the site is positioned close to shore and it has a relatively large perimeter. Therefore, deep excavations at this location would have pronounced (and therefore easily observable) effects on modeled sediment transport patterns at the shoreline.

Model runs were made for several excavated depths at Site M8, including 2, 3, 5, 7, and 9 m. The results of sediment transport potential calculations from these model runs are shown in Figure 4-5. This figure shows transport potential computed for Site M8 alone, without sites A1 and A2 included in the analysis. Included with the plot of transport difference is a shaded area that represents the envelope of maximum change allowed by the impact significance criterion. According to the significance criterion, excavation depths greater than 5 m would not be permitted, as the allowable limit criterion is exceeded along the shoreline south of Corsons Inlet. In this case, borrow site excavations greater than 5 m would be rejected no matter how small a section of shoreline that the significance criterion is exceeded.

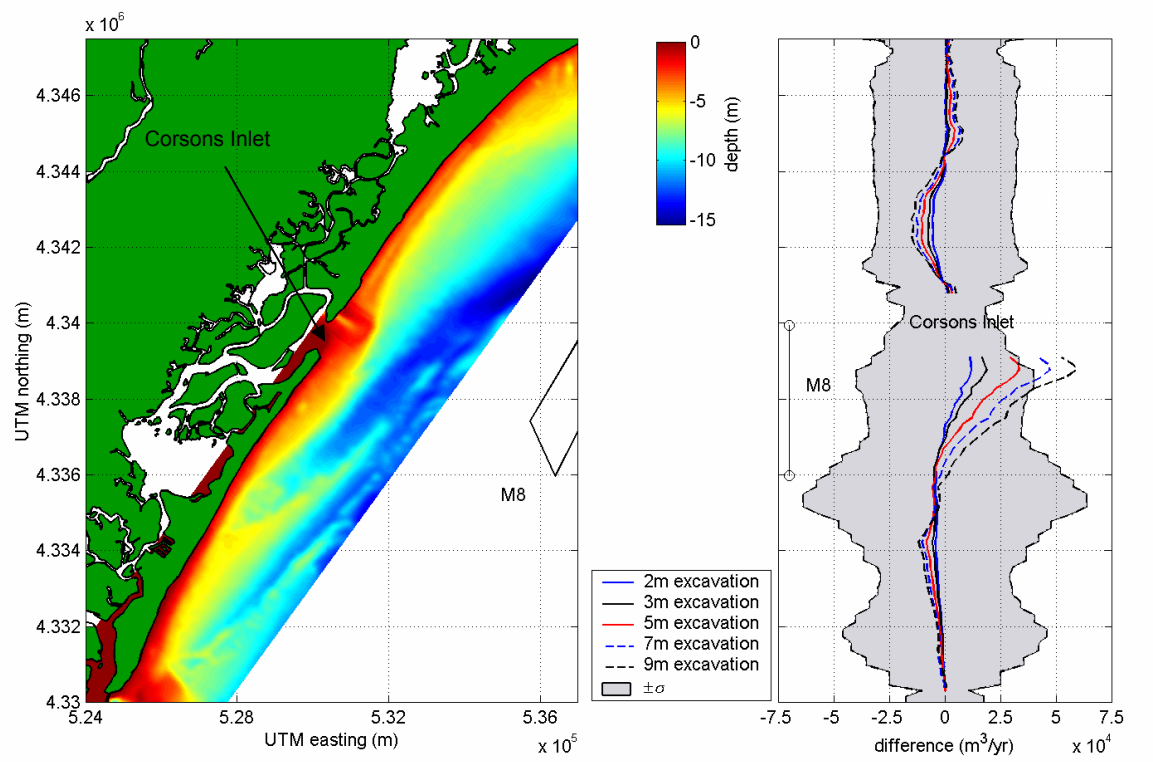

Figure 4-5. Plot of change in sediment transport potential computed for five excavated depths at site M8, offshore Corsons Inlet, New Jersey. The shaded area represents the envelope of maximum transport influence that is allowed by the impact significance criterion.

From the five model runs, change in transport potential is seen to vary linearly with depth of excavation. Figure 4-6 is a plot showing this relationship. The maximum-modeled differences are plotted with a least squares fit of the data. The fit correlates very well with the model data.

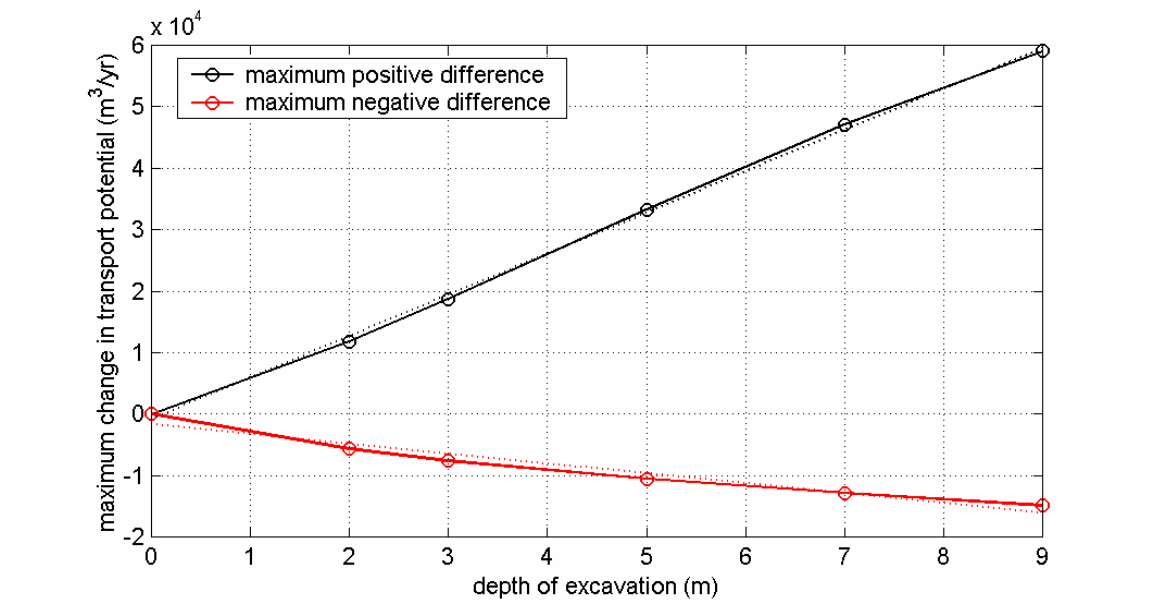

Figure 4-6. Plot of excavation depth *versus* change in modeled sand transport potential. Dotted lines represent linear least squares fits of the model output (for black line r^2=0.999, and for the red line r^2=0.954).

5.0 CONCLUSIONS

A four-phase approach was implemented to assess the potential for negative impacts from alterations to the local wave climate and sediment transport regime associated with offshore sand mining. First, a detailed evaluation of three readily-available, project-tested spectral wave models was conducted to determine the most effective simulation routine for predicting potential wave impacts due to dredging at offshore borrow sites. Second, a standard method was developed to qualify the significance of changes associated with borrow site excavation to determine the influence of borrow site geometry on local wave refraction and sediment transport patterns. The method developed for this study is based on historical wave climate variability, as well as local wave climate changes directly attributable to borrow site excavation. The third phase of the project focused on wave spectra development, wave transformation modeling, and coastal sediment transport calculations. Wave transformation modeling and sediment transport potential calculations were performed for existing and post-dredging bathymetric conditions at four sites along the U.S. East Coast. In addition, a site-specific determination of acceptable limits of borrow site impacts relative to sediment transport potential was determined for each case. The fourth and most significant phase of the project addressed potential cumulative effects of sand dredging from offshore sand borrow sites. These analyses were designed to determine how potential wave impacts at individual sites may interact to produce additive physical environmental effects along the coast.

5.1 WAVE MODEL ASSESSMENT

The primary quantitative technique used to evaluate nearshore processes is wave transformation modeling. Wave models have been developed to numerically solve the equations governing change in wave height and direction (through processes such as refraction, shoaling, and breaking). As better offshore wave data sets have been developed (both wave gauge and hindcast information), wave transformation models have become standard tools for evaluating the nearshore wave climate. The analysis techniques presented in this report involve spectral wave modeling, based primarily on wave hindcast information, combined with standard longshore sediment transport equations to evaluate impacts associated with offshore sand mining.

A comparison of numerical wave transformation models was performed to determine the most appropriate tool for assessing impacts associated with offshore borrow sites. The results of this analysis are shown in Appendix A. STWAVE, REF/DIF S, and SWAN were selected for this comparison because they all are spectral wave models and are easily accessible to the coastal engineering community. Spectral models can simulate real ocean wave conditions, where waves of varying frequency and direction propagate simultaneously through the same physical domain. These models can be described as either action density models, like STWAVE and SWAN, or as propagation models like REF/DIF S. Action density models use the distribution of energy in a spectrum to compute wave transformations, whereas propagation models propagate individual waves through the model domain, each with a different frequency and different initial direction.

Based on this model comparison and other factors, it is recommended that future MMS wave modeling projects use STWAVE. This recommendation is provided because:

- STWAVE is a fully spectral model with an efficient numerical scheme that requires a minimum of computing resources and which has acceptable accuracy when compared to physical model data.
- The USACE is actively updating STWAVE for its own use, and further improvements to the model will be made (e.g., diffraction is currently being added).
- STWAVE is able to compute mean wave angles, which is necessary input in sediment transport modeling, whereas currently available versions of REF/DIF S do not have a rigorous method for mean wave angle computations.
- Though the basic model approach of SWAN is very similar to STWAVE, it has many additional features that are not included in STWAVE. However, these advanced capabilities will not be required in the wave modeling projects for the MMS. Otherwise SWAN offers no performance advantage over STWAVE.

5.2 MANAGEMENT TOOL FOR ASSESSING IMPACT SIGNIFICANCE

To directly assess the impacts of offshore sand mining to coastal wave and sediment transport processes, an approach was developed that considers spatial (longshore) and temporal aspects of the local wave climate. This method uses a similar wave modeling effort as that applied by Basco (1999) and Byrnes et al. (1999); however, wave modeling is performed for the entire 20-year WIS record and five 4-year blocks of the WIS record. As such, temporal variations in wave climate are considered relative to average annual conditions. From these wave model runs, sediment transport potential curves are derived for average annual conditions (based on the full 20-year WIS record) and each 4-year period (based on the five 4-year wave records parsed from the full record). Based on this information, the average and standard deviation in calculated longshore sediment transport potential is determined every 200 m along the shoreline.

Assuming the temporal component of sediment transport potential is normally distributed, the suggested criterion for accepting or rejecting a potential borrow site is based on a range of one standard deviation about the mean. If any portion of the sediment transport potential curve associated with a sand mining project exceeds one standard deviation of the natural temporal variability (which incorporates 2/3 of the variability) in sediment transport potential, the site would be rejected. Although using the standard deviation of each 4-year period is more conservative than using a 1-year period, the methodology provides a useful indication of sediment transport variability relative to the natural system.

As a management tool for the MMS, this methodology provides several advantages over methods previously employed to assess the significance of borrow site impacts. The primary advantages include:

- Observed long-term shoreline change is compared with computed longshore change in sediment transport potential. Close comparison between these two curves indicates that longshore sediment transport potential calculations are appropriate for assessing long-term natural change. Therefore, this methodology has a model-independent component (observed shoreline change) used to ground truth the model results.

- The method is directly related to sediment transport potential and associated shoreline change. Therefore, impacts associated with borrow site excavation can be directly related to their potential influence on observed coastal processes (annualized variability in shoreline position).
- Site-specific temporal variability in wave climate and sediment transport potential is calculated as part of the methodology. For sites that show little natural variability in inter-annual wave climate, allowable coastal processes impacts associated with borrow site dredging similarly would be limited, and *vice versa*. In this manner, the inter-annual temporal component of the natural wave climate is a major component in the determination of impact significance.
- Similar to methodologies incorporated in previous MMS studies, the longshore spatial distribution of borrow site impacts is considered. However, the allowable limit of longshore sediment transport variability is computed from the temporal component of the analysis. Therefore, the final results of this analysis provide a spatially-varying envelope of allowable impacts in addition to the modeled impacts directly associated with borrow site excavation. The methodology accounts for spatial and temporal variability in wave climate, as well as providing a defensible means of assessing significance of impacts relative to site-specific conditions.

5.3 WAVE AND SEDIMENT TRANSPORT ANALYSIS

Spectral wave input for STWAVE model runs performed for each of the study areas was developed using WIS hindcast data for borrow sites offshore southern New Jersey, Dam Neck/Sandbridge Beach (Virginia), Dare County North Carolina, and Cape Canaveral (Florida). Alternatively, for the Sandbridge Shoal area offshore southeastern Virginia, a five-year spectral wave data record from an offshore buoy maintained by the National Data Buoy Center (NDBC) was used to develop model input spectra. The NDBC data were used over available WIS data for southeastern Virginia because the buoy record was adequately long and represented actual long-term wave conditions in the area. Along with input spectra, bathymetry grids were developed for existing and post-dredging scenarios. For each of the four modeled areas, two coarse grids were developed that have the same geographical coverage and differ only by modifications to bathymetry in the borrow area. The maximum cumulative dredged volumes and mean depths for the modeled borrow sites for each region are shown in Table 3-6.

Overall, post-dredging wave model output for the four study sites illustrates reduced wave heights landward of borrow sites and increased wave heights at the longshore limits of the borrow site. This effect is more pronounced for cases with larger wave heights and longer periods. As waves propagate across a borrow site (deeper water than the surrounding area), wave refraction bends waves away from the center of the borrow site and toward the shallower edges. The net effect is to create a shadow zone of reduced wave energy immediately landward of the borrow site and a zone of increased wave energy updrift and downdrift of the borrow site. The effect of this redirected wave energy is to alter nearshore wave patterns responsible for longshore sediment transport.

By developing average annual sediment transport potential curves from wave modeling results, the influence of borrow site excavation on nearshore sediment transport quantitatively can be quantified. Comparisons of average annual sediment transport potential were performed for existing and post-dredging conditions to indicate

the relative impact of dredging to longshore sediment transport processes. Sediment transport potential is a useful indicator of shoreline impacts caused by offshore borrow sites because the computations include the borrow site influence on wave height and direction.

5.4 APPLICATION OF MANAGEMENT TOOL

To establish useful criteria for estimating impacts of sand mining on the nearshore littoral system, a comparison of sediment transport potential analysis and long-term shoreline change was performed at each of the four sand borrow sites. The analysis provided a quantitative method for determining whether longshore wave-induced transport was responsible for observed shoreline change and whether the long-term shoreline change trends were consistent with the shorter time-period (20-year) sediment transport potential analysis. In general, the comparison indicated that the longshore gradient in computed wave-induced sediment transport followed similar trends as observed long-term shoreline change for nearly all cases. Exceptions occurred at locations where STWAVE modeling was not applicable (areas where wave diffraction was important) or where wave-induced processes may not govern sediment transport (in the vicinity of tidal inlets).

For the southern New Jersey shoreline, erosion and accretion trends are predicted well at all locations, including in the vicinity of tidal inlets. Along the southeastern Virginia coast, model results predict similar trends as observed long-term shoreline change, where much of the coastline is stable or slightly erosional. The location of highest erosion rates is predicted accurately by the modeling analysis. Overall agreement between modeled trends and measured shoreline change also was achieved for the North Carolina coast north of Oregon Inlet. Discrepancies between predicted and measured results likely are a result of the significant historical migration of Oregon Inlet. Along the Cape Canaveral coast, STWAVE modeling was not capable of evaluating changes in wave climate resulting from wave diffraction processes across Canaveral Shoals. In addition, these shoals likely serve as a sediment source to the beach in this region. South of Port Canaveral, away from the influence of the Cape's topographic and bathymetric features, the trends predicted by the sediment transport potential model match well with historical shoreline change.

Because modeled longshore gradients in sediment transport potential generally matched the trends in observed shoreline change, wave and sediment transport modeling provided an appropriate basis for evaluating long-term impacts associated with offshore sand mining. The methodology utilized to determine impact significance depended on a region's site-specific wave characteristics, where the method considered temporal (inter-annual) and spatial variability in wave conditions. Because the natural variability in inter-annual shoreline migration changes along the coast, certain portions of a given shoreline naturally will be more tolerant of alterations to the wave climate and associated sediment transport. The methodology used to evaluate borrow site impacts provided a reliable quantitative technique for developing acceptable site-specific limits associated with changes in sediment transport potential. Based on site-specific analyses for each of the four sites, the impacts associated with dredging at all borrow sites were deemed acceptable. However, due to limitations with the wave modeling effort, further analyses would be required to accurately assess impacts caused by dredging for the shoreline north of Port Canaveral.

5.5 CUMULATIVE EFFECTS

To evaluate cumulative impacts associated with incremental dredging of a single site and/or the combined effects of dredging borrow sites in the same region, a cumulative assessment strategy was developed. For evaluating cumulative impacts of sand dredging at an offshore borrow site, two types of borrow site configurations were investigated. The first group of cumulative impacts involves the interaction of multiple sites in close proximity, such that they have overlapping areas of shoreline impact. The second grouping of cumulative impacts involves multiple dredging events at a single site.

For the analysis of borrow sites in close proximity to each other, two case studies were evaluated: 1) Sandbridge Shoal, offshore southeastern Virginia, and 2) offshore North Carolina, in the vicinity of Oregon Inlet. At Sandbridge Shoal, the two borrow sites are oriented side-by-side and parallel to the shoreline. For offshore North Carolina, sites 3 East and 3 West are oriented front-to-back in a line perpendicular to the shoreline. To evaluate the influence of individual borrow sites relative to the combined influence of both borrow site excavations, wave model runs were performed for cases where each borrow site was excavated individually and both borrow sites were excavated in a single event. Annual sediment transport calculations were then performed for each wave modeling scenario. Superimposing the effects of individual borrow site excavations onto the sediment transport potential curve developed from the combined excavation model run was used as the basis for comparison. The results from these two cases (Virginia and North Carolina) suggest that borrow sites located in close proximity illustrate additive impacts. Therefore, the influence of multiple sites on sediment transport along a coastline is a simple additive effect, rather than a more complicated non-linear effect or amplification.

The second type of cumulative impact analysis evaluated the effect of multiple dredging events at a single site. As a borrow site is excavated to greater depths, the impact that it has on sediment transport along the shoreline will increase. Taken to extreme depths, the magnitude of impacts would be expected to reach some asymptotic value, but how these impacts vary through a range of reasonable depths was the emphasis of this study. In addition, the performance significance criterion established in Chapter 3 was tested to see what depths of excavation the criterion would be violated. Site M8, offshore southern New Jersey, was used in this analysis because the site is positioned close to shore and it has a relatively large perimeter. Therefore, deep excavations at this location would have pronounced (and therefore easily observable) effects on modeled sediment transport patterns at the shoreline. From the five model runs, change in transport potential varied linearly with depth of excavation.

6.0 REFERENCES

Basco, D.R., 1999. A methodology and criteria to assess the impacts of sand volume removed in federal waters on the nearshore wave climate. Coastal Engineering Centre, Old Dominion University, Norfolk, VA.

Battjes, J.A. and J.P. Janssen, 1978. Energy loss and set-up due to breaking of random waves. Proc. 23rd Int. Conf. Coastal Engineering, ASCE, pp. 569-587.

Bretschneider, C.L., 1968. Significant waves and wave spectrum. Ocean Industry, pp. 40-46.

Byrnes, M.R. and M.W. Hiland, 1994. Compilation and analysis of shoreline and bathymetry data (Appendix B). In: N.C. Kraus, L.T. Gorman, and J. Pope (editors), Kings Bay Coastal and Estuarine Monitoring and Evaluation Program: Coastal Studies. Technical Report CERC-94-09, Coastal Engineering Research Center, Vicksburg, MS, p. B1-B90.

Byrnes, M.R. and N.C. Kraus, 1999. Regional sediment transport patterns adjacent to Canaveral Harbor, Florida. In: N.C. Kraus and W.G. McDougal (editors), Coastal Sediments '99, American Society of Civil Engineers, New York, NY, pp. 750-760.

Byrnes, M.R., R.M. Hammer, B.A. Vittor, J.S. Ramsey, D.B. Snyder, K.F. Bosma, J.D. Wood, T.D. Thibaut, and N.W. Phillips, 1999. Environmental Study of Identified Sand Resource Areas Offshore Alabama: Volume I: Main Text, Volume II: Appendices. U.S. Department of the Interior, Minerals Management Service, International Activities and Marine Minerals Division (INTERMAR), Herndon, VA. OCS Report MMS 99-0052, 326 pp. + 132 pp. appendices.

Byrnes, M.R., R.M. Hammer, B.A. Vittor, J.S. Ramsey, D.B. Snyder, J.D. Wood, K.F. Bosma, T.D. Thibaut, N.W. Phillips, 2000. Environmental Survey of Potential Sand Resource Sites: Offshore New Jersey. U.S. Department of the Interior, Minerals Management Service, International Activities and Marine Minerals Division (INTERMAR), Herndon, VA. OCS Report MMS 2000-052, Volume I: Main Text 380 pp. + Volume II: Appendices 291 pp.

Byrnes, M.R., R.M. Hammer, B.A. Vittor, J.S. Ramsey, D.B. Snyder, J.D. Wood, T.D. Thibaut, N.W. Phillips, 2001. Collection Of Environmental Data Within Sand Resource Areas Offshore North Carolina And The Implications Of Sand Removal For Coastal And Beach Restoration. U.S. Department of the Interior, Minerals Management Service, International Activities and Marine Minerals Division (INTERMAR), Herndon, VA. OCS Report MMS 2000-056, Volume I: Main Text + Volume II: Appendices.

Dean, R.G., 1977. Equilibrium beach profiles: U.S. Atlantic and Gulf coasts. Dept of Civil Engineering, Ocean Engineering Rept. No. 12, Univ. of Delaware, Newark, DE.

Goda, Y., 1985. Random Seas and Design of Maritime Structures. University of Tokyo Press, Tokyo, Japan.

Hammer, R.M., B.J. Balcom, M.J. Cruickshank, and C.L. Morgan, 1993. Synthesis and Analysis of Existing Information Regarding Environmental Effects of Marine Mining. Final Report by Continental Shelf Associates, Inc. for the U.S. Department of the Interior, Minerals Management Service, Office of International Activities and Marine Minerals, Herndon, VA, OCS Study MMS 93-0006, 392 pp.

Hoffman, C.W., 1998. Preliminary Assessment of Potential Sand Resource Areas Offshore of Nags Head, Kitty Hawk, and Kill Devil Hills, North Carolina. North Carolina Geological Survey, Raleigh, NC, 12 pp.

Inman, D.L. and R. Dolan, 1989. The Outer Banks of North Carolina: Budget of sediment and inlet dynamics along a migrating barrier system. Journal of Coastal Research, 5(2): 193-237.

Jensen, R.E., 1983. "Methodology for the calculation of a shallow-water wave climate." WIS Report 8, U.S. Army Engineer Waterways Experiment Station, Vicksburg, MS.

Kamphuis, J.W., 1990. Alongshore sediment transport rate. Proc. 22nd Coastal Engineering Conference, ASCE.

Kimball, S.M. and J.K. Dame, 1989. Geotechnical Evaluation of Sand Resources on the Inner Shelf of Southern Virginia. Final Report to the City of Virginia Beach, Two Volumes. Virginia Institute of Marine Science, College of William and Mary, Gloucester Point, VA.

Kimball, S.M., J.K. Dame, and C.H. Hobbs, 1991. Investigation of Isolated Sand Shoals on the Inner Shelf of Southern Virginia. Final Contract Report. Virginia Institute of Marine Science, College of William and Mary, Gloucester Point, VA, 73 pp. plus Appendices.

Kraus, N.C., M.R. Byrnes, and A.L. Lindquist, 1999. Coastal processes assessment for Brevard County, Florida, with special reference to test plaintiffs. Technical Report CHL-99-6, U.S. Army Engineer Waterways Experiment Station, Vicksburg, MS.

McKinney, T.G., W.L. Stubblefield, and D.J.P. Swift, 1974. Large-scale current lineations, central New Jersey shelf: Investigations by sidescan sonar. Marine Geology, 17: 79-102.

Mitsuyasu, H. et al., 1975. Observation of the directional spectrum of ocean waves using a cloverleaf buoy. Journal of Physical Oceanography, 5(4), 750-760.

National Ocean Service, 1998. Geophysical data system for hydrographic survey data. Version 4.0, National Ocean Service, Washington, DC.

Rosati, J.D., and N.C. Kraus, 1991. Practical Considerations in Longshore Transport Calculations. CETN II-24, U.S. Army Engineer Waterways Experiment Station, Coastal and Hydraulics Laboratory, Vicksburg, MS, 6 pp.

Smith, J.M., D.T. Resio, and A.K. Zundel, 1999. STWAVE: Steady-state spectral wave model. Instruction Report CHL-99-March 1999, U.S. Army Engineer Waterways Experiment Station, Vicksburg, MS.

Svendson, I.A., and I.G. Jonsson, 1976. Hydrodynamics of Coastal Regions. Technical University of Denmark, 285 pp.

Swift, D.J.P., J.W. Kofoed, F.P. Salsbury, and P. Sears, 1972. Holocene evolution of the shelf surface, central and southern Atlantic shelf of North America. In: D.J.P. Swift, D.B Duane, and O.H. Pilkey (editors), Shelf Sediment Transport: Process and Pattern. Dowden Hutchinson, and Ross. Stroudsburg, PA, p. 499-575.

USACE, 1984. Shore Protection Manual. U.S. Army Engineer Waterways Experiment Station, Coastal Engineering Research Center, Vicksburg MS.

USACE, 1999. Final Environmental Assessment and Finding of No Significant Impact, Canaveral Shoals Borrow Area II. USACE-Jacksonville District, Jacksonville, FL, 13 pp.

Williams, S.J., 1987. Geological Framework and Sand Resources of Quaternary Deposits Offshore Virginia, Cape Henry to Virginia Beach. U.S. Geological Survey Open-File Report 87-667, 60 pp.

COMPARISON OF NUMERICAL SPECTRAL WAVE TRANSFORMATION MODELS FOR EVALUATING THE PHYSICAL ENVIRONMENTAL IMPACTS OF OFFSHORE SAND MINING

by Sean W. Kelley
John S. Ramsey
Mark R. Byrnes

Applied Coastal Research and Engineering, Inc.
766 Falmouth Road, Building A, Unit 1C
Mashpee, MA 02649

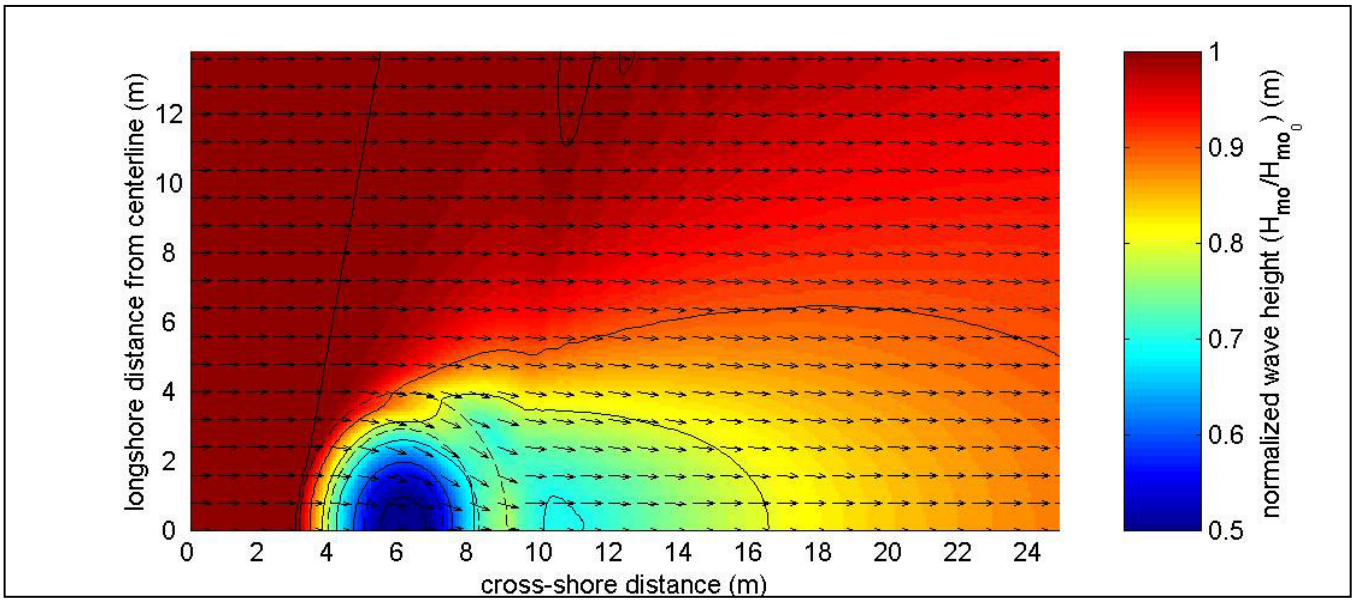

Technical Report – October 1999

Prepared for: U.S. Department of the Interior
Minerals Management Service
Office of International Activities and
Marine Minerals (INTERMAR)
381 Elden Street, MS 4030
Herndon, VA 22070

TABLE OF CONTENTS

Chapter **Page**

LIST OF FIGURES

Figure **Page**

Figure **Page**

LIST OF TABLES

Table **Page**

1. Introduction

There are currently several nearshore wave transformation models available for use in practical engineering and research problems. Generally, these models differ greatly with regard to the basic modeling approach, the selection of model inputs, as well as user control over the formulation of the model. For this initial study, three models were selected for comparison: REF/DIF S v1.2 (Combined Refraction/Diffraction Model for Spectral Wave Conditions) by Kirby and Özkah (1994), STWAVE v2 (Steady State Spectral Wave Model) by Smith, Resio, and Zundel (1999), and SWAN v30.74 (Simulation of Waves Nearshore) by Ris *et al.* (1998).

One key factor in selecting these particular models is their current use and acceptance by the coastal engineering community. It is also important that the model computations utilize wave spectra, which is a statistical representation of a measured wave field. A two-dimensional wave spectrum describes a random wave field as a distribution of wave energy in terms of frequency and direction. A wave spectrum can be thought of as describing a collection of several individual monochromatic wave trains, with varying wave height and direction of travel.

For the purposes of the MMS Offshore Sand Resources Program, a single wave transformation model should be selected for the sake of consistency throughout the course of program development. Ultimately, the selection of a wave model for this work should be based upon model accuracy in predicting wave transformation from federally controlled offshore waters into the nearshore. Accuracy of the model is required to assess the impact of potential borrow sites on the wave climate at the coastline, and the resulting transport of sediment along the coast. The selection of a model should take into account the ease of model set-up and use to assist in quickly generating future analyses of potential coastal impacts from real borrow sites, as required by the MMS for program implementation.

A comparison of model results for an area of open coastline is presented, showing the magnitude of difference between model simulations. This discussion also includes the differences in computational resources necessary to achieve similar results from each model.

2. General Modeling Approach

Major features and limitations of each model are presented in the following discussion. First, basic assumptions used in the formulation of each model are presented. Later, a more detail discussion concerning modeling of some specific phenomena, such as wave breaking criteria included in each model, is presented.

2.1 STWAVE

Developed by the U.S. Army Corps of Engineers (USACE) Waterways Experiment Station (WES), STWAVE v2.0 is a steady state, spectral wave transformation model, based on a form of the wave action balance equation of Jonsson (1990). A wave *action* spectrum is the product of the interaction between a wave *energy* spectrum and a current field. STWAVE is able to simulate wave refraction and shoaling induced by changes in bathymetry and by wave interactions with currents. The model includes wave breaking models based on water depth and wave steepness. Other features of

STWAVE include wind induced wave growth, and influences of wave white capping on the distribution and dissipation of energy in the wave spectrum.

STWAVE is most applicable to wave transformation problems where the following assumptions can be made:

Mild bottom slope and negligible wave reflection. STWAVE can only propagate waves within a sector of a circle that includes ±87.5° from the cross-shore axis of the grid, where the 0 deg axis points in the onshore direction. Generally, this limitation is not important for applications involving areas of open coastline, with bathymetric contours that are for the most part parallel, as is the case in this study. Wave reflection caused by sharp gradients in bottom contours or from coastal structures is not accounted for in the model, even for waves reflected in directions within the ±87.5° sector of model propagation. This assumption too is valid for offshore sand resource areas under consideration.

Spatially homogeneous offshore wave conditions with steady state wave, current, and wind conditions. STWAVE assumes that the input wave spectrum does not vary over the length of the offshore open boundary. Even over the large lengths of coastline (~25 km) considered in this study, this assumption is valid. The steady state assumption is valid for applications where conditions vary slowly with time. Model inputs and results therefore represent a single snapshot in time, where wind driven waves are fully developed. Other assumptions include a spatially homogeneous wind field and water level offset, due to the ocean tide, therefore these quantities are constant over the whole computational domain. The current field input is depth averaged, but is not required to be spatially homogeneous.

Linear wave refraction and shoaling with negligible effects from bottom friction. The model is formulated using strictly linear wave theory, and therefore will slightly underestimate wave heights in shallow water. Energy dissipation from bottom friction is not included in STWAVE. The authors of the model state that the cumulative energy dissipation caused by bottom friction in the nearshore is small enough that it is not included in the model. Finally, a simplified wave diffraction model is incorporated into STWAVE by laterally smoothing wave energy without changing the direction of wave approach. Diffraction is the processes by which wave energy is spread laterally, perpendicular to the direction of travel of the incident wave, and is the dominant method of wave propagation in sheltered areas behind coastal structures, such as breakwaters and jetties.

STWAVE is an efficient program that requires minimal computing resources to run well. The model is implemented using a finite-difference scheme, on a regular Cartesian grid (grid increments in the *x* and *y* directions are equal). During a model run, the solution is computed starting from the offshore open boundary and is marched in the onshore direction in a single pass of the model domain. This is why STWAVE can propagate waves only in directions within the ±87.5 ° half plane. A benefit of using this single pass approach is that it uses minimal computer memory, because the only memory-resident spectral data are for two grid columns. As such, the changing wave spectra across each grid column are in turn computed using the information solely from the previous grid column.

To assist the user with model set-up and visualization of model output, an interface was designed with the Surface-Water Modeling System (SMS) of the Brigham and Young

University Engineering Computer Graphics Laboratory (1997). SMS also supports other models, such as the hydrodynamic models RMA-2 and ADCIRC. The SMS interface for STWAVE is useful for constructing the computational grid, generating input wave spectra, and visualizing raw model output, including significant wave height (H_s), peak period (T_p), and peak wave direction (θ_p).

2.2 SWAN

The numerical wave transformation model SWAN was developed at Delft University of Technology, Delft, The Netherlands. Like STWAVE, the formulation of SWAN is based on the spectral wave action balance equation. This model currently has many well-developed features, which give the user many options on how each model run is executed. These features range from purely convenient options that allow several different formats for input and output data, to options that allow control of fundamental physical processes in the model, like wave generation, dissipation, and interaction.

SWAN and STWAVE have many similarities. SWAN is a finite difference model, and can directly use an STWAVE formatted bathymetry grid. SWAN does not model wave diffraction or reflection, and is therefore most useful in applications where accuracy of the computed wave field is not required in the immediate vicinity of obstacles. Similar sources of input and dissipation of energy in the wave spectrum are a part of SWAN, including wind wave generation, whitecapping, non-linear wave interactions, and depth induced wave breaking.

Users of SWAN must consider the following model assumptions and features when considering its utility in a specific application:

Mild bottom slope with negligible wave reflection. As with STWAVE, SWAN uses a wave spectrum to describe two-dimensional wave propagation. The spectral definition of the wave field is used even in areas of the model domain where non-linear phenomena dominate, such as the surf zone, or any location where waves are breaking. The authors of SWAN suggest that even in these areas, reasonable accuracy is still possible in the second order moment (the standard deviation) of the wave spectrum (Ris *et al*., 1998). Wave reflections are not included in SWAN, and therefore results may not be accurate in the vicinity of structures or any general obstruction to wave propagation.

Input wave conditions vary spatially along open boundary, and wind, water level elevation, and current inputs vary spatially over the entire computational domain. Unlike STWAVE, in SWAN it is possible to define different spectral conditions at different points along the open boundary of a model domain. This feature is most useful when nested grid runs are executed. A nested grid uses output from a grid that included a larger physical domain, but at the same time has a much coarser grid mesh. Using nested grids, more detailed computations are possible, without requiring the same degree of detail throughout the computational domain. This approach can decrease the total computational time, with little sacrifice in accuracy. In addition to the varying spectral input, other model inputs (wind, water level elevation, and currents) are allowed to vary spatially over the model domain. This feature makes SWAN useful for the computation of wave fields during storm surges in large estuaries, where it is possible to have significant variations in surge levels throughout a model domain.

Simulations may be steady state or dynamic. SWAN has the ability to compute a time dependent, time varying solution, rather that just a series of steady state solutions. The difference between steady state and dynamic solutions is most apparent in applications where wind driven waves do not have sufficient time to reach the maximum height possible, for a given wind strength and duration. Waves that reach the maximum height are described as fetch-limited waves. During hurricanes and other fast moving storms, it is possible that wave conditions may not be fetch limited, due to the quickly changing wind field. For the type of wave conditions and results necessary for this study however, the dynamic capabilities of SWAN are not required.

Linear wave refraction with bottom friction included. Only linear wave refraction is included in the model. Bottom friction can be included in the model computations, but by default it is not. Bottom friction is often used as a tuning parameter, which allows small adjustments in the model output for better comparison to actual data.

SWAN is a full 360° model, which means that it can propagate waves in any direction. Input wave spectra can have a full 360° directional spread, but it is also possible to activate only a sector of a full circle. The ability of SWAN to propagate waves in all directions is the result of its numerical scheme, which makes four separate passes of the model domain, one for each quadrant of a full circle. This is in contrast to STWAVE, which uses a single pass of the model domain. The numerical scheme used by SWAN is a first order implicit, upwind scheme in geographic space.

Because the four passes require that all data remain in memory during the computation, SWAN uses a much larger data array. This requires substantially more machine memory to run than STWAVE. For example, a model domain with dimensions 200 by 300 grid cells would run quickly on an ordinary PC computer with STWAVE, and would require about 3.3 MB of storage to run. In contrast, the same grid run with SWAN using the same input spectrum would require more than 336 MB of storage to run. The amount of memory required for an application can be reduced through the use of nested grids, which is a feature included in SWAN. A nested grid is a fine mesh that uses boundary conditions supplied from a previous run of a spatially larger and courser mesh.

2.3 REF/DIF S

The last model under consideration for MMS borrow site impact studies is REF/DIF S, developed at the Center for Applied Coastal Research, at the University of Delaware. This spectral wave transformation model is a further development of the REF/DIF 1 model, which solves for monochromatic waves only. The modeling approach used in the REF/DIF models is fundamentally different than that used in both STWAVE and SWAN. Rather than basing computations on wave spectra action balance, REF/DIF uses a form of the mild-slope equation, and the complex amplitude of each separate wave component.

REF-DIF S is also a finite difference model and uses a Cartesian grid. Because the mild-slope form of the governing equation is used, the model includes the effects of wave diffraction, unlike STWAVE and SWAN. This is probably the most important distinctive feature of this model compared to the others.

The basic model assumptions that reflect the governing philosophy used in the formulation of REF/DIF S are given as (Kirby and Özkan, 1994):

Mild bottom slope and weak non-linearlity. The REF/DIF models are based on a parabolic formulation of the mild-slope equation of Berkoff (1972). The mild slope assumption has been found to be accurate up to a bottom slope of 1:3 (Booij, 1983), which for most coastal applications that will be encountered in this study is fairly steep. The formulation of REF/DIF S is based on a third order Stokes perturbation expansion. The authors of the model suggest that the Ursell parameter U is a useful indicator of the linearity of waves, where $U = HL^2 / h^3$. The suggested maximum value of U = 40 sets the limit of where REF/DIF S should be applied.

Negligable wave reflection and wave propagation in ±45° sector from the mean wave direction. Just as with STWAVE and SWAN, this model does not include wave reflection. The propagation of wave energy is confined to a 90° sector, which is more restrictive than STWAVE. Ris, et al. (1998) states that wave energy distribution is typically no greater than ±40°, so this characteristic of REF/DIF-S does not appear to be a practical limitation of the model.

Spatially homogeneous offshore wave conditions with steady state wave and current conditions. REF/DIF S is a steady state model. Input spectra can be generated using the preprocessing program SPECGEN, which is distributed with REF-DIF S. Current data are included in the input file containing grid bathymetry. REF/DIF S does not include wind generated waves. Forms of energy dissipation included in the model are damping from different effects of bottom friction and wave breaking.

A major difference of REF/DIF S from the other two models is that the solution computed by the model is greatly dependent on the spacing of the computational grid. REF/DIF S will add subdivisions to the input grid if there are fewer than five points in the x-direction per wavelength of the highest frequency wave being modeled. The number of subdivisions added will thus impact the time required to complete a model run, often resulting in a model total run time that is significantly longer than either STWAVE or SWAN, for the same input grid dimensions. The other two models have no such restriction on grid spacing, because their computations are based on wave energy distribution, not the propagation of individual wave components. Table 1 provides a summary of the attributes for each of the wave transformation models.

Table 1. Attributes for the spectral wave transformation models used for the comparison study.

Model Attribute	REF/DIF S	STWAVE	SWAN
Basis of model formulation	complex amplitude	action density spectrum	action density spectrum
Sector of wave propagation	±45°	±87.5°	360°
Valid wave theory	Stokes/ weakly non-linear	linear	linear
Steady-state or time dependent solution	steady state	steady state	time dependent
Grid spacing dependence on maximum modeled wave length	dependent	independent	independent
Solution quality dependence on grid spacing	high	low	low
Nested Grids/ spatially varying input spectra	yes	no [(b)]	yes
Current input/ wave current interaction	yes	yes	yes
Wind field input	no	spatially homogeneous	spatially varying
Wave diffraction	yes	no [(a), (b)]	no
Wave reflection	no	no	no
Wave breaking model	statistical - Thornton and Guza (1983)	simple breaking criterion [(c)]	statistical - Battjes and Janssen (1978)
Bottom friction	yes	no	yes

Notes: [(a)] currently, wave diffraction is partially included through the lateral spreading of spectral energy around an obstruction, but accompanying direction changes are not modeled.

[(b)] versions of STWAVE soon available will incorporate nested grid and improved diffraction routines.

[(c)] the Battjes and Janssen statistical wave breaking model has been successfully incorporated into STWAVE, though not yet in official distributions of the model.

3. Model Formulation Comparison

The following section focuses on a direct comparison of wave transformation processes represented in each model under consideration. Though these models include several sources of wave energy input and dissipation, the only process that is considered fundamentally important for this study, beyond the formulation of the governing equation, is the process of wave breaking. For the most part, the model selected will be used to solve the distribution of wave heights along a stretch of coastline where the model is driven solely by an input spectrum at the open boundary. Other phenomena included in the wave transformation models under consideration (i.e., the effects of wind, whitecapping, water currents and wave diffraction) are considered less important to the scope of the study (i.e., open coastline with incident wave spectrum driving the open boundary), and are not discussed in detail here.

3.1 Wave Propagation Model

In each of the three models under consideration, a single governing equation characterizes the process of wave transformation through a model domain. This equation may be composed of several individual terms that define energy inputs or losses in the system (e.g., wind-induced waves and wave breaking). Each computer model is an algebraic formulation of the governing equation, which is often more elegantly expressed as a partial differential equation (PDE). Both STWAVE and SWAN are fully spectral models that compute wave characteristics in the model domain based on the transformation of the wave energy density spectrum. On the other hand, computations in REF/DIF S are based on the mild-slope equation and the complex amplitude of individual components in a wave field, not the energy spectrum.

Action Balance Models. Both STWAVE and SWAN are based on forms of the wave action balance equation. In these models, the wave action density spectrum, which includes the effects of currents, is conserved along wave rays. In the absence of currents, wave rays correspond to wave orthogonals, and the action density spectrum is equivalent to the wave energy density spectrum. The governing equation of wave transformation, using the action balance spectrum, in geographical space is written (Ris, *et al*., 1998)

$$\frac{\partial}{\partial t}N + \frac{\partial}{\partial x}c_x N + \frac{\partial}{\partial y}c_y N + \frac{\partial}{\partial \sigma}c_\sigma N + \frac{\partial}{\partial \theta}c_\theta N = \frac{S}{\sigma} \tag{1}$$

where

$N(\sigma,\theta)$ = action density spectrum,

$S(\sigma,\theta)$ = wave energy sources and sinks (e.g., wind induced growth, depth induced breaking),

c = propagation velocities of wave action (energy and currents).

The first term is the change in action density with time. Only SWAN includes this term, as STWAVE is purely a steady state model. The second and third terms represent wave propagation in geographical space. The fourth term represents the shifting of the relative frequency due to variations of depth and currents, while the fifth term represents changes in the action spectrum due to depth and current induced refraction.

Mild Slope Model. A different modeling approach is used in REF/DIF S, where the transformation of discrete wave components is tracked individually rather than as a part of an action or energy spectrum. A simplified, linear form of the mild slope equation with general wave energy dissipation and a separate wave breaking term is formulated as (Kirby and Özkan, 1994):

$$\frac{\partial A_n}{\partial x} = \frac{i}{2k}\frac{\partial^2 A_n}{\partial y^2} - \frac{w_n}{2C_{gn}}A_n - \alpha A_n \tag{2}$$

where

A_n = is the complex amplitude of wave component *n*, related to the water surface displacement by $\eta = Ae^{i(kx-\omega t)}$,

w_n = dissipation factor depending on nature of energy dissipation (e.g., bottom friction),

α = wave breaking coefficient,

k = wave number, $2\pi/L$,

C_{gn} = wave component group velocity.

The actual formulation of the mild slope equation used in REF/DIF S includes the effects of wave–current interaction, and is based on third order Stokes waves, a higher-order wave theory than the given linear wave representation. An important difference between this model and the model used in SWAN and STWAVE is that this is a parabolic equation, of the form $\frac{\partial A}{\partial x} = \frac{\partial^2 A}{\partial y^2} + S$, whereas the previous models are first order partial differential equations.

3.2 Wave Breaking Model

For coastal sites included as part of the offshore borrow site impact study, the dominant process of wave energy dissipation is depth induced breaking. The exact method used to simulate the effects of breaking waves is different in each model. STWAVE depends on a breaking parameter, which determines the maximum wave height for given conditions. REF/DIF S and SWAN use similar methods, where wave breaking is always included as a dissipation term in the model's governing equation. After the discussion of the basis of each breaking model, a comparison of model output for breaking waves on a planar beach is provided.

STWAVE. The breaking model in STWAVE is based on a form of the Miche criterion as discussed by Battjes and Janssen (1978). It sets a maximum limit on the zero-moment wave height (H_{mo}), the wave height based on the distribution of energy in the wave spectrum. The formulation of this model is

$$H_{mo(max)} = 0.1L \tanh(kd) \tag{3}$$

where L is the wavelength, k is the wave number ($k = 2\pi/L$), and d is the depth at the point where the breaking limit is being evaluated. This equation is used together with a simpler breaking model, which was used alone in earlier versions of STWAVE, where the maximum H_{mo} wave height is always expressed as a constant ratio of water depth

$$H_{mo(max)} = 0.64\ d\ . \tag{4}$$

An advantage of using Equation 3 over Equation 4 is that it accounts for increased wave breaking resulting from wave steepening caused by wave-current interactions. Once model wave heights exceed $H_{mo(max)}$, STWAVE uses a simple method to reduce the energy spectrum, essentially to set the value of $H_{mo} = H_{mo(max)}$. Energy at each frequency and direction is reduced by the same percentage. As a result, non-linear transfers of energy to high frequencies during breaking are not included in STWAVE.

SWAN. In contrast to STWAVE, where wave breaking is turned on only after a maximum wave height is surpassed, the wave breaking model in SWAN is always on. The amount of energy dissipation at any point is still a strong function of depth and wave height. The model takes advantage of the full work of Battjes and Janssen (1978), where in addition to specifying a maximum limit to H_{mo}, it uses a dissipation function to compute the fraction of waves in a random wave field that will break at a point. By applying this dissipation model, wave breaking begins earlier, in deeper water, but very gradually at first. The equation used to determine the fraction of breaking waves Q_b is

$$\frac{1-Q_b}{\ln Q_b} = -8\frac{E_{tot}}{H_{mo(\max)}^2} \tag{5}$$

where E_{tot} is the total energy contained in the wave spectrum. The maximum wave height is computed using an equation of the form $H_{mo(max)} = \gamma\ d$, similar to Equation 3. However for most bottom conditions γ is not a constant value, but rather a function of bottom slope β expressed as

$$\gamma = 0.55 + 0.88\ \exp(-0.012\ \cot\beta). \tag{6}$$

In circumstances where there is a negative bottom slope (increasing depth) SWAN uses a constant value for the breaking criterion, γ = 0.73. After computing Q_b and $H_{mo(max)}$, the mean energy dissipation rate D_{tot} is then computed using the relationship

$$D_{tot} = -\frac{1}{4}\alpha Q_b\left(\frac{\overline{\sigma}}{2\pi}\right)H_{mo(\max)}^2 \tag{7}$$

where $\overline{\sigma}$ is the peak frequency and α is a constant of the order 1 (Battjes and Janssen, 1978). Finally, the dissipation rate $S(\sigma,\theta)$ of each spectral component is determined by the expression

$$S(\sigma,\theta) = -D_{tot}\frac{E(\sigma,\theta)}{E_{tot}} \tag{8}$$

where $E(\sigma,\theta)$ is the energy contained within the spectral component with frequency σ and direction θ.

REF/DIF S. The breaking model in REF/DIF S is similar to that included in SWAN, in that wave energy dissipation due to breaking is always included as a term in the governing equation, no matter how small a contribution it is. REF/DIF S uses the

breaking model by Thornton and Guza (1983) where energy dissipation is a function of a bore dissipation parameter ε_b, and

$$\varepsilon_b = \frac{3\sqrt{\pi}}{16} \frac{\rho g \sigma_p B^3}{\gamma^4 d^5} H_{rms}^7 \tag{9}$$

where

γ, B = constants with values 0.6 and 1.0 respectively,
σ_p = peak frequency of the frequency energy spectrum, and
H_{rms} = is the root mean square wave height, $H_{rms} = (2)^{-0.5} H_{mo}$.

The term included in the governing equation for energy dissipation due to wave breaking is $-\alpha A_n$, where A_n is the complex amplitude of wave component n, and α is a function of ε_b

$$\alpha = \frac{4\varepsilon_b}{\rho g H_{rms}^2}. \tag{10}$$

The value of α in deep water is negligible, but as depth increases, α becomes more significant and a greater amount of energy is dissipated from the system.

4. Comparison of Model Output

Simulations from each model were made to demonstrate model behavior for a few different test cases where real data are available from laboratory or field measurements. Three cases where chosen for this comparison:

- Waves breaking on a simple planar beach (Thornton and Guza, 1986),
- Wave refraction about a simple elliptical shoal (Vincent and Briggs, 1989),
- Wave refraction along a prototype coastline (Smith and Harkins, 1997).

The following analysis is not an exhaustive comparison, but the results provide a useful guide for judging model performance. For each case, the FORTRAN computer code of each model was compiled using single precision on an Intel Pentium III platform.

4.1 Simple Planar Beach

Model performance in the breaker zone is critical if computed results are to be used as input to a sediment transport model. The amount of sediment transport caused by wave-induced longshore currents is greatly impacted by the offshore extent of the surf zone as well as the distribution of wave heights across the surf zone. A run of each model was completed for a beach with constant slope in order to make a simple comparison of breaking model performance. Data from field measurements in the surf zone of a planar beach are available in Thornton and Guza (1986).

Results of the planar beach model runs are given in Figure 1, which shows the cross-shore distribution of the H_{rms} wave height through the breaker zone. These model runs are based on conditions listed in Table 1. A TMA spectrum was developed for this

comparison, based on the given wave conditions, and assuming a narrow frequency and directional spectral spread.

Table 2.	Wave and beach conditions used with model runs for breaking waves on a planar beach (Thornton and Guza, 1986).
Max offshore depth of grid (m)	9.1
peak frequency, f_p (Hz)	0.07
peak direction, θ_p (deg)	18.4
incident wave height, H_{rms} (m)	0.52
Bottom Slope	0.038

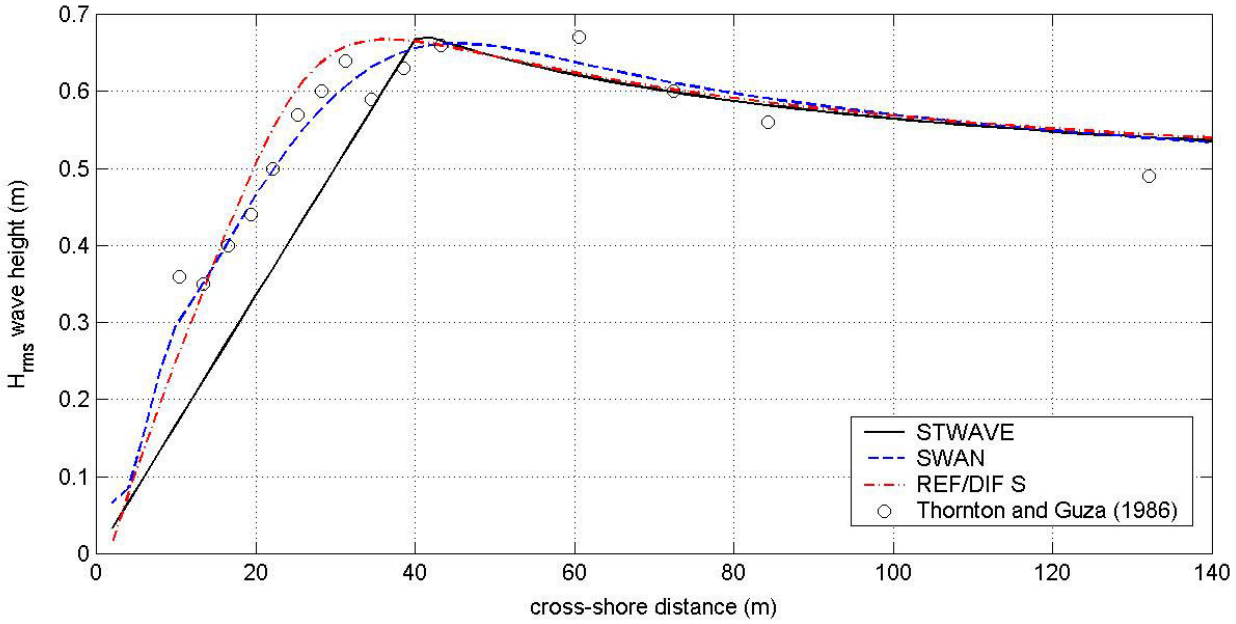

Figure 1. Comparison of modeled and measured wave height distributions in surf zone of a planar beach (parallel contours) with approximate 1:26 slope.

The results of these runs show the difference between the breaking model in STWAVE based on a simple breaking criterion, and the breaking models used in SWAN and REF/DIF S, which are statistical models. Waves in STWAVE gradually increase in height as they move toward shore, and once the maximum wave height breaking criterion is exceeded at about 40 m from the shore, wave heights are reduced at a constant rate until all wave energy is dissipated. The other two models exhibit a different behavior that more closely models the wave height transformation in the breaker zone seen in the field data. In these models, wave breaking is more gradually applied at first, which results in higher wave heights closer to the shoreline. Though the wave breaking model in STWAVE does not model the distribution of wave heights through the surfzone as well as the other two models, it is still able to accurately predict the maximum wave height at the beginning of the surfzone.

In order to improve the performance of STWAVE in the breaker zone, it would be necessary to make changes to the original wave-breaking routine to incorporate a probabilistic wave breaking model like those used in REF/DIF S and SWAN.

4.2 Elliptical Shoal

Model runs were made to simulate physical model testing done by Vincent and Briggs (1989), for a simple elliptical shoal with breaking waves. For this case, the shoal does not break the water surface, and beyond the shoal the bottom is at a constant depth of 0.47 m. A three-dimensional contour plot of shoal bathymetry is given in Figure 2. A TMA spectrum was developed for these model runs, based on the conditions given by Vincent and Briggs for a narrow frequency spread spectrum, with a wide directional spread. The incident wave conditions are given in Table 2.

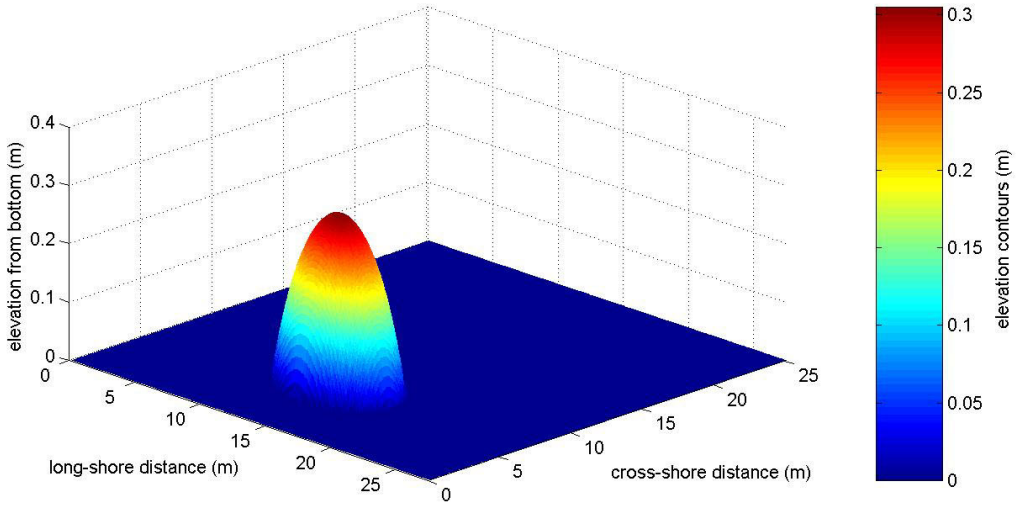

Figure 2. Color contour plot of depths for elliptical shoal used in wave model comparison.

Table 3. Wave conditions used in model runs of elliptical shoal to simulate breaking wave conditions (Vincent and Briggs, 1989).	
maximum depth of grid (m)	0.47
peak frequency, f_p (Hz)	0.77
peak direction, θ_p (deg)	0
incident wave height, H_{mo} (m)	0.19
TMA peak enhancement factor, γ	2
directional spreading factor, σ_m (deg)	30

The results of these model runs are shown in Figures 3 through 7. Wave height contours and vectors indicating mean wave direction are shown for the entire model domain, for each model in Figures 3, 4,and 5. For the output from STWAVE and REF/DIF S, only half of the model domain is shown because the solution is axisymmetric about the minor axis of the shoal, as would be expected. However, the output from

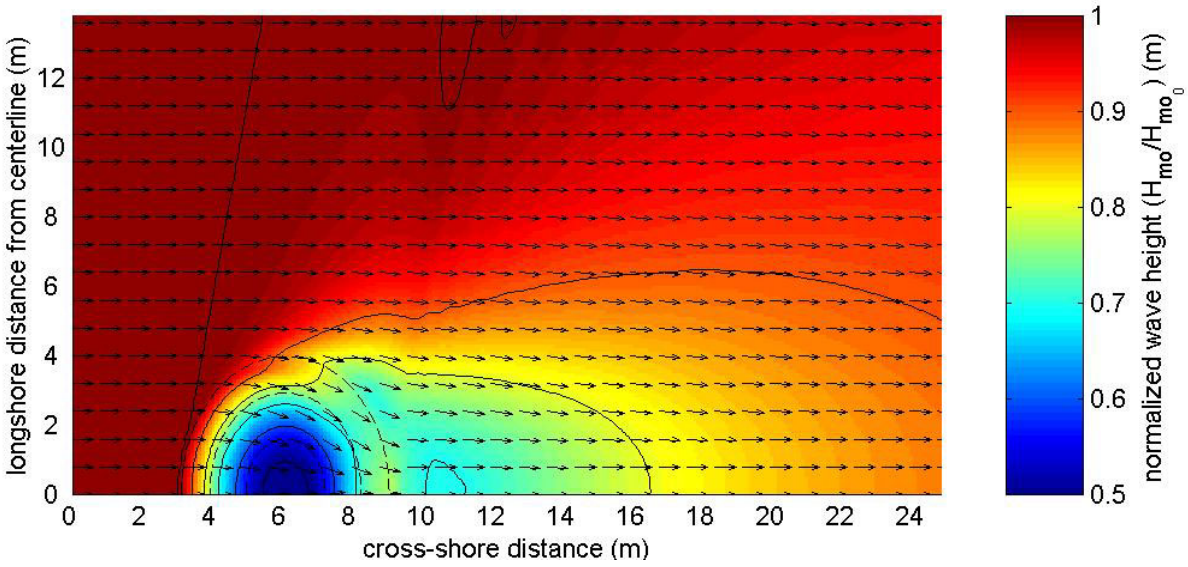

Figure 3. Contour plot of STWAVE model results for elliptical shoal with incident wave height H_{mo} = 0.19 m, showing mean wave direction (arrows) and shoal position (dashed contor lines) . Model results are shown for half the grid.

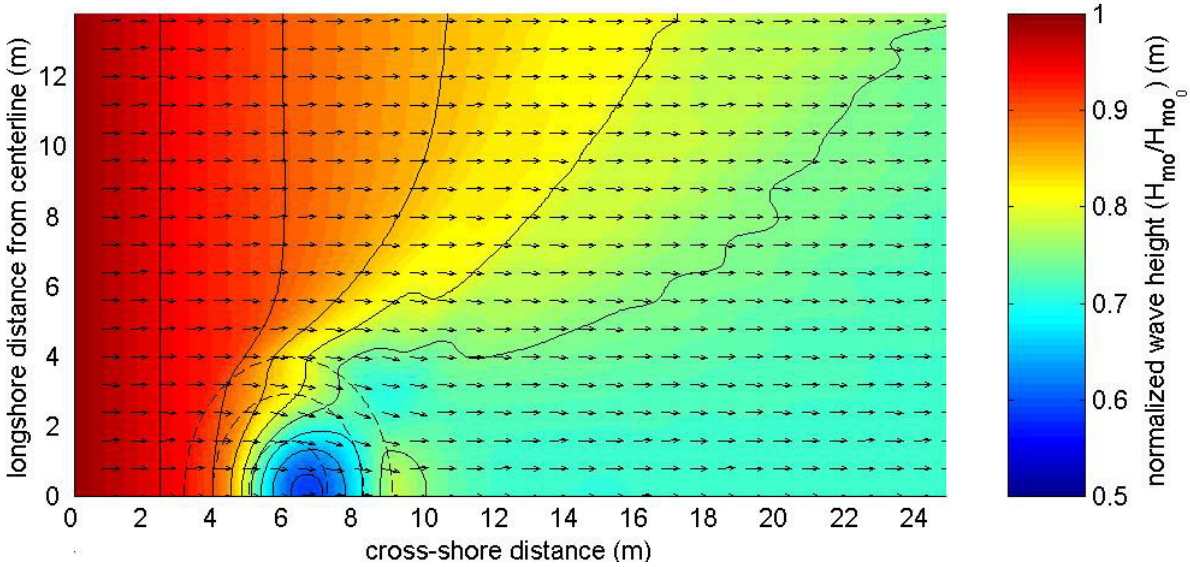

Figure 4. Contour plot of REF/DIF S model results for elliptical shoal with incident wave height H_{mo} = 0.19 m, showing mean wave direction (arrows) and shoal position (dashed contor lines) . Model results are shown for half the grid.

SWAN (Figure 5) shows a solution that is asymmetric. The unexpected asymmetry of the solution is probably a residual of the solving technique used by SWAN, which is based on four passes of the model domain, one for each quadrant of a full circle. Because the solution is asymmetric, this might indicate that SWAN is sensitive to physically small domains. In fact, the SWAN users manual recommends that the minimum spatial resolution of a grid should be no smaller than 50 m, which is two orders of magnitude larger than the 0.1 m grid spacing used in this comparison.

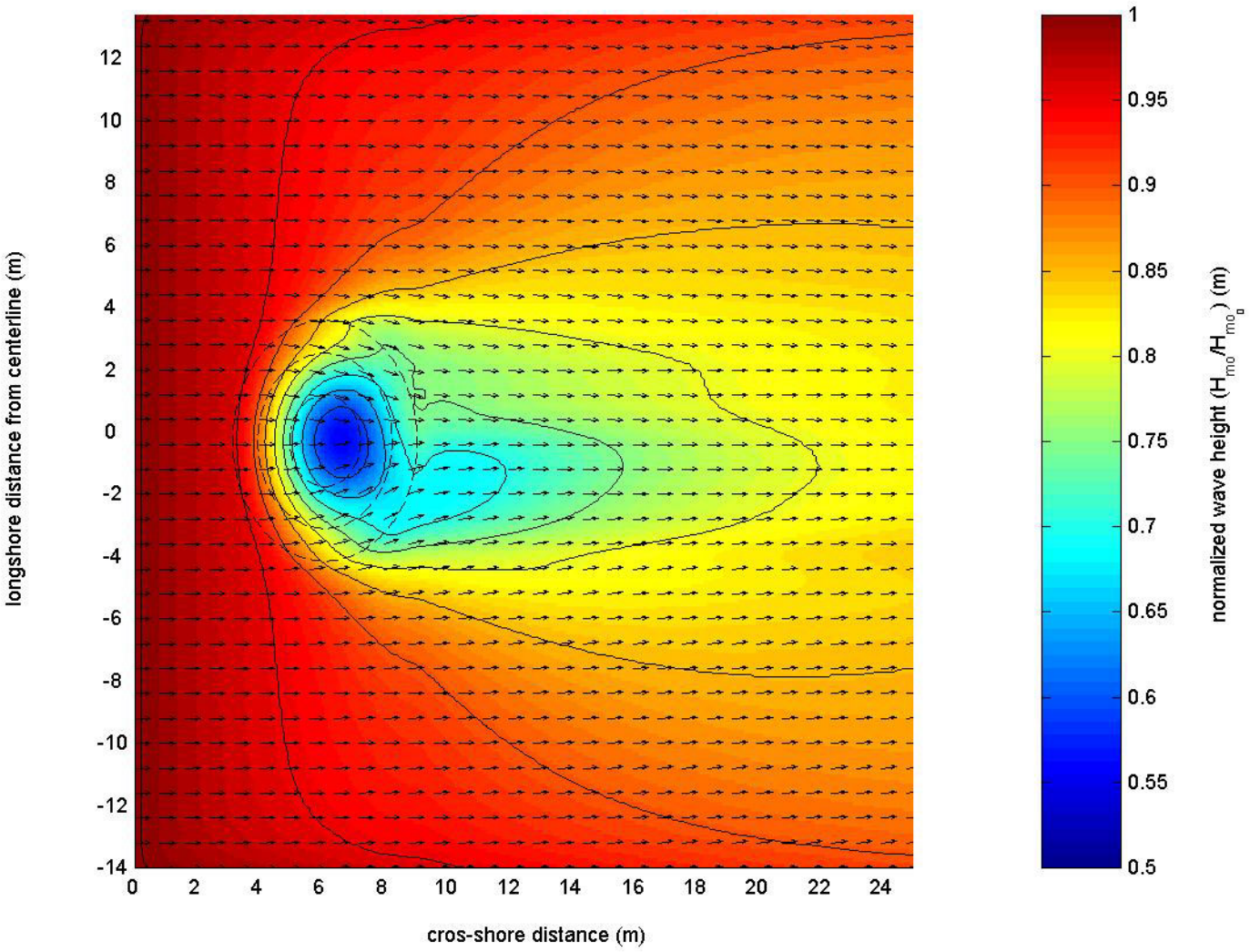

Figure 5. Contour plot of SWAN model results for elliptical shoal with incident wave height H_{mo} = 0.19 m, showing mean wave direction (arrows) and shoal position (dashed contor lines) .

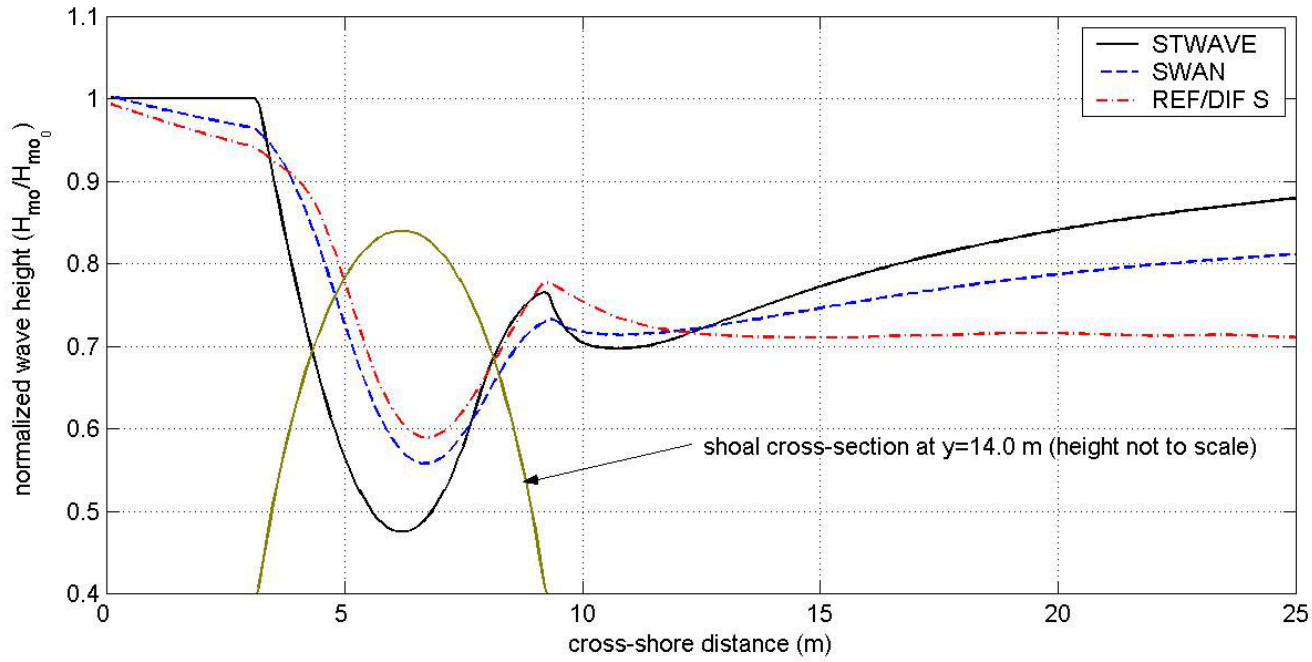

Figure 6. Comparison of wave height distributions for three wave models at the cross-shore centerline of the elliptical shoal (y = 14.0 m), including the shoal profile.

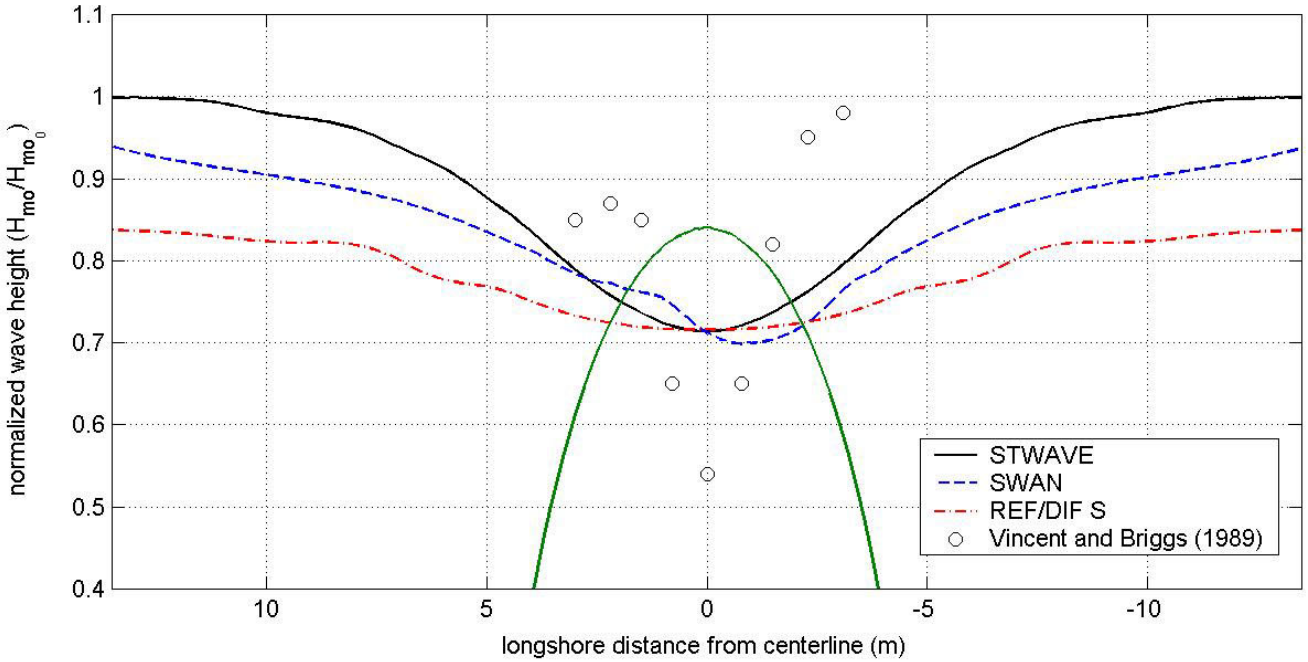

Figure 7. Comparison of wave height distributions behind elliptical shoal for three wave models at x = 12.2 m, including test data collected by Vincent and Briggs (1989) (Case B5), and including the shoal profile.

In Figures 6 and 7, model output is shown for two transects of the model domain. In Figure 6 the transect is located along the centerline of the shoal, and in Figure 7 the transect is located approximately 6 m behind the major axis of the shoal. The effects of lateral diffusion incorporated into STWAVE and SWAN, used to make up for the lack of proper diffraction in these models, is apparent in Figure 6; wave heights increase quickly in the wake of the shoal. It is possible that REF/DIF S may not be diffusive enough, as indicated by relatively constant wave heights behind the shoal after wave focusing. For all models, the correlation to laboratory data from Vincent and Briggs (1989) is not good. In the lab data, wave heights behind the shoal are smaller further away from the shoal, and heights seem to increase moving out from the shoal at a much greater rate.

Differences in model output due to the different wave breaking models are also apparent in Figure 6. Initially wave heights decrease in SWAN and REF/DIF S as a result of the statistical breaking model, but in STWAVE wave heights remain constant until the wave height breaking criterion is exceeded.

In addition to the wave directions shown as part of Figures 3, 4, and 5, a close-up comparison of mean wave angles computed by each model, along a line located behind the shoal (Figure 8). This figure indicates that STWAVE has the greatest change in mean wave angle at this transect. Direction changes are simply caused by refraction over the shoal.

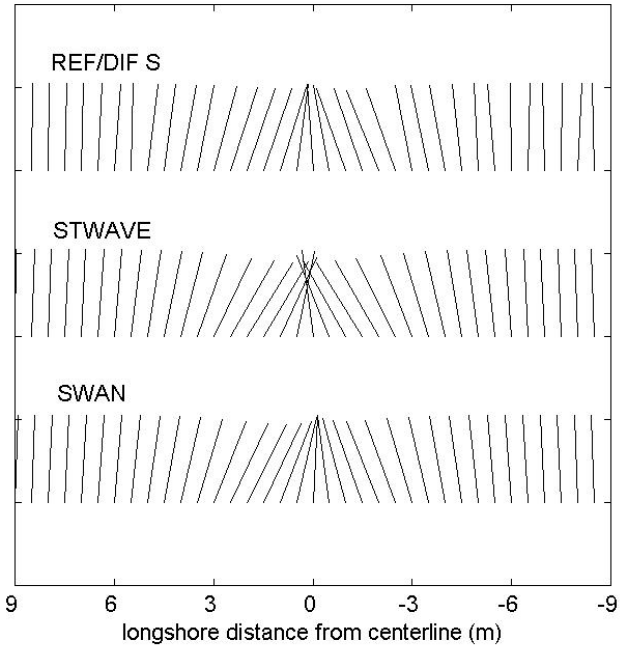

Figure 8. Quiver plot indicating mean wave directions along line located at x = 12.2 m for three wave models.

4.3 Ponce de Leon Inlet

An additional set of wave model runs were made for a full-scale section of coastline. The section of coastline used is around Ponce de Leon Inlet, located on the east coast of Florida, near Daytona Beach. Scale model tests (100:1) of the Ponce de Leon Inlet where made by Smith and Harkin (1997) at WES, and the resulting test data provide an excellent source for comparison of wave model performance on a prototype coastline. Figure 9 shows bathymetric contours for the entire grid used in the model runs. Wave conditions used in the model runs are listed in Table 3. A TMA spectrum based on these characteristics was generated for the model runs.

The physical model extends approximately 2 km offshore. Water depths begin at the bottom of the test basin (at -30.5 m from Mean Low Water, MLW), which is deeper than the prototype bottom in this area. From the bottom of the basin there is a steep 1:5 transition to the –10.7 m (MLW) contour of the model. The grid used in the numerical wave model runs uses the same bathymetry as the physical model, including the –30.5 m offshore depth. Prototype-scale water depths of the numerical grid were adjusted to include a +1.07 m tide.

Waves in the physical model were generated using the Directional Spectral Wave Generator (DSWG) at WES. Wave data were collected using 30 capacitive wave gauges. Locations of the wave gauges are indicated in Figure 9.

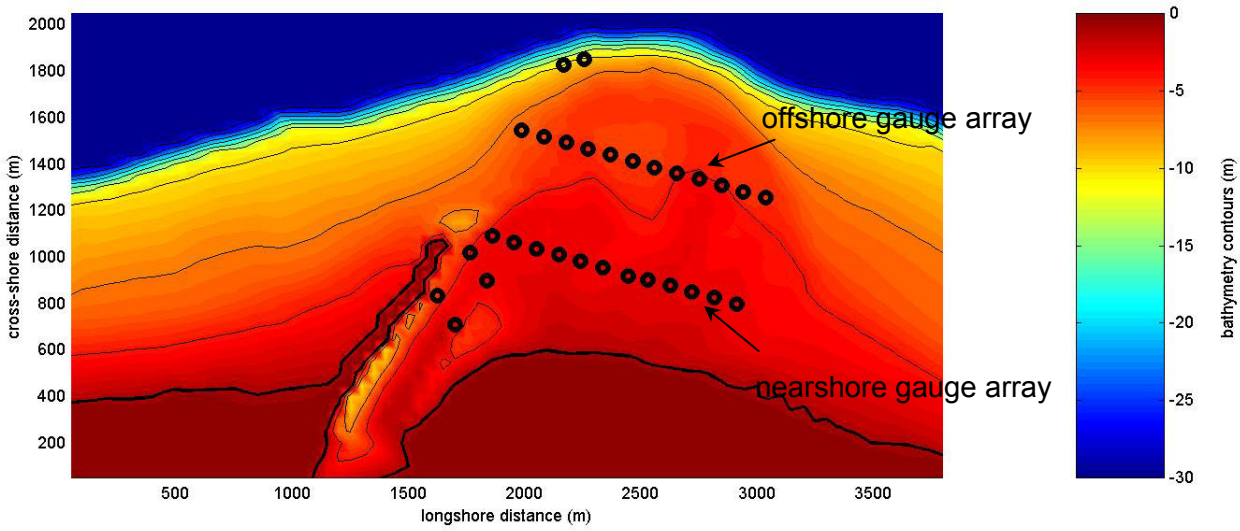

Figure 9. Bathymetric contours of numerical grid used to model Ponce de Leon Inlet, Florida. Solid lines indicate bathymetric contours. Locations of wave gauges (°) used in physical model tests are also indicated.

Table 4. Case 02 wave conditions used in model runs of Ponce de Leon inlet (Smith and Harkins, 1997).	
maximum depth of grid (m)	18
peak frequency, f_p (Hz)	0.125
peak dir. (from cross-shore axis), θ_p (deg)	0
incident wave height, H_{mo} (m)	1.01
TMA peak enhancement factor, γ	3.3
directional spreading factor, σ_m (deg)	30

Output for the entire numerical grid for the three model runs is shown in Figures 10, 11, and 12. The highest computed wave heights appear in the STWAVE solution, near the shore. Generally, STWAVE and SWAN output show similar trends in wave growth over the shoal area near the inlet (Figures 10 and 12). The output from REF/DIF S shows lower computed wave heights and a streaky appearance (Figure 11). The shadow of reduced wave heights behind the jetty is also much more pronounced in the REF/DIF S solution.

Figures 13 through 18 illustrate numerical model wave heights at the offshore and nearshore wave gauge arrays plotted with prototype-scaled wave heights measured in the physical model. Wave heights from the numerical models at the gauge locations are interpolated from the global model output using a linear interpolation function in MATLAB.

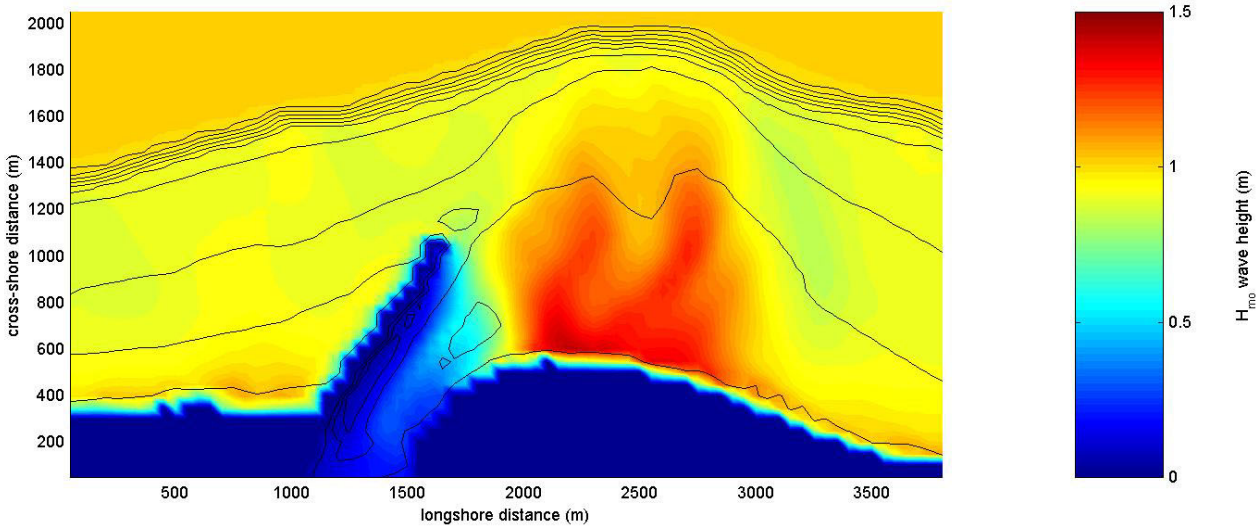

Figure10. Global output of H_{mo} wave heights output from STWAVE for Ponce de Leon inlet, with peak incident wave direction θ_p = 0° from cross-shore axis, incident H_{mo} = 1.01, and peak period T_p = 8 sec. Solid lines indicate bathymetric contours.

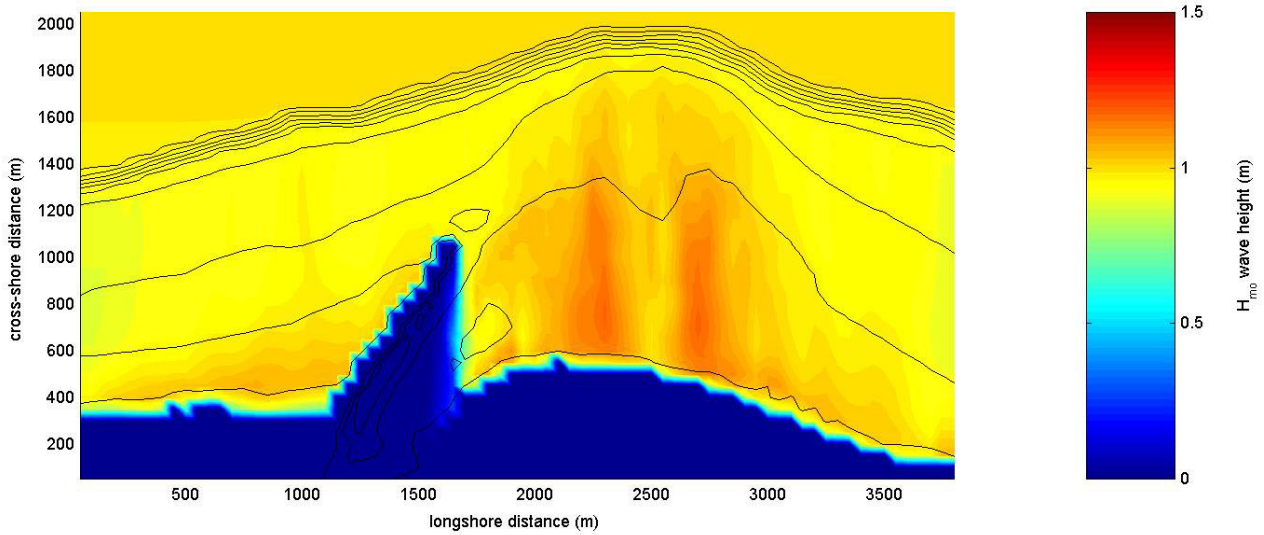

Figure11. Global output of H_{mo} wave heights output from REF/DIF S for Ponce de Leon inlet, with peak incident wave direction θ_p = 0° from cross-shore axis, incident H_{mo} = 1.01, and peak period T_p = 8 sec. Solid lines indicate bathymetric contours.

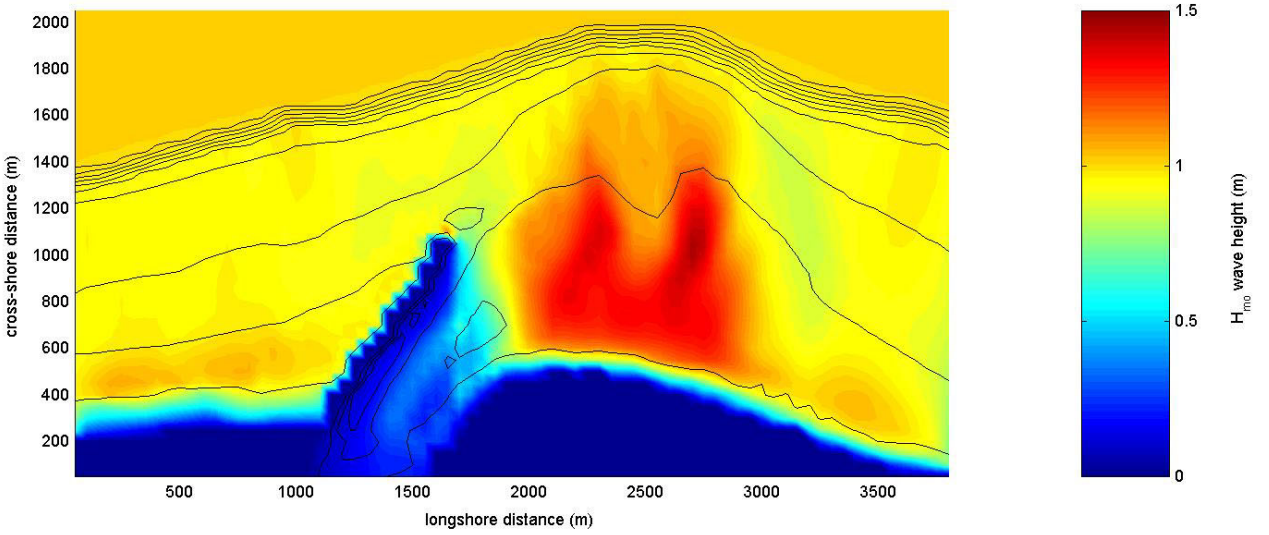

Figure12. Global output of H_{mo} wave heights output from SWAN for Ponce de Leon inlet, with peak incident wave direction θ_p = 0° from cross-shore axis, incident H_{mo} = 1.01, and peak period T_p = 8 sec. Solid lines indicate bathymetric contours.

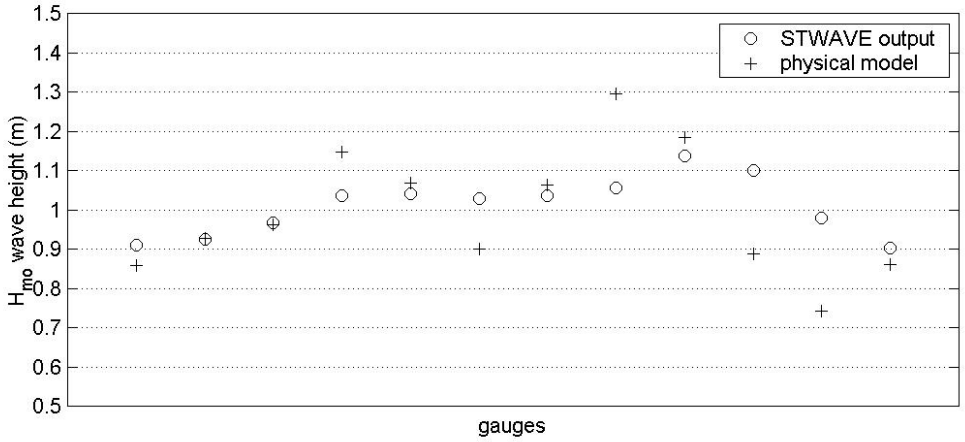

Figure 13. STWAVE output comparison with physical model data for offshore wave gauge array for physical model tests of Ponce de Leon Inlet.

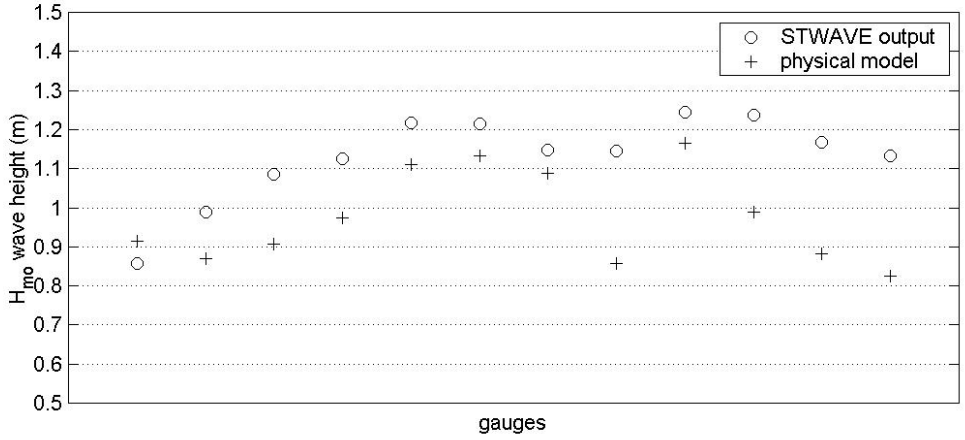

Figure 14. STWAVE output comparison with physical model data for nearshore wave gauge array for physical model tests of Ponce de Leon Inlet.

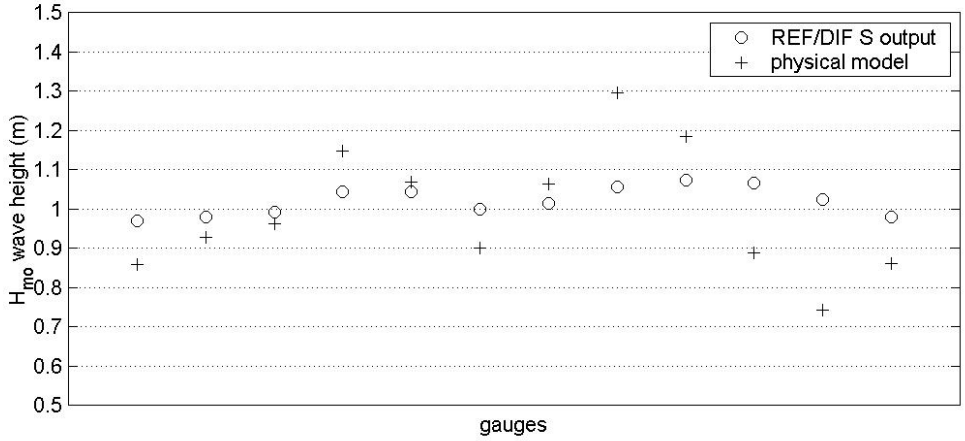

Figure 15. REF/DIF S output comparison with physical model data for offshore wave gauge array for physical model tests of Ponce de Leon Inlet.

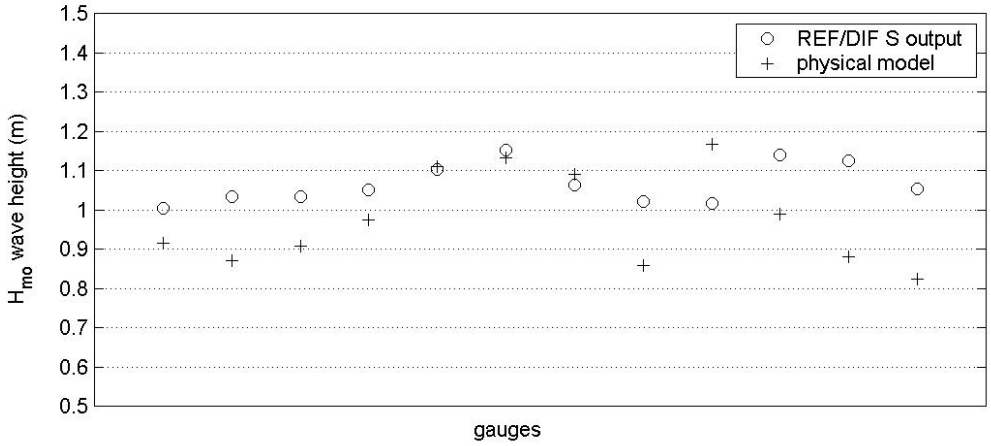

Figure 16. REF/DIF S output comparison with physical model data for nearshore wave gauge array for physical model tests of Ponce de Leon Inlet.

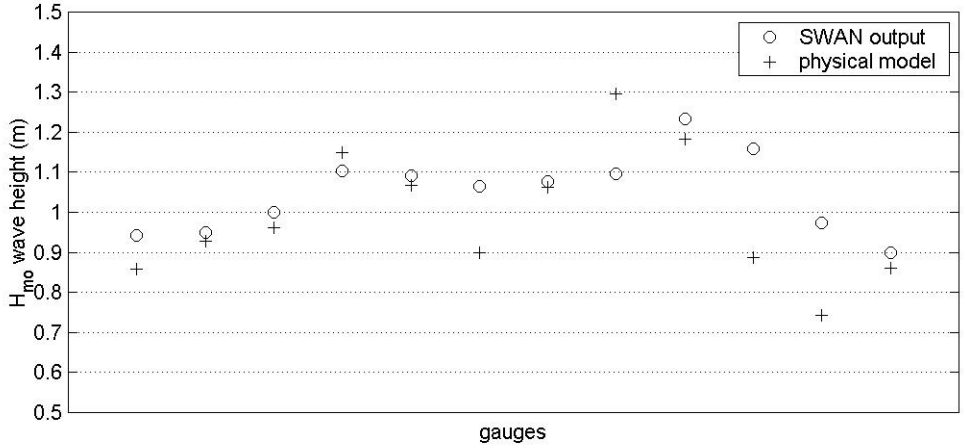

Figure 17. SWAN output comparison with physical model data for offshore wave gauge array for physical model tests of Ponce de Leon Inlet.

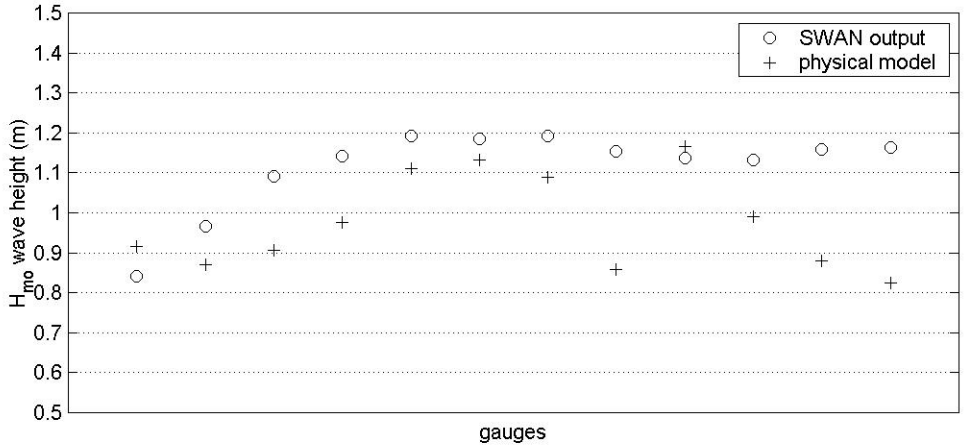

Figure 18. SWAN output comparison with physical model data for nearshore wave gauge array for physical model tests of Ponce de Leon Inlet.

The plots of model output along the wave gauge arrays show that the models generally exhibit similar wave height distributions. Differences between measured data and computed solutions may be caused by small differences between the bathymetry of physical model and the numerical grid used by the computer models. To quantify the performance of each model compared with measured physical model data, it is useful to perform an error analysis. This analysis can also be useful as a gauge of relative performance between each of the numerical models.

Table 5. RMS and mean error values computed using 12 offshore and 12 nearshore wave gauges, for case 02 conditions.

data array	RMS error (%)	mean error (%)
STWAVE offshore array	13.9	3.7
STWAVE nearshore array	21.0	16.7
REF/DIF S offshore array	15.5	5.0
REF/DIF S nearshore array	15.8	10.4
SWAN offshore array	14.9	7.4
SWAN nearshore array	29.1	24.6

Results of a RMS error analysis of computer model output plotted in Figures 13 through 18 are presented in Table 4. The RMS error (E_{rms}) and mean error (E_{mean}) are determined by (Smith and Harkins, 1997)

$$E_{rms}(\%) = \sqrt{\frac{1}{N}\sum_{i=1}^{N}\left(\frac{H(c)_i - H(m)_i}{H(m)_i}\right)^2} \times 100\% \tag{11}$$

and

$$E_{mean}(\%) = \frac{1}{N}\sum_{i=1}^{N}\frac{(H(c)_i - H(m)_i)}{H(m)_i} \times 100\% \tag{12}$$

where $H(c)_i$ is the computed value of wave height at gauge location i, $H(m)_i$ is the measured value of wave height from the physical model, and N is the total number of data points in each array.

This error analysis shows that the three models perform almost equally well in modeling wave heights at the offshore gauge array, but differences become more pronounced at the nearshore gauge array, after waves have propagated farther along the shoal area near the inlet. The STWAVE model results could be improved by incorporating a better representation of wave diffraction into the model, which may help to reduce wave heights nearer to shore. The larger error computed from the SWAN solution for the nearshore array of gauges may be the effect of the numerical scheme used by this model, which is very fast compared to even STWAVE, but may result in lower model accuracy.

5. Summary and Recommendations

A comparison of numerical wave transformation models has been presented. STWAVE, REF/DIF S, and SWAN were selected for this comparison because they are spectral wave models and are easily accessible. Spectral models can simulate real ocean wave conditions, where waves of varying frequency and direction propagate simultaneously through the same physical domain. These models can be described as either action density models, like STWAVE and SWAN, or as propagation models like REF/DIF S. Action density models use the distribution of energy in a spectrum to compute wave transformations, whereas propagation models propagate individual waves through the model domain, each with a different frequency and different initial direction.

The time to complete a solution is roughly the same for the three models, as long as REF/DIF S does not add additional grid subdivisions. When making computations on large physical domains REF/DIF S will often require several additional grid divisions for stability. These additional grid divisions are automatically included by the model in the x direction if required, and can greatly affect the amount of computer time necessary to complete a simulation. STWAVE and SWAN are much less sensitive to grid cell size, and do not add grid subdivisions. The numerical scheme used by SWAN is the fastest, but it requires much more computer memory to run, and solution accuracy is lower.

The three wave models differ by how wave breaking is represented. STWAVE has a simple wave breaking model, based on a breaking criterion that is a function of wave length. SWAN and REF/DIF S include more sophisticated breaking models that are based on the dissipation of energy as a wave breaks. These dissipation-based models compute wave height distributions in the surf zone that compare better to actual data than the STWAVE breaking model, though the STWAVE breaking model does accurately predict maximum wave heights in the surfzone. Wave height distribution in the surf zone is important for sediment transport calculations. Applied Coastal has already incorporated the Battjes and Janssen breaking model into the STWAVE source code so that it includes this better breaking model.

Based this model comparison and other factors, it is recommended that future wave modeling projects use STWAVE. This recommendation is based on:

- STWAVE is a fully spectral model with an efficient numerical scheme that requires a minimum of computing resources and which has acceptable accuracy when compared to physical model data.
- The USACE is actively updating STWAVE for its own use, and further improvements to the model will be made (e.g., diffraction is currently being added).
- STWAVE is able to compute mean wave angles, which is necessary input in sediment transport modeling, whereas currently available versions of REF/DIF S do not have a rigorous method for mean wave angle computations.
- Though the basic model approach of SWAN is very similar to STWAVE, it has many additional features that are not included in STWAVE. However, these advanced capabilities will not be required in the wave modeling projects for the MMS. Otherwise SWAN offers no performance advantage over STWAVE.

Finally, it is recommended that the Battjes and Janssen (1978) wave height distribution model be used with STWAVE. Applied Coastal has already successfully incorporated

this model into a copy of the STWAVE source code. This breaking model improves STWAVE's performance in the surfzone, and could potentially improve the performance of the model elsewhere as well.

6. Acknowledgments

Applied Coastal would like to thank Jarrell Smith, at the U.S. Army Engineering Waterways Experiment Station in Vicksburg, MS, for providing test data and computer grids for the Ponce de Leon inlet physical model tests used in this paper.

7. References

Battjes, J.A., and Janssen, J.P.F.M. (1978). "Energy loss and set-up due to breaking of random waves." *Proc. 16th Coastal Engineering Conf.*, ASCE, Reston, VA, 569-587.

Berkhoff, J.C.W. (1972). "Computation of combined refraction-diffraction." *Proceedings 13th International Conf. of Coastal Engineering*, ASCE, Reston, VA.

Booij, N. (1983). *Gravity waves on water with non-uniform depth and current*, Ph.D. dissertation, Technical University of Delft, The Netherlands.

Kirby, J.T., and Özkan, H.T. (1994). "Combined refraction/diffraction model for spectral wave conditions." *CACR Report No. 94-04*, Center for Applied Coastal Research, University of Delaware, Newark, DE.

Ris, R.C., Booij, N., Holthuijsen, L.H., Padilla-Hernandez, R., and Haagsma, I.G. (1998). *User manual SWAN cycle 2 version 30.75*, Delft University of Technology, Department of Civil Engineering, Delft, The Netherlands.

Smith, J.M., Resio, D.T., and Zundel, A.K. (1999). "STWAVE: Steady-state spectral wave model." *Instruction Report CHL-99-March 1999*, U.S. Army Engineering Waterways Experiment Station, Vicksburg, MS.

Smith, S.J., and Harkins, G.S. (1997). "Numerical wave model Evaluations using laboratory data." *Proc. Waves '97 Conf.*, ASCE, Reston, VA.

Thornton, E.B., and Guza, R.T. (1983). "Transformation of wave height distribution." *Journal of Geophysical Research*, 88, 5925-5938.

Thornton, E.B. and Guza, R.T. (1986). "Surf zone longshore currents and random waves: Field data and models." *Journal of Physical Oceanography*, 16, 1165-1178.

Vincent , C.L., and Briggs, M.J. (1989). "Refraction-diffraction of irregular waves over a mound." *Journal of Waterway, Port, Coastal, and Ocean Engineering*, 115(2), 269-284.

APPENDIX B: NEW JERSEY WAVE MODEL OUTPUT

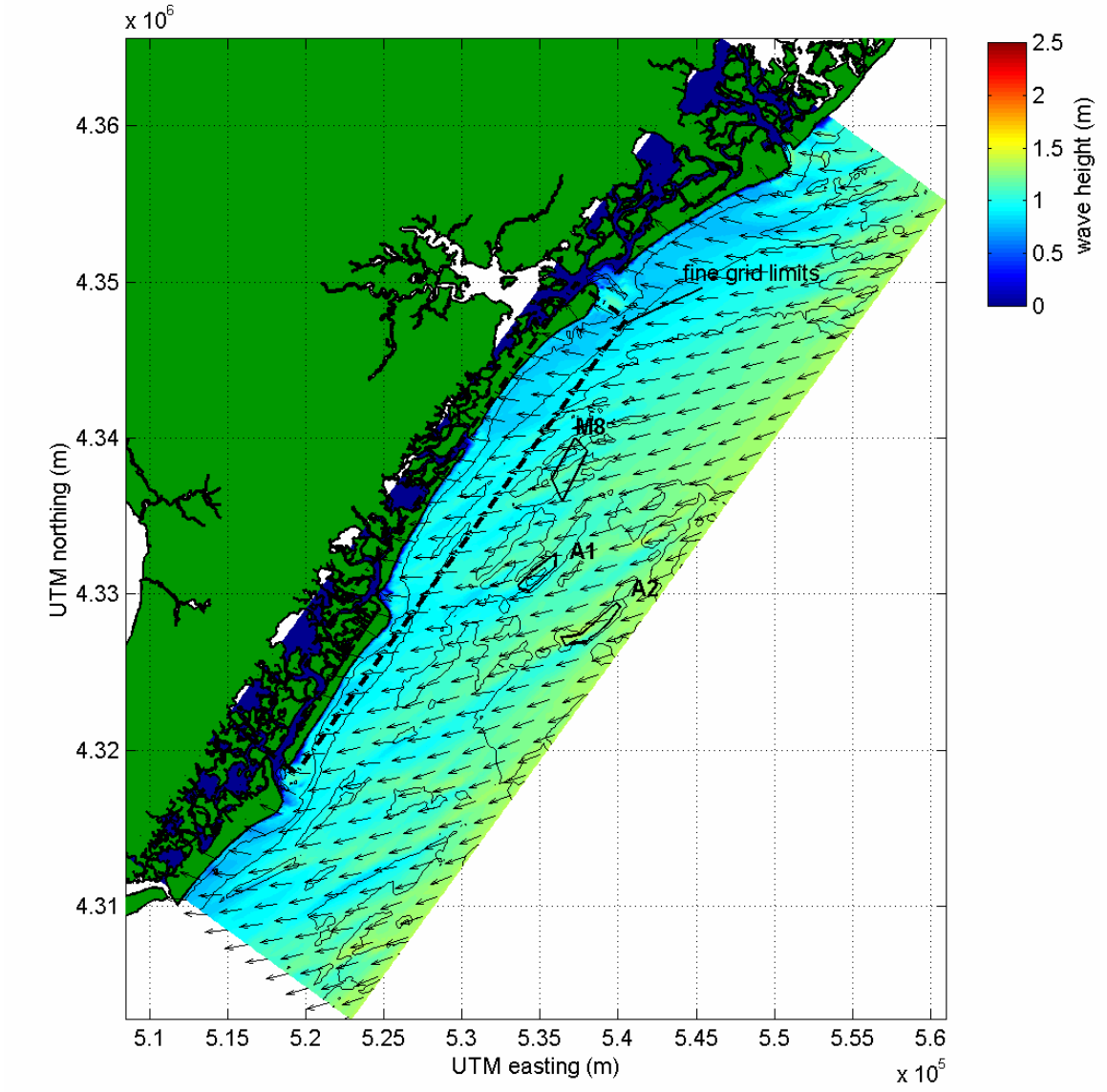

Figure B-1. Plot of STWAVE model output for southern New Jersey, existing conditions, wave Case 1 (H_s=1.4 m, T_{peak}=7.7 sec, θ_{peak}=61 deg). Color contours indicate wave height, and vectors show mean direction of wave propagation.

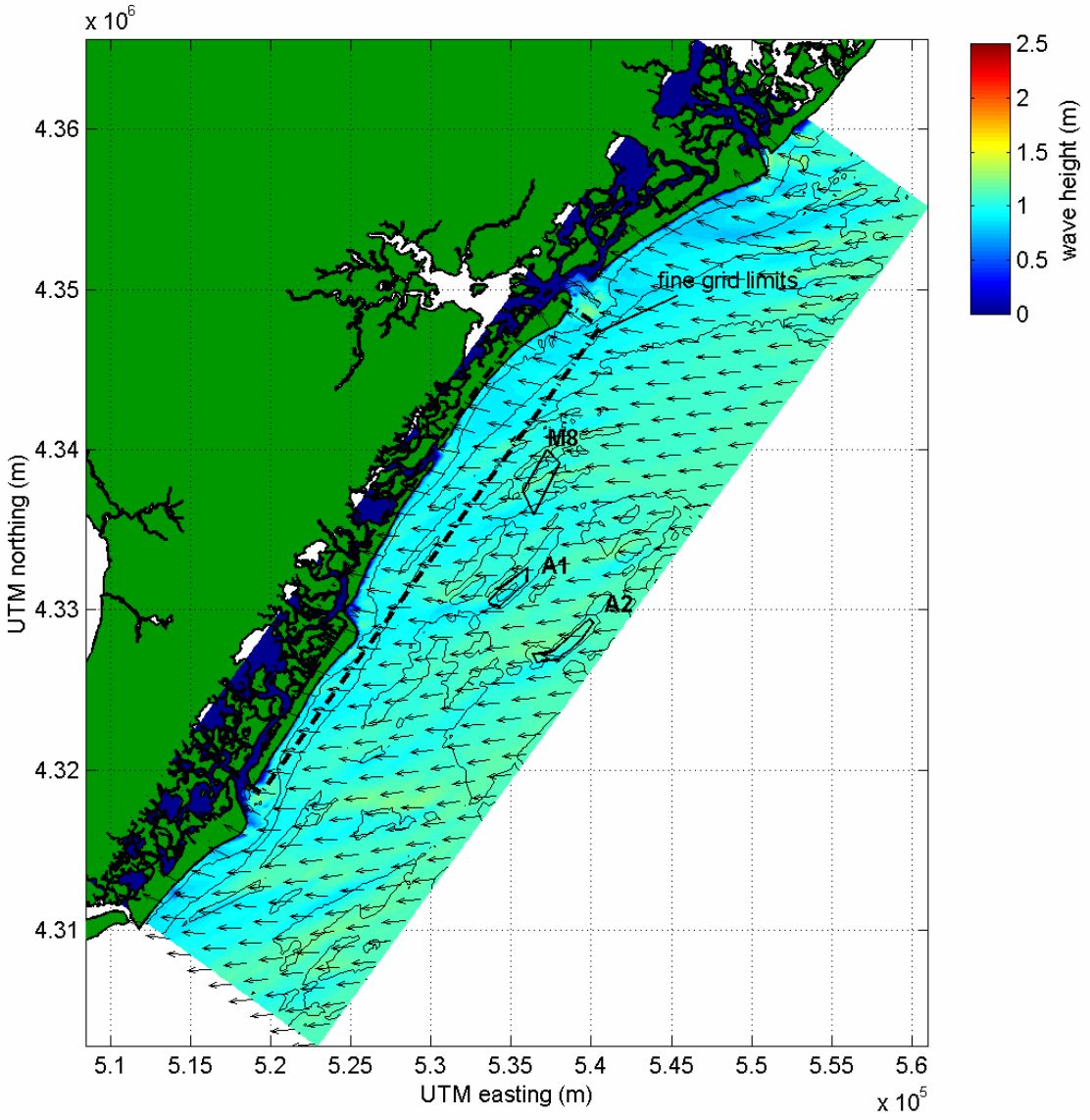

Figure B-2. Plot of STWAVE model output for southern New Jersey, existing conditions, wave Case 2 (H_s=1.1 m, T_{peak}=8.3 sec, θ_{peak}=86 deg). Color contours indicate wave height, and vectors show mean direction of wave propagation.

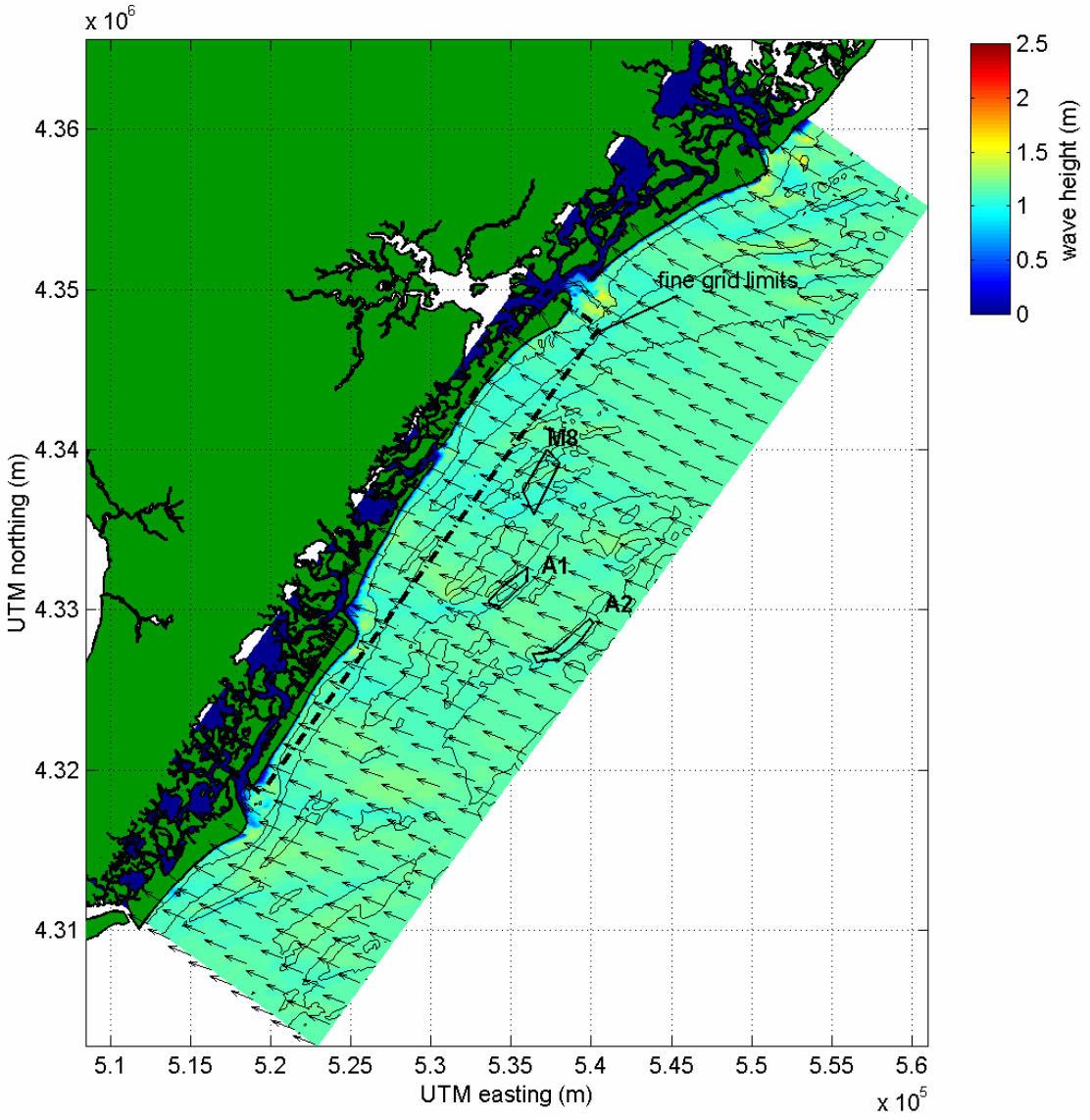

Figure B-3. Plot of STWAVE model output for southern New Jersey, existing conditions, wave Case 3 (H_s=1.2 m, T_{peak}=7.7 sec, θ_{peak}=111 deg). Color contours indicate wave height, and vectors show mean direction of wave propagation.

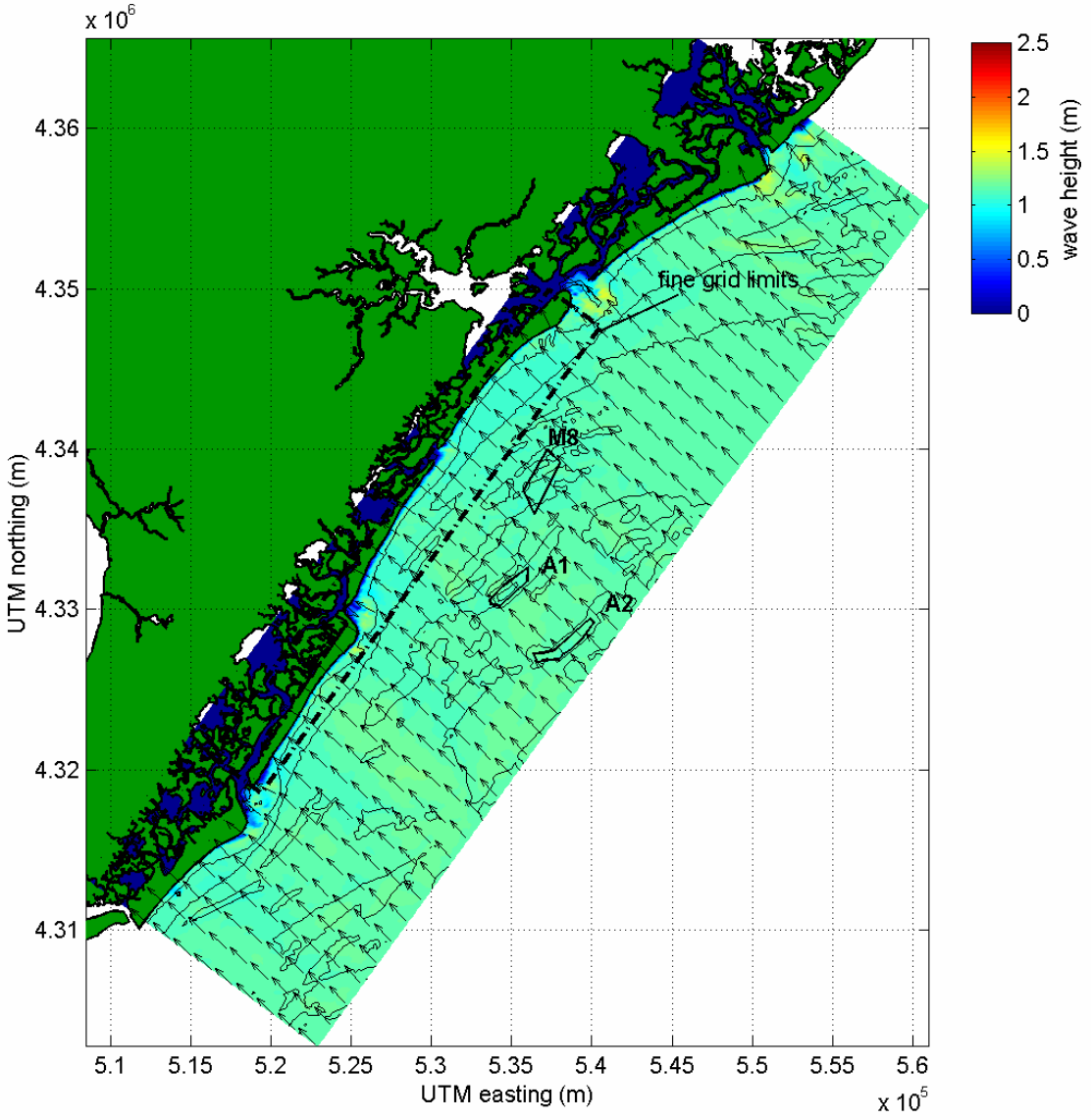

Figure B-4. Plot of STWAVE model output for southern New Jersey, existing conditions, wave Case 4 (H_s=1.2 m, T_{peak}=7.1 sec, θ_{peak}=131 deg). Color contours indicate wave height, and vectors show mean direction of wave propagation.

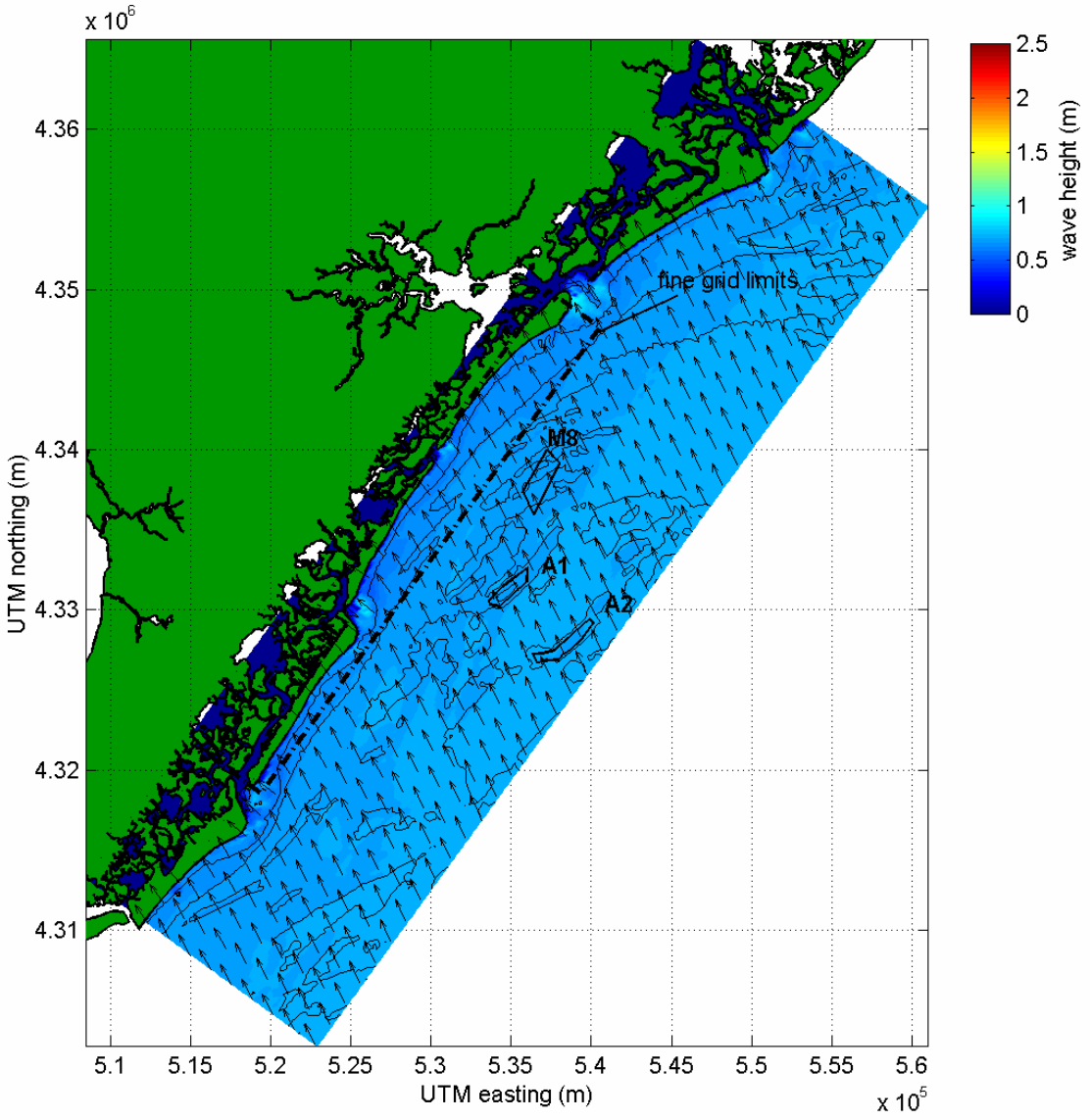

Figure B-5. Plot of STWAVE model output for southern New Jersey, existing conditions, wave Case 5 (H_s=0.8 m, T_{peak}=5.0 sec, θ_{peak}=161 deg). Color contours indicate wave height, and vectors show mean direction of wave propagation.

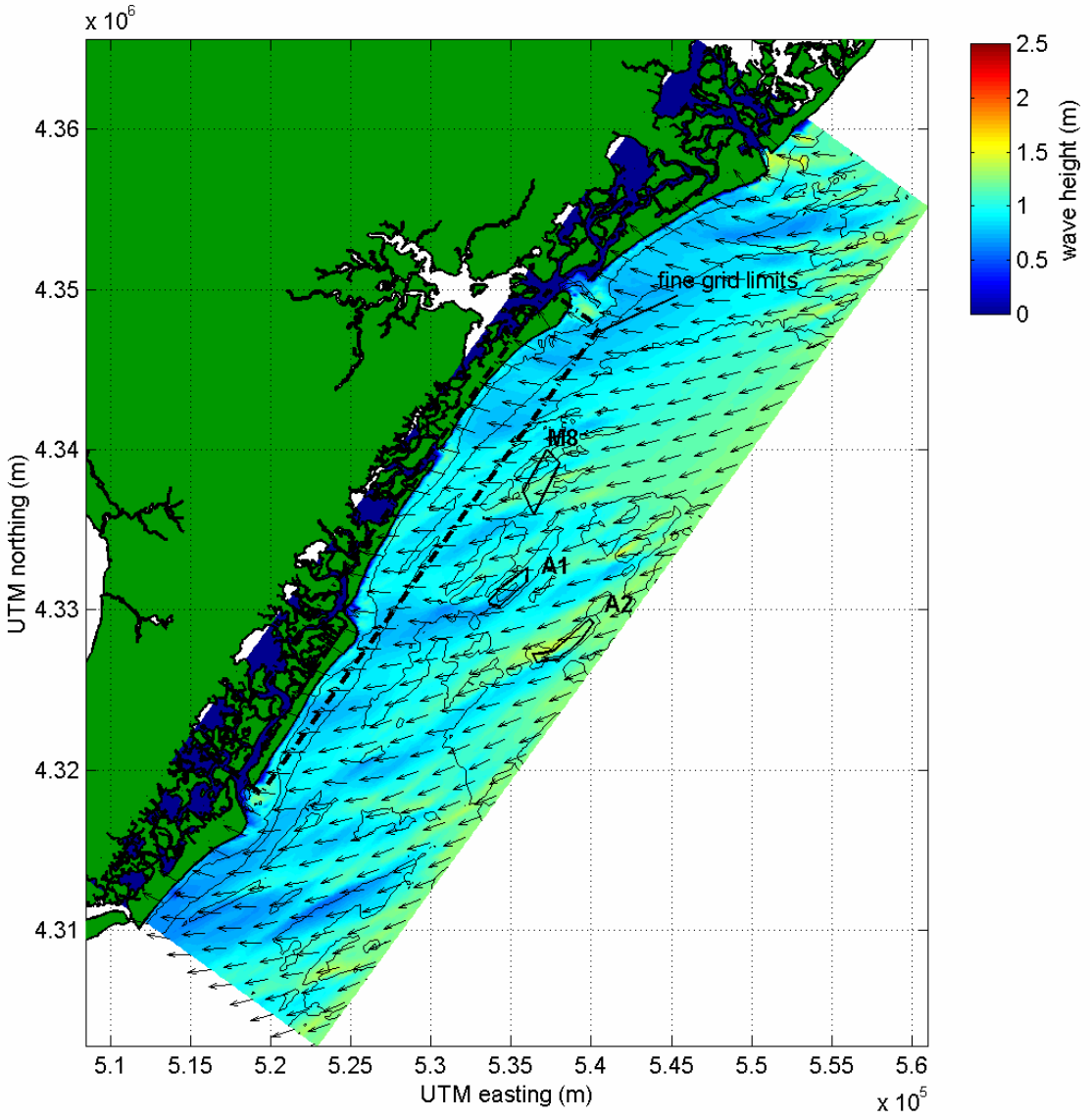

Figure B-6. Plot of STWAVE model output for southern New Jersey, existing conditions, wave Case 6 (H_s=1.3 m, T_{peak}=11.1 sec, θ_{peak}=61 deg). Color contours indicate wave height, and vectors show mean direction of wave propagation.

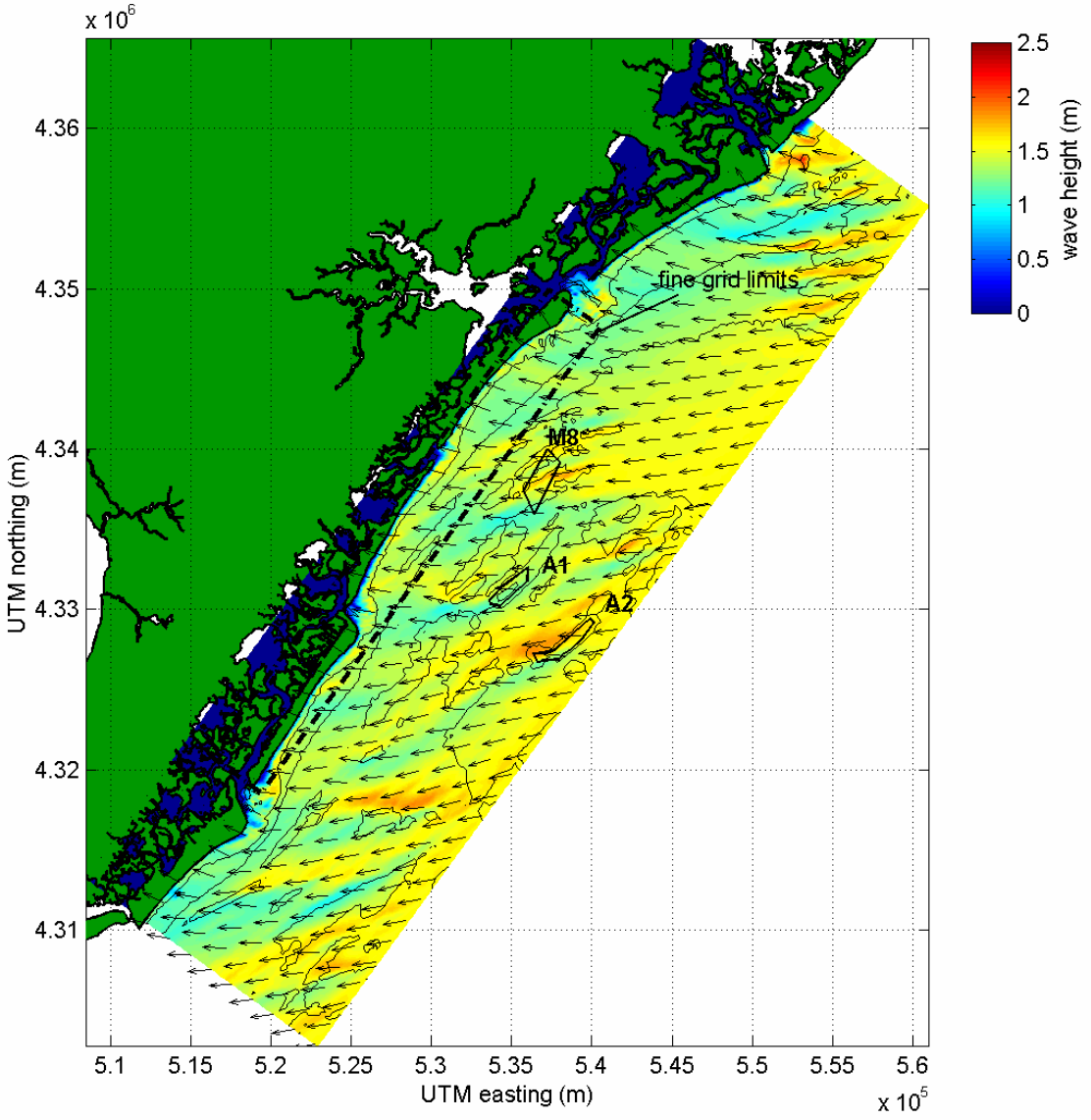

Figure B-7. Plot of STWAVE model output for southern New Jersey, existing conditions, wave Case 7 (H_s=1.6 m, T_{peak}=11.1 sec, θ_{peak}=81 deg). Color contours indicate wave height, and vectors show mean direction of wave propagation.

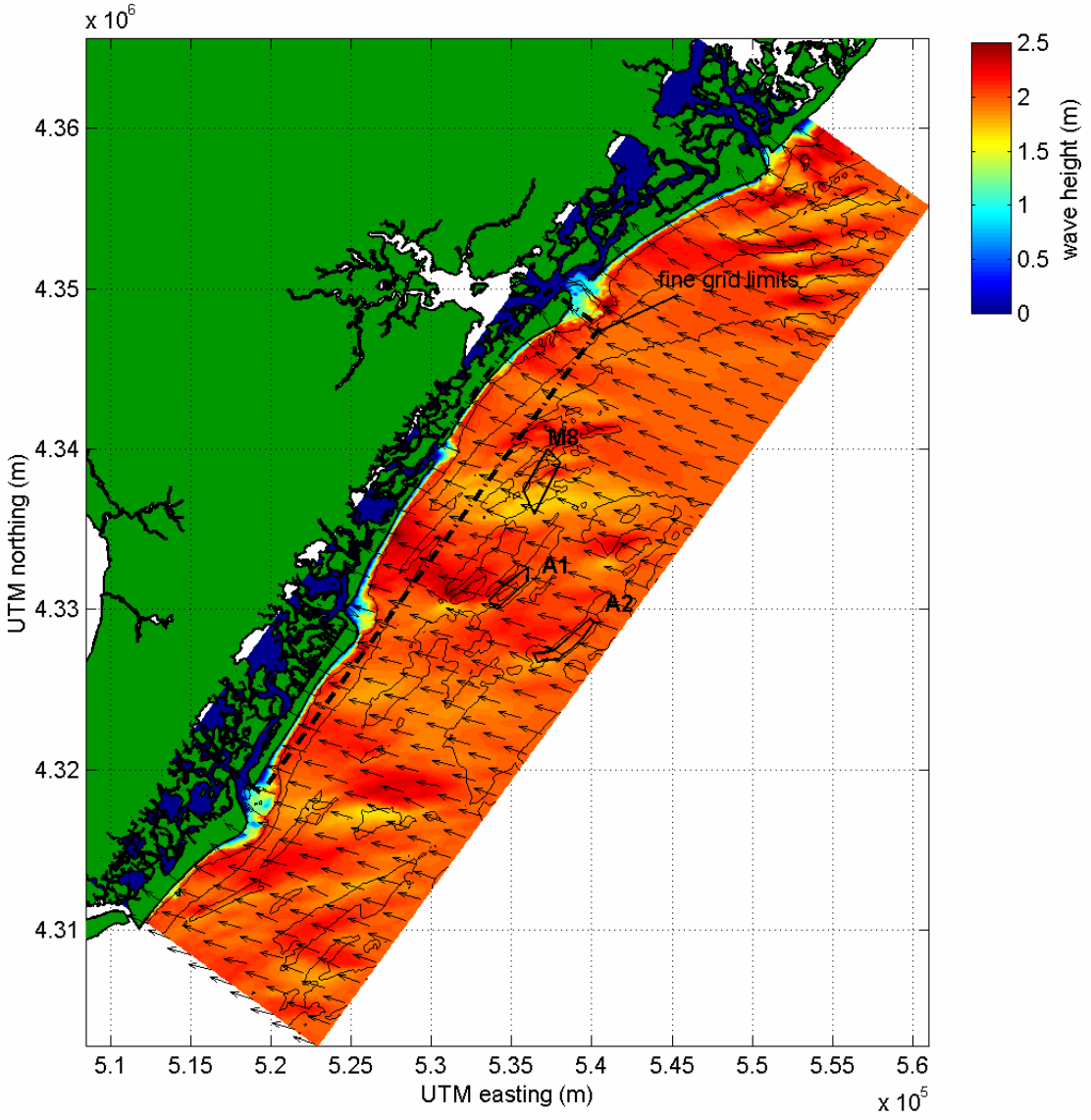

Figure B-8. Plot of STWAVE model output for southern New Jersey, existing conditions, wave Case 8 (H_s=2.0 m, T_{peak}=10.0 sec, θ_{peak}=96 deg). Color contours indicate wave height, and vectors show mean direction of wave propagation.

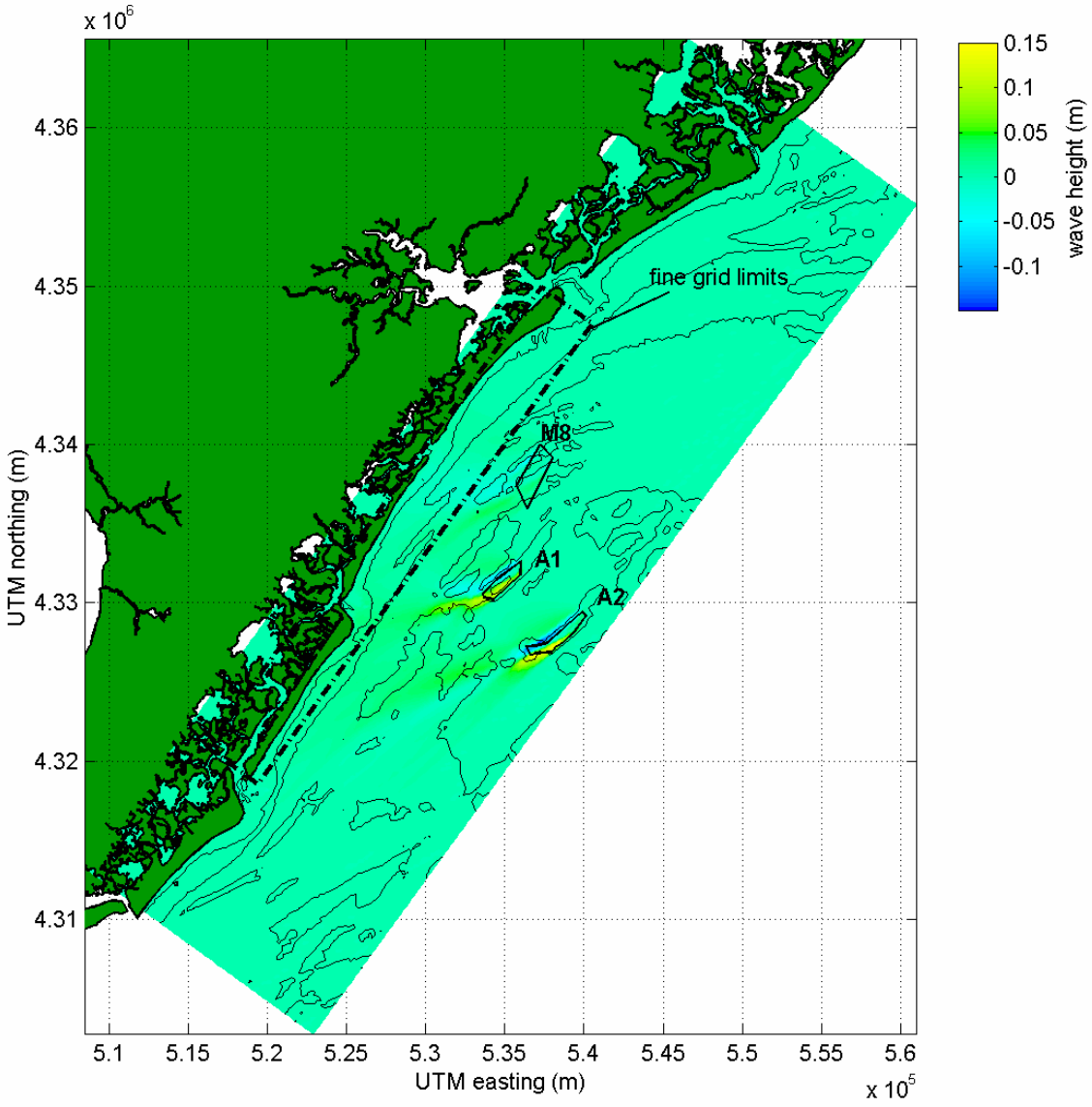

Figure B-9. Plot of wave height change between pre- and post-dredge ($\Delta=H_{post}-H_{pre}$) conditions at indicated borrow sites, for STWAVE model output of New Jersey wave Case 1 (H_s=1.4 m, T_{peak}=7.7 sec, θ_{peak}=61 deg).

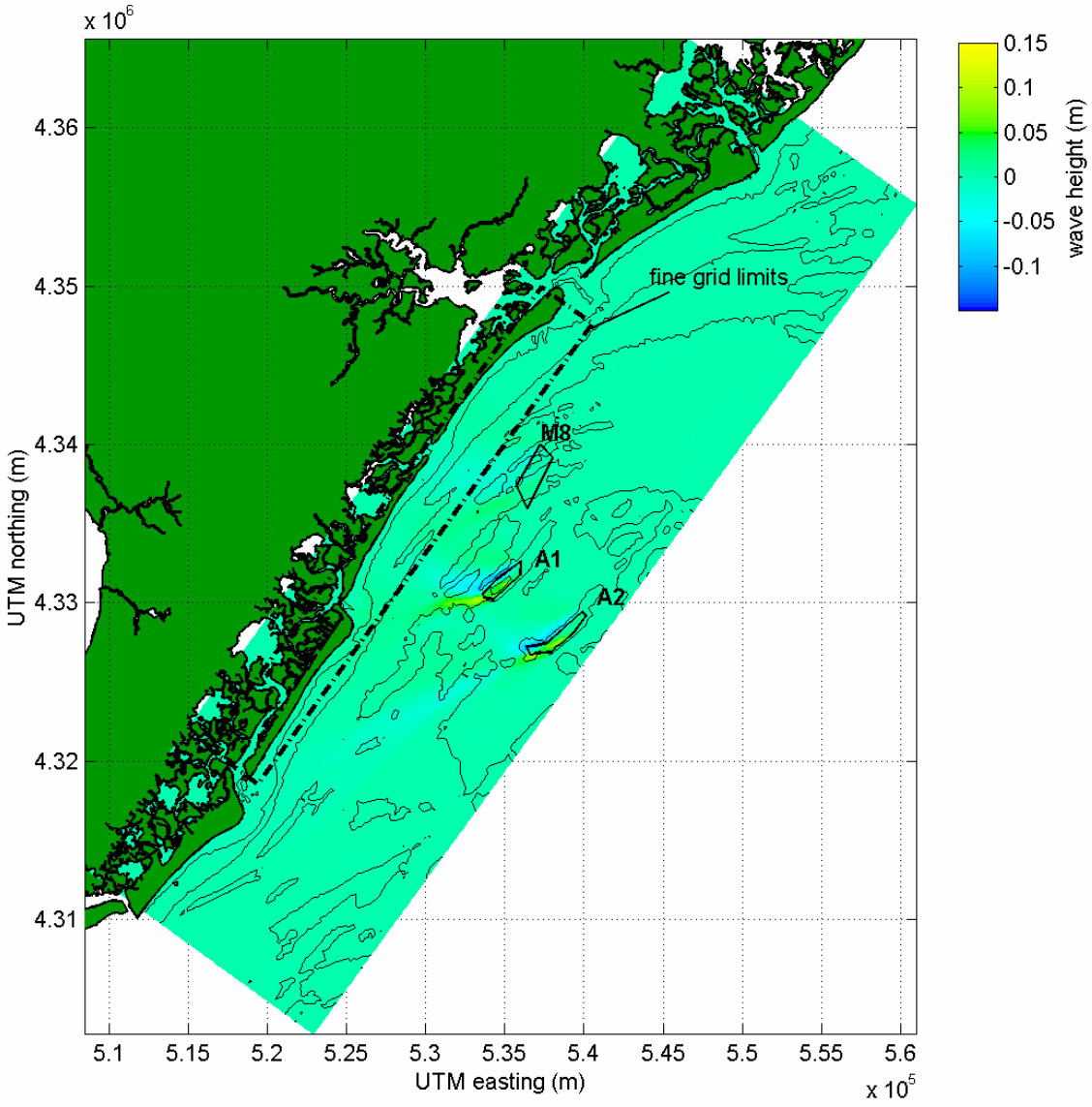

Figure B-10. Plot of wave height change between pre- and post-dredge ($\Delta=H_{post}-H_{pre}$) conditions at indicated borrow sites, for STWAVE model output of New Jersey wave Case 2 (H_s=1.1 m, T_{peak}=8.3 sec, θ_{peak}=86 deg).

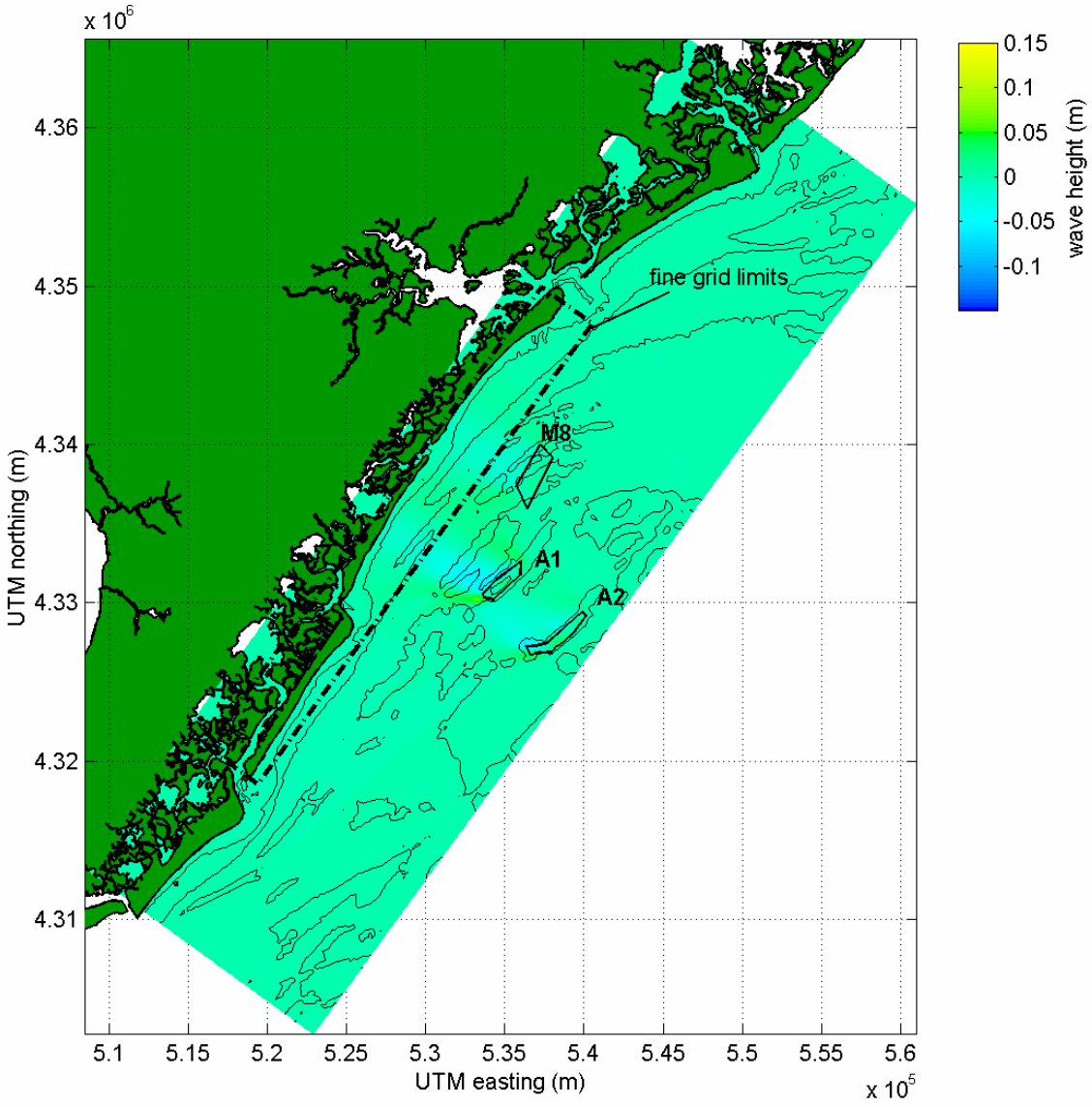

Figure B-11. Plot of wave height change between pre- and post-dredge ($\Delta=H_{post}-H_{pre}$) conditions at indicated borrow sites, for STWAVE model output of New Jersey wave Case 3 (H_s=1.2 m, T_{peak}=7.7 sec, θ_{peak}=111 deg).

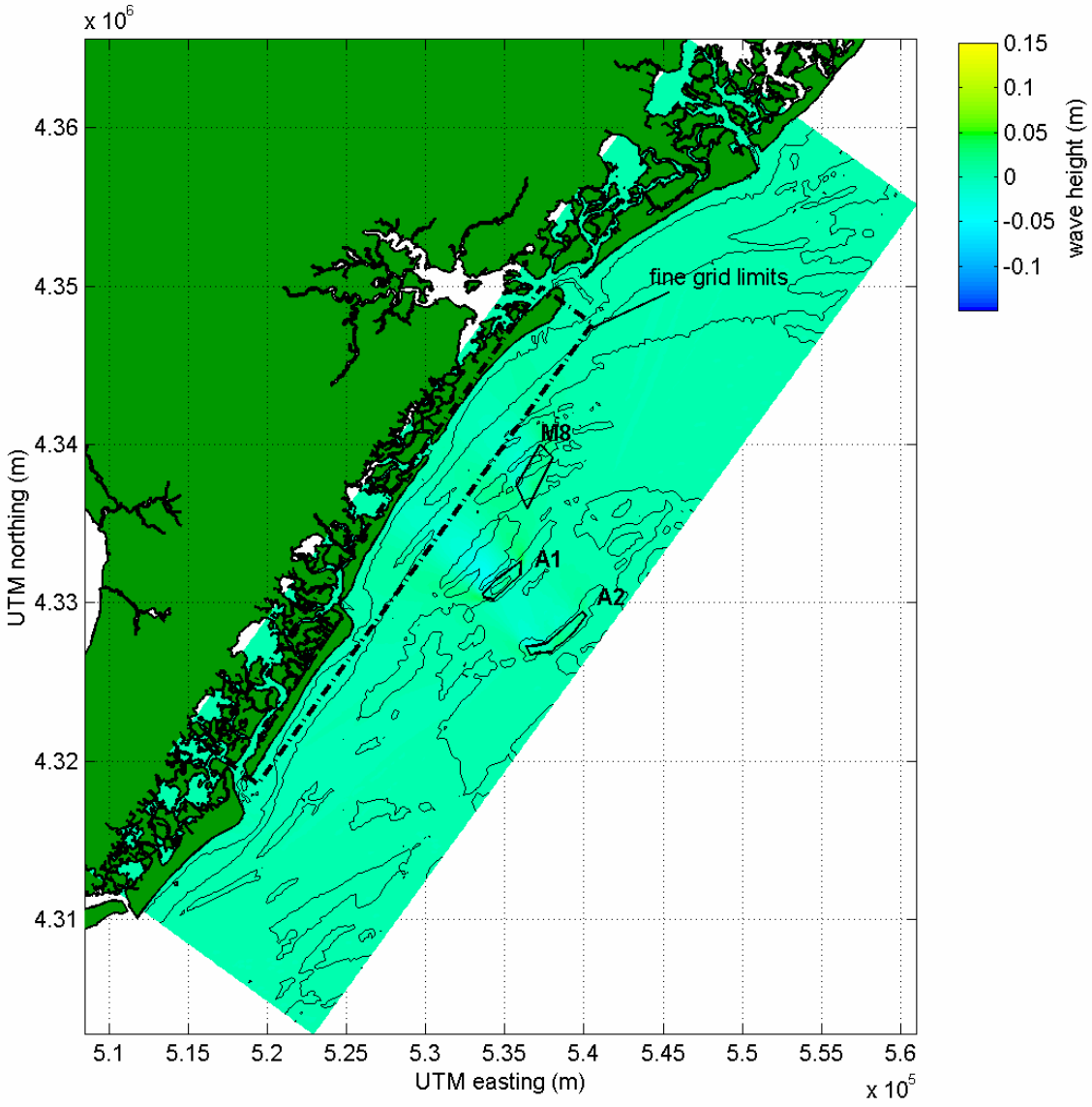

Figure B-12. Plot of wave height change between pre- and post-dredge ($\Delta=H_{post}-H_{pre}$) conditions at indicated borrow sites, for STWAVE model output of New Jersey wave Case 4 (H_s=1.2 m, T_{peak}=7.1 sec, θ_{peak}=131 deg).

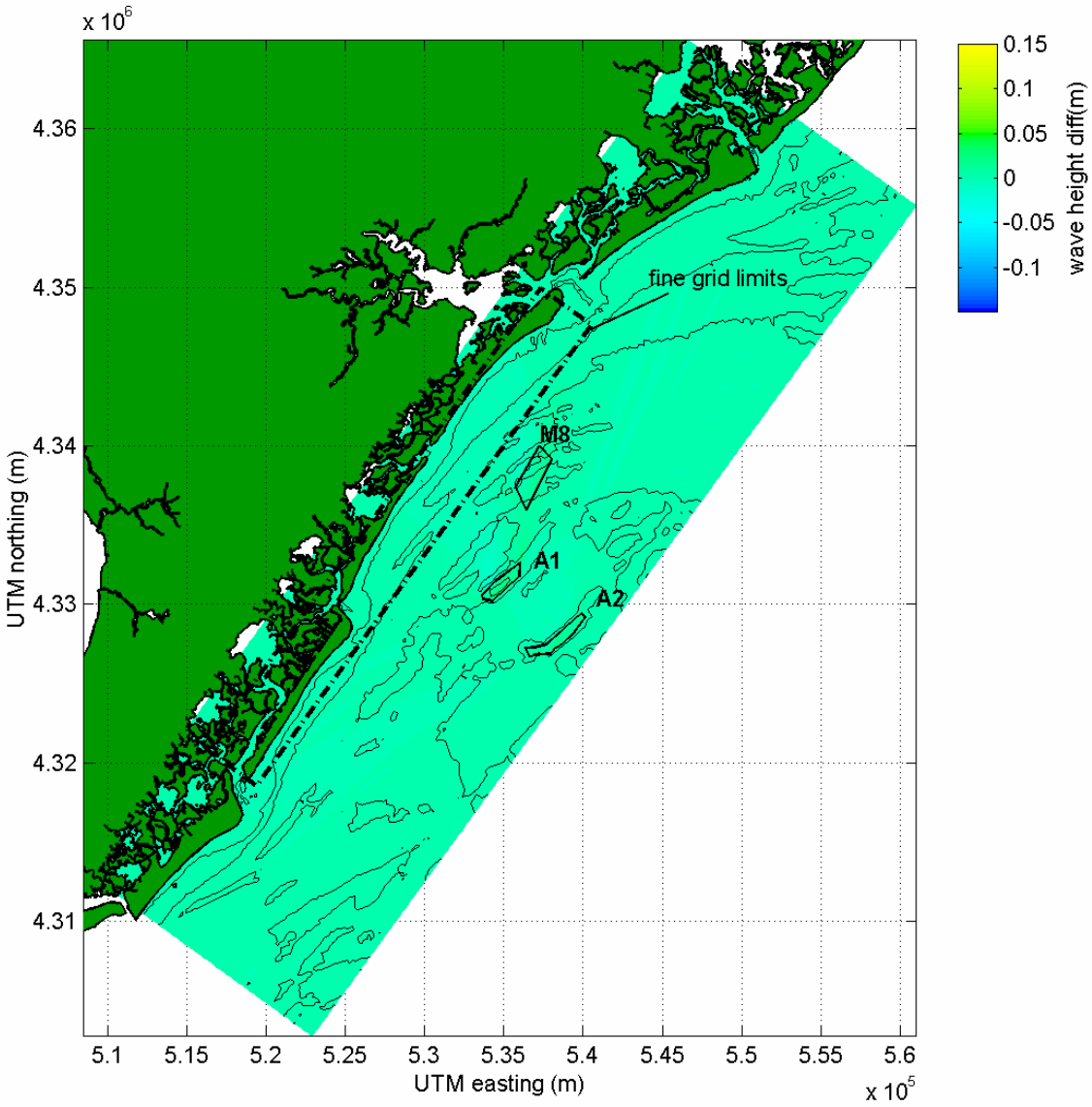

Figure B-13. Plot of wave height change between pre- and post-dredge ($\Delta=H_{post}-H_{pre}$) conditions at indicated borrow sites, for STWAVE model output of New Jersey wave Case 5 (H_s=0.8 m, T_{peak}=5.0 sec, θ_{peak}=161 deg).

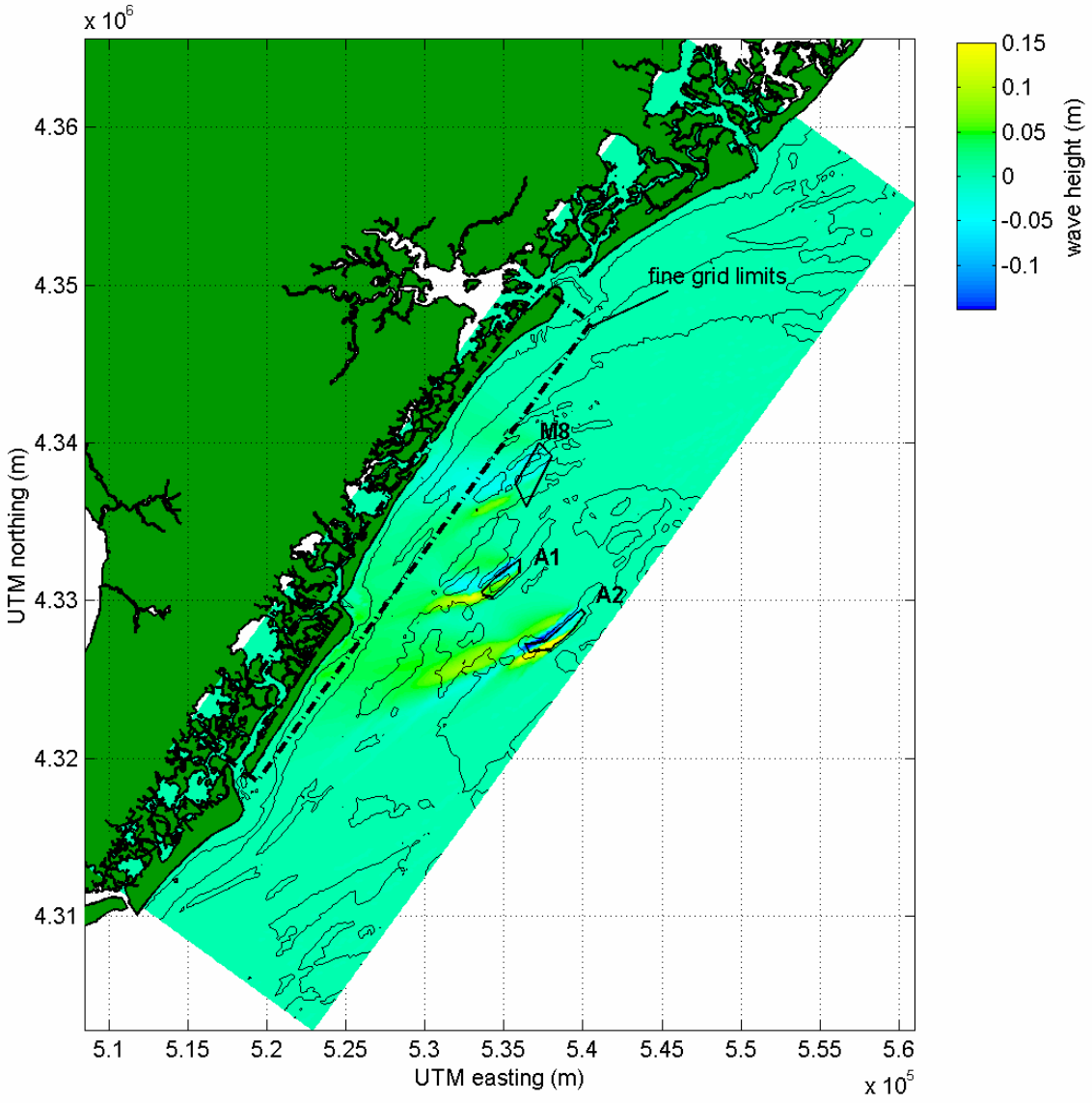

Figure B-14. Plot of wave height change between pre- and post-dredge ($\Delta=H_{post}-H_{pre}$) conditions at indicated borrow sites, for STWAVE model output of New Jersey wave Case 6 (H_s=1.3 m, T_{peak}=11.1 sec, θ_{peak}=61 deg).

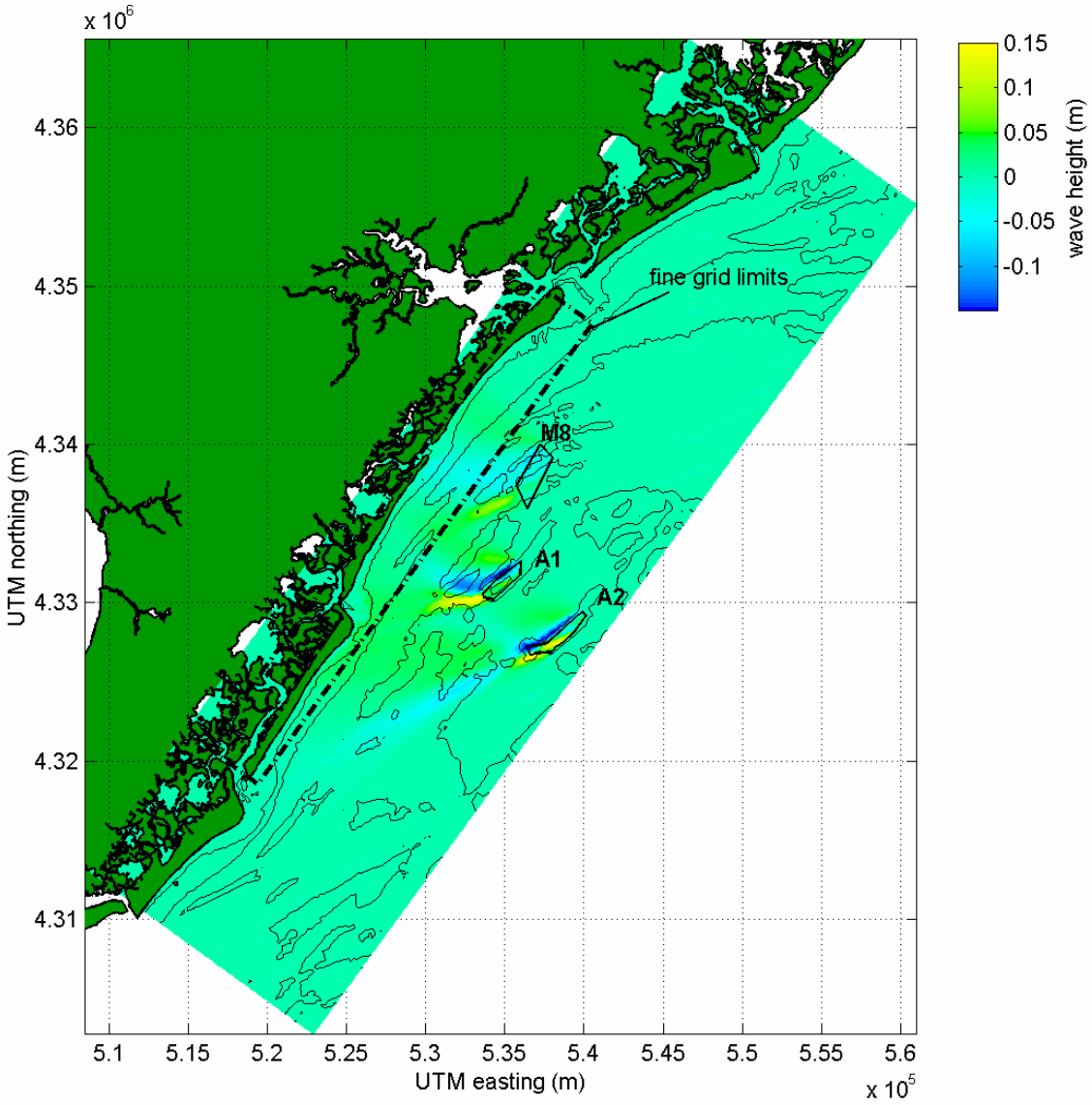

Figure B-15. Plot of wave height change between pre- and post-dredge ($\Delta=H_{post}-H_{pre}$) conditions at indicated borrow sites, for STWAVE model output of New Jersey wave Case 7 (H_s=1.6 m, T_{peak}=11.1 sec, θ_{peak}=81 deg).

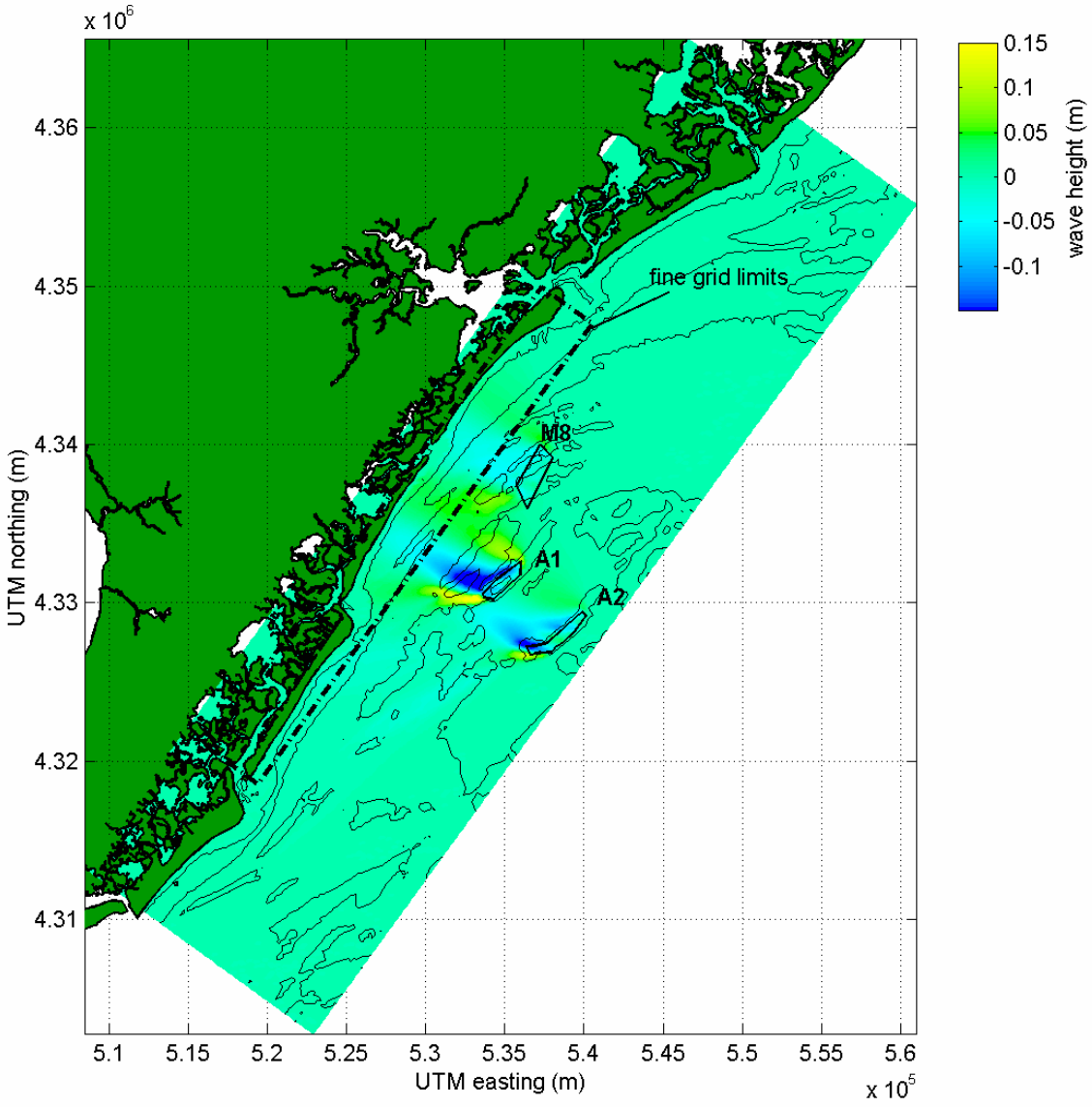

Figure B-16. Plot of wave height change between pre- and post-dredge ($\Delta=H_{post}-H_{pre}$) conditions at indicated borrow sites, for STWAVE model output of New Jersey wave Case 8 (H_s=2.0 m, T_{peak}=10.0 sec, θ_{peak}=96 deg).

APPENDIX C: VIRGINIA WAVE MODEL OUTPUT

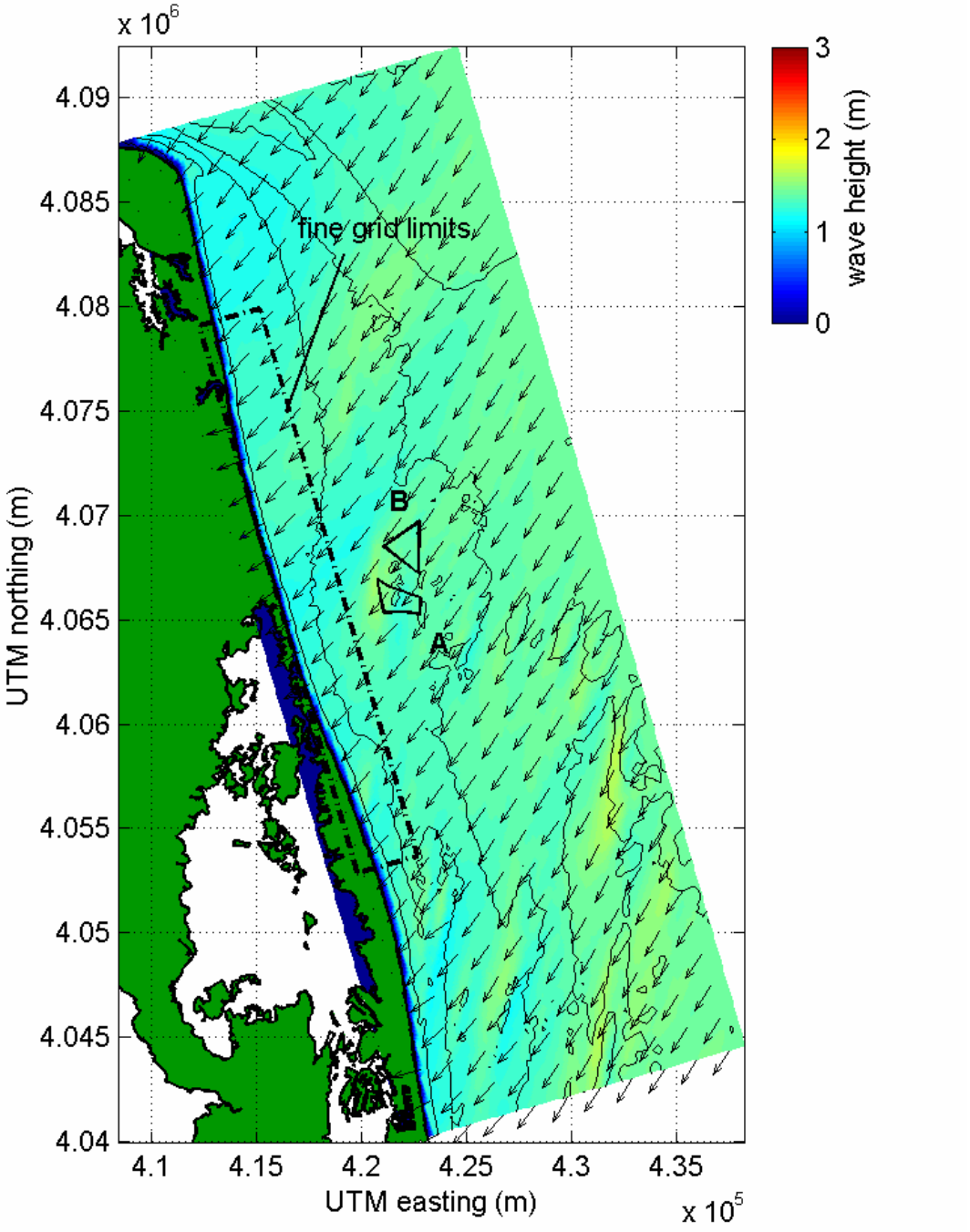

Figure C-1. Plot of STWAVE model output for Virginia, existing conditions, wave Case 1 (H_s=1.6 m, T_{peak}=7.7 sec, θ_{peak}=359 deg). Color contours indicate wave height, and vectors show mean direction of wave propagation.

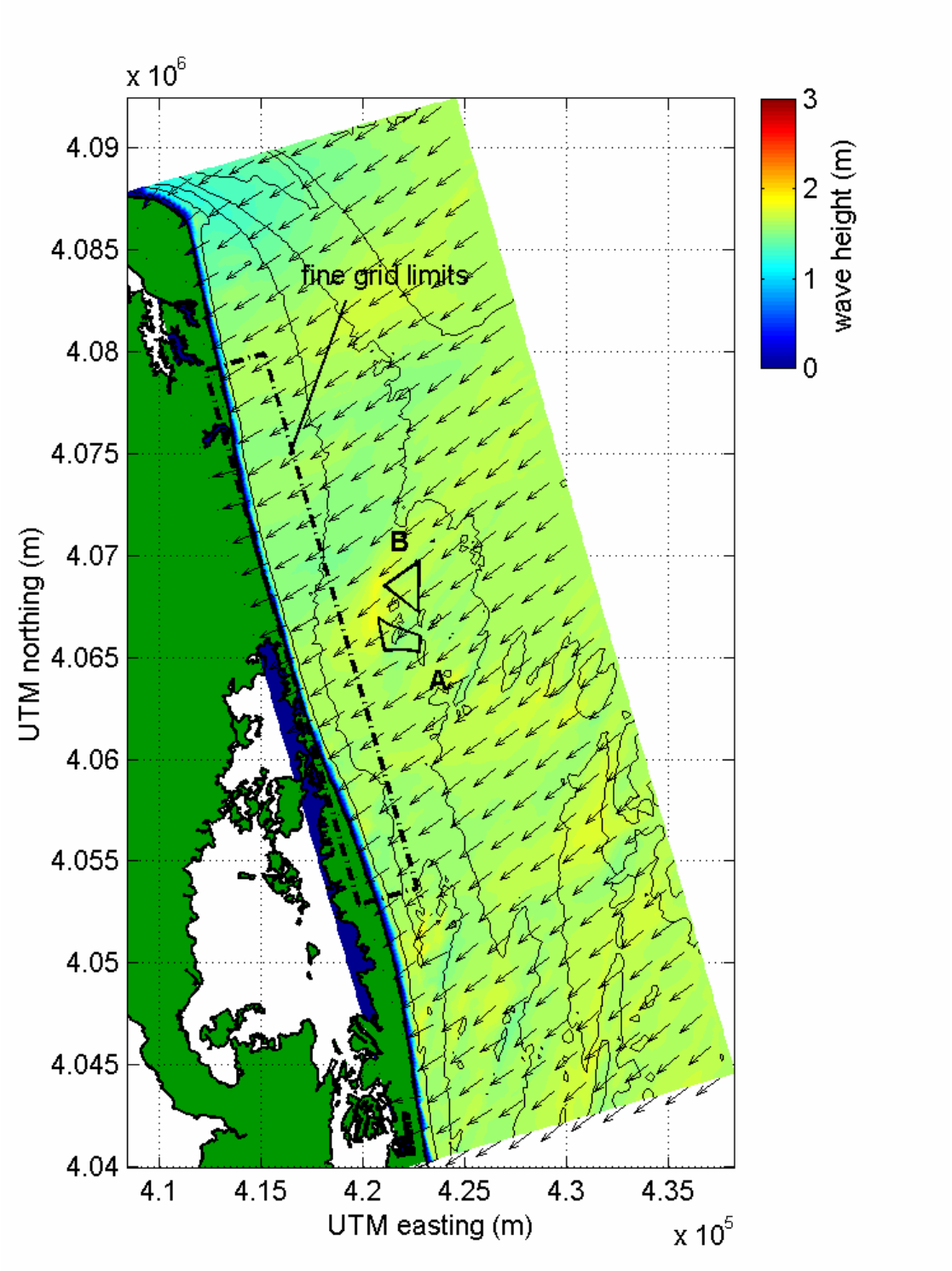

Figure C-2. Plot of STWAVE model output for Virginia, existing conditions, wave Case 2 (H_s=1.6 m, T_{peak}=8.3 sec, θ_{peak}=34 deg). Color contours indicate wave height, and vectors show mean direction of wave propagation.

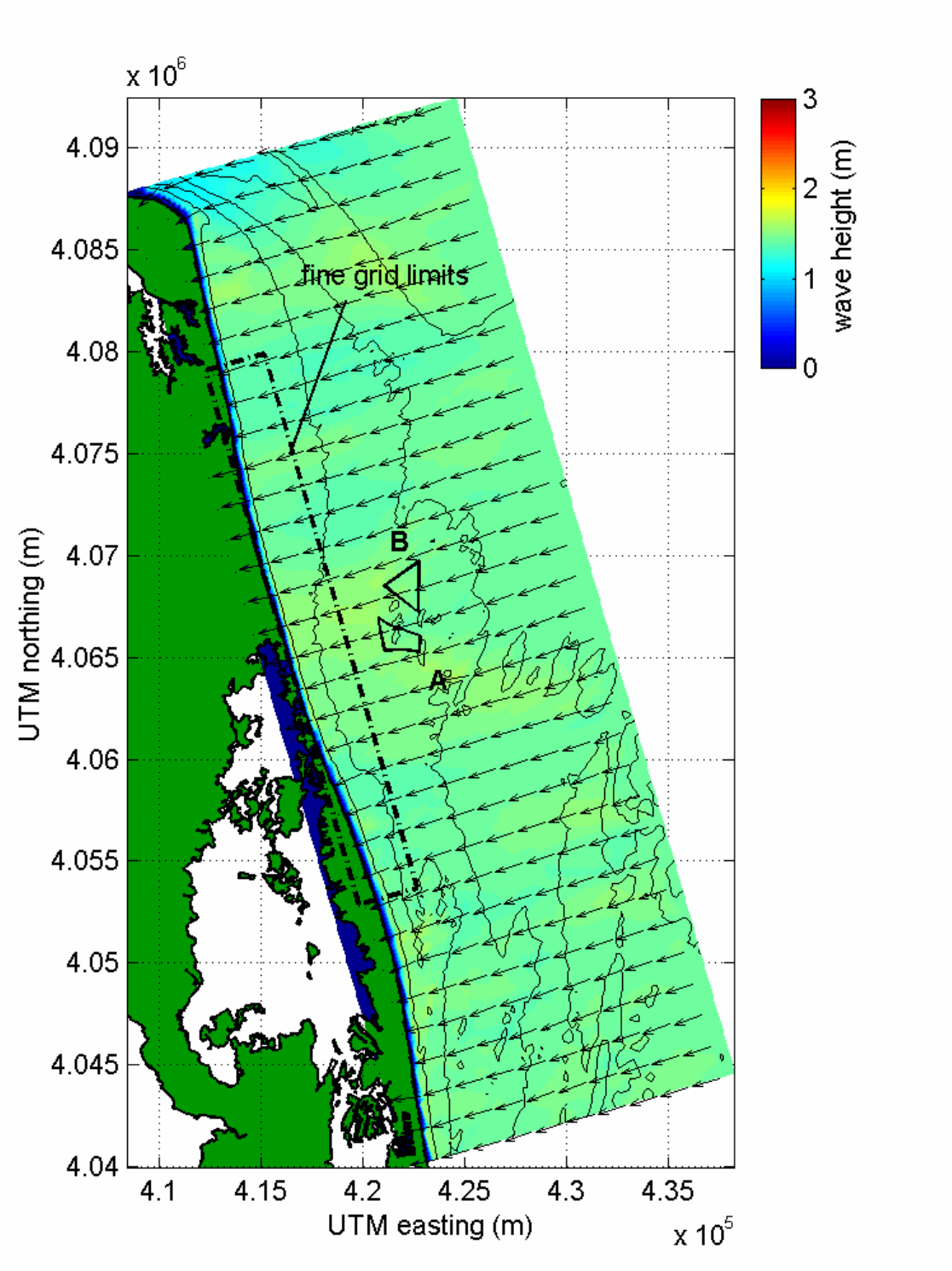

Figure C-3. Plot of STWAVE model output for Virginia, existing conditions, wave Case 3 (H_s=1.4 m, T_{peak}=9.1 sec, θ_{peak}=54 deg). Color contours indicate wave height, and vectors show mean direction of wave propagation.

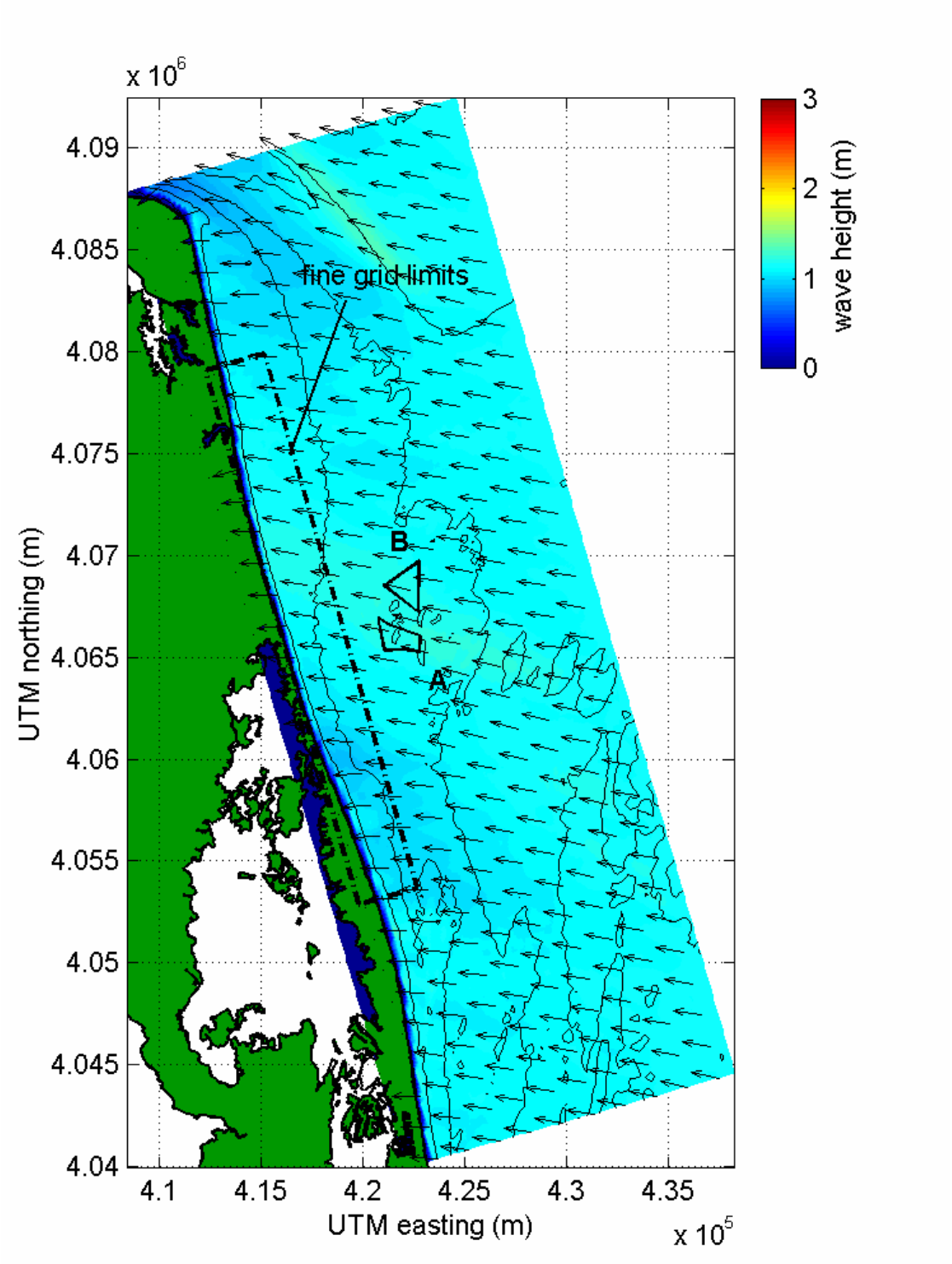

Figure C-4. Plot of STWAVE model output for Virginia, existing conditions, wave Case 4 (H_s=1.1 m, T_{peak}=8.3 sec, θ_{peak}=104 deg). Color contours indicate wave height, and vectors show mean direction of wave propagation.

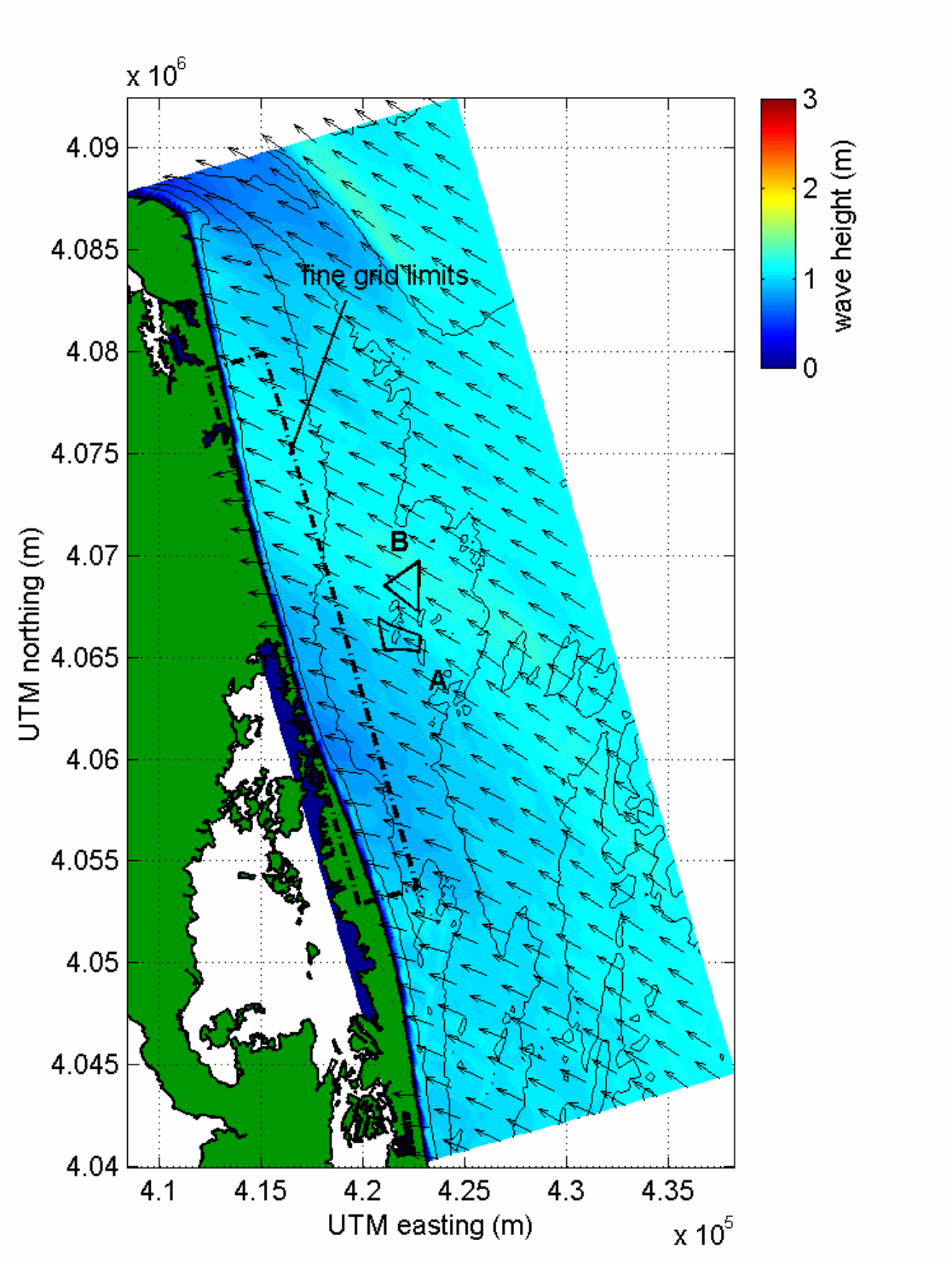

Figure C-5. Plot of STWAVE model output for Virginia, existing conditions, wave Case 5 (H_s=1.1 m, T_{peak}=8.3 sec, θ_{peak}=119 deg). Color contours indicate wave height, and vectors show mean direction of wave propagation.

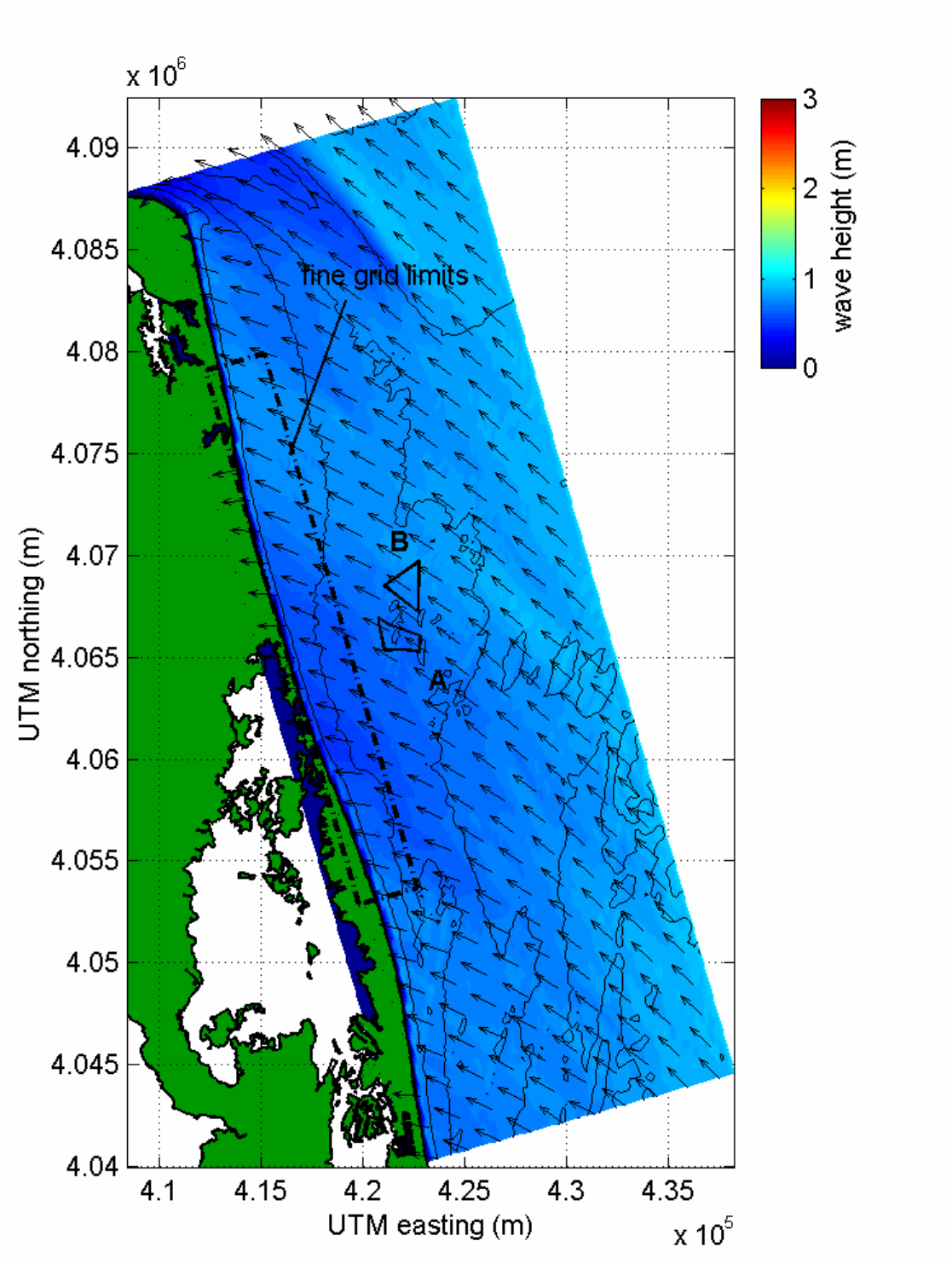

Figure C-6. Plot of STWAVE model output for Virginia, existing conditions, wave Case 6 (H_s=1.2 m, T_{peak}=8.3 sec, θ_{peak}=149 deg). Color contours indicate wave height, and vectors show mean direction of wave propagation.

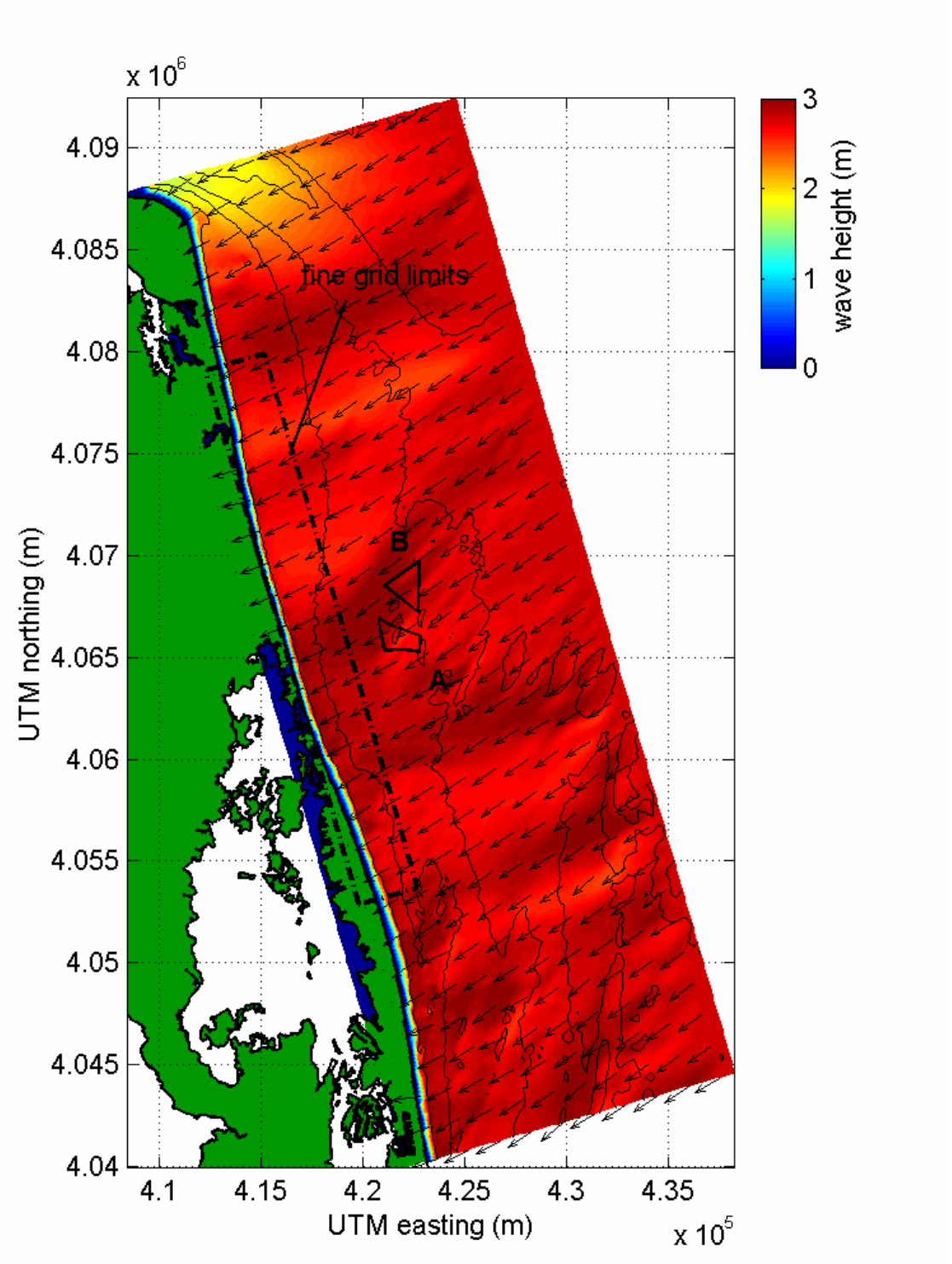

Figure C-7. Plot of STWAVE model output for Virginia, existing conditions, wave Case 7 (H_s=2.8 m, T_{peak}=11.1 sec, θ_{peak}=39 deg). Color contours indicate wave height, and vectors show mean direction of wave propagation.

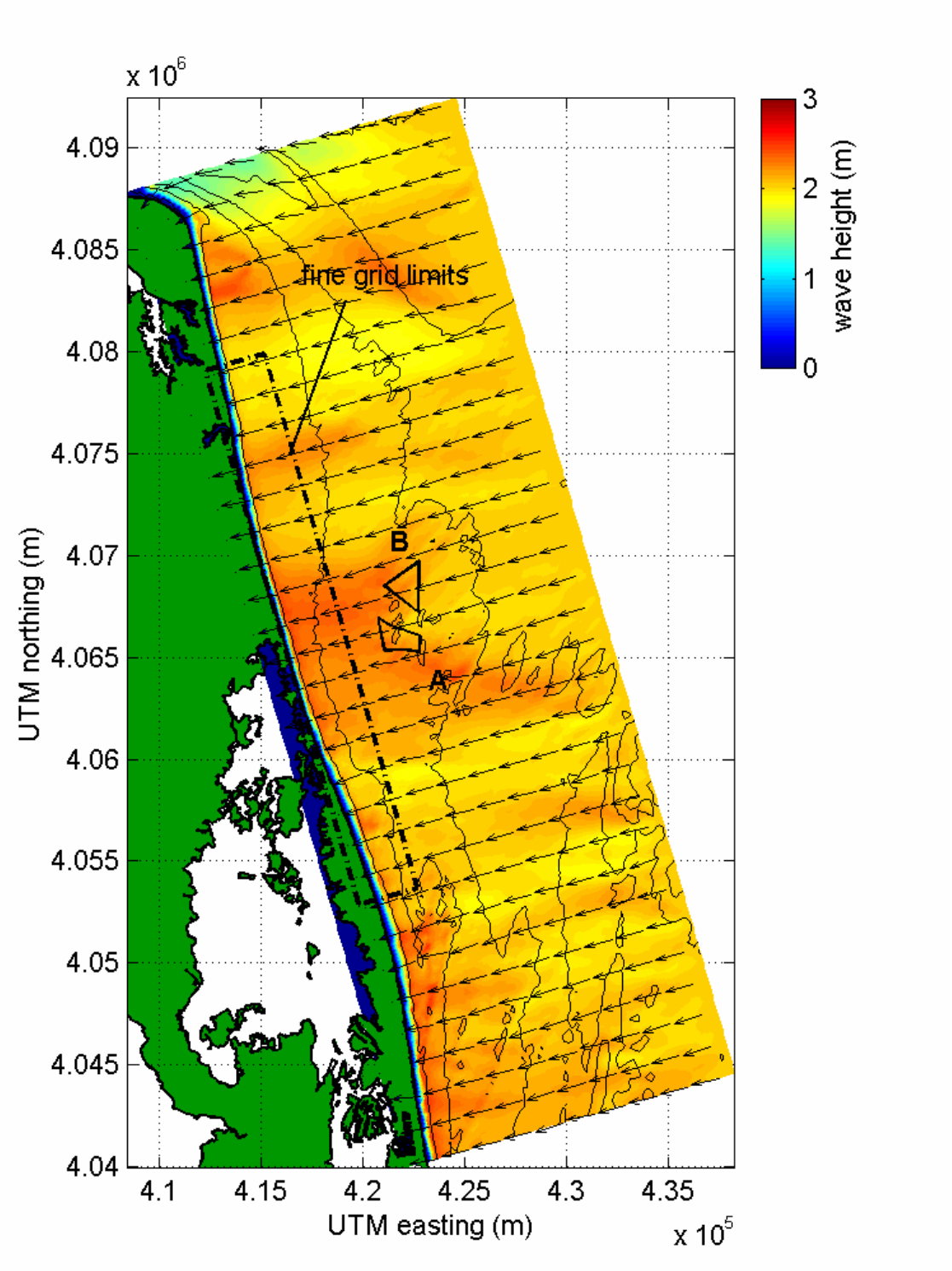

Figure C-8. Plot of STWAVE model output for Virginia, existing conditions, wave Case 8 (H_s=2.0 m, T_{peak}=11.1 sec, θ_{peak}=64 deg). Color contours indicate wave height, and vectors show mean direction of wave propagation.

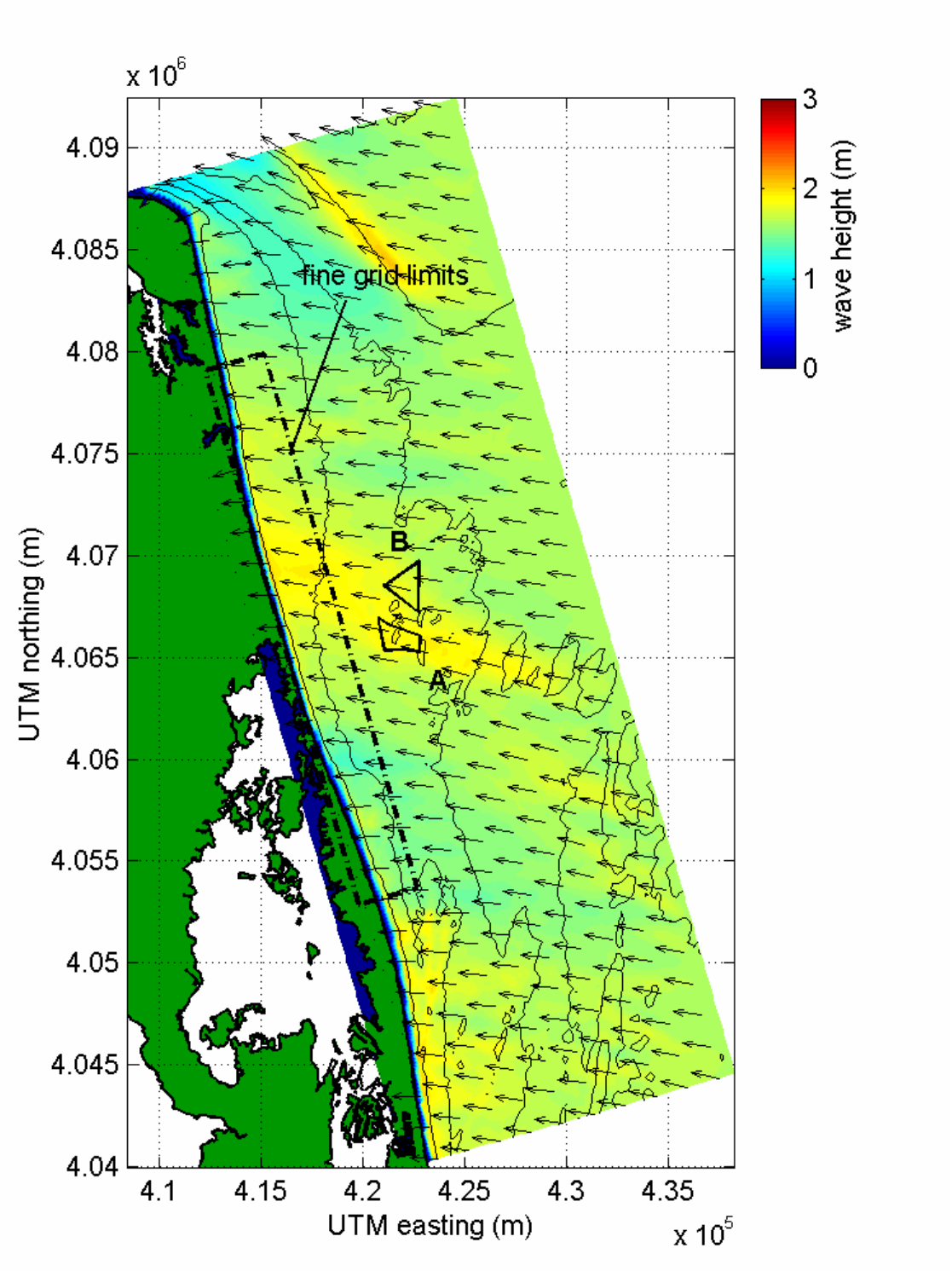

Figure C-9. Plot of STWAVE model output for Virginia, existing conditions, wave Case 9 (H_s=1.6 m, T_{peak}=11.1 sec, θ_{peak}=79 deg). Color contours indicate wave height, and vectors show mean direction of wave propagation.

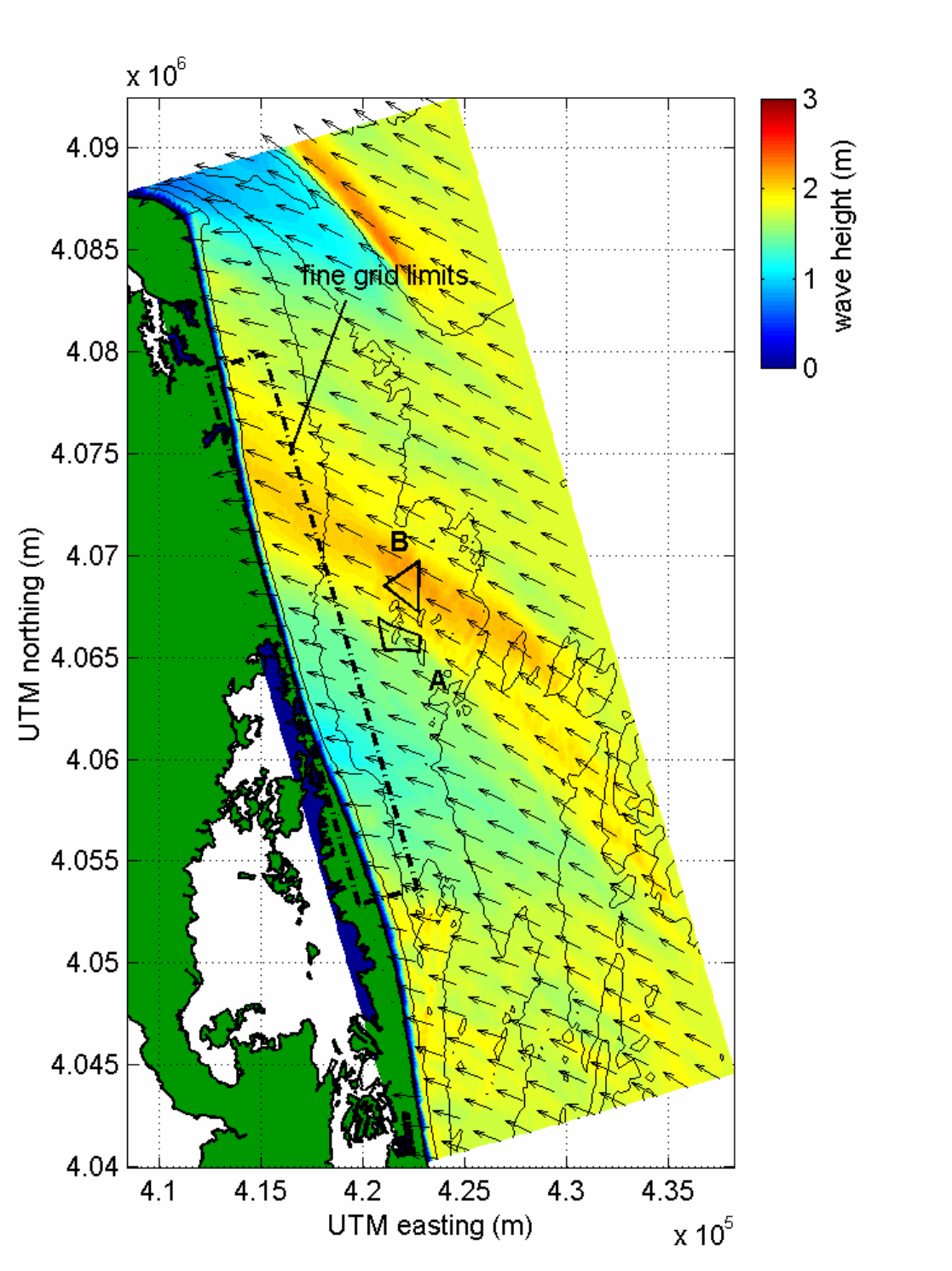

Figure C-10. Plot of STWAVE model output for Virginia, existing conditions, wave Case 10 (H_s=1.8 m, T_{peak}=10.0 sec, θ_{peak}=134 deg). Color contours indicate wave height, and vectors show mean direction of wave propagation.

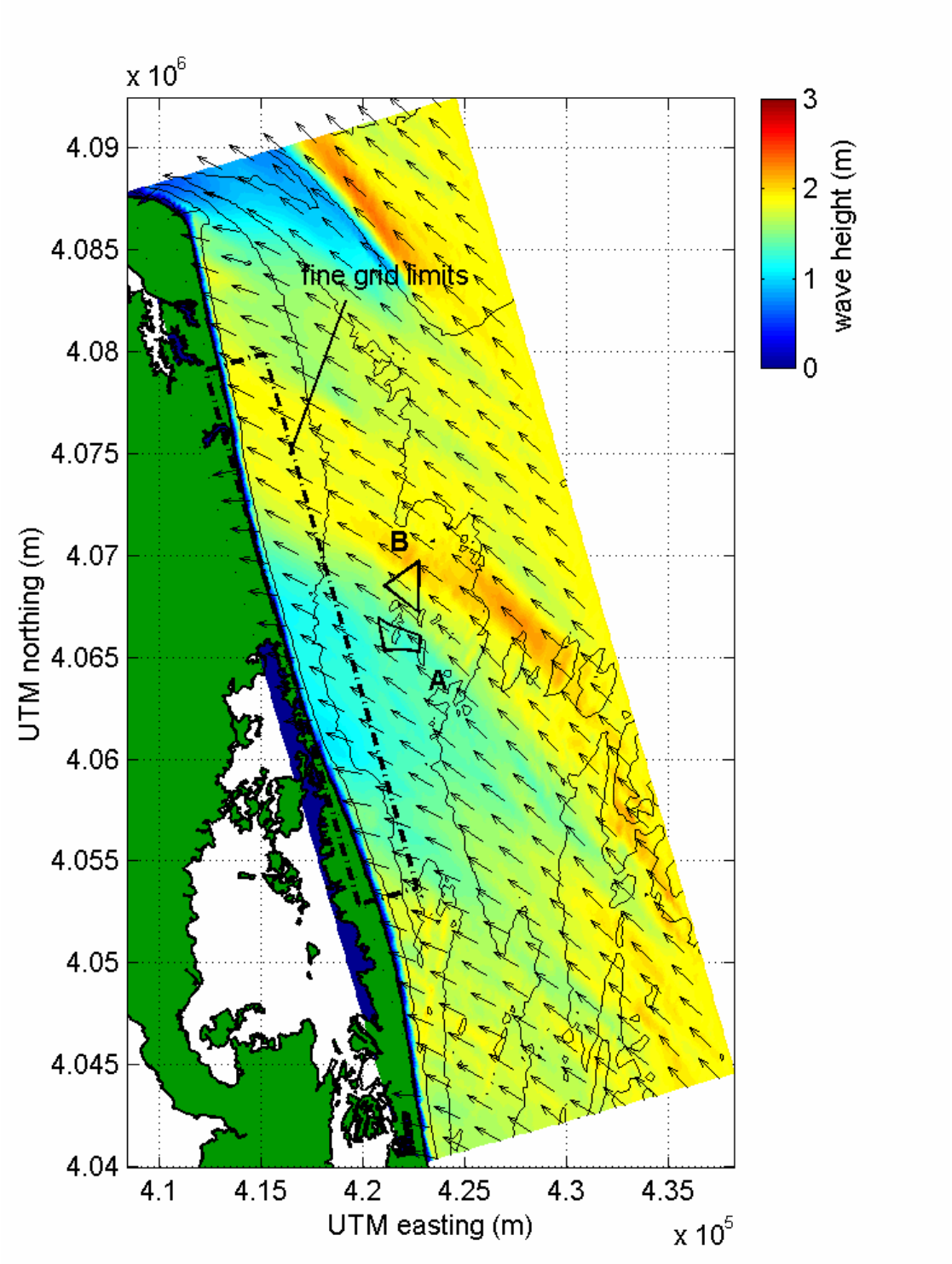

Figure C-11. Plot of STWAVE model output for Virginia, existing conditions, wave Case 7 (H_s=2.4 m, T_{peak}=10.0 sec, θ_{peak}=144 deg). Color contours indicate wave height, and vectors show mean direction of wave propagation.

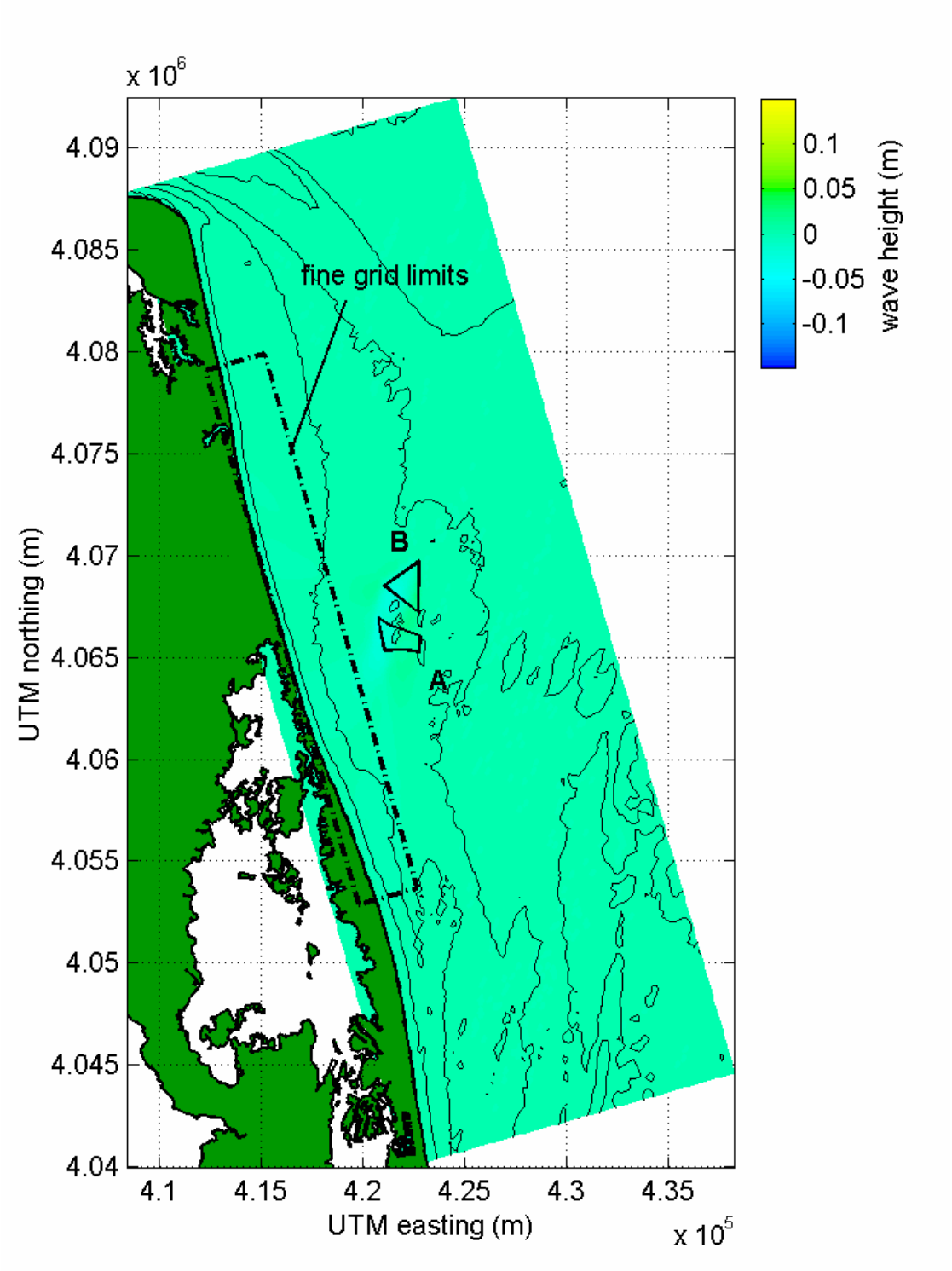

Figure C-12. Plot of wave height change between pre- and post-dredge ($\Delta=H_{post}-H_{pre}$) conditions at indicated borrow sites, for STWAVE model output of Virginia wave Case 1 (H_s=1.6 m, T_{peak}=7.7 sec, θ_{peak}=359 deg).

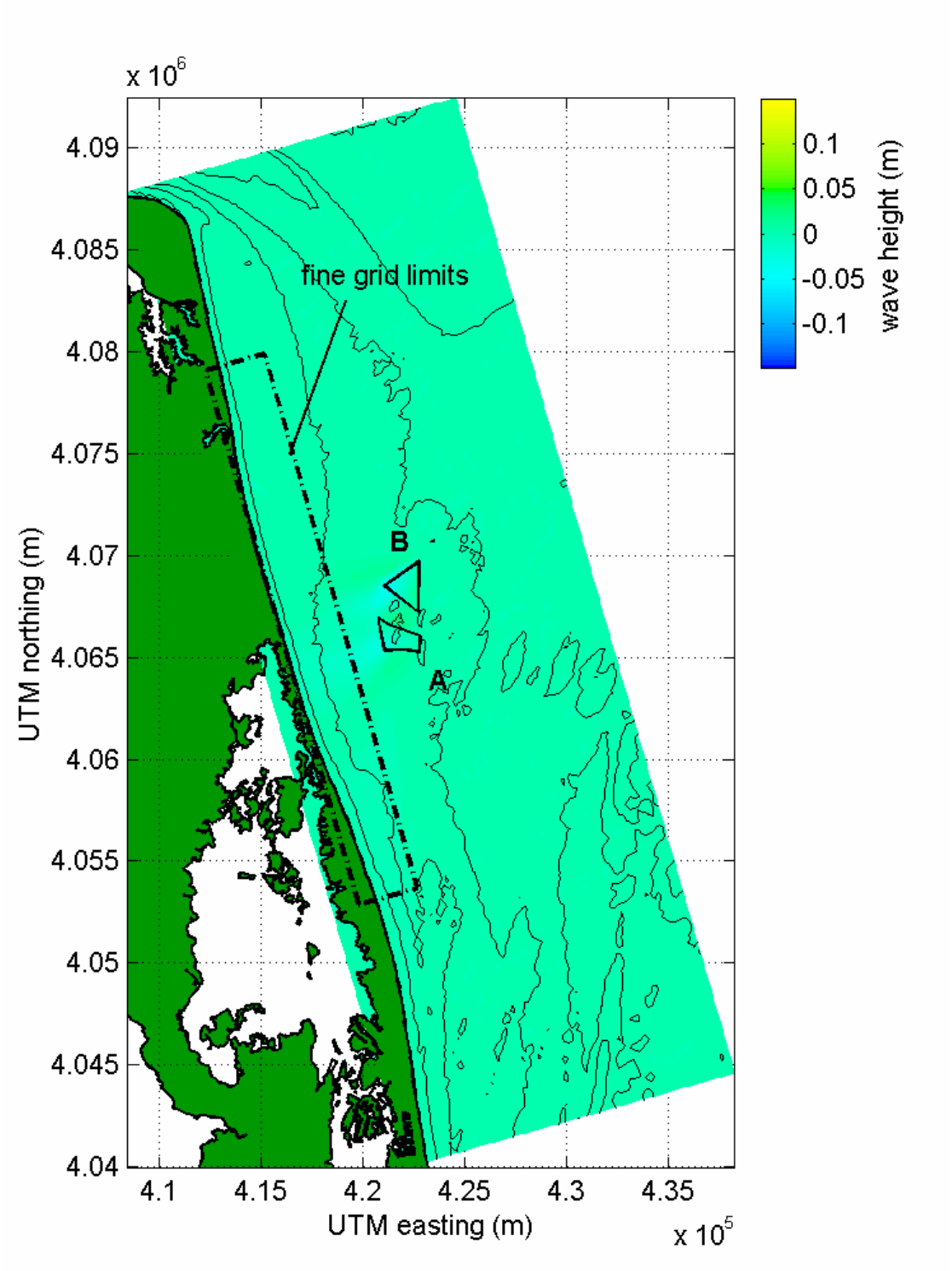

Figure C-13. Plot of wave height change between pre- and post-dredge ($\Delta=H_{post}-H_{pre}$) conditions at indicated borrow sites, for STWAVE model output of Virginia wave Case 2 (H_s=1.6 m, T_{peak}=8.3 sec, θ_{peak}=34 deg).

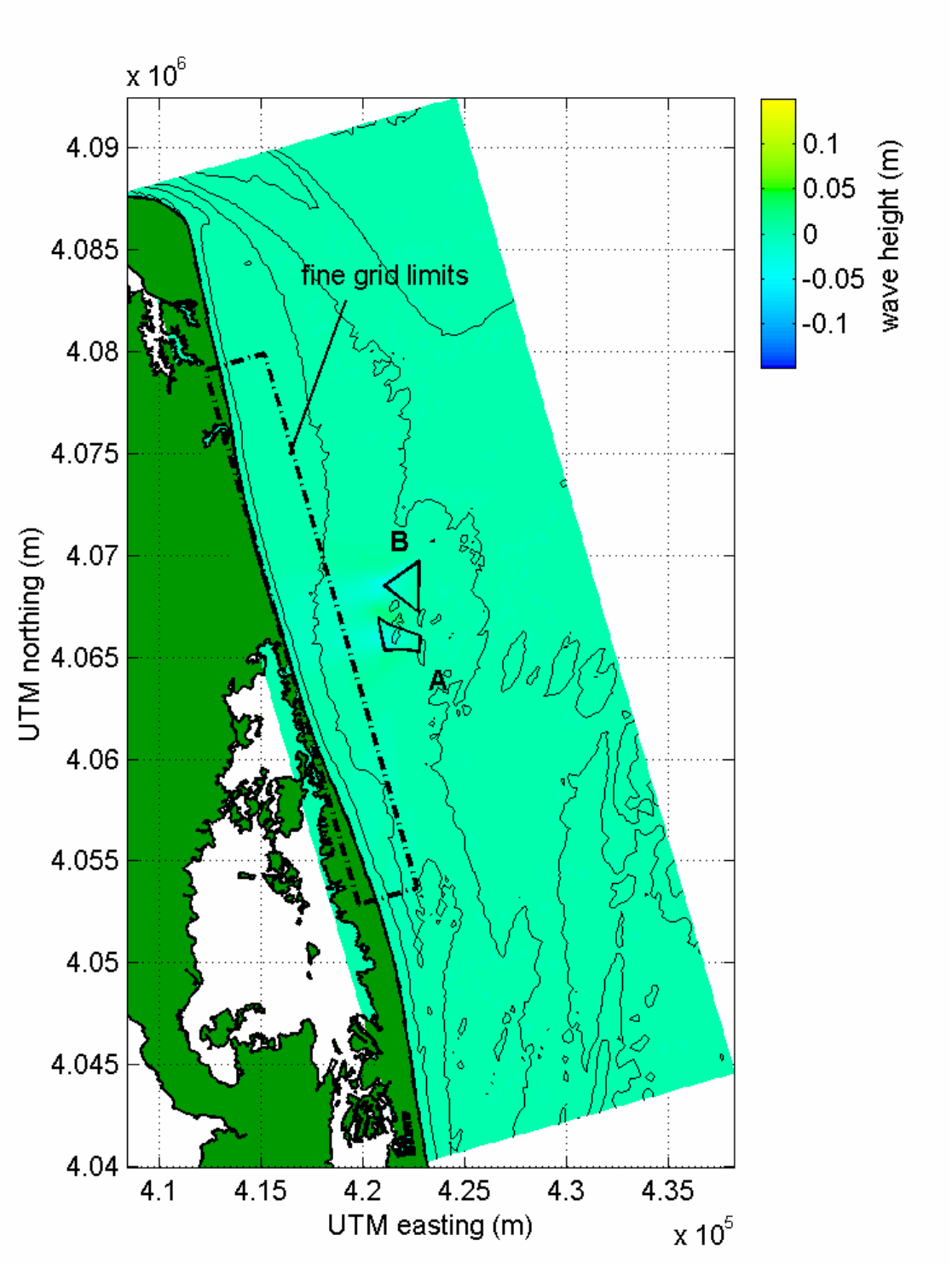

Figure C-14. Plot of wave height change between pre- and post-dredge ($\Delta=H_{post}-H_{pre}$) conditions at indicated borrow sites, for STWAVE model output of Virginia wave Case 3 (H_s=1.4 m, T_{peak}=9.1 sec, θ_{peak}=54 deg).

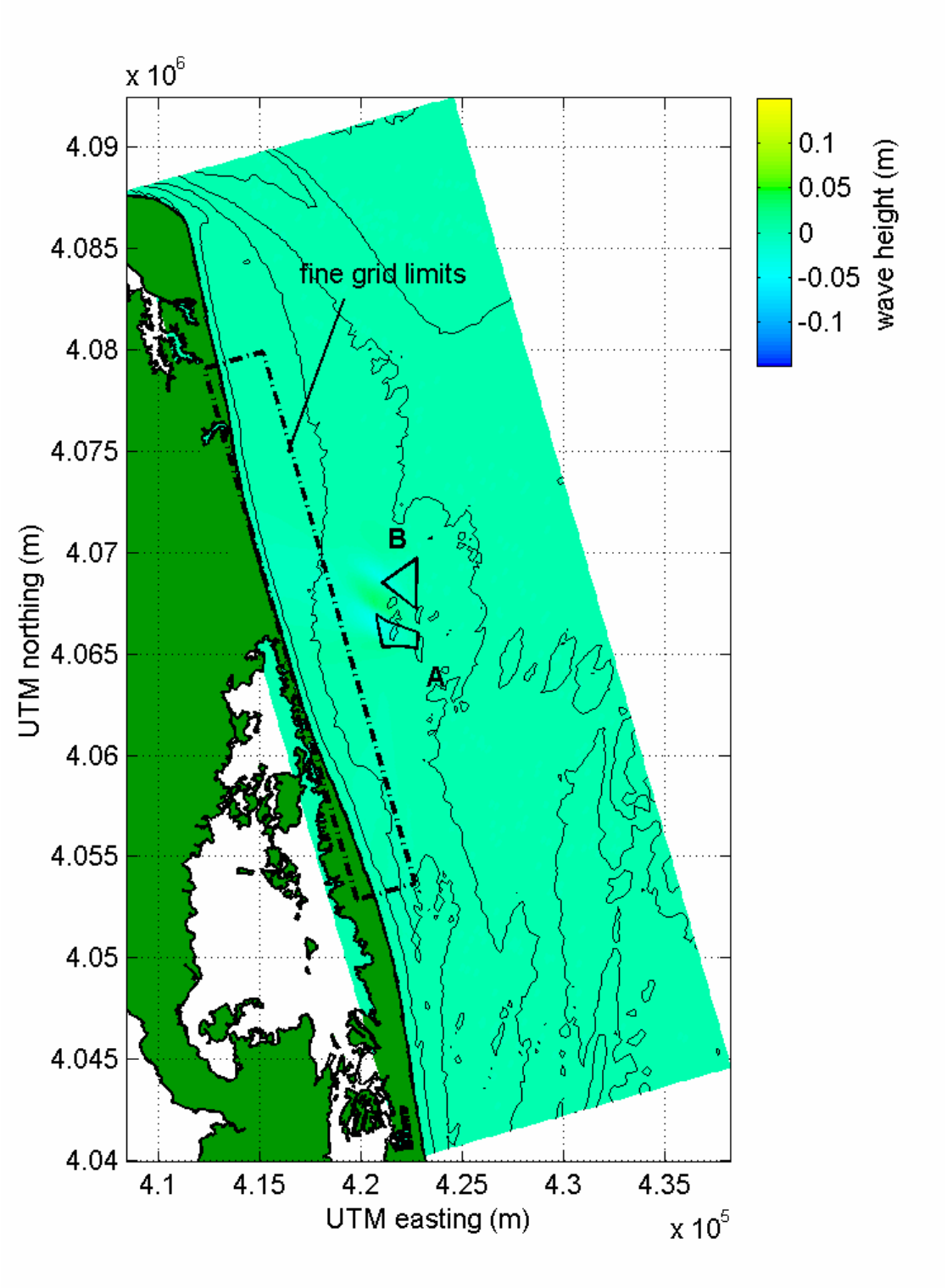

Figure C-15. Plot of wave height change between pre- and post-dredge ($\Delta=H_{post}-H_{pre}$) conditions at indicated borrow sites, for STWAVE model output of Virginia wave Case 4 (H_s=1.1 m, T_{peak}=8.3 sec, θ_{peak}=104 deg).

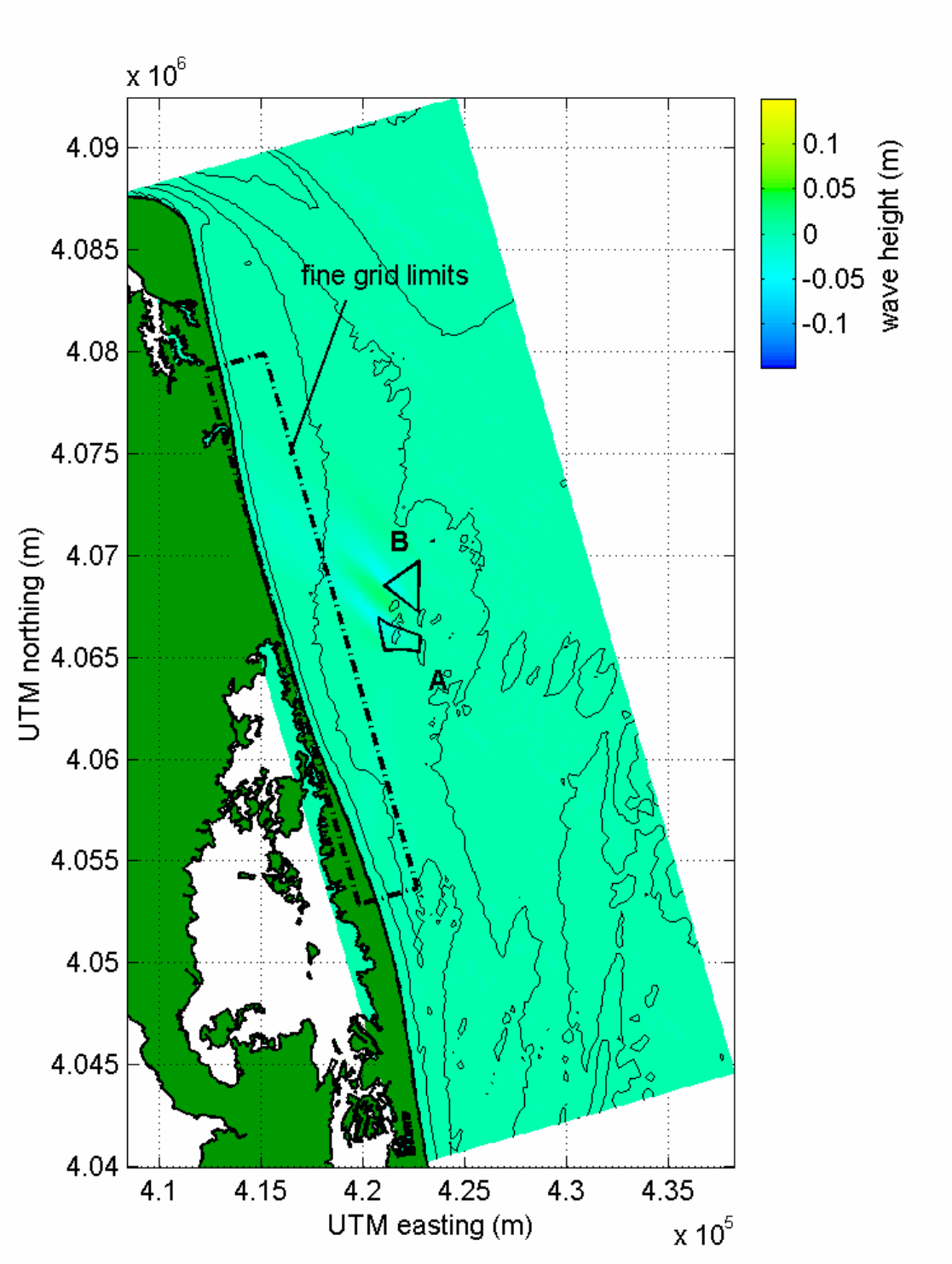

Figure C-16. Plot of wave height change between pre- and post-dredge ($\Delta=H_{post}-H_{pre}$) conditions at indicated borrow sites, for STWAVE model output of Virginia wave Case 5 (H_s=1.1 m, T_{peak}=8.3 sec, θ_{peak}=119 deg).

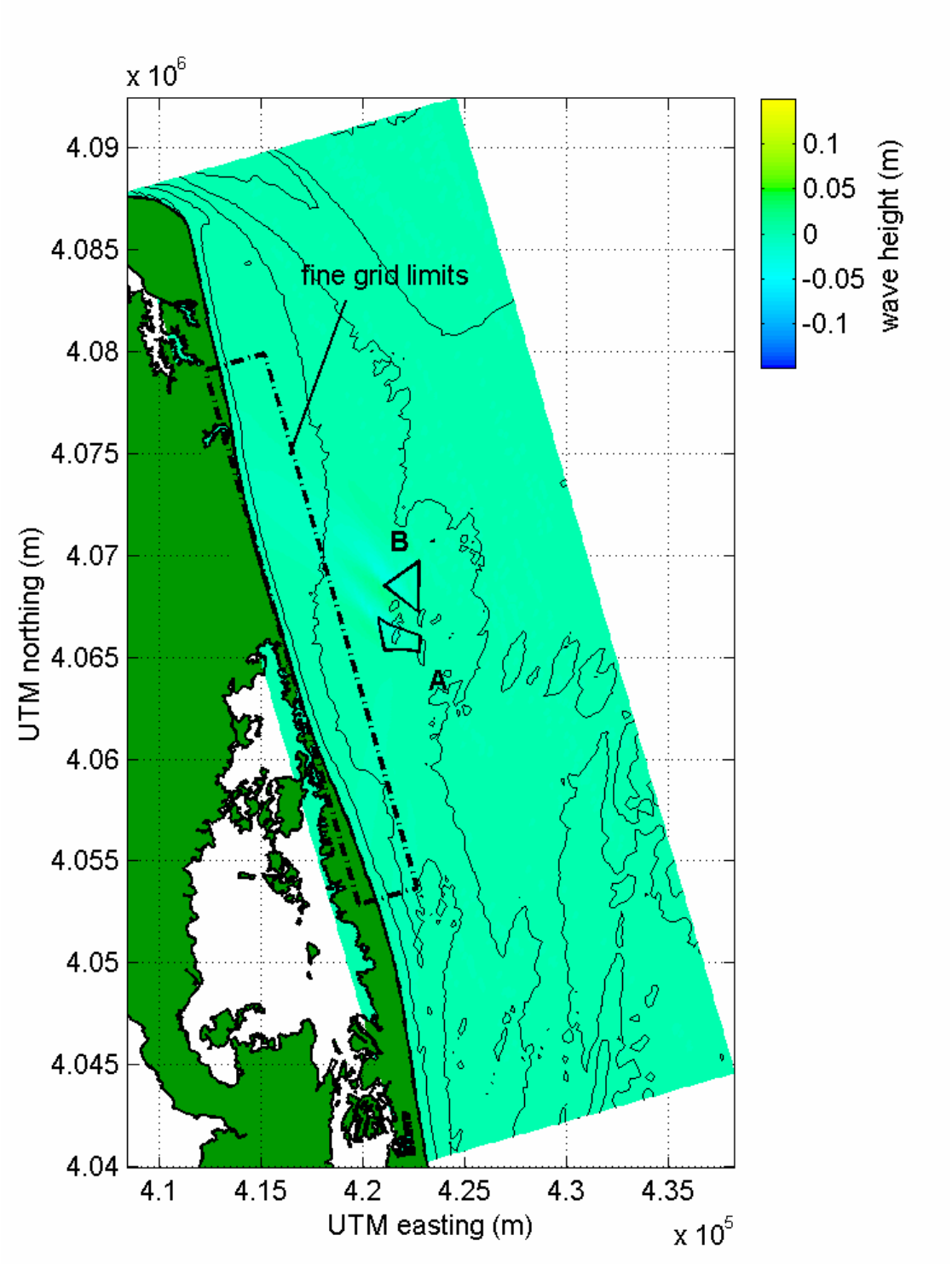

Figure C-17. Plot of wave height change between pre- and post-dredge ($\Delta=H_{post}-H_{pre}$) conditions at indicated borrow sites, for STWAVE model output of Virginia wave Case 6 (H_s=1.2 m, T_{peak}=8.3 sec, θ_{peak}=149 deg).

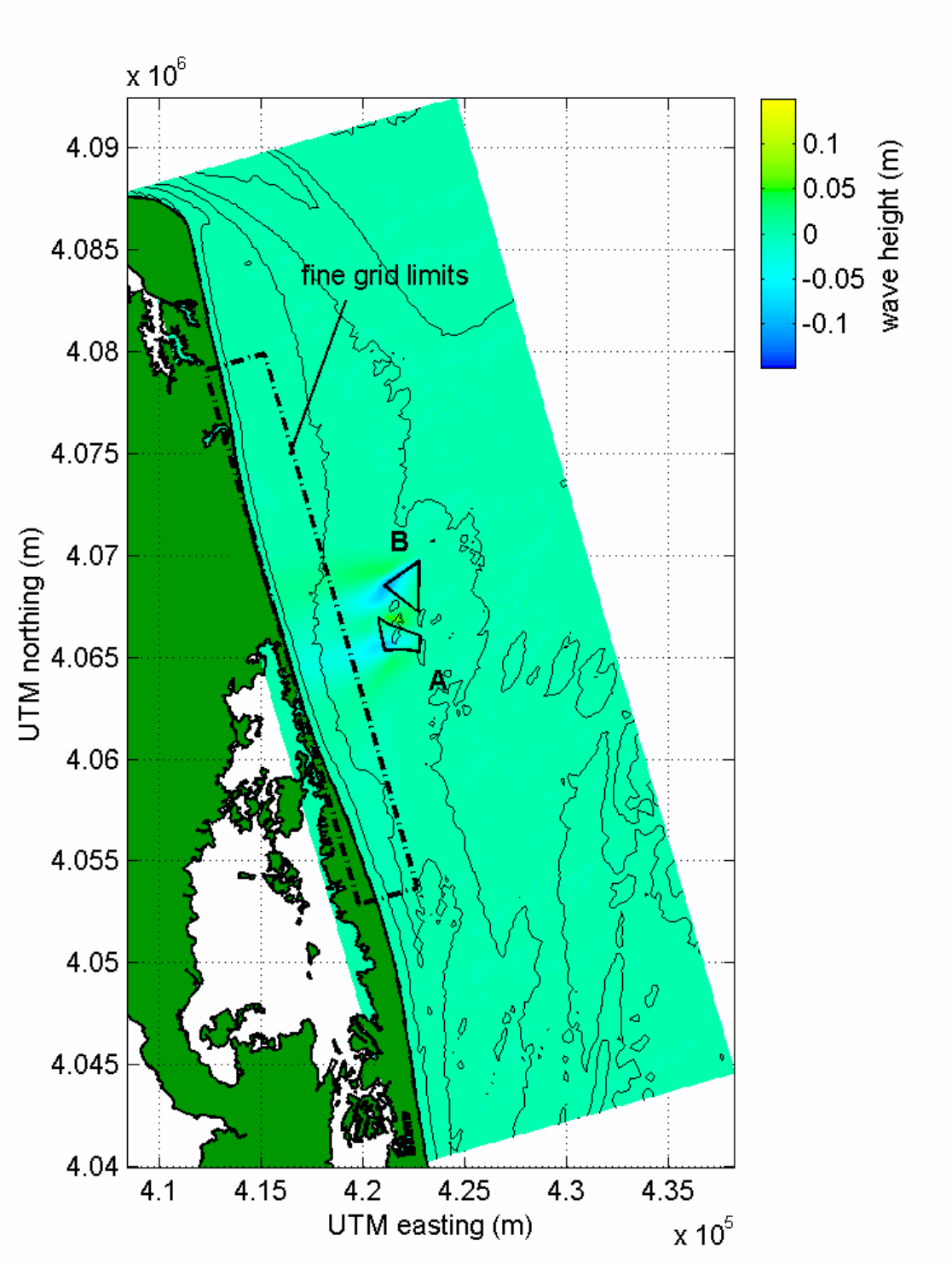

Figure C-18. Plot of wave height change between pre- and post-dredge ($\Delta=H_{post}-H_{pre}$) conditions at indicated borrow sites, for STWAVE model output of Virginia wave Case 7 (H_s=2.8 m, T_{peak}=11.1 sec, θ_{peak}=39 deg).

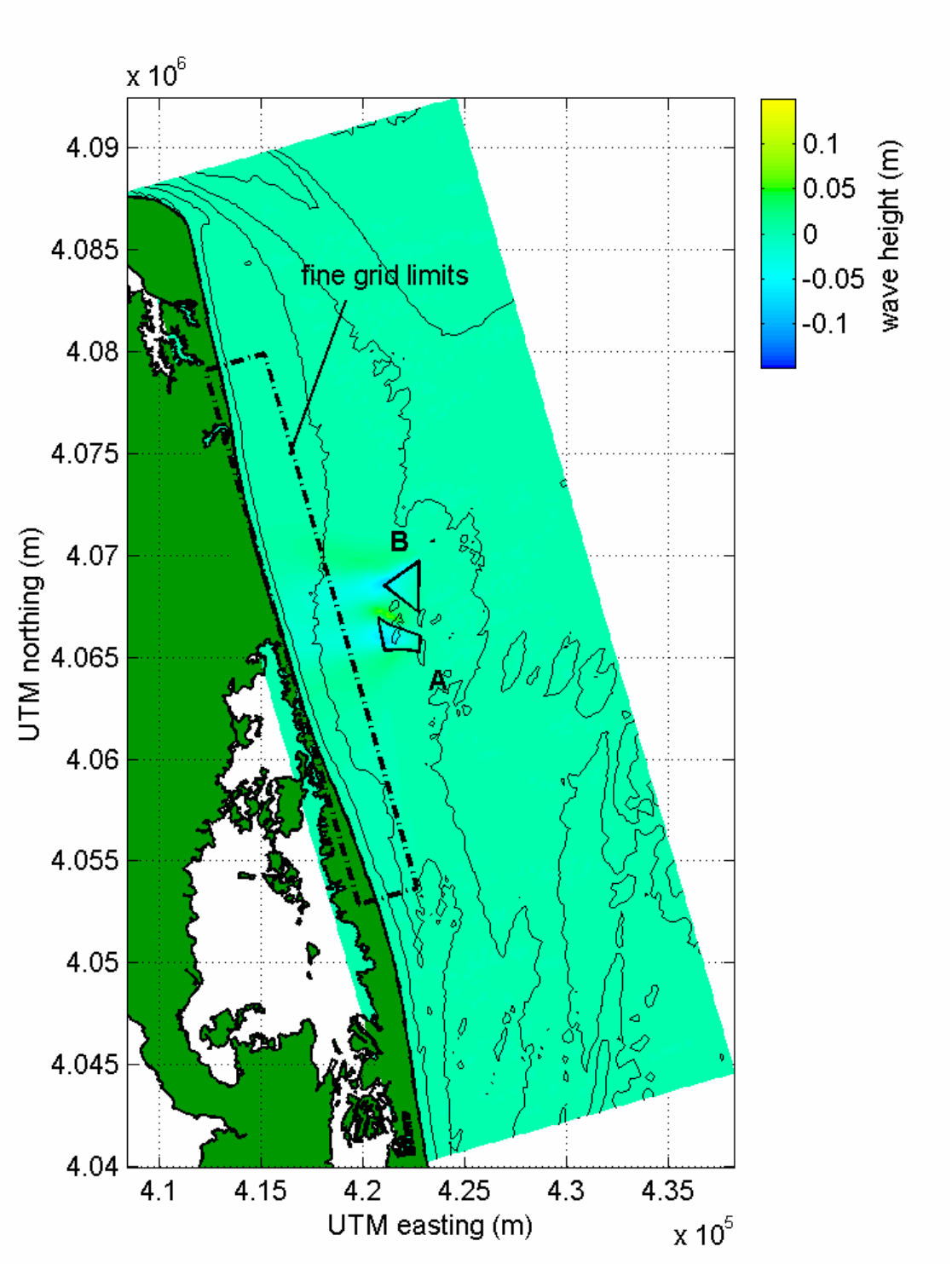

Figure C-19. Plot of wave height change between pre- and post-dredge ($\Delta=H_{post}-H_{pre}$) conditions at indicated borrow sites, for STWAVE model output of Virginia wave Case 8 (H_s=2.0 m, T_{peak}=11.1 sec, θ_{peak}=64 deg).

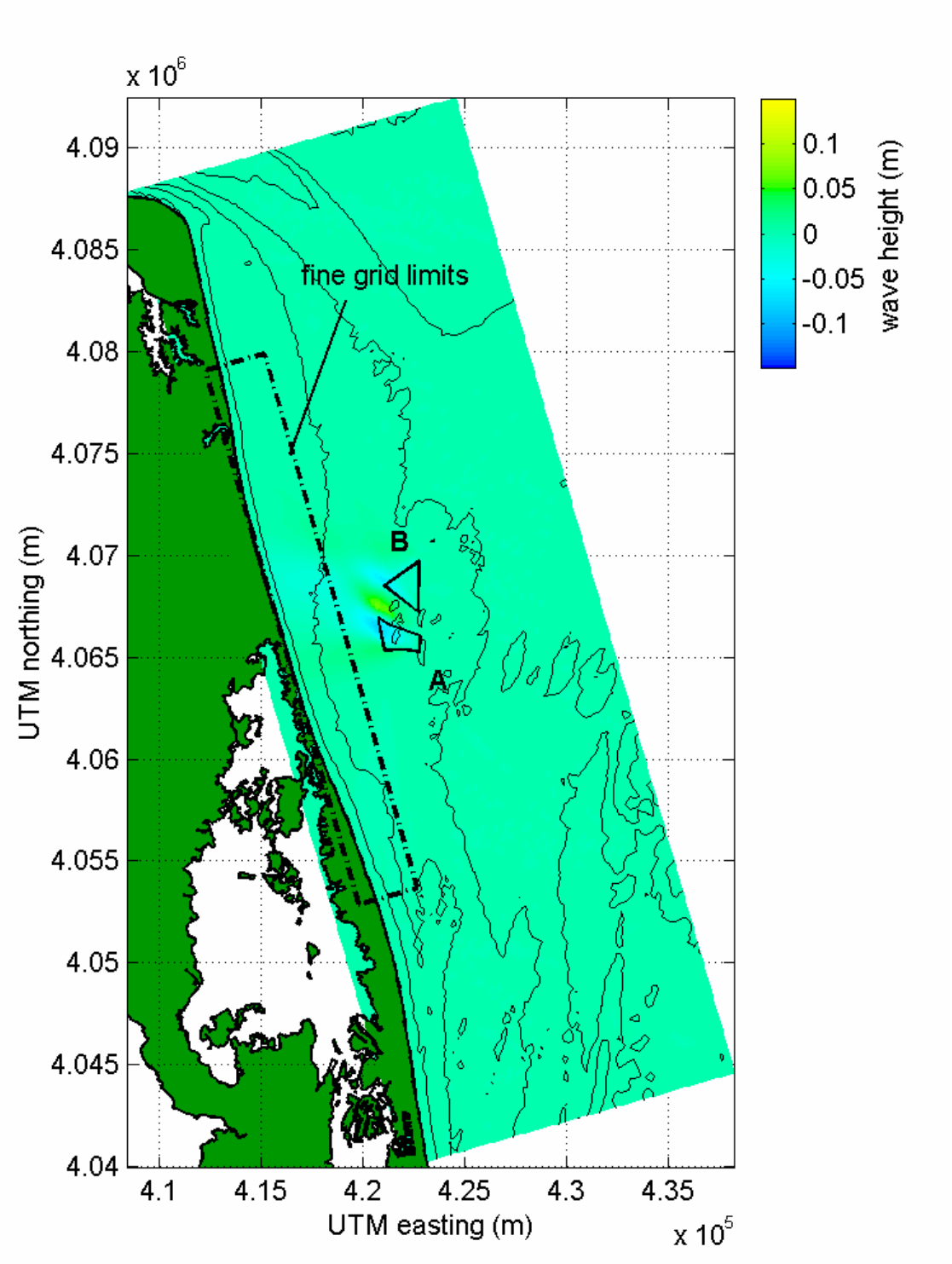

Figure C-20. Plot of wave height change between pre- and post-dredge ($\Delta=H_{post}-H_{pre}$) conditions at indicated borrow sites, for STWAVE model output of Virginia wave Case 9 (H_s=1.6 m, T_{peak}=11.1 sec, θ_{peak}=79 deg).

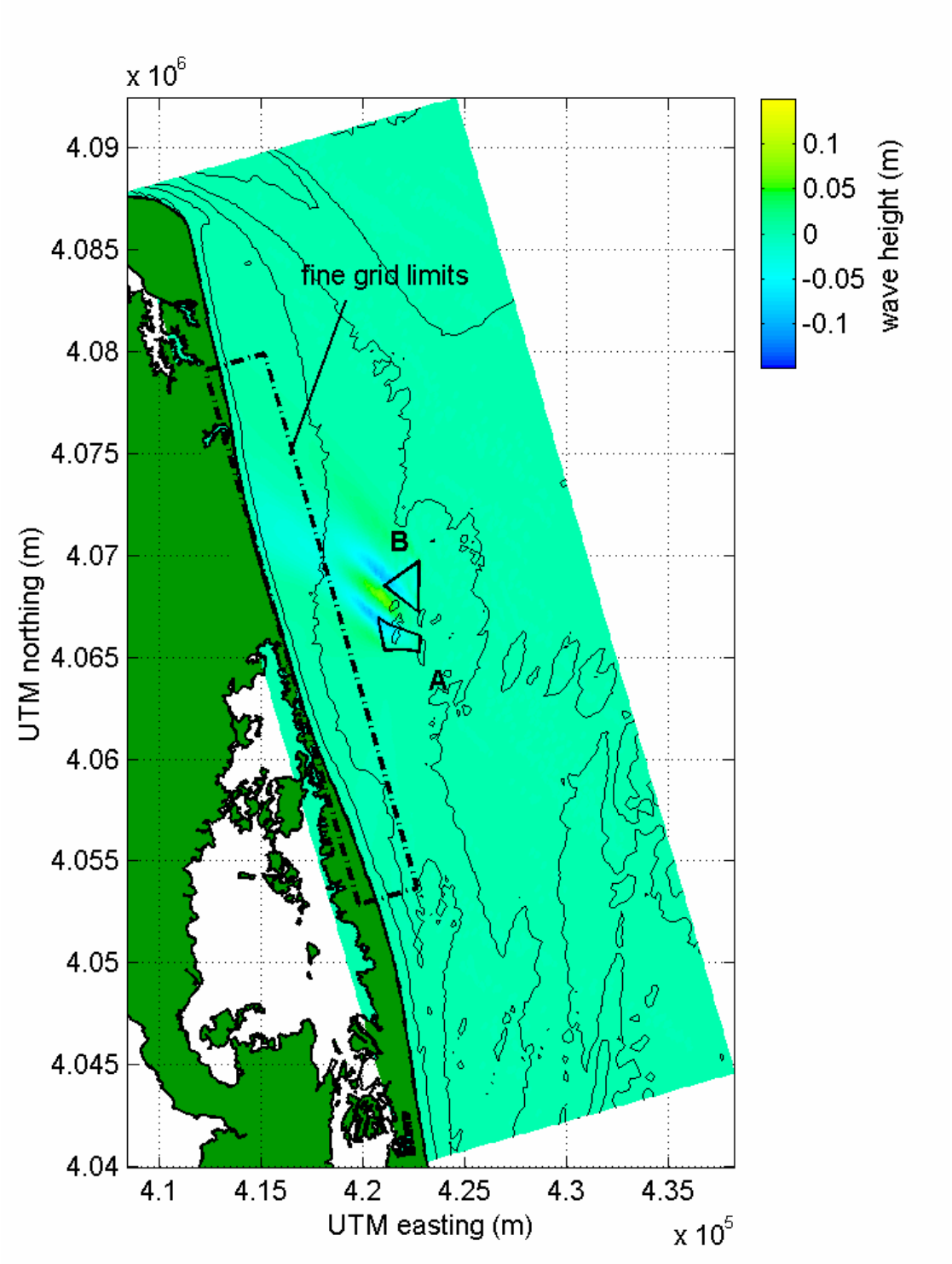

Figure C-21. Plot of wave height change between pre- and post-dredge ($\Delta=H_{post}-H_{pre}$) conditions at indicated borrow sites, for STWAVE model output of Virginia wave Case 10 (H_s=1.8 m, T_{peak}=10.0 sec, θ_{peak}=134 deg).

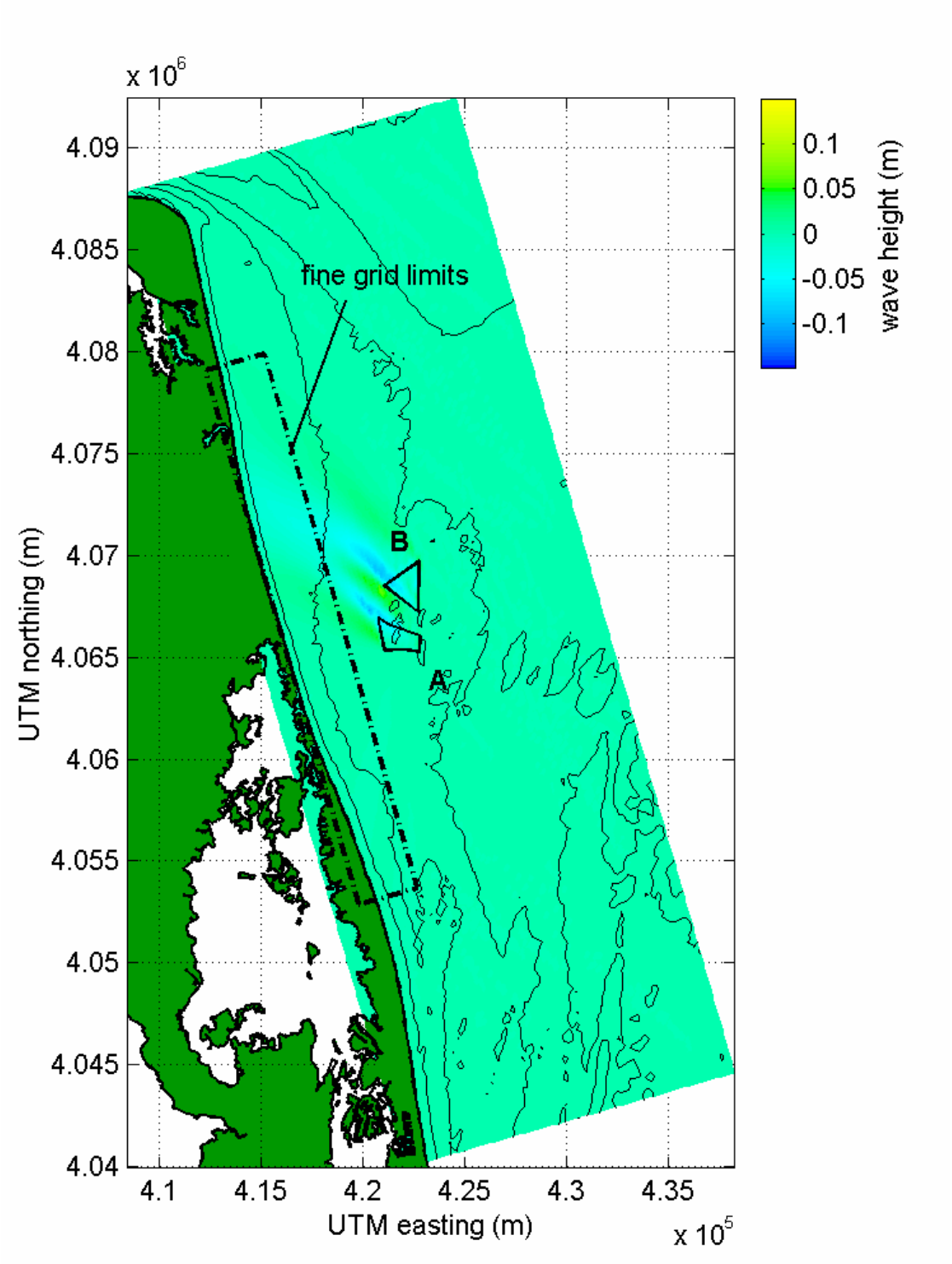

Figure C-22. Plot of wave height change between pre- and post-dredge ($\Delta=H_{post}-H_{pre}$) conditions at indicated borrow sites, for STWAVE model output of Virginia wave Case 11 (H_s=2.4 m, T_{peak}=10.0 sec, θ_{peak}=144 deg).

APPENDIX D: NORTH CAROLINA WAVE MODEL OUTPUT

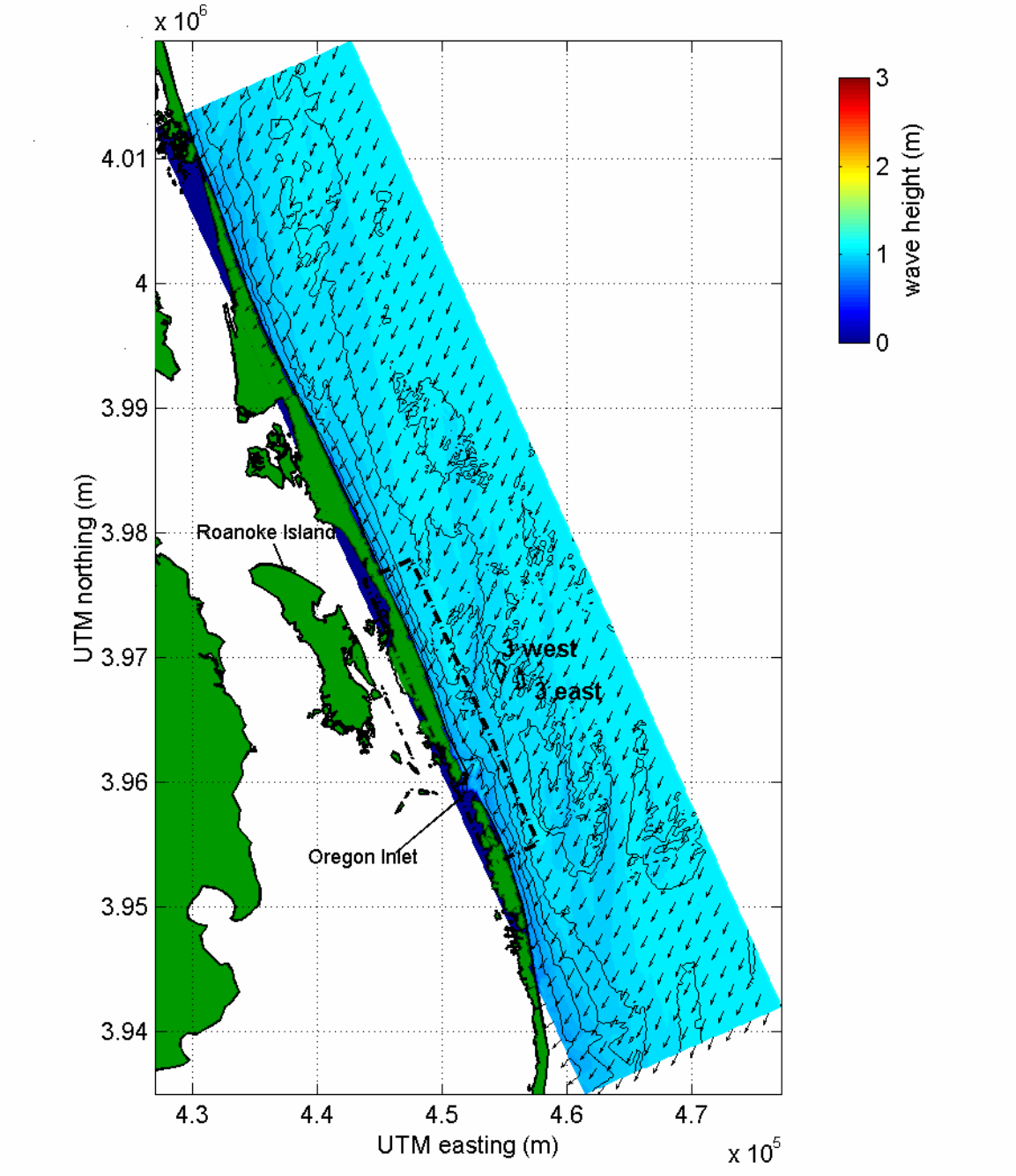

Figure D-1. Plot of STWAVE model output for North Carolina, existing conditions, wave Case 1 (H_s=1.1 m, T_{peak}=5.1 sec, θ_{peak}=1 deg). Color contours indicate wave height, and vectors show mean direction of wave propagation.

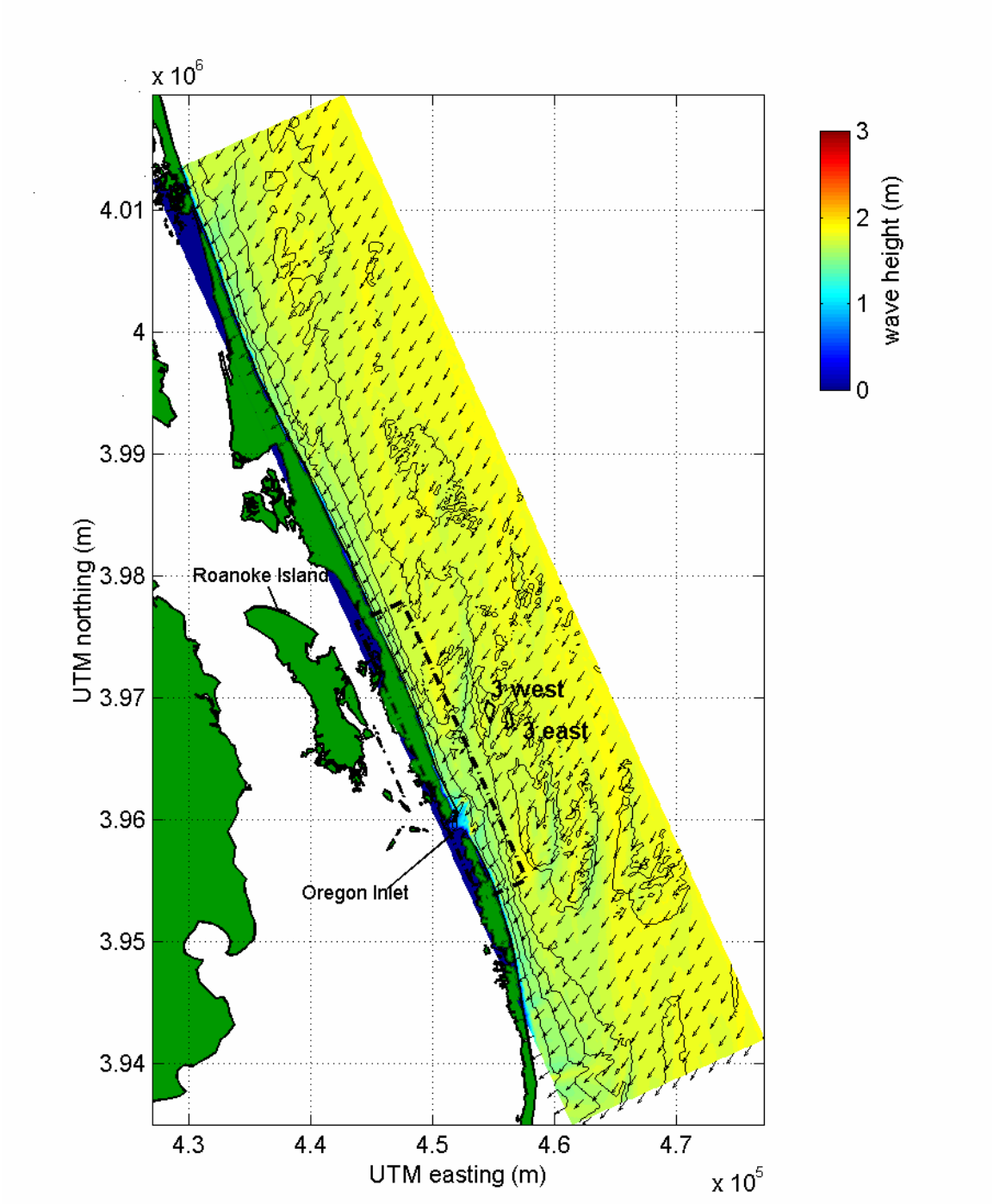

Figure D-2. Plot of STWAVE model output for North Carolina, existing conditions, wave Case 2 (H_s=1.9 m, T_{peak}=6.0 sec, θ_{peak}=21 deg). Color contours indicate wave height, and vectors show mean direction of wave propagation.

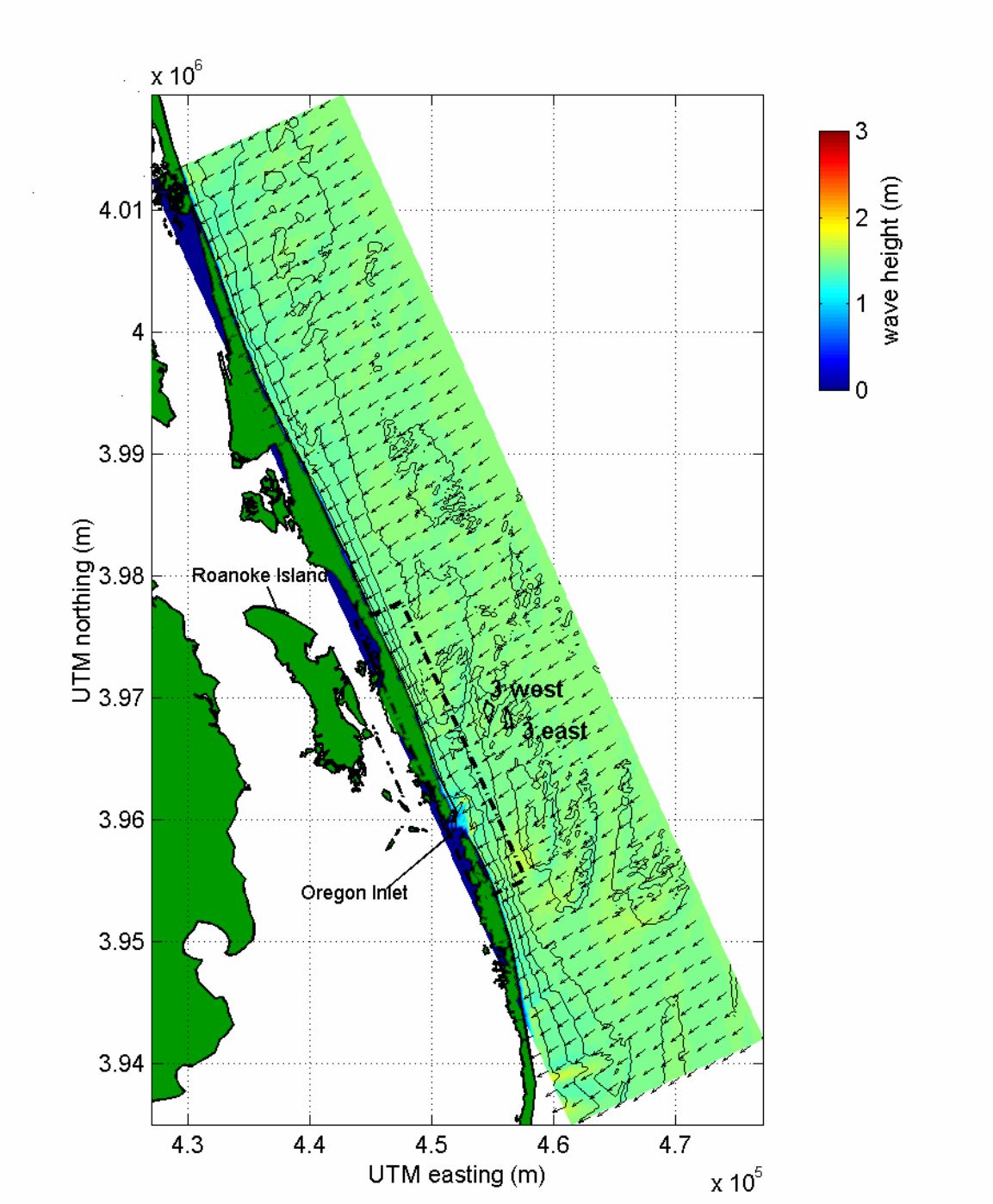

Figure D-3. Plot of STWAVE model output for North Carolina, existing conditions, wave Case 3 (H_s=1.5 m, T_{peak}=6.7 sec, θ_{peak}=56 deg). Color contours indicate wave height, and vectors show mean direction of wave propagation.

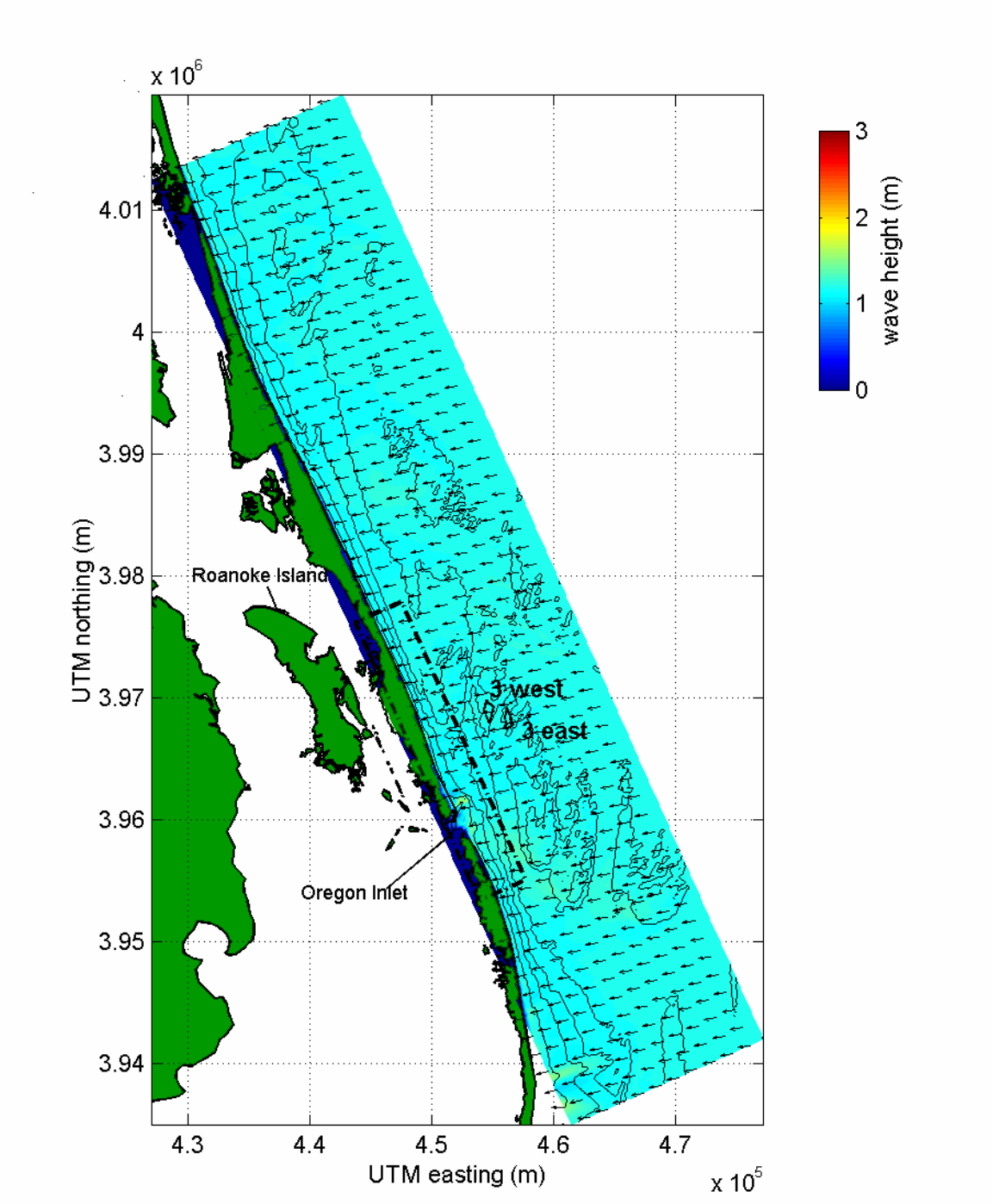

Figure D-4. Plot of STWAVE model output for North Carolina, existing conditions, wave Case 4 (H_s=1.2 m, T_{peak}=7.4 sec, θ_{peak}=86 deg). Color contours indicate wave height, and vectors show mean direction of wave propagation.

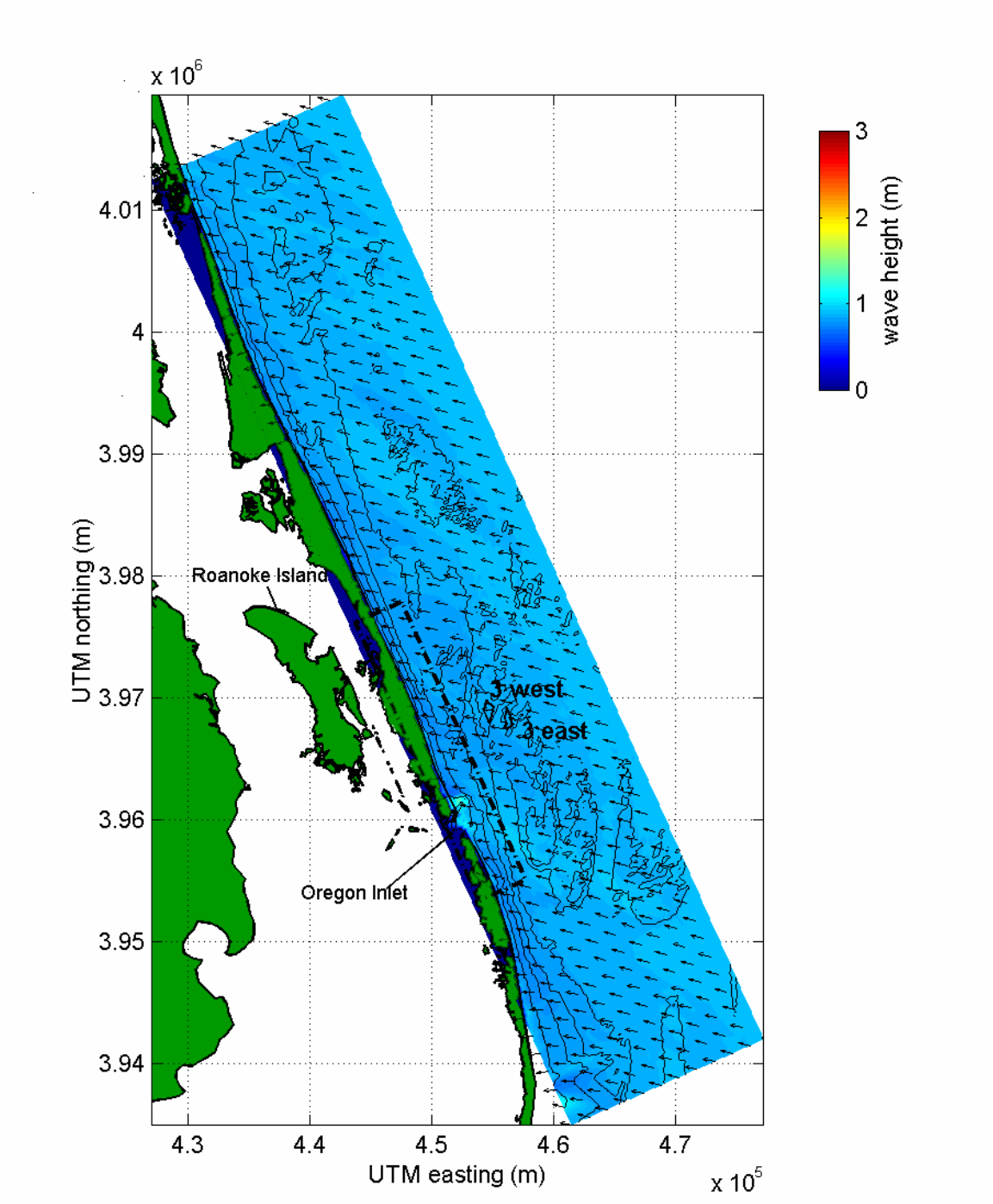

Figure D-5. Plot of STWAVE model output for North Carolina, existing conditions, wave Case 5 (H_s=0.9 m, T_{peak}=7.6 sec, θ_{peak}=106 deg). Color contours indicate wave height, and vectors show mean direction of wave propagation.

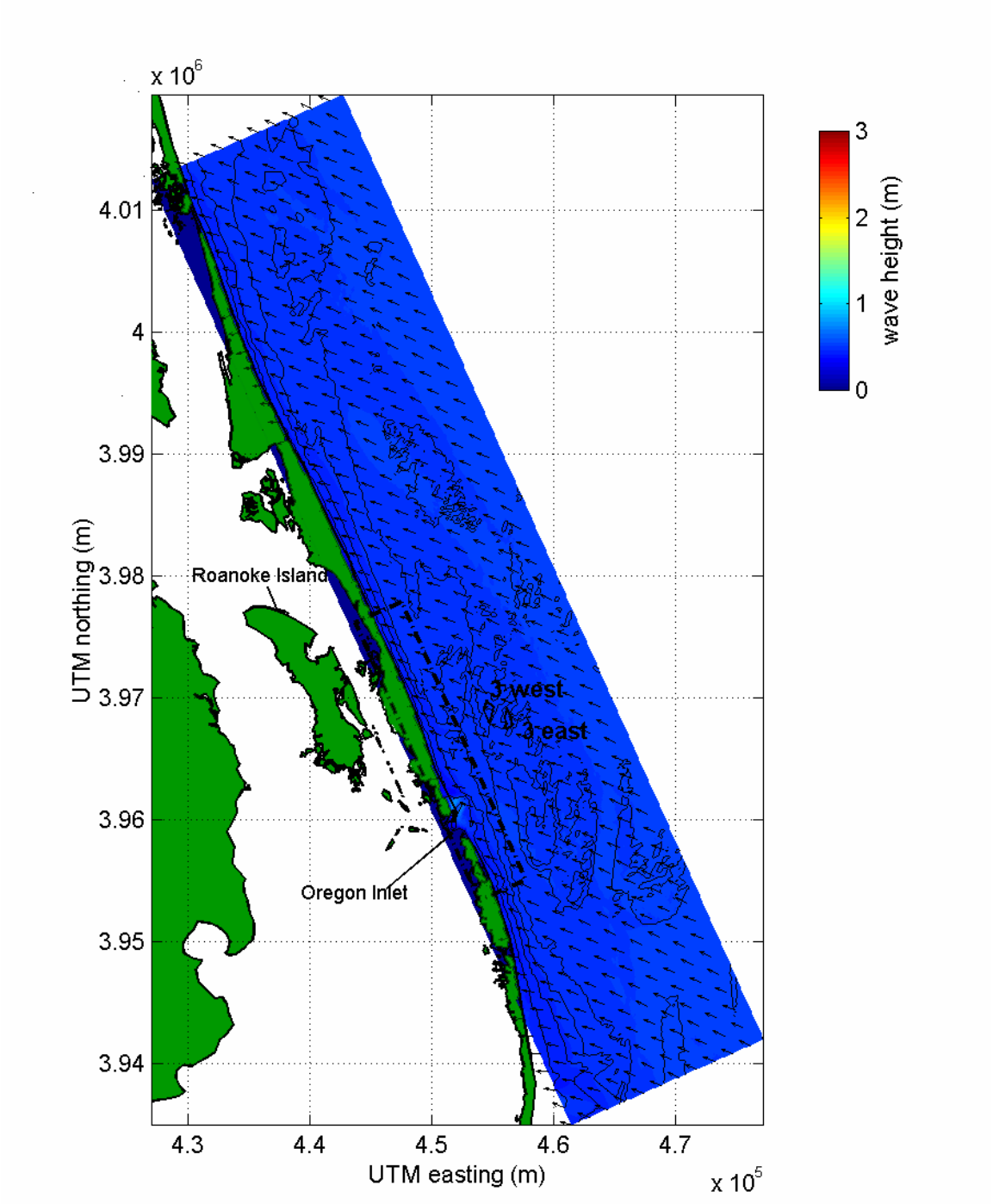

Figure D-6. Plot of STWAVE model output for North Carolina, existing conditions, wave Case 6 (H_s=0.6 m, T_{peak}=4.6 sec, θ_{peak}=131 deg). Color contours indicate wave height, and vectors show mean direction of wave propagation.

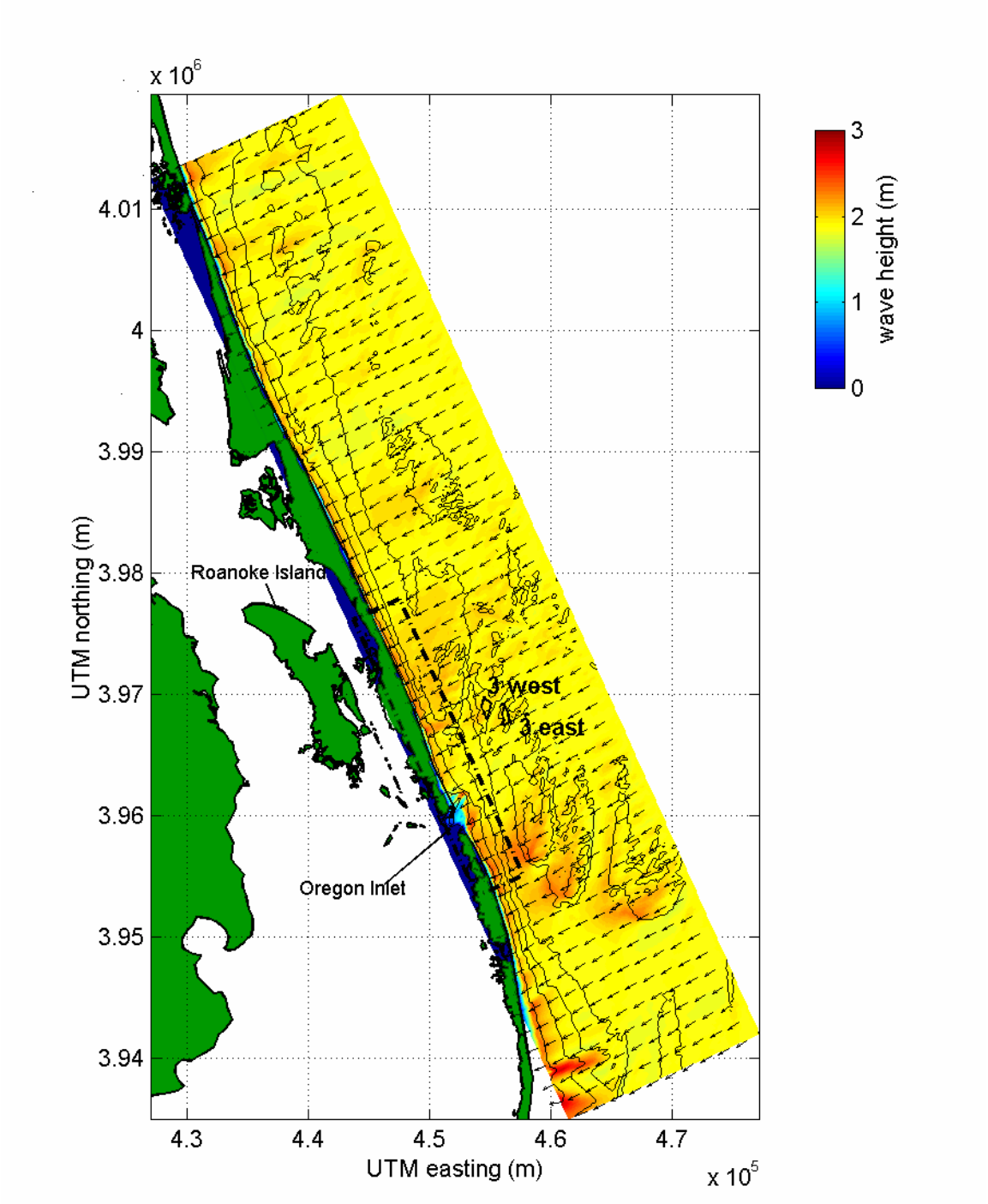

Figure D-7. Plot of STWAVE model output for North Carolina, existing conditions, wave Case 7 (H_s=1.9 m, T_{peak}=11.5 sec, θ_{peak}=66 deg). Color contours indicate wave height, and vectors show mean direction of wave propagation.

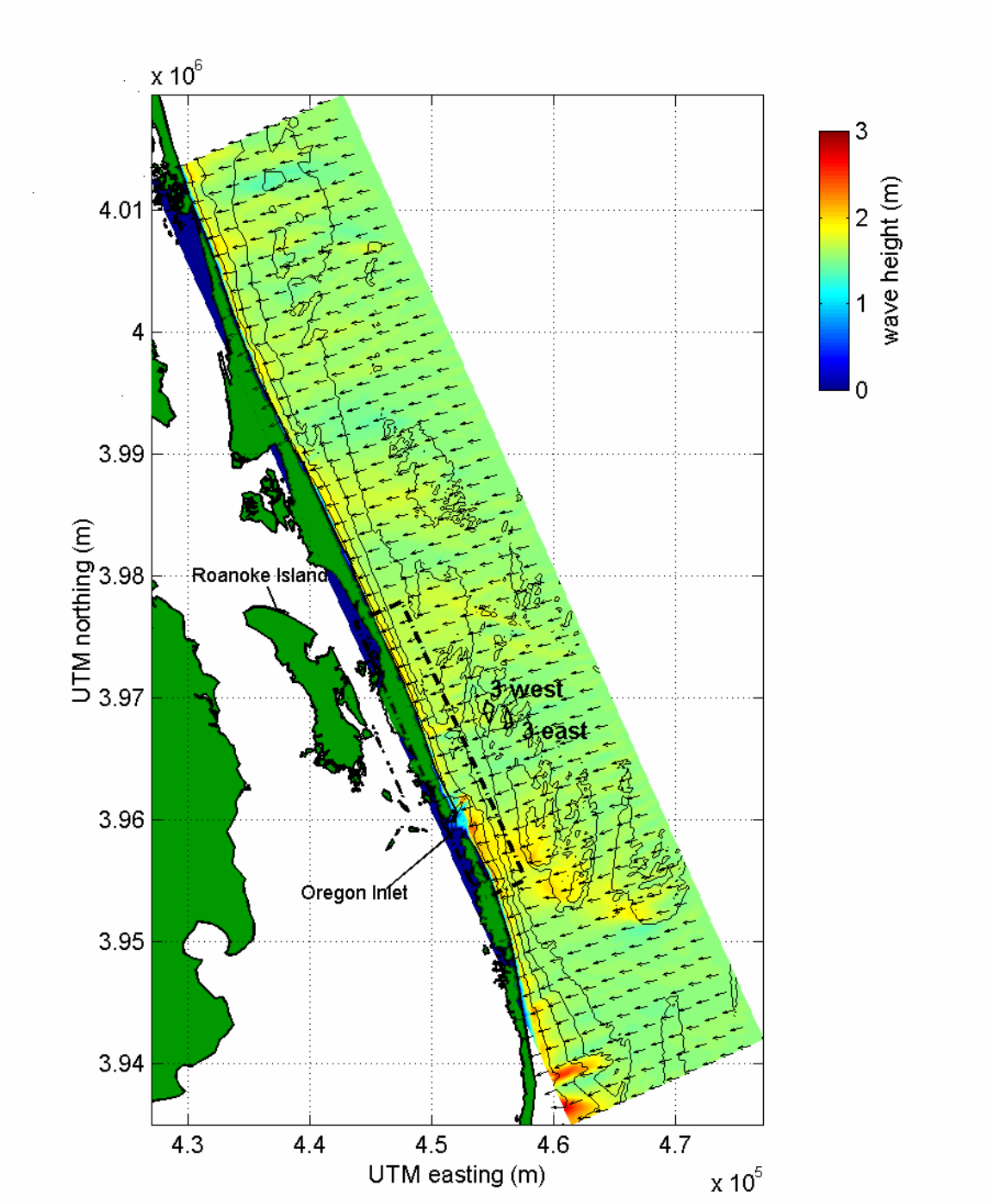

Figure D-8. Plot of STWAVE model output for North Carolina, existing conditions, wave Case 8 (H_s=1.5 m, T_{peak}=12.8 sec, θ_{peak}=71 deg). Color contours indicate wave height, and vectors show mean direction of wave propagation.

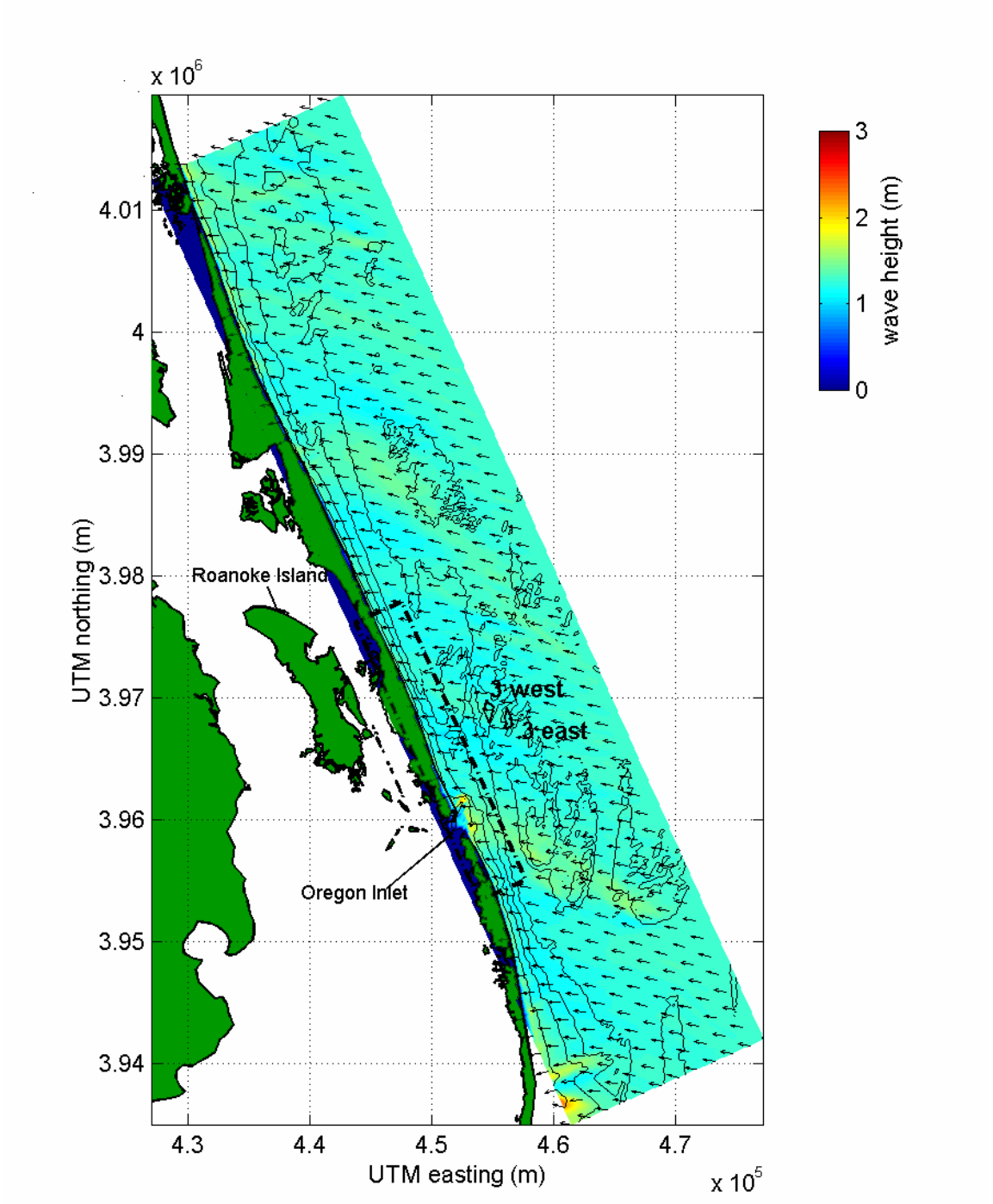

Figure D-9. Plot of STWAVE model output for North Carolina, existing conditions, wave Case 9 (H_s=1.3 m, T_{peak}=11.3 sec, θ_{peak}=101 deg). Color contours indicate wave height, and vectors show mean direction of wave propagation.

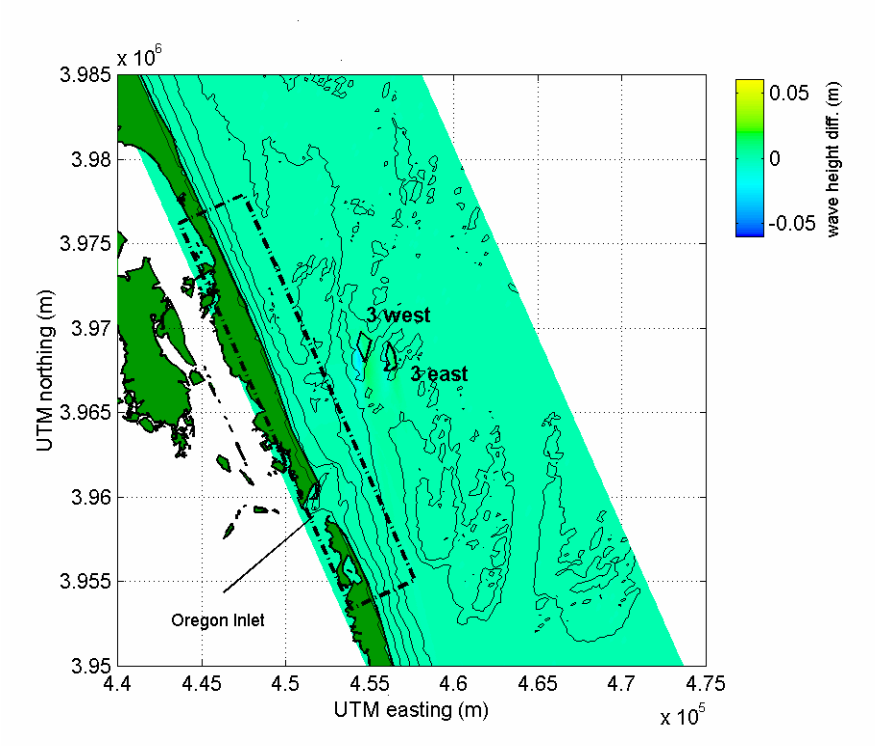

Figure D-10. Plot of wave height change between pre- and post-dredge ($\Delta=H_{post}-H_{pre}$) conditions at indicated borrow sites, for STWAVE model output of North Carolina wave Case 1 (H_s=1.1 m, T_{peak}=5.1 sec, θ_{peak}=1 deg).

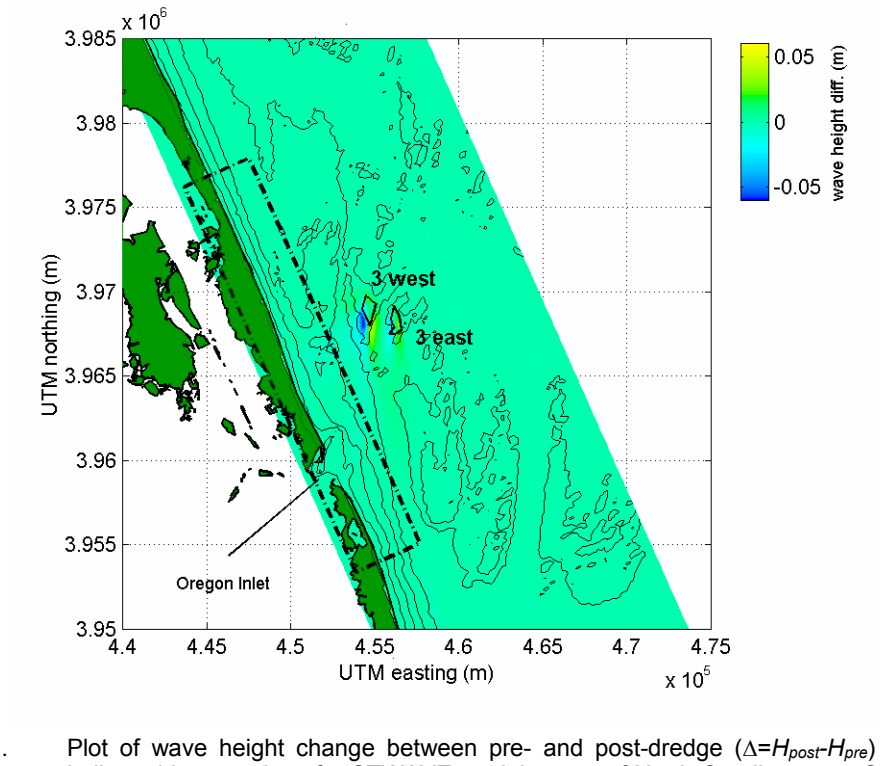

Figure D-11. Plot of wave height change between pre- and post-dredge ($\Delta=H_{post}-H_{pre}$) conditions at indicated borrow sites, for STWAVE model output of North Carolina wave Case 2 (H_s=1.9 m, T_{peak}=6.0 sec, θ_{peak}=21 deg).

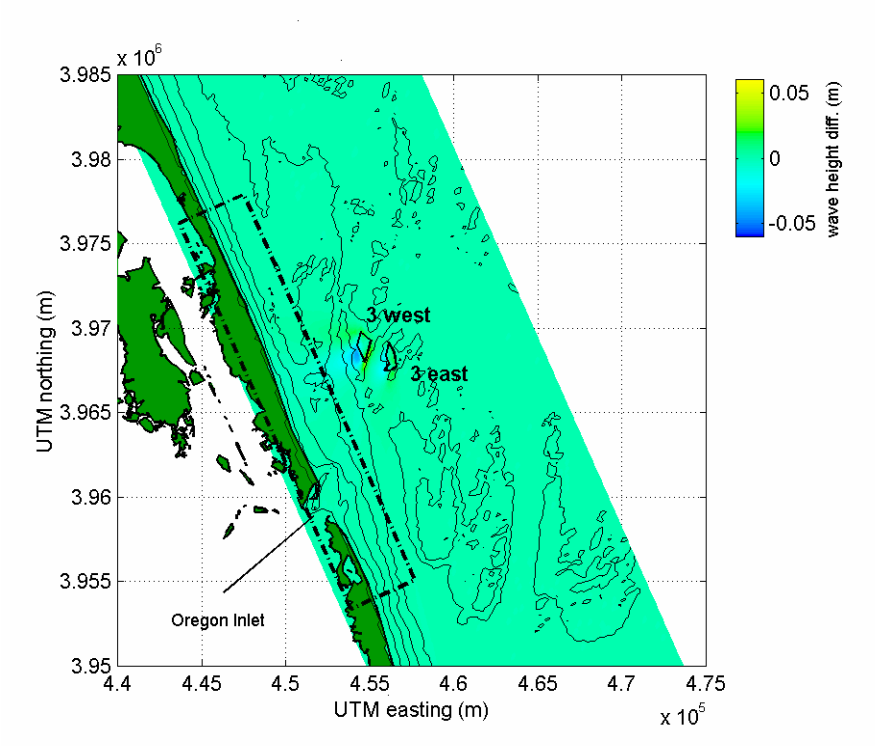

Figure D-12. Plot of wave height change between pre- and post-dredge ($\Delta=H_{post}-H_{pre}$) conditions at indicated borrow sites, for STWAVE model output of North Carolina wave Case 3 (H_s=1.5 m, T_{peak}=6.7 sec, θ_{peak}=56 deg).

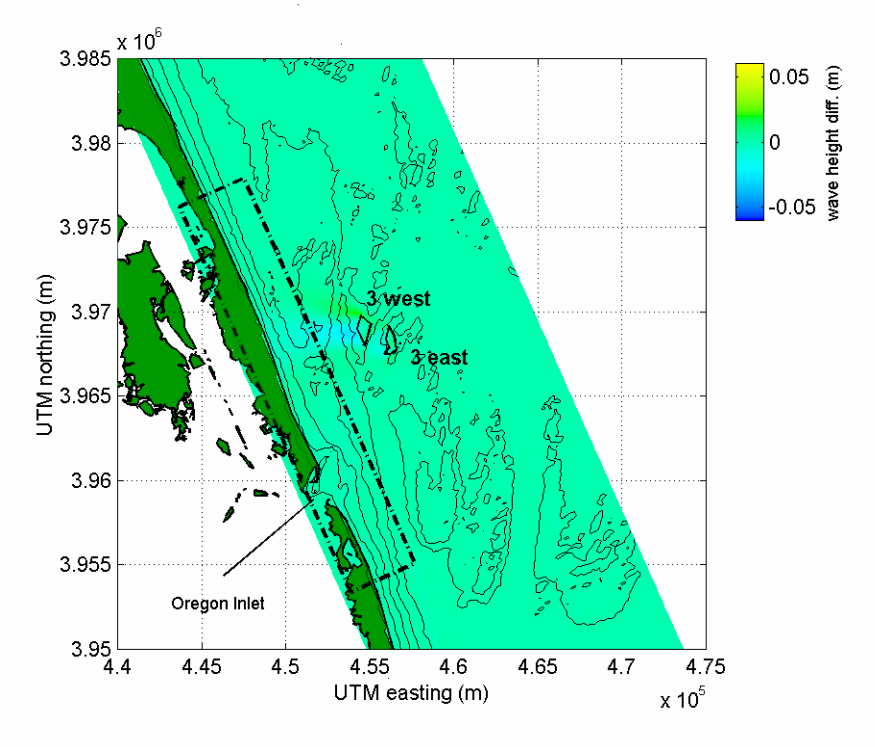

Figure D-13. Plot of wave height change between pre- and post-dredge ($\Delta=H_{post}-H_{pre}$) conditions at indicated borrow sites, for STWAVE model output of North Carolina wave Case 4 (H_s=1.2 m, T_{peak}=7.4 sec, θ_{peak}=86 deg).

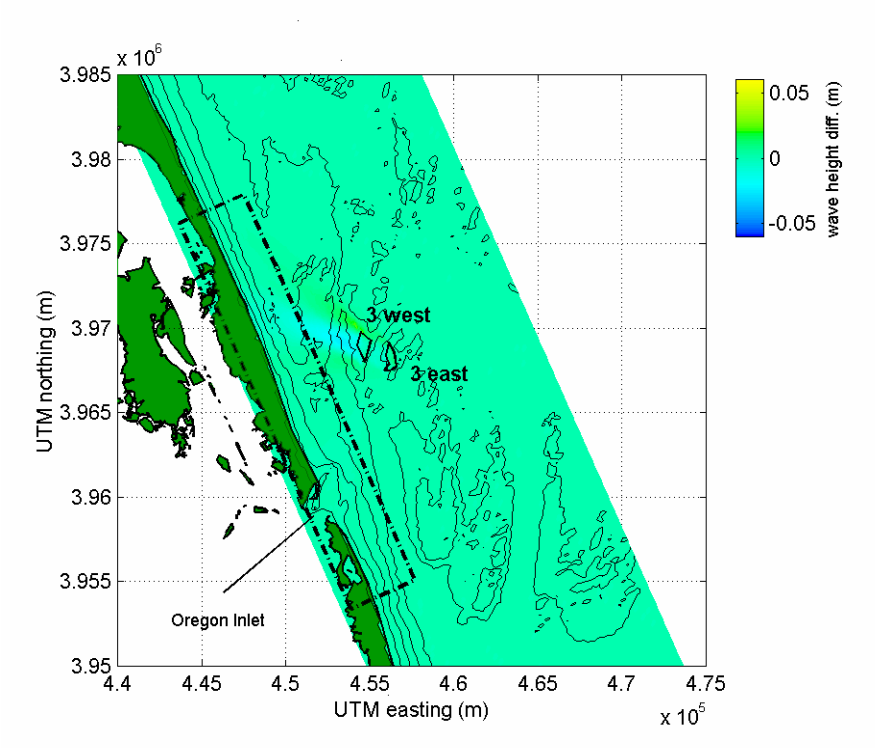

Figure D-14. Plot of wave height change between pre- and post-dredge ($\Delta=H_{post}-H_{pre}$) conditions at indicated borrow sites, for STWAVE model output of North Carolina wave Case 5 (H_s=0.9 m, T_{peak}=7.6 sec, θ_{peak}=106 deg).

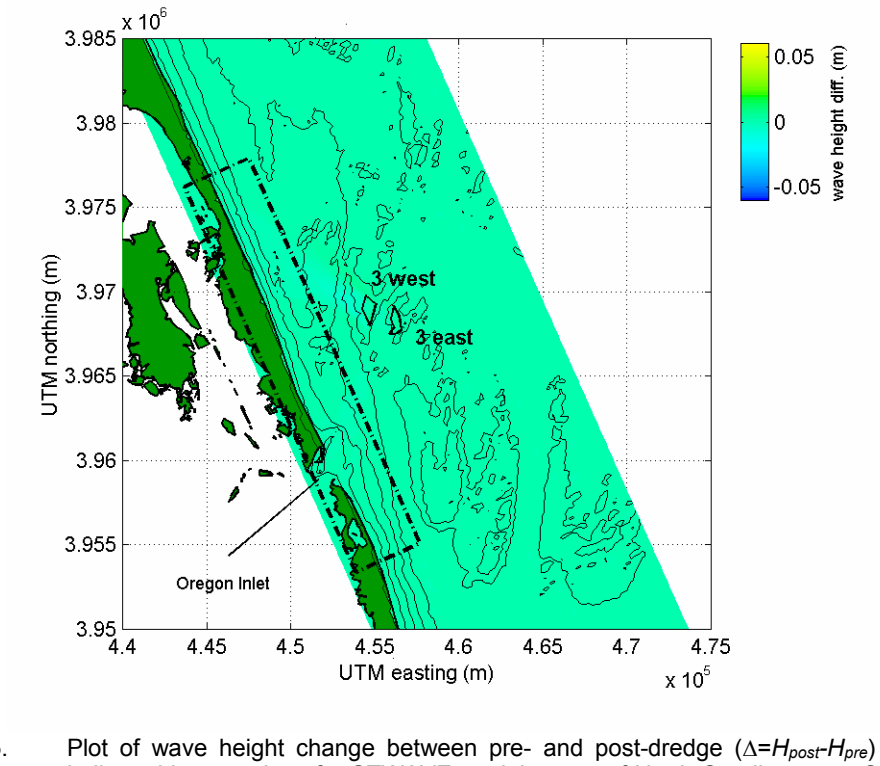

Figure D-15. Plot of wave height change between pre- and post-dredge ($\Delta=H_{post}-H_{pre}$) conditions at indicated borrow sites, for STWAVE model output of North Carolina wave Case 6 (H_s=0.6 m, T_{peak}=4.6 sec, θ_{peak}=131 deg).

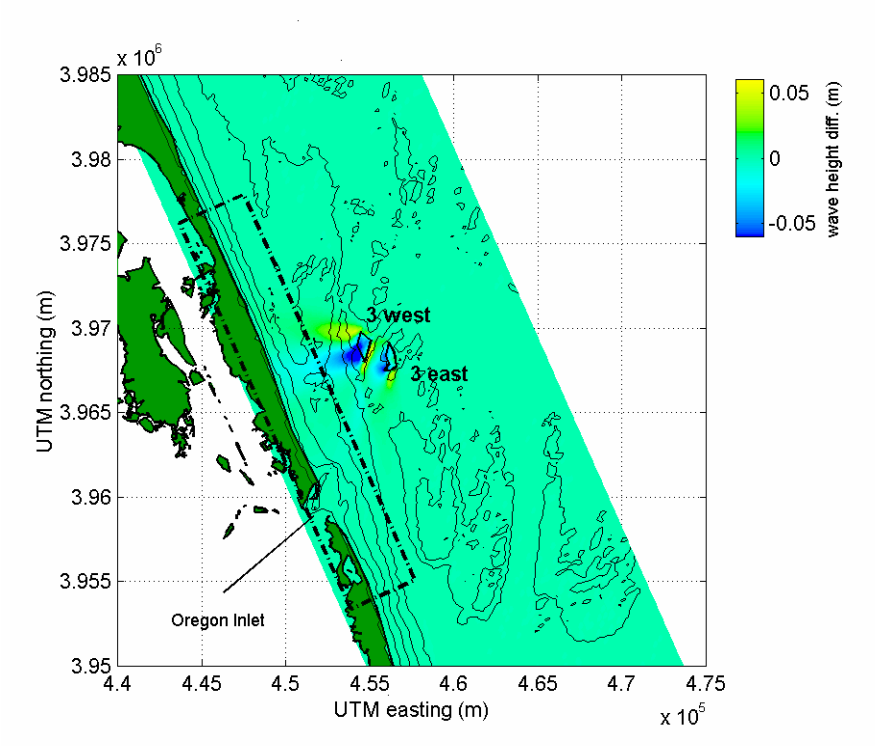

Figure D-16. Plot of wave height change between pre- and post-dredge ($\Delta=H_{post}-H_{pre}$) conditions at indicated borrow sites, for STWAVE model output of North Carolina wave Case 7 (H_s=1.9 m, T_{peak}=11.5 sec, θ_{peak}=66 deg).

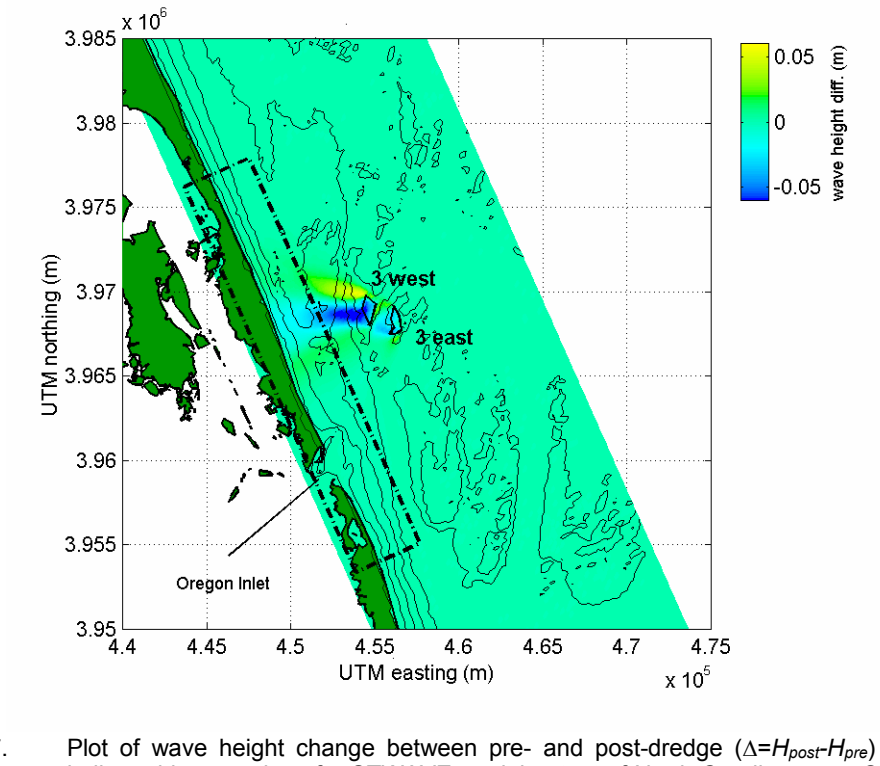

Figure D-17. Plot of wave height change between pre- and post-dredge ($\Delta=H_{post}-H_{pre}$) conditions at indicated borrow sites, for STWAVE model output of North Carolina wave Case 8 (H_s=1.5 m, T_{peak}=12.8 sec, θ_{peak}=71 deg).

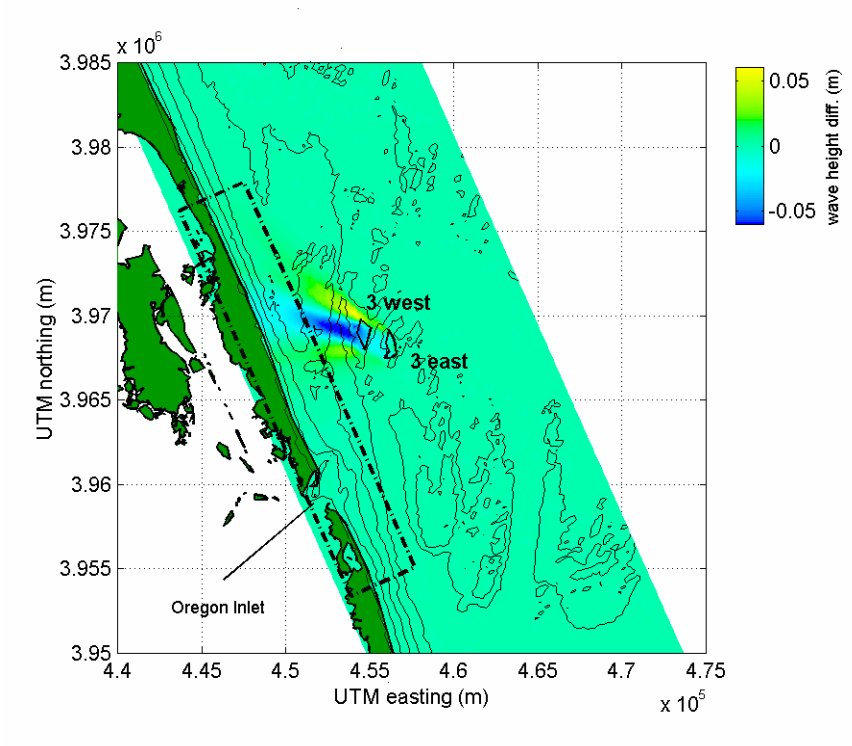

Figure D-18. Plot of wave height change between pre- and post-dredge ($\Delta=H_{post}-H_{pre}$) conditions at indicated borrow sites, for STWAVE model output of North Carolina wave Case 9 (H_s=1.3 m, T_{peak}=11.3 sec, θ_{peak}=101 deg).

APPENDIX E: FLORIDA WAVE MODEL OUTPUT

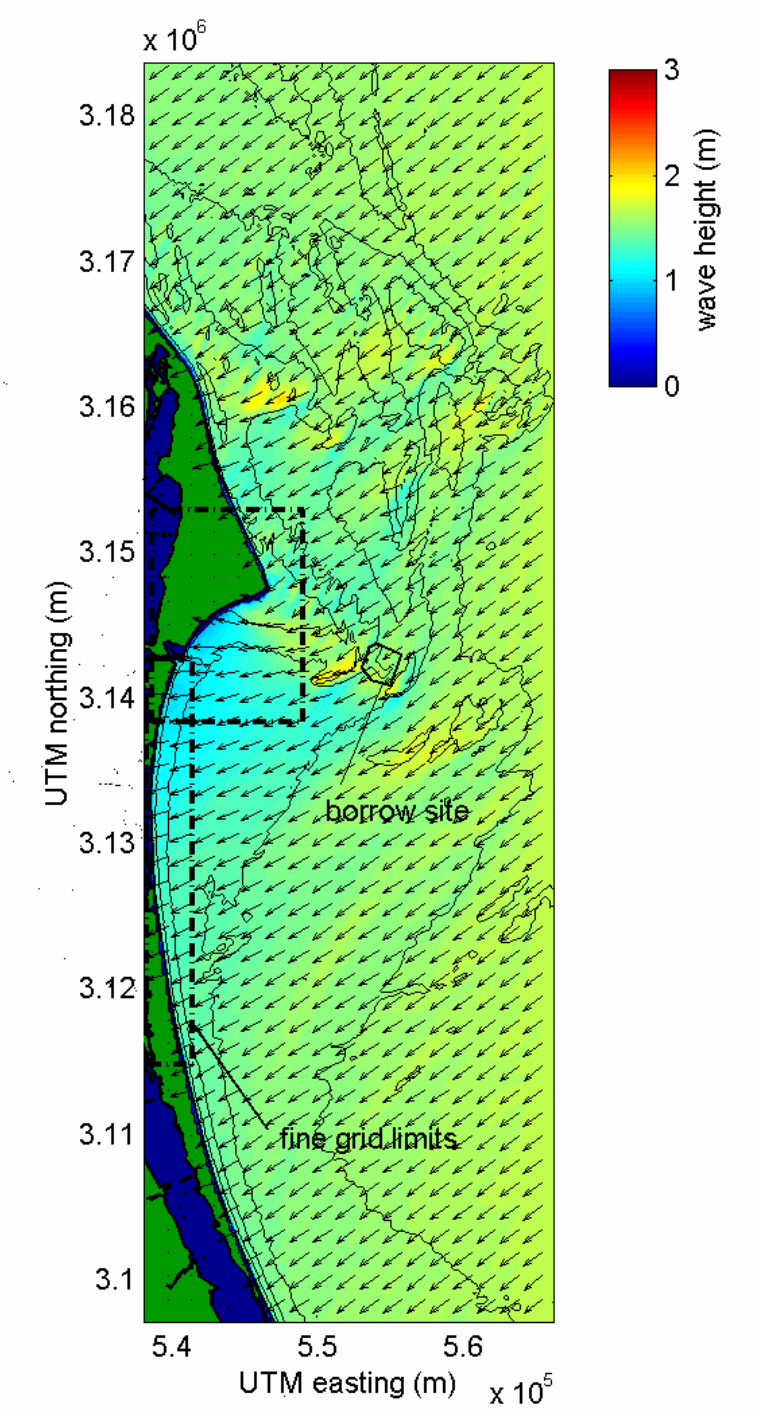

Figure E-1. Plot of STWAVE model output for Cape Canaveral, Florida, existing conditions, wave Case 1 (H_s=1.7 m, T_{peak}=7.7 sec, θ_{peak}=55 deg). Color contours indicate wave height, and vectors show mean direction of wave propagation.

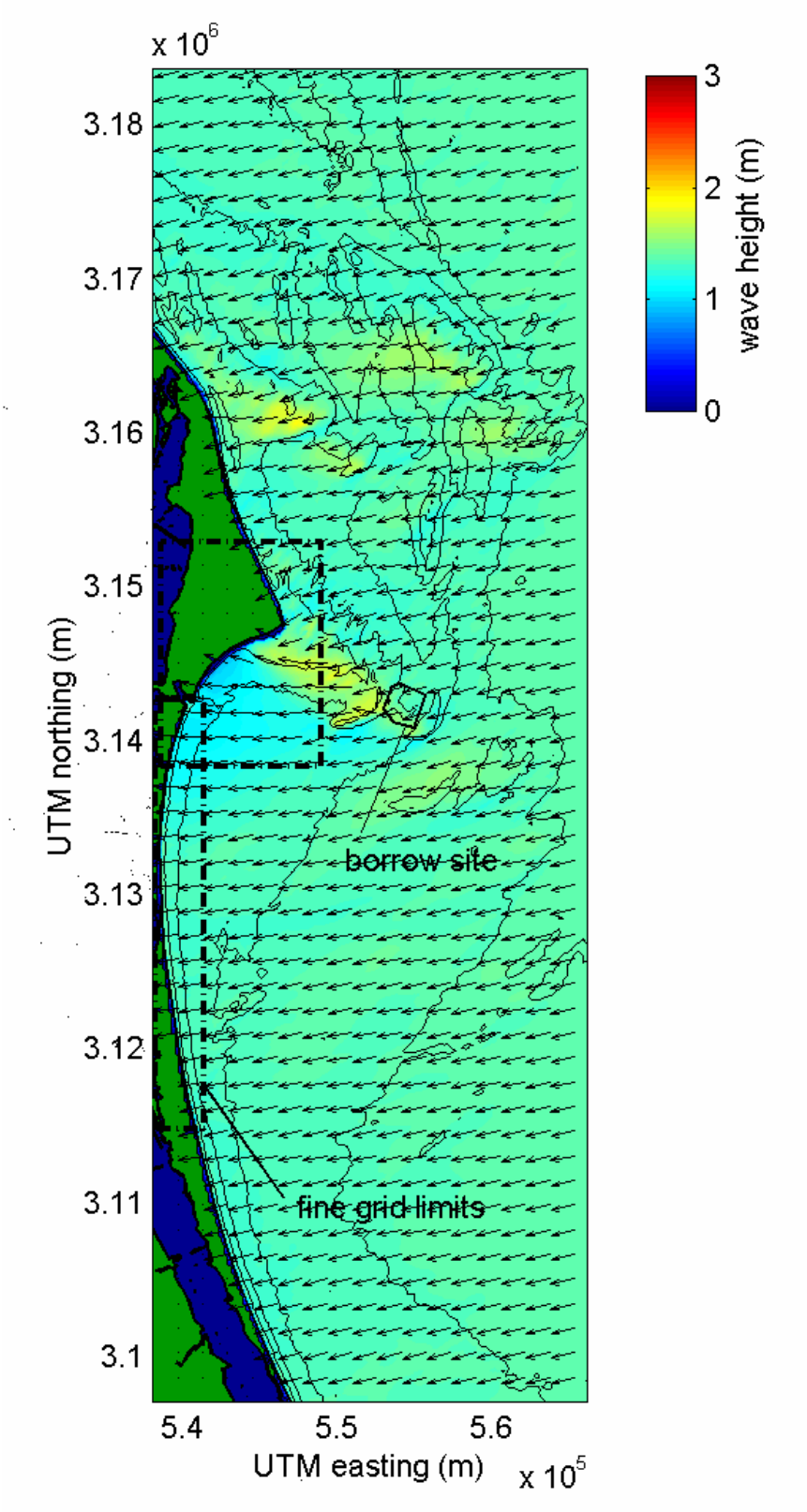

Figure E-2. Plot of STWAVE model output for Cape Canaveral, Florida, existing conditions, wave Case 2 (H_s=1.4 m, T_{peak}=7.7 sec, θ_{peak}=80 deg). Color contours indicate wave height, and vectors show mean direction of wave propagation.

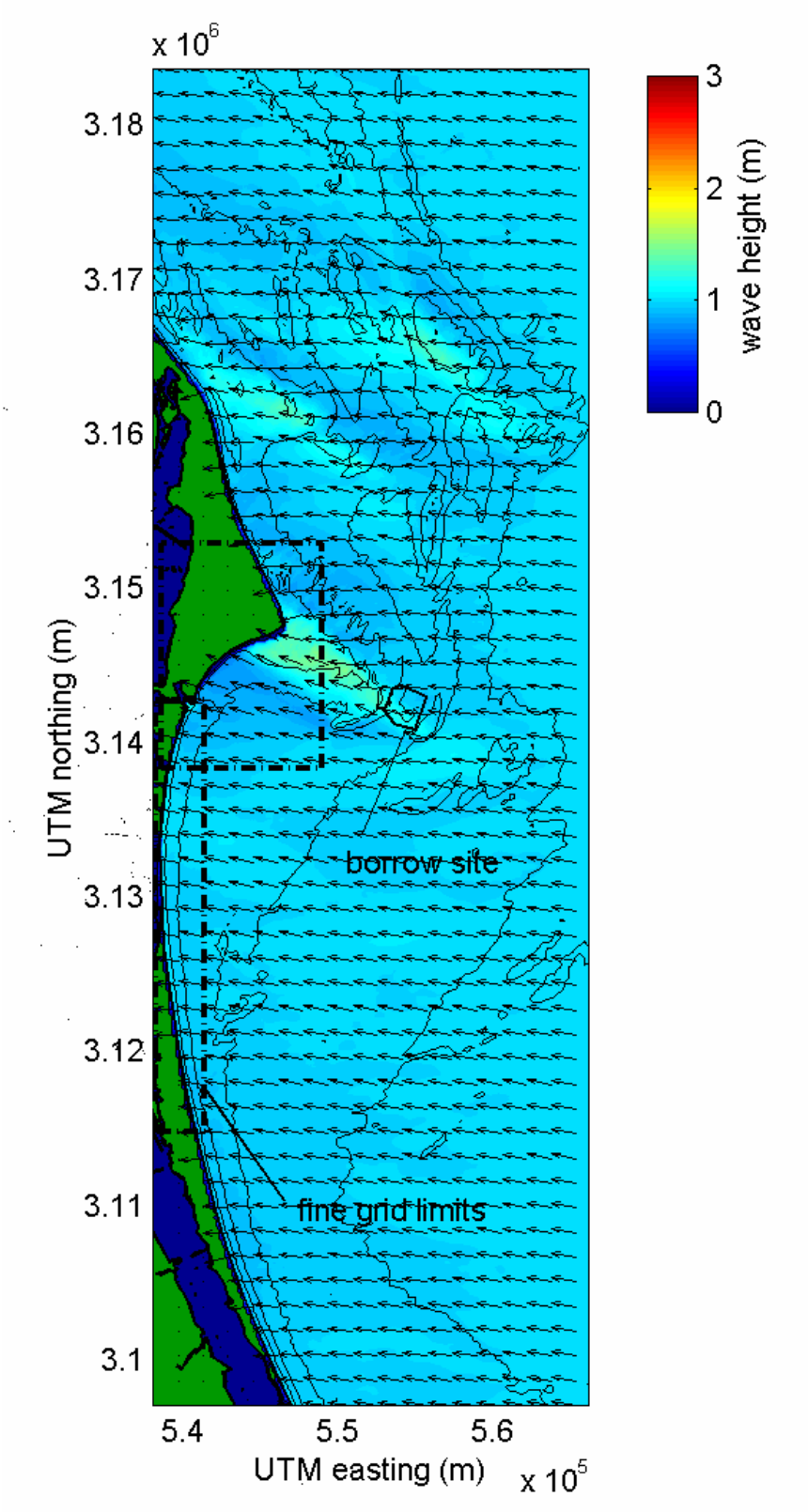

Figure E-3. Plot of STWAVE model output for Cape Canaveral, Florida, existing conditions, wave Case 3 (H_s=1.0 m, T_{peak}=7.7 sec, θ_{peak}=100 deg). Color contours indicate wave height, and vectors show mean direction of wave propagation.

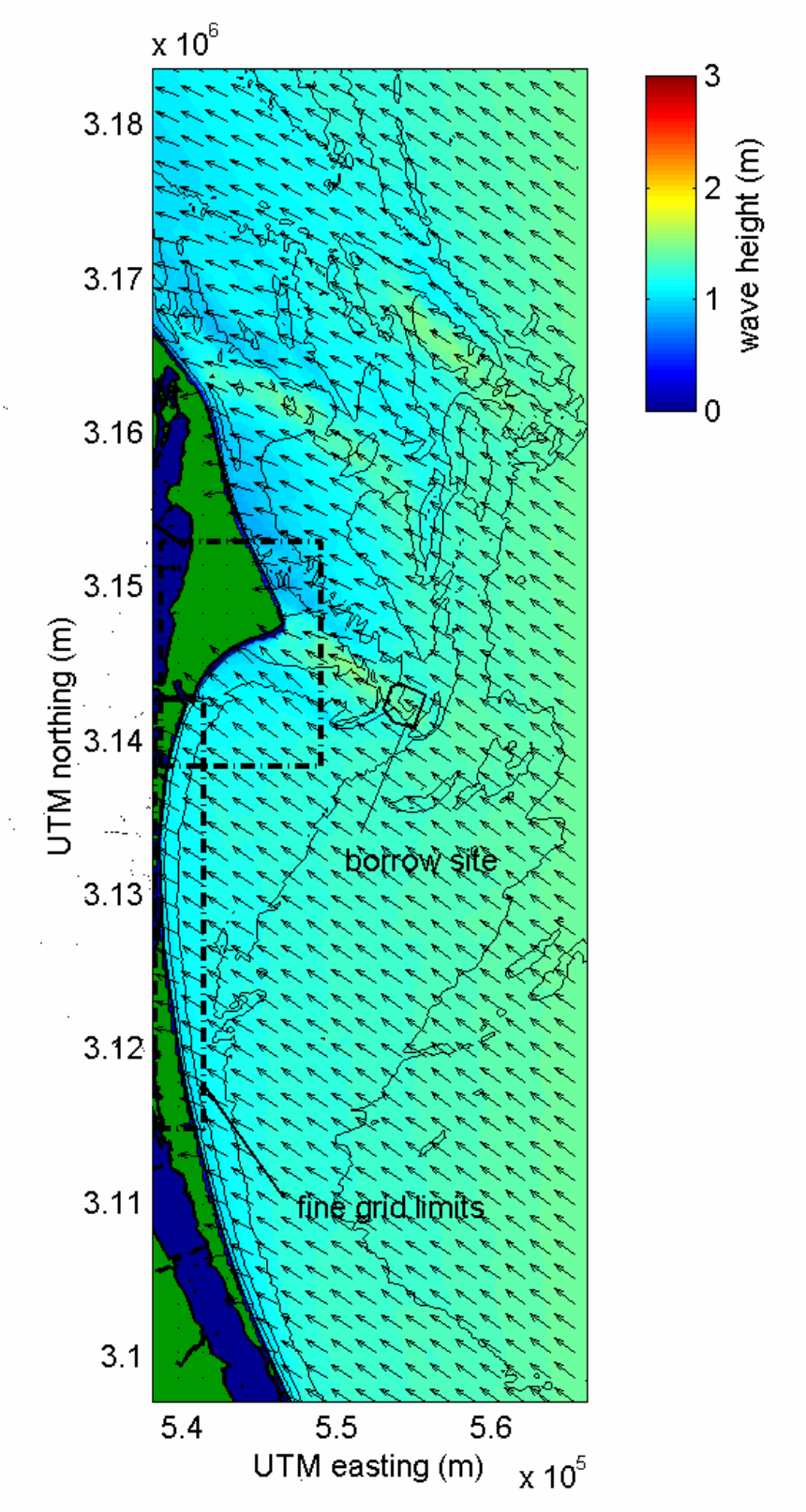

Figure E-4. Plot of STWAVE model output for Cape Canaveral, Florida, existing conditions, wave Case 4 (H_s=1.5 m, T_{peak}=6.3 sec, θ_{peak}=130 deg). Color contours indicate wave height, and vectors show mean direction of wave propagation.

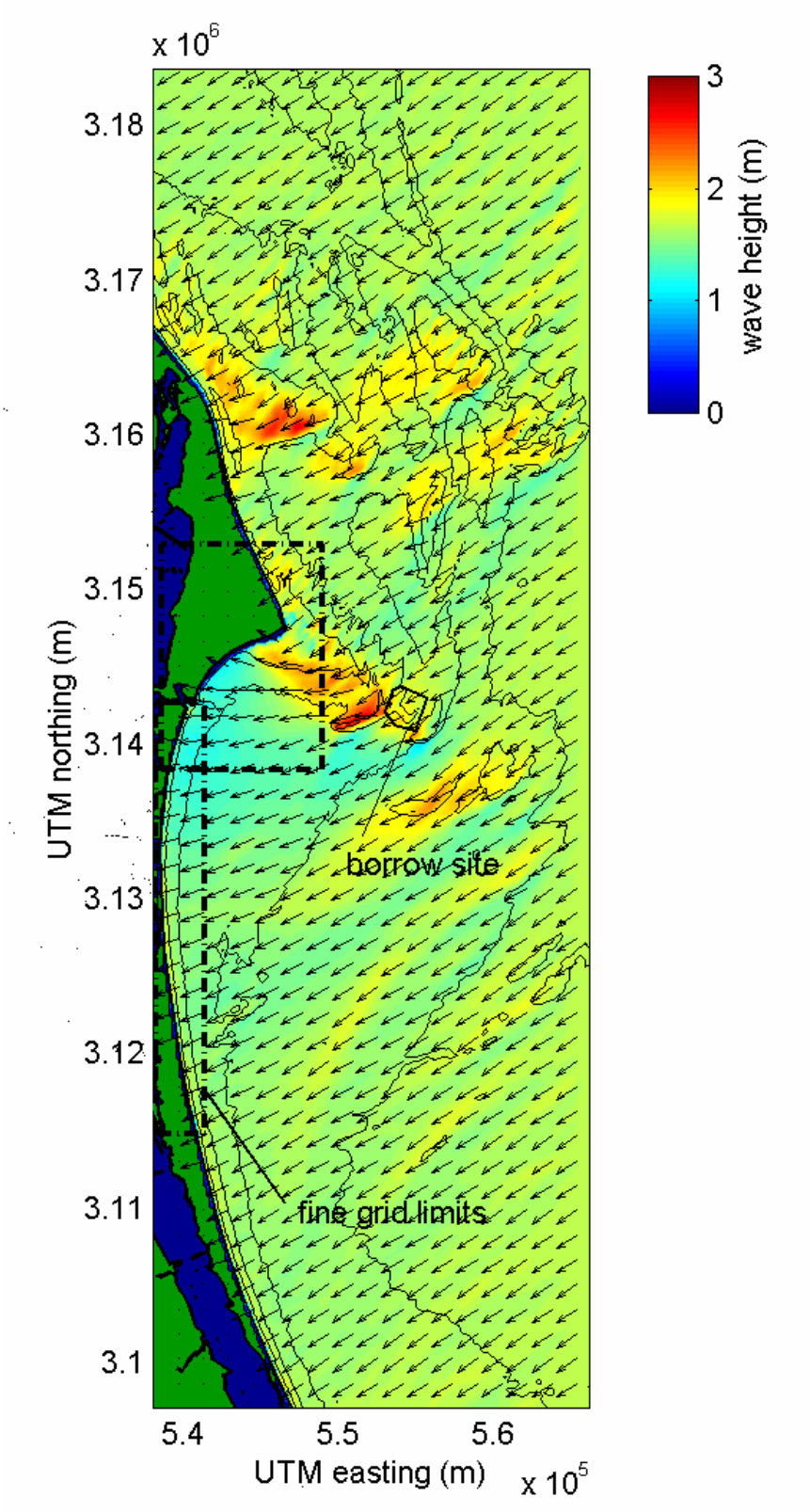

Figure E-5. Plot of STWAVE model output for Cape Canaveral, Florida, existing conditions, wave Case 5 (H_s=1.7 m, T_{peak}=12.5 sec, θ_{peak}=60 deg). Color contours indicate wave height, and vectors show mean direction of wave propagation.

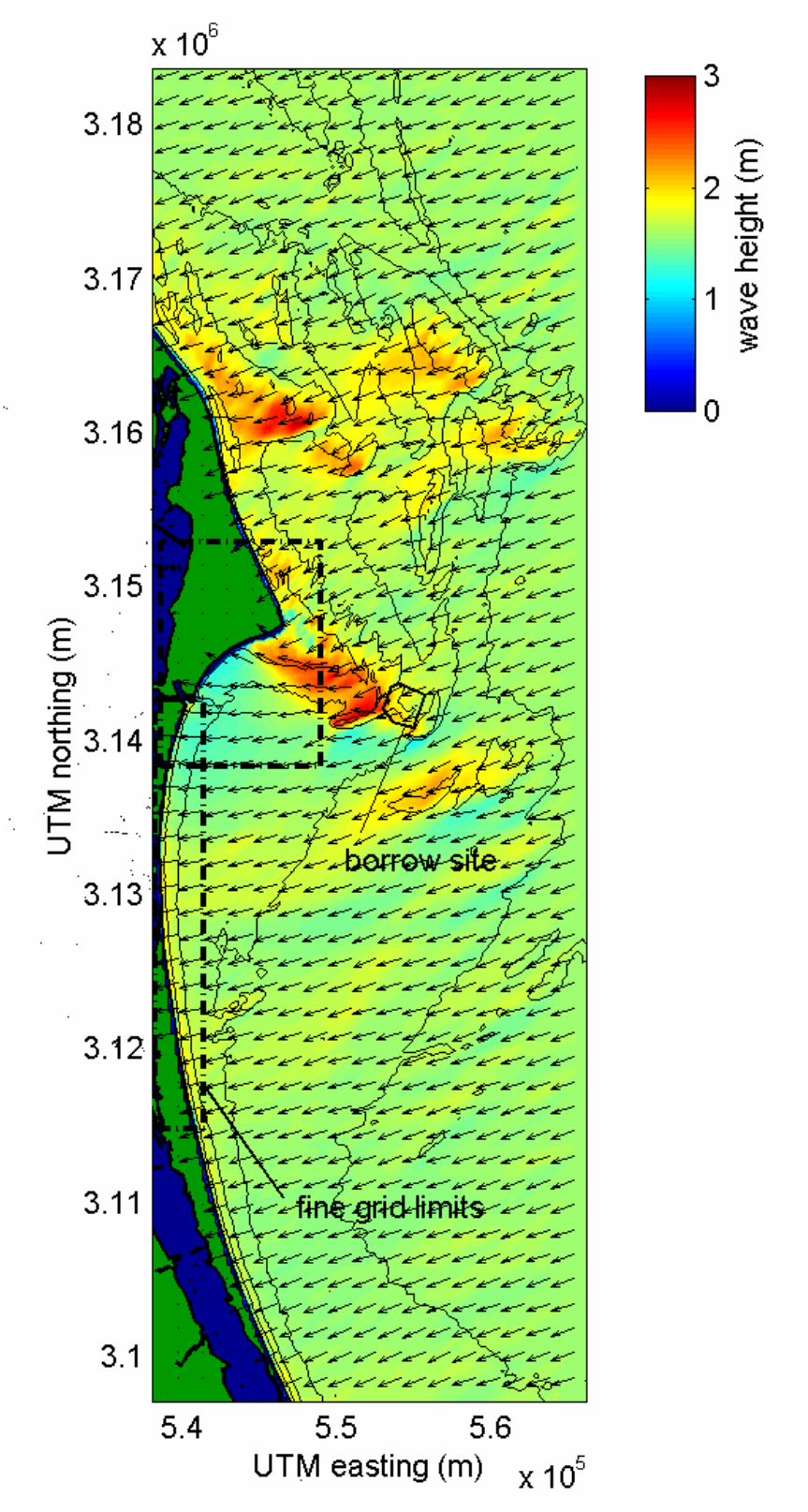

Figure E-6. Plot of STWAVE model output for Cape Canaveral, Florida, existing conditions, wave Case 6 (H_s=1.6 m, T_{peak}=14.3 sec, θ_{peak}=65 deg). Color contours indicate wave height, and vectors show mean direction of wave propagation.

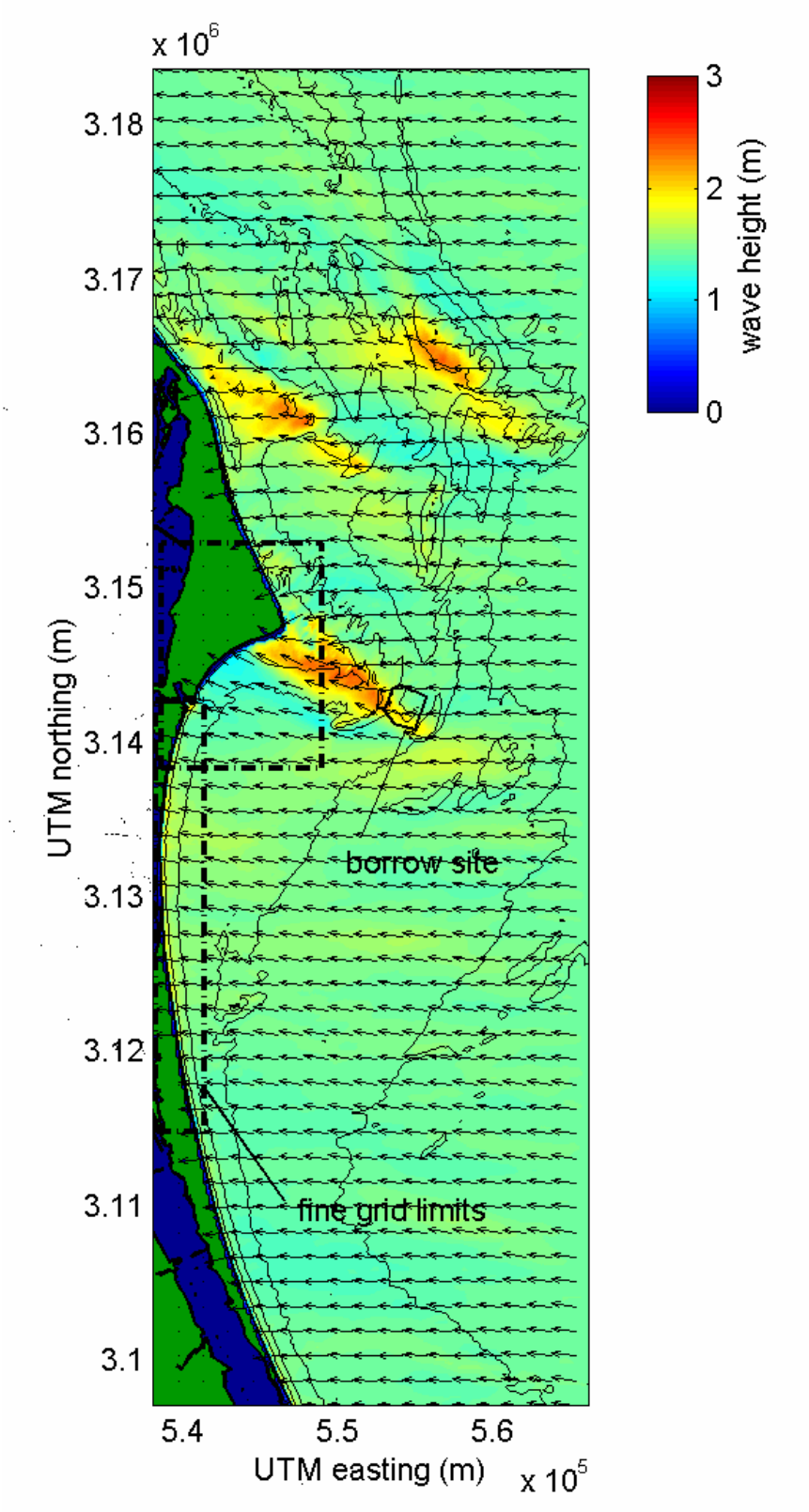

Figure E-7. Plot of STWAVE model output for Cape Canaveral, Florida, existing conditions, wave Case 7 (H_s=1.5 m, T_{peak}=11.1 sec, θ_{peak}=100 deg). Color contours indicate wave height, and vectors show mean direction of wave propagation.

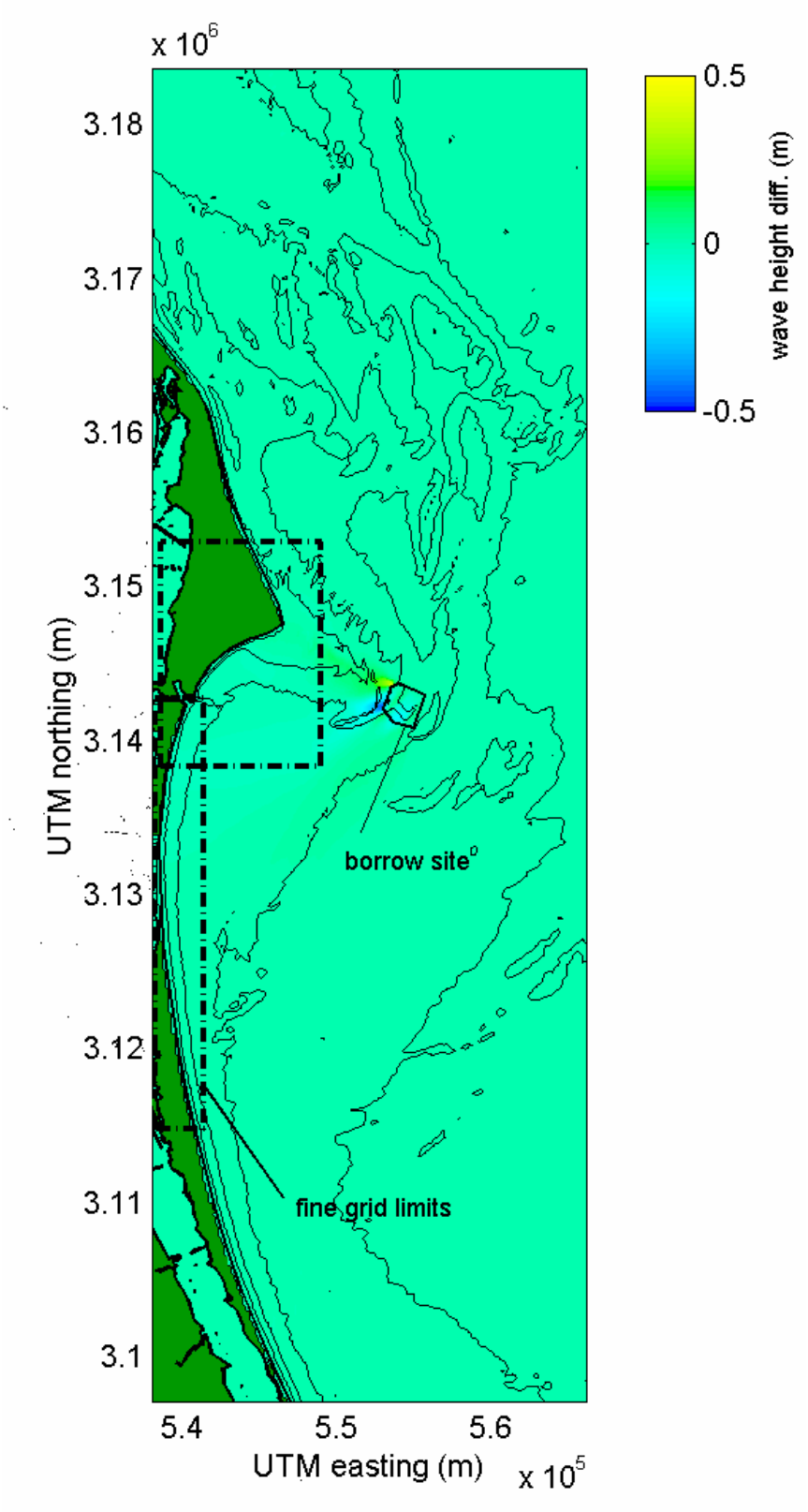

Figure E-8. Plot of wave height change between pre- and post-dredge ($\Delta=H_{post}-H_{pre}$) conditions at indicated borrow sites, for STWAVE model output of Cape Canaveral, Florida wave Case 1 (H_s=1.7 m, T_{peak}=7.7 sec, θ_{peak}=55 deg).

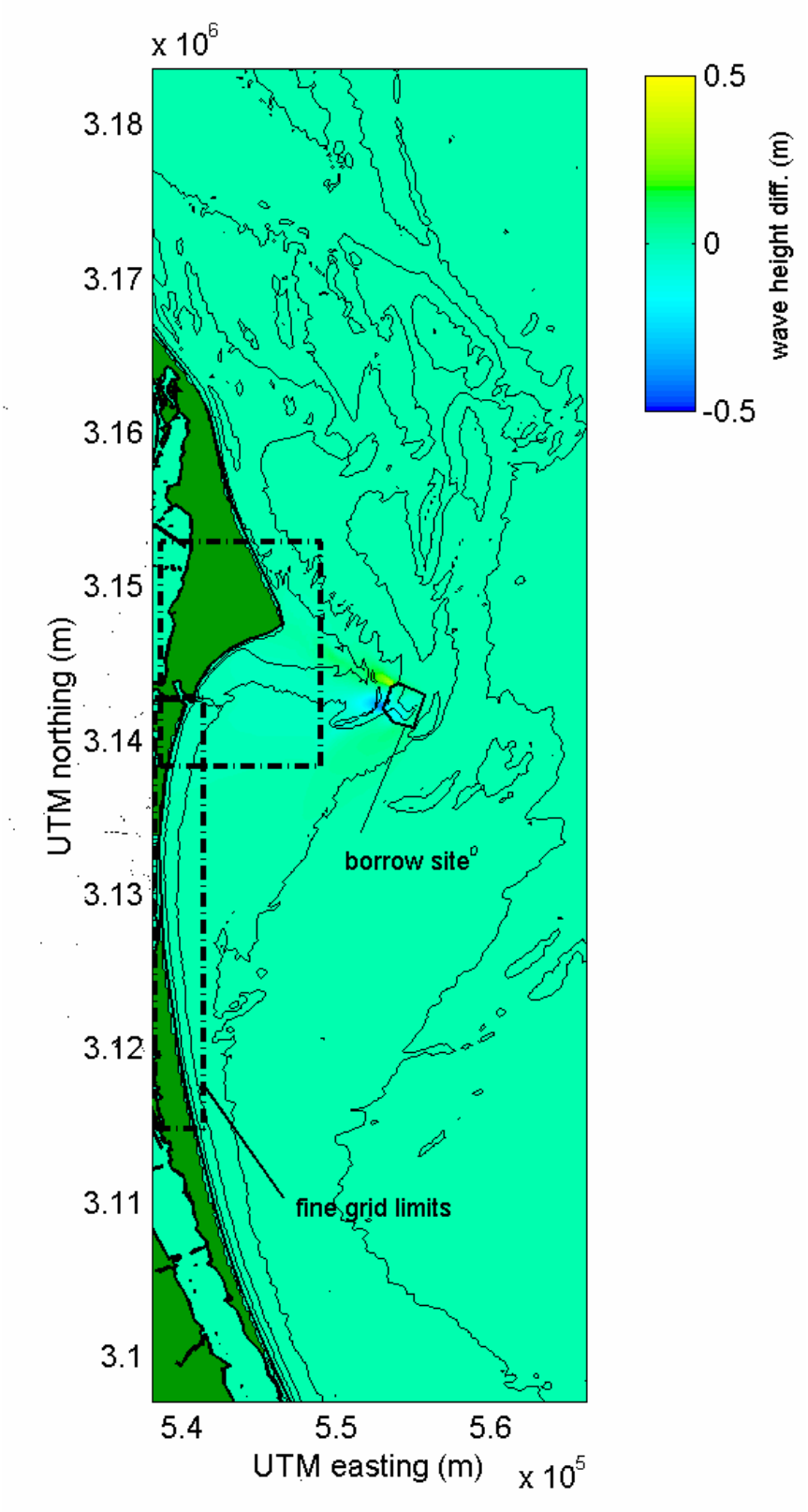

Figure E-9. Plot of wave height change between pre- and post-dredge ($\Delta=H_{post}-H_{pre}$) conditions at indicated borrow sites, for STWAVE model output of Cape Canaveral, Florida wave Case 2 (H_s=1.4 m, T_{peak}=7.7 sec, θ_{peak}=80 deg).

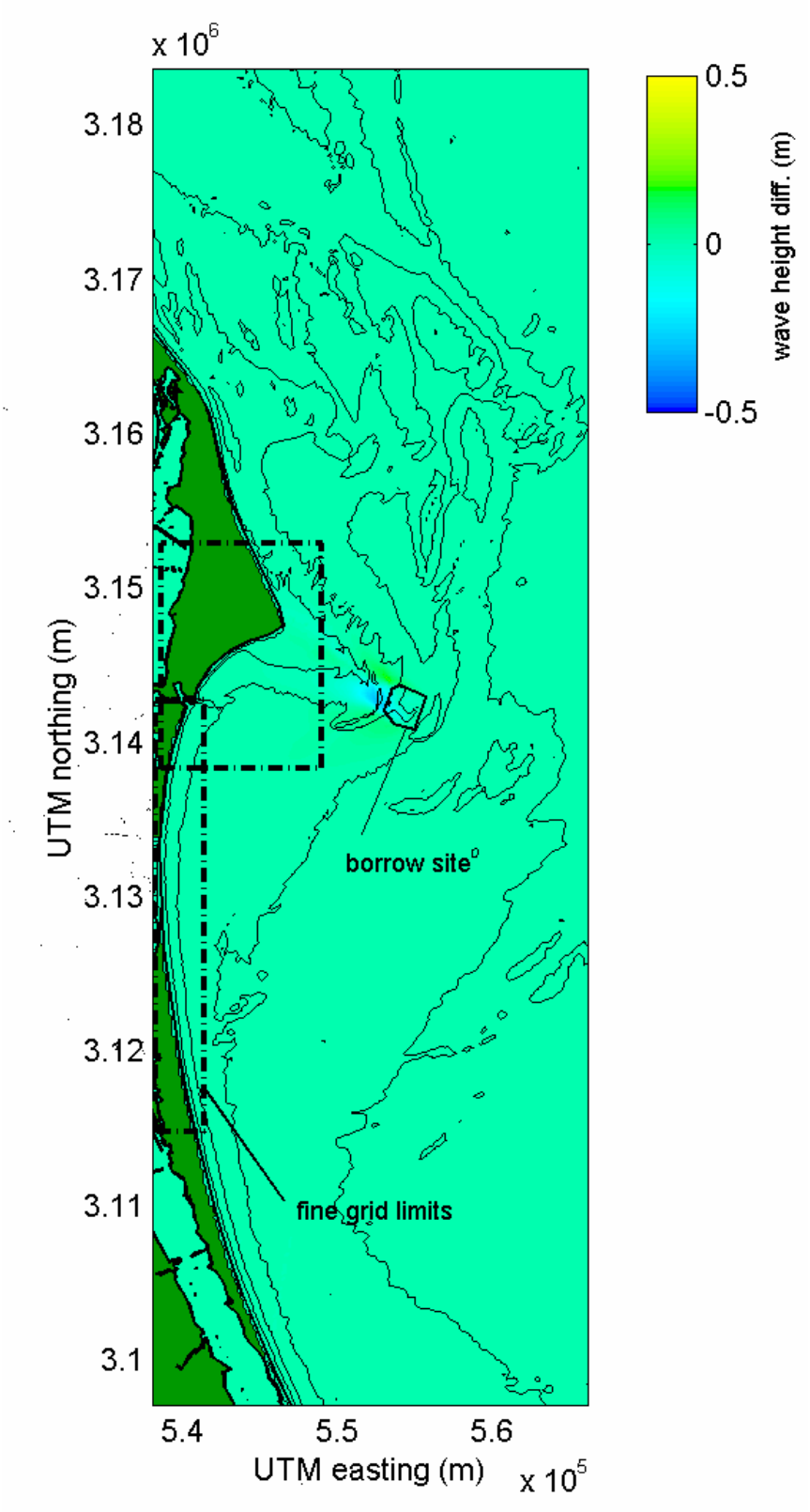

Figure E-10. Plot of wave height change between pre- and post-dredge ($\Delta=H_{post}-H_{pre}$) conditions at indicated borrow sites, for STWAVE model output of Cape Canaveral, Florida wave Case 3 (H_s=1.0 m, T_{peak}=7.7 sec, θ_{peak}=100 deg).

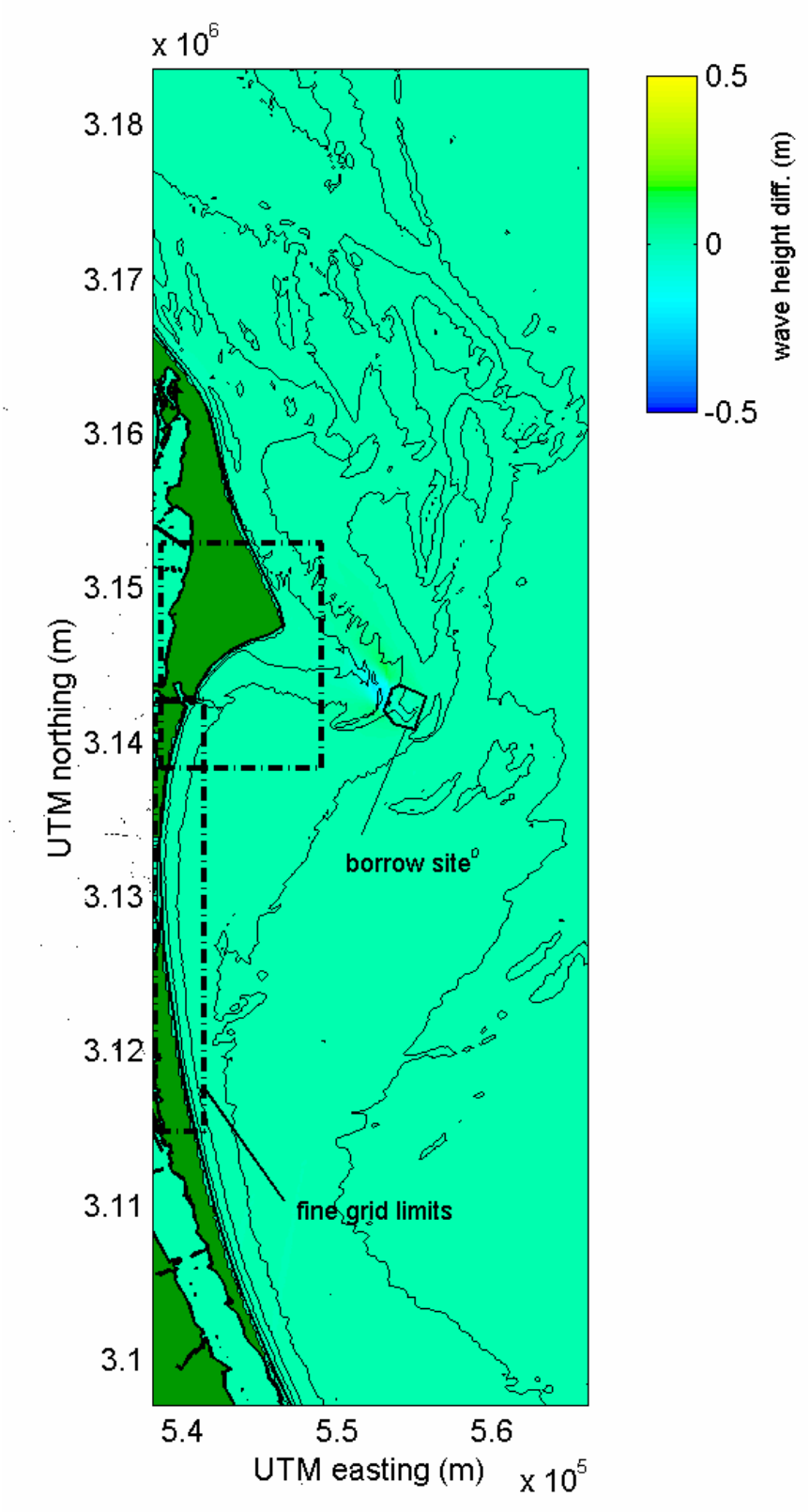

Figure E-11. Plot of wave height change between pre- and post-dredge ($\Delta=H_{post}-H_{pre}$) conditions at indicated borrow sites, for STWAVE model output of Cape Canaveral, Florida wave Case 4 (H_s=1.5 m, T_{peak}=6.3 sec, θ_{peak}=130 deg).

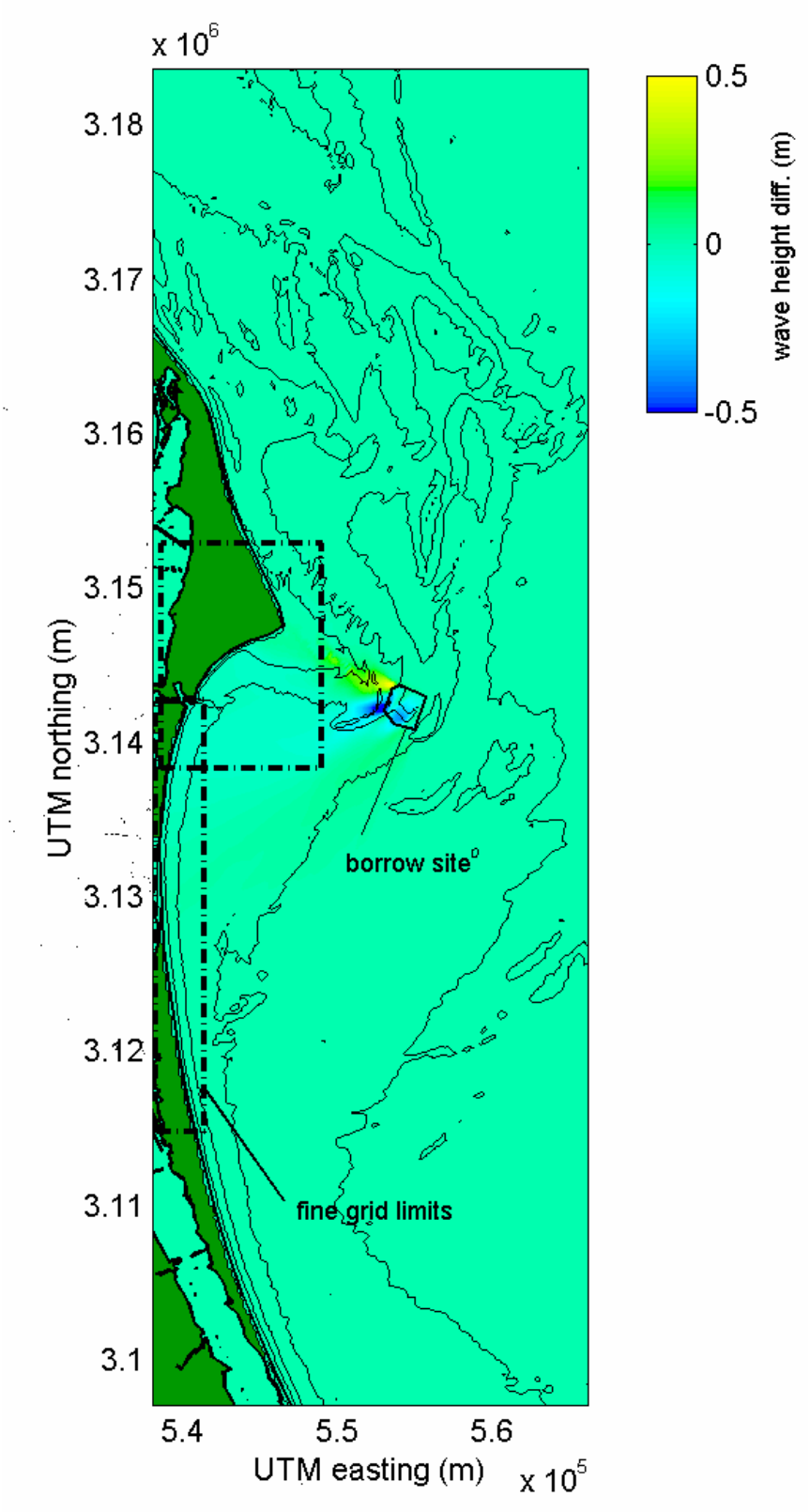

Figure E-12. Plot of wave height change between pre- and post-dredge ($\Delta=H_{post}-H_{pre}$) conditions at indicated borrow sites, for STWAVE model output of Cape Canaveral, Florida wave Case 5 (H_s=1.7 m, T_{peak}=12.5 sec, θ_{peak}=60 deg).

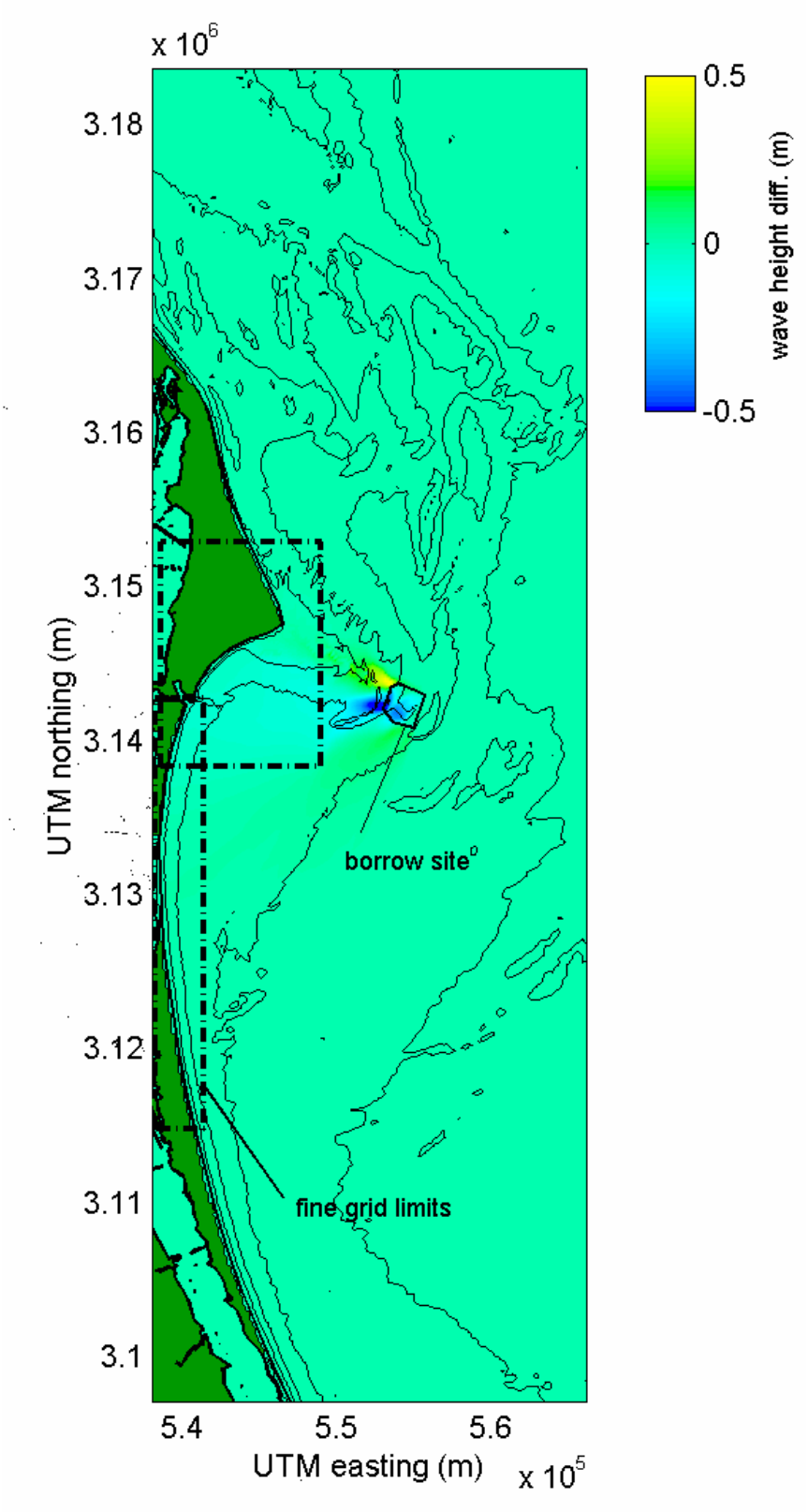

Figure E-13. Plot of wave height change between pre- and post-dredge ($\Delta=H_{post}-H_{pre}$) conditions at indicated borrow sites, for STWAVE model output of Cape Canaveral, Florida wave Case 6 (H_s=1.6 m, T_{peak}=14.3 sec, θ_{peak}=65 deg).

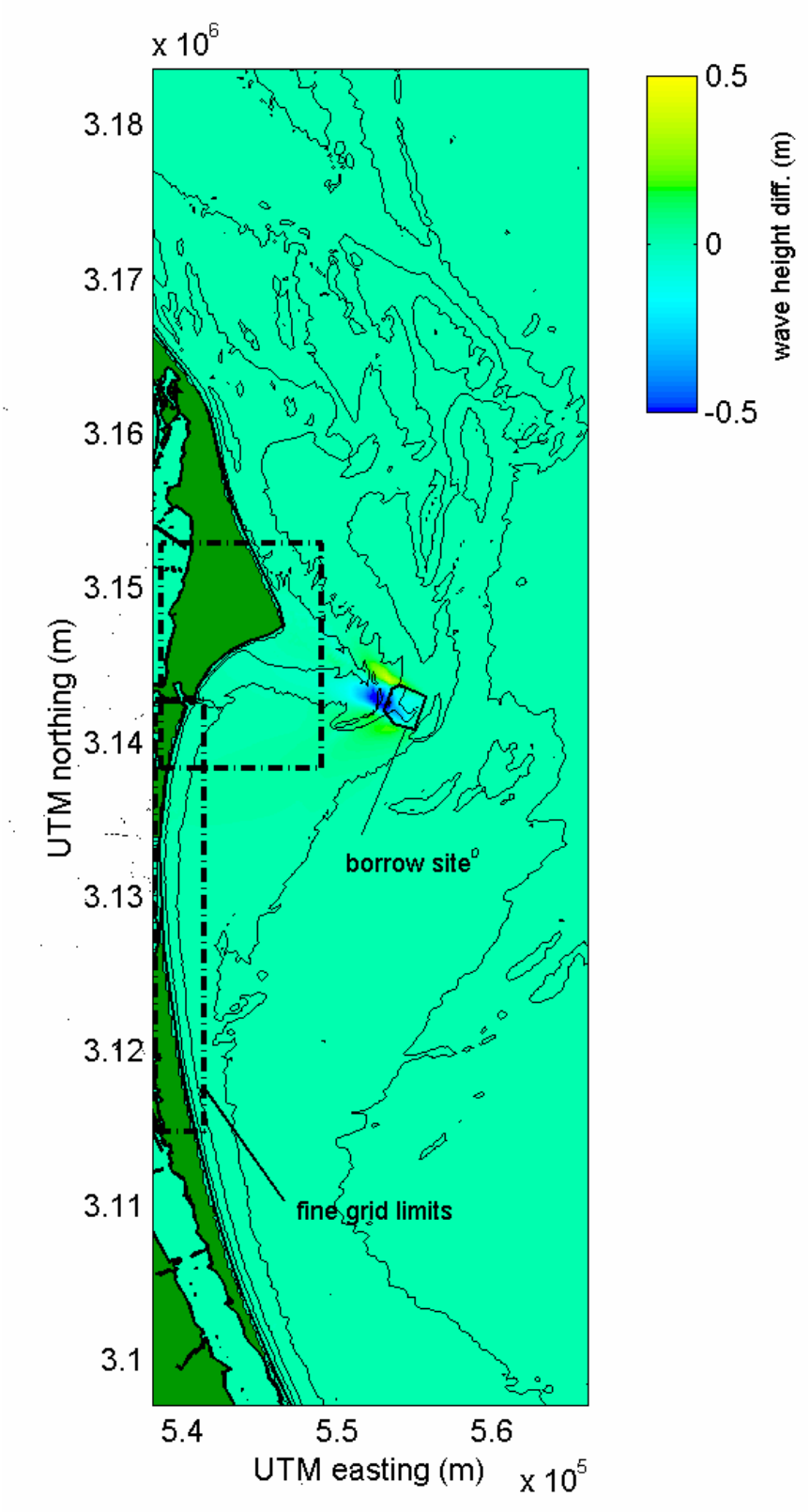

Figure E-14. Plot of wave height change between pre- and post-dredge ($\Delta=H_{post}-H_{pre}$) conditions at indicated borrow sites, for STWAVE model output of Cape Canaveral, Florida wave Case 1 (H_s=1.5 m, T_{peak}=11.1 sec, θ_{peak}=100 deg).